AFWL-TR-
71-118

A STUDY OF ENERGY GENERATION FROM IMPACT ON PIEZOELECTRIC MATERIALS

R. C. Dove W. E. Baker M. Valathur

University of New Mexico

TECHNICAL REPORT NO. AFWL-TR-71-118

December 1971

AIR FORCE WEAPONS LABORATORY
Air Force Systems Command
Kirtland Air Force Base
New Mexico

Approved for public release; distribution unlimited.

291

UNCLASSIFIED

Security Classification

DOCUMENT CONTROL DATA - R & D

(Security classification of title, body of abstract and indexing annotation must be entered when the overall report is classified)

1. ORIGINATING ACTIVITY (Corporate author)	2a. REPORT SECURITY CLASSIFICATION
University of New Mexico Department of Mechanical Engineering Albuquerque, New Mexico 87106	UNCLASSIFIED 2b. GROUP

3. REPORT TITLE

A STUDY OF ENERGY GENERATION FROM IMPACT ON PIEZOELECTRIC MATERIALS

4. DESCRIPTIVE NOTES (Type of report and inclusive dates)

December 1968 through July 1971

5. AUTHOR(S) (First name, middle initial, last name)

R. C. Dove, W. E. Baker, and M. Valathur

6. REPORT DATE	7a. TOTAL NO. OF PAGES	7b. NO. OF REFS
December 1971	~~198~~ 201	35

8a. CONTRACT OR GRANT NO.	9a. ORIGINATOR'S REPORT NUMBER(S)
F29601-69-C-0023 b. PROJECT NO. 5791 c. Task 32 d.	AFWL-TR-71-118 9b. OTHER REPORT NO(S) (Any other numbers that may be assigned this report)

10. DISTRIBUTION STATEMENT

Approved for public release; distribution unlimited.

11. SUPPLEMENTARY NOTES	12. SPONSORING MILITARY ACTIVITY
	AFWL (SRA) Kirtland AFB, NM 87117

13. ABSTRACT

(Distribution Limitation Statement A)

The feasibility of using piezoelectric or ferroelectric materials to generate useful amounts of electrical energy when subjected to impact was investigated. A survey of the current literature in this area was made and abstracts of pertinent articles are included. The basic principles and equations are placed in a form convenient for use in this work and examples given of their application. Significant material properties of common piezoelectric and ferroelectric materials are tabulated. Experimental work on crystals of selected materials was conducted. Static tests were conducted to check the specified piezoelectric coefficients. Two types of dynamic tests were conducted. The first utilized a low pressure shock tube for applying the impulse to the crystal. This series of tests was conducted primarily to study the effect of various circuit parameters on the energy available for dissipation in a fixed resistor. Since the impulse applied was small, the energy levels were quite small. The second type of dynamic test investigated in depth was one which utilized a split Hopkinson pressure bar for loading the crystals. Tests were conducted in which the impact speeds on the pressure bar ranged from about 30 ft/sec to 8000 ft/sec. A computer code was developed for predicting current from the crystal and energy dissipated in a fixed resistor. Results from the experimental work were used to show that the code gave reasonably good agreement between the computed current and energy functions as compared to the measured ones.

DD FORM 1 NOV 65 1473

UNCLASSIFIED

Security Classification

AFWL-TR-71-118

AIR FORCE WEAPONS LABORATORY
Air Force Systems Command
Kirtland Air Force Base
New Mexico 87117

When US Government drawings, specifications, or other data are used for any purpose other than a definitely related Government procurement operation, the Government thereby incurs no responsibility nor any obligation whatsoever, and the fact that the Government may have formulated, furnished, or in any way supplied the said drawings, specifications, or other data, is not to be regarded by implication or otherwise, as in any manner licensing the holder or any other person or corporation, or conveying any rights or permission to manufacture, use, or sell any patented invention that may in any way be related thereto.

This report is made available for study with the understanding that proprietary interests in and relating thereto will not be impaired. In case of apparent conflict or any other questions between the Government's rights and those of others, notify the Judge Advocate, Air Force Systems Command, Andrews Air Force Base, Washington, DC 20331.

DO NOT RETURN THIS COPY. RETAIN OR DESTROY.

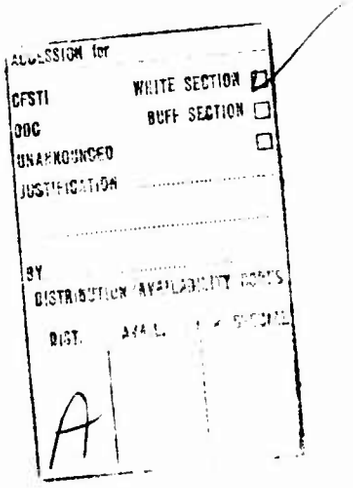

14. KEY WORDS	LINK A		LINK B		LINK C	
	ROLE	WT	ROLE	WT	ROLE	WT
Piezoelectric material Impact fuze						

ABSTRACT

The feasibility of using piezoelectric or ferroelectric materials to generate useful amounts of electrical energy when subjected to impact was investigated. A survey of the current literature in this area was made and abstracts of pertinent articles are included. The basic principles and equations are placed in a form convenient for use in this work and examples given of their application. Significant material properties of common piezoelectric and ferroelectric materials are tabulated.

Experimental work on crystals of selected materials was conducted. Static tests were conducted to check the specified piezoelectric coefficients. Two types of dynamic tests were conducted. The first utilized a low pressure shock tube for applying the impulse to the crystal. This series of tests was conducted primarily to study the effect of various circuit parameters on the energy available for dissipation in a fixed resistor. Since the impulse applied was small, the energy levels were quite small.

The second type of dynamic test investigated in depth was one which utilized a split Hopkinson pressure bar for loading the crystals. Tests were conducted in which the impact speeds on the pressure bar ranged from about 30 ft/sec to 8000 ft/sec. A computer code was developed for predicting current from the crystal and energy dissipated in a fixed resistor. Results from the experimental work were used to show that the code gave reasonably good agreement between the computed current and energy functions as compared to the measured ones.

(Distribution Limitation Statement A)

AFWL-TR-71-118

A STUDY OF ENERGY GENERATION FROM IMPACT ON PIEZOELECTRIC MATERIALS

R. C. Dove W. E. Baker M. Valathur

TECHNICAL REPORT NO. AFWL-TR-71-118

FOREWORD

This report was prepared by the University of New Mexico, Albuquerque, New Mexico, under Contract F29601-69-C-0023. The research was performed under Program Element 62601F, Project 5791, Task 32.

Inclusive dates of research were December 1968 through July 1971. The report was submitted 11 November 1971 by the Air Force Weapons Laboratory Project Officer, Lt Ervin P. Jaskolski (SRA).

The assistance and support provided by the Atmospheric Sciences Laboratory, White Sands Missile Range, is greatly appreciated. In particular, the expertise and cooperative attitude of Mr. Williamson and his subordinates were significant factors in the successful completion of the test program. Special mention is also made of Lt John F. Hodges, who initiated this program and was instrumental in ensuring its success.

This technical report has been reviewed and is approved.

Ervin P. Jaskolski

ERVIN P. JASKOLSKI
Lieutenant, USAF
Project Officer

Carl G. Weis

CARL G. WEIS
Lt Colonel, USAF
Chief, Applications Branch

Durward D. Young, Jr.

DURWARD D. YOUNG, JR.
Lt Colonel, USAF
Chief, Radiation Division

CONTENTS

CONTENTS, continued

ILLUSTRATIONS

ILLUSTRATIONS, continued

ILLUSTRATIONS, continued

ILLUSTRATIONS, continued

TABLES

LIST OF SYMBOLS

A	Area of the crystal face on which the load is applied
C	Capacitance
C_{Bond}	Bond capacitance
C_{Dist}	Distributed capacitance
C_{Load}	Load capacitance
C_p	Crystal capacitance
C_s	Shunt capacitance
C_{SCOPE}	Input capacitance of oscilloscope
C_{TOTAL}	Total capacitance in the crystal circuit
E	Energy
E_o	Elastic modulus of loading bar
F	Gage factor of resistance strain gage
K_3	Relative dielectric constant measured along the poling axis
K_1	Relative dielectric constant measured at right angles to the poling axis
K_o	Dielectric constant of empty space
P_r	Remanent polarization
Q_e	Electrical charge
Q_{max}	Maximum electrical charge
R_{Bond}	Bond resistance
R_{Cal}	Resistance of parallel calibrate resistor
R_{Dist}	Distributed resistance
R_L	Load resistance
R_p	Crystal resistance
R_{SCOPE}	Input resistance of oscilloscope

LIST OF SYMBOLS, continued

R_{TERM}	Terminating resistance
RC	Circuit time constant
U_o	Impact speed
V	Voltage
XK	Pulse rise time divided by circuit time constant
Y_{33}^E	Elastic modulus measured in a constant electric field in the 3 direction
Y_{11}^E	Elastic modulus measured in a constant electric field in the 1 direction
Y_{55}^E	Shear modulus measured in a constant electric field
Z_{Bond}	Bond impedance
C_o or C	One-dimensional elastic wave propagation speed
d_{em}	General piezoelectric charge coefficient, e identifying the electrical direction and m the mechanical direction
d_{33}	Direct piezoelectric charge coefficient
d_{31}	Transverse piezoelectric charge coefficient
d_{15}	Shear piezoelectric charge coefficient
e	Voltage
e_{11}^s	Permittivity of the crystal
g_{33}	Direct piezoelectric voltage coefficient
g_{31}	Transverse piezoelectric voltage coefficient
g_{15}	Shear piezoelectric voltage coefficient
h	Crystal thickness
i_c	Current through the parallel capacitance in a crystal circuit
i_q	Current generated by a crystal during the first wave passage

LIST OF SYMBOLS, continued

i_R	Current through the parallel resistance in a crystal circuit
i_{sc}	Current through a short circuit across a crystal during first wave passage
k_{33}	Direct electromechanical coupling coefficient
k_{31}	Transverse electromechanical coupling coefficient
k_{15}	Shear electromechanical coupling coefficient
t	Time
u	Particle displacement
v	Particle speed
x	Particle position
$\Delta\sigma$	Difference in uniaxial stress on two parallel faces of a crystal
ε	One-dimensional strain
ϕ	Angle of wavefront in crystal
θ	Angle between impacting surfaces
σ	One-dimensional stress
σ_m	Stress on the "m" face of a crystal
τ_R	Pulse rise time

SECTION I

INTRODUCTION

The general problem to which this work was directed was that of generating a usable amount of energy with piezoelectric or ferroelectric materials. The input to the active material of interest was to be a forcing function on one face of the crystal, and the desired output was an electrical current which would be dissipated in a fixed resistor.

The forcing functions which would be applied to the material were investigated in the work reported on in Volume I of the final reports of the contract supporting this work. The problem of particular interest was to maximize the energy available for dissipation in the fixed resistor.

Important factors which influence the amount of energy available for use are certain material properties of the piezoelectric or ferroelectric material, the geometry of the material, the pulse signature of the input forcing function, the fixity or support of the material, and the circuits used with the crystal. The work done for this study included consideration of each of these factors.

SECTION II

LITERATURE REVIEW

Initial studies on this problem included a search of the literature to determine the current state of the art of energy generation from piezoelectric and ferroelectric crystals, as defined by the published works on the subject. Because of the broad nature of this problem and to present the information as efficiently as possible, the list of papers considered as pertinent are given as the references, and the author's abstract of each of the more significant works are given in Appendix A. The first four references give information of a general, introductory nature, and do not have abstracts given for this reason.

SECTION III

REVIEW OF BASIC RELATIONSHIPS AND THEORY

Since the primary purpose of this study is the determination of the energy that a piezoelectric or ferroelectric device can deliver to some electrical load, a review of the necessary computations and theory are in order.

a. Charge generated by the crystal.

$$Q_e = d_{em}\sigma_m A \tag{1}$$

The above relation implies a linear relation between charge and force. In general, this is not true, particularly over a wide stress range for quartz, and for ferroelectric materials.

b. Capacitance.

$$C = \frac{K_o A \varepsilon_{11}^s}{h} \tag{2}$$

The above relation implies that ε_{11}^s is constant. It has been shown that this may change under strong shock conditions.

c. Voltage between faces of crystal for open circuit conditions ($R_L \to \infty$)

$$V = Q_e/C \tag{3}$$

d. Current through a short circuit across faces of a crystal during initial passage of a shock wave.

$$i_{sc}(t) = \frac{d_{em}\sigma_m(t)Ac}{h}, \quad \text{for } t<\frac{h}{c} \tag{4}$$

Reference 9 shows that this relation is good for quartz for the time for passage of the first wave through the crystal. The subscript "sc" indicates this is for a short circuit from one face of the crystal to another. It neglects the effect of any crystal capacitance, lead capacitance, or line resistance, which cannot be zero.

Since Equation (4) is the basis of the work done reported herein, the limitations of this equation as related to piezoelectric and ferroelectric materials are discussed below.

The equation is based upon a stress induced polarization which is a linear function of the stress in the direction normal to the surface upon which charge is being collected. This is true only in limited cases. One of these is a state of uniaxial strain. Another is uniaxial stress, where the strain in other directions be written as a function of the stress in the normal direction by use of appropriate constitutive relations. Similarly, it is also necessary that the electric field generated in the crystal be a linear function of the normal stress.

It is also necessary that stress is a linear function of strain. This allows the relation for the current output to be written as a linear function of stress, even though it is the strain in the crystal which produces the current. In order to keep the relation one-dimensional, it is assumed that the stress on the charge collecting face is uniform on that face.

Other necessary conditions related to the properties of the piezoelectric material are

1. Shock velocity is independent of stress amptitude.
2. Shock velocity is steady.
3. Resistivity of the material is infinite. This is particularly true in short circuit mode.
4. Dielectric constant is unchanged. This is normally the case, except for high strain rates, as when a shock wave passes.

These are reasonably valid for most piezoelectric or ferroelectric materials.

Necessary conditions for Equation (4) to be applicable which are valid for quartz but are in general not valid for ferroelectrics are the condition of linear polarization with stress and an electromechanical coupling effect which is negligible. For ferroelectrics, the polarization is approximately linear with stress for very low stress levels, but for high stress levels it is highly nonlinear. The results of later experimental tests make this quite apparent.

The effect of a large electromechanical coupling coefficient is to convert some of the electrical energy generated in the crystal back into mechanical energy through induced stress. For a material such as quartz where the coupling coefficient is small ($K \doteq .1$), this effect is negligible. But in a ferroelectric where the coupling coefficient can be large ($K = .3$ to $.6$), the effects are certainly not negligible. They are, however, difficult to calculate and account for.

Even though this equation does have significant limitation on when it is valid, it will be used as a basis for a first approximation in the studies for determining energy outputs from dynamically loaded piezoelectric and ferroelectric materials.

e. Current through a short circuit across faces of a crystal during passage of a pulse whose duration is long relative to h/c.

$$i_{sc}(t) = \frac{d_{em}\Delta\sigma_m(t)Ac}{h} \qquad (5)$$

In the above expression, $\Delta\sigma(t)$ is the stress difference between the front and rear electroded surfaces of the generator. This equation is applicable for any degree of fixity at each face of the crystal and is based upon an extension of Equation (4), which represents the output of the crystal as explained on the basis of piezoelectric theory and observed experiments.

f. Energy available under open circuit conditions ($R_L = \infty$).

$$E = \frac{Q^2}{2C} \tag{6}$$

In this expression, E is in joules when Q is in coulombs and C is in farads. The energy value determined from this expression is <u>not</u> a realizeable value under actual conditions of use, i.e., when the generator is connected to a finite load. Rather, it gives an upper limit on the amount of energy available.

In the practical application of a piezoelectric or ferroelectric as an energy generator, the problem is to find the energy delivered to the external load. The generator, circuit, and external load are shown in Figure 1. The inductive effect of the elements has been assumed negligible. If the following further assumptions are made

$$\begin{aligned} R_P &>> R_L \\ R_{Dist} &<< R_L \\ Z_{Bond} &\to 0 \ , \\ C_{Load} &<< C_p + C_{Dist} \end{aligned} \tag{7}$$

then the circuit can be approximated as shown in Figure 2. If it is assumed that the energy generated by the crystal in the real circuit of Figure 2 is the same as when in a short circuit, the following expression is obtained:

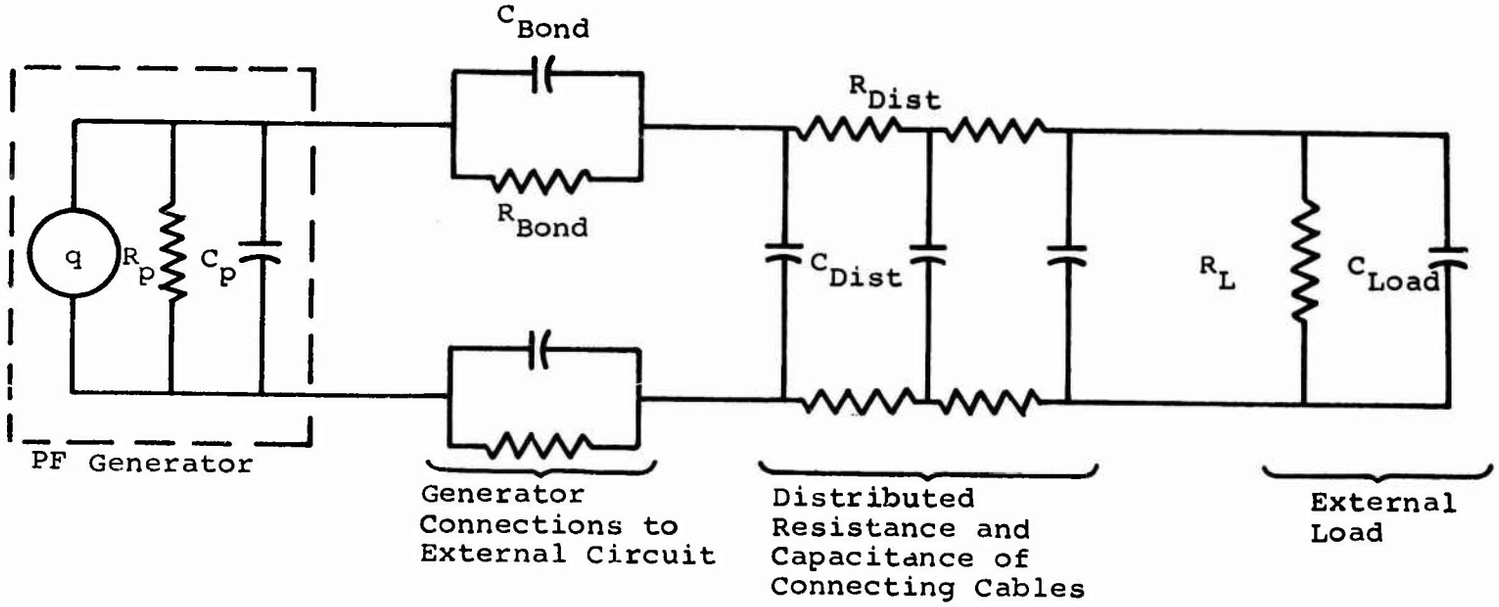

Figure 1. Generator, Circuit and External Load Schematic

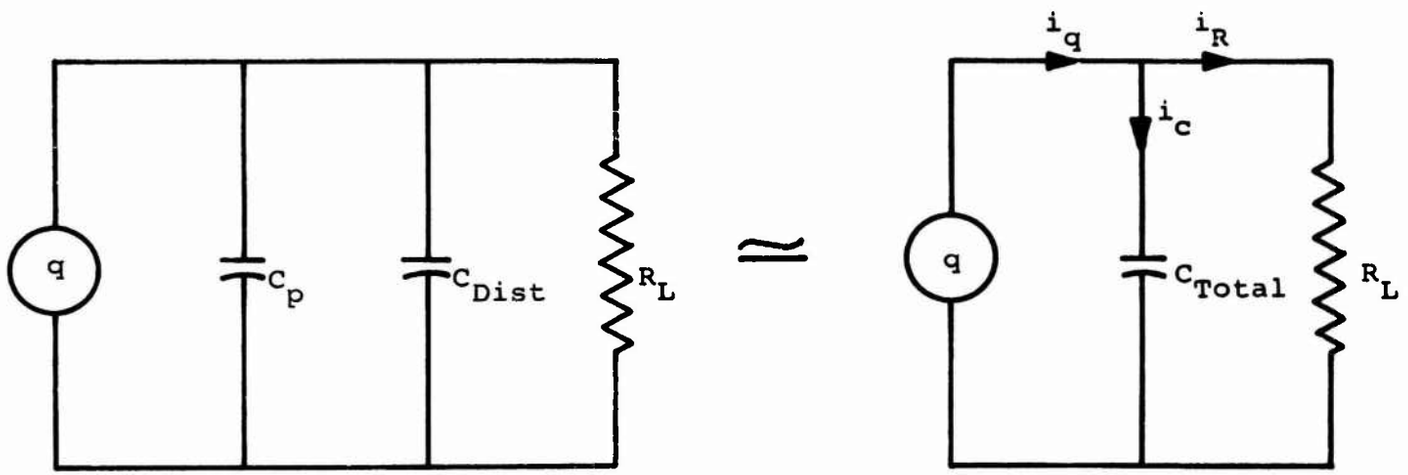

Figure 2. Idealized Circuit

$$i_{sc}(t) = i_q(t) = \frac{d_{em}\sigma(t)Ac}{h}, \quad \text{for } t < h/c \qquad (8)$$

This expression is subject to all the assumptions previously discussed in connection with Equation (4).

The current through the load resistor may be found from circuit theory

$$i_q = i_c + i_R$$

$$i_c = C_{Total} \frac{de}{dt}$$

where e is the voltage drop across C_{Total}. The first of the above equations may be written as

$$C_T \frac{de}{dt} + i_R = i_q \qquad (9)$$

This equation may be solved for the current delivered to the external load if the input, $i_q(t)$, is known.

g. Energy delivered to the external load,

$$E = \int_o^t i_R{}^2 R_L dt \qquad (10)$$

It must be remembered that i_R in the above equation has been obtained utilizing i_q. which is based upon the assumption that the load resistance in the circuit is zero. However, the energy available is now a function of R_L. Experiment has shown that for R_L small, say less than 100 ohms, the equation may still be used for quartz (Ref. 9).

As before, in many practical applications the rise time of the stress pulse will not be less than the transit time

of the pulse through the piezoelectric generator. It is necessary to extend Equation (8) to cover these cases. To do this, Equation (8) is reinterpreted to the form:

$$i_q(t) = \frac{d_{em}\Delta\sigma_m(t)Ac}{h} \tag{11}$$

where $\Delta\sigma_m(t)$ is the stress difference between the front and rear surface of the crystal.

The above discussion is based upon the energy generation from the piezoelectric effect. Ferroelectric materials also generate charge in a mode different from the piezoelectric one, i.e., by depoling from passage of a shock wave. Reference 6 gives a discussion of phenomenon.

The maximum charge release possible under these conditions is determined from the expression

$$Q_{max} = P_r A \tag{12}$$

Actual tests show that all of this amount cannot be obtained (Ref. 10). The percentage which can be obtained is dependent on such factors as the intensity of the shock wave and the planeness of the shock front.

In general, a greater charge may be released from the remanent polarization than with the piezoelectric effect. This phenomenon has been given the name "charge bulge."

SECTION IV

SUMMARY OF IMPORTANT PROPERTIES CF COMMON MATERIALS

There are many materials which exhibit a piezoelectric or ferroelectric effect, and consideration must be given to the ones most suitable for use in energy generation. This section gives information on the more important properties of materials currently listed in catalogs of certain manufacturers. The balues have been obtained primarily from the manufacturer's literature, but some has come from technical journals. The values are summarized here for convenience. Information is given on the following materials:

- Quartz
- HD-11
- HS-21
- G-53
- HDT-31
- G-1408
- G-1500
- HST-41
- G-1512
- G-2000

Manufactured by Gulton Industries, Inc.

- Ceramic "B"
- PZT-2
- PZT-4
- PZT-5A
- PZT-5H

Manufactured by Clevite Corporation

Blanks on these sheets indicate that the information was either not readily available or the quantity was not applicable for that material.

MATERIAL: Quartz MANUFACTURER: Gulton Industries, Inc.

DENSITY: = 2.65 gm/cm^3

SPECIFIC WEIGHT: = 0.095 lb/in^3

ELASTIC MODULI: Y^E_{33} = 8.0** x 10^{10} $\frac{newtons}{m^2}$ or 1.16 x 10^7 psi

Y^E_{11} = x 10^{10} $\frac{newtons}{m^2}$ or psi

Y^E_{55} = x 10^{10} $\frac{newtons}{m^2}$

ONE-DIMENSIONAL WAVE VELOCITY: c = 5.5 x 10^5 cm/sec or 2.16 x 10^5 in/sec

CURIE TEMPERATURE: °C

FREE DIELECTRIC CONSTANTS: K_3 = 4.5*

K_1 =

PIEZOELECTRIC CHARGE COEFFICIENTS: d_{33} = -2.3* $\frac{pcb}{newton}$ or -10.2 $\frac{pcb}{lb}$

d_{31} = 0.7* $\frac{pcb}{newton}$ or 0.31 $\frac{pcb}{lb}$

d_{15} = $\frac{pcb}{newton}$ or $\frac{pcb}{lb}$

PIEZOELECTRIC VOLTAGE COEFFICIENTS: g_{33} = 50# x 10^{-3} volt meters/newton

g_{31} = x 10^{-3} volt meters/newton

g_{15} = x 10^{-3} volt meters/newton

COUPLING COEFFICIENTS: k_{33} = 0.10**

k_{31} =

k_{15} =

REMANENT POLARIZATION:

* An Introduction to Piezoelectric Transducers, Valpey Corp., May 1965.

** Piezoelectricity, by Hans Jaffe, Reprinted from the Encyclopedia Britannica, Copyright 1961.

\# A Primer on Ferroelectricity and Piezoelectric Ceramics, Bernard Jaffe, Electronic Research Division, Clevite Corp., Engr. Memo #60-14, 1960.

MATERIAL: HD-11 (Barium Titanate)

MANUFACTURER: Gulton Industries, Inc.

DENSITY: $= >5.6 \ gm/cm^3$

SPECIFIC WEIGHT: $= 0.2 \ lb/in^3$

ELASTIC MODULI:

$Y^E_{33} = 13.0 \times 10^{10} \frac{newtons}{m^2}$ or 1.89×10^7 psi

$Y^E_{11} = 13.7 \times 10^{10} \frac{newtons}{m^2}$ or 1.99×10^7 psi

$Y^E_{55} = 5.7 \times 10^{10} \frac{newtons}{m^2}$ or 0.83×10^7 psi

ONE-DIMENSIONAL WAVE VELOCITY: $c = 4.8 \times 10^5$ cm/sec or 1.89×10^5 in/sec

CURIE TEMPERATURE: °C >135

FREE DIELECTRIC CONSTANTS:

$K_3 = 600$

$K_1 = 570$

PIEZOELECTRIC CHARGE COEFFICIENTS:

$d_{33} = 86 \ \frac{pcb}{newton}$ or $382 \ \frac{pcb}{lb}$

$d_{31} = -30 \ \frac{pcb}{newton}$ or $-133 \ \frac{pcb}{lb}$

$d_{15} = 125 \ \frac{pcb}{newton}$ or $555 \ \frac{pcb}{lb}$

PIEZOELECTRIC VOLTAGE COEFFICIENTS:

$g_{33} = 16 \times 10^{-3}$ volt meters/newton

$g_{31} = -5.5 \times 10^{-3}$ volt meters/newton

$g_{15} = 25 \times 10^{-3}$ volt meters/newton

COUPLING COEFFICIENTS:

$k_{33} = 0.45$

$k_{31} = 0.16$

$k_{15} = 0.42$

REMANENT POLARIZATION: $P_r = 9.4 \ \mu coul/cm^2$

MATERIAL: HS-21 (Barium Titanate)

MANUFACTURER: Gulton Industries, Inc.

DENSITY: = >5.6 gm/cm^3

SPECIFIC WEIGHT: = 0.2 lb/in^3

ELASTIC MODULI: $Y^E_{33} = 11.1 \times 10^{10} \frac{newtons}{m^2}$ or 1.61×10^7 psi

$Y^E_{11} = 11.5 \times 10^{10} \frac{newtons}{m^2}$ or 1.67×10^7 psi

$Y^E_{55} = 4.4 \times 10^{10} \frac{newtons}{m^2}$ or 0.64×10^7 psi

ONE-DIMENSIONAL WAVE VELOCITY: $c = 4.45 \times 10^5$ cm/sec or 1.75×10^5 in/sec

CURIE TEMPERATURE: °C >125

FREE DIELECTRIC CONSTANTS: $K_3 = 1150$

$K_1 = 1050$

PIEZOELECTRIC CHARGE COEFFICIENTS: $d_{33} = 148 \frac{pcb}{newton}$ or $658 \frac{pcb}{lb}$

$d_{31} = -50 \frac{pcb}{newton}$ or $-220 \frac{pcb}{lb}$

$d_{15} = 225 \frac{pcb}{newton}$ or $1000 \frac{pcb}{lb}$

PIEZOELECTRIC VOLTAGE COEFFICIENTS: $g_{33} = 16 \times 10^{-3}$ volt meters/newton

$g_{31} = -5.2 \times 10^{-3}$ volt meters/newton

$g_{15} = 25 \times 10^{-3}$ volt meters/newton

COUPLING COEFFICIENTS: $k_{33} = 0.51$

$k_{31} = 0.18$

$k_{15} = 0.48$

REMANENT POLARIZATION: $P_r = 50$ $\mu coul/cm^2$

MATERIAL: G-53 MANUFACTURER: Gulton Industries, Inc.
(Lead Zirconate Titanate)

DENSITY: $= >7.6 \ gm/cm^3$

SPECIFIC WEIGHT: $= 0.27 \ lb/in^3$

ELASTIC MODULI: $Y^E_{33} = 6.5 \times 10^{10} \frac{newtons}{m^2}$ or 0.94×10^7 psi

$Y^E_{11} = 8.1 \times 10^{10} \frac{newtons}{m^2}$ or 1.18×10^7 psi

$Y^E_{55} = 3.8 \times 10^{10} \frac{newtons}{m^2}$ or 0.55×10^7 psi

ONE-DIMENSIONAL WAVE VELOCITY: $c = 2.92 \times 10^5$ cm/sec or 1.15×10^5 in/sec

CURIE TEMPERATURE: °C >330

FREE DIELECTRIC CONSTANTS: $K_3 = 720$

$K_1 = 960$

PIEZOELECTRIC CHARGE COEFFICIENTS: $d_{33} = 190 \ \frac{pcb}{newton}$ or $845 \ \frac{pcb}{lb}$

$d_{31} = -84 \ \frac{pcb}{newton}$ or $-370 \ \frac{pcb}{lb}$

$d_{15} = 300 \ \frac{pcb}{newton}$ or $1330 \ \frac{pcb}{lb}$

PIEZOELECTRIC VOLTAGE COEFFICIENTS: $g_{33} = 30 \times 10^{-3}$ volt meters/newton

$g_{31} = -13 \times 10^{-3}$ volt meters/newton

$g_{15} = 36 \times 10^{-3}$ volt meters/newton

COUPLING COEFFICIENTS: $k_{33} = 0.60$

$k_{31} = 0.29$

$k_{15} = 0.64$

REMANENT POLARIZATION: $P_r = 26 \ \mu coul/cm^2$

MATERIAL: HDT-31 (Lead Zirconate Titanate) MANUFACTURER: Gulton Industries, Inc.

DENSITY: $= >7.6 \ gm/cm^3$

SPECIFIC WEIGHT: $= 0.27 \ lb/in^3$

ELASTIC MODULI:

$Y_{33}^E = 6.7 \times 10^{10} \frac{newtons}{m^2}$ or 0.97×10^7 psi

$Y_{11}^E = 8.1 \times 10^{10} \frac{newtons}{m^2}$ or 1.18×10^7 psi

$Y_{55}^E = 3.2 \times 10^{10} \frac{newtons}{m^2}$ or 0.46×10^7 psi

ONE-DIMENSIONAL WAVE VELOCITY: $c = 2.98 \times 10^5$ cm/sec or 1.17×10^5 in/sec

CURIE TEMPERATURE: $°C \quad >330$

FREE DIELECTRIC CONSTANTS:

$K_3 = 1300$

$K_1 = 1350$

PIEZOELECTRIC CHARGE COEFFICIENTS:

$d_{33} = 280 \ \frac{pcb}{newton}$ or $1243 \ \frac{pcb}{lb}$

$d_{31} = -120 \ \frac{pcb}{newton}$ or $-534 \ \frac{pcb}{lb}$

$d_{15} = 360 \ \frac{pcb}{newton}$ or $1600 \ \frac{pcb}{lb}$

PIEZOELECTRIC VOLTAGE COEFFICIENTS:

$g_{33} = 23 \times 10^{-3}$ volt meters/newton

$g_{31} = -11 \times 10^{-3}$ volt meters/newton

$g_{15} = 29 \times 10^{-3}$ volt meters/newton

COUPLING COEFFICIENTS:

$k_{33} = 0.66$

$k_{31} = 0.35$

$k_{15} = 0.59$

REMANENT POLARIZATION: $P_r = 27 \ \mu coul/cm^2$

MATERIAL: G-1408 MANUFACTURER: Gulton Industries, Inc.

DENSITY: $= >7.5 \quad gm/cm^3$

SPECIFIC WEIGHT: $= 0.27 \quad lb/in^3$

ELASTIC MODULI: $Y^E_{33} = 8.2 \times 10^{10} \frac{newtons}{m^2}$ or 1.19×10^7 psi

$Y^E_{11} = 9.0 \times 10^{10} \frac{newtons}{m^2}$ or 1.30×10^7 psi

$Y^E_{55} = 4.0 \times 10^{10} \frac{newtons}{m^2}$ or 0.58×10^7 psi

ONE-DIMENSIONAL WAVE VELOCITY: $c = 3.3 \times 10^5$ cm/sec or 1.3×10^5 in/sec

CURIE TEMPERATURE: °C >300

FREE DIELECTRIC CONSTANTS: $K_3 = 1000$

$K_1 = 1250$

PIEZOELECTRIC CHARGE COEFFICIENTS: $d_{33} = 200 \frac{pcb}{newton}$ or $890 \frac{pcb}{lb}$

$d_{31} = -80 \frac{pcb}{newton}$ or $356 \frac{pcb}{lb}$

$d_{15} = 315 \frac{pcb}{newton}$ or $1401 \frac{pcb}{lb}$

PIEZOELECTRIC VOLTAGE COEFFICIENTS: $g_{33} = 22 \times 10^{-3}$ volt meters/newton

$g_{31} = -9.0 \times 10^{-3}$ volt meters/newton

$g_{15} = 29 \times 10^{-3}$ volt meters/newton

COUPLING COEFFICIENTS: $k_{33} = 0.60$

$k_{31} = 0.26$

$k_{15} = 0.60$

REMANENT POLARIZATION: $P_r = 22 \quad \mu coul/cm^2$

MATERIAL: G-1500 (Lead Zirconate Titanate) MANUFACTURER: Gulton Industries, Inc.

DENSITY: = >7.6 gm/cm^3

SPECIFIC WEIGHT: = 0.27 lb/in^3

ELASTIC MODULI: $Y^E_{33} = 4.9 \times 10^{10} \frac{newtons}{m^2}$ or 0.71×10^7 psi

$Y^E_{11} = 6.3 \times 10^{10} \frac{newtons}{m^2}$ or 0.91×10^7 psi

$Y^E_{55} = 2.2 \times 10^{10} \frac{newtons}{m^2}$ or 0.32×10^7 psi

ONE-DIMENSIONAL WAVE VELOCITY: $c = 2.54 \times 10^5$ cm/sec or 1×10^5 in/sec

CURIE TEMPERATURE: °C >360

FREE DIELECTRIC CONSTANTS: $K_3 = 1700$

$K_1 = 1700$

PIEZOELECTRIC CHARGE COEFFICIENTS: $d_{33} = 370 \frac{pcb}{newton}$ or $1642 \frac{pcb}{lb}$

$d_{31} = -166 \frac{pcb}{newton}$ or $-739 \frac{pcb}{lb}$

$d_{15} = 540 \frac{pcb}{newton}$ or $2400 \frac{pcb}{lb}$

PIEZOELECTRIC VOLTAGE COEFFICIENTS: $g_{33} = 25 \times 10^{-3}$ volt meters/newton

$g_{31} = -11 \times 10^{-3}$ volt meters/newton

$g_{15} = 36 \times 10^{-3}$ volt meters/newton

COUPLING COEFFICIENTS: $k_{33} = 0.69$

$k_{31} = 0.34$

$k_{15} = 0.65$

REMANENT POLARIZATION: $P_r = 24$ $\mu coul/cm^2$

MATERIAL: HST-41 (Lead Zirconate Titanate)

MANUFACTURER: Gulton Industries, Inc.

DENSITY: = >7.6 gm/cm^3

SPECIFIC WEIGHT: = 0.27 lb/in^3

ELASTIC MODULI:

$Y^E_{33} = 5.9 \times 10^{10} \frac{newtons}{m^2}$ or 0.86×10^7 psi

$Y^E_{11} = 7.0 \times 10^{10} \frac{newtons}{m^2}$ or 1.01×10^7 psi

$Y^E_{55} = 1.8 \times 10^{10} \frac{newtons}{m^2}$ or 0.26×10^7 psi

ONE-DIMENSIONAL WAVE VELOCITY: $c = 2.79 \times 10^5$ cm/sec or 1.10×10^5 in/sec

CURIE TEMPERATURE: °C >270

FREE DIELECTRIC CONSTANTS:

$K_3 = 1800$

$K_1 = 2100$

PIEZOELECTRIC CHARGE COEFFICIENTS:

$d_{33} = 325 \frac{pcb}{newton}$ or $1445 \frac{pcb}{lb}$

$d_{31} = -157 \frac{pcb}{newton}$ or $-698 \frac{pcb}{lb}$

$d_{15} = 625 \frac{pcb}{newton}$ or $2780 \frac{pcb}{lb}$

PIEZOELECTRIC VOLTAGE COEFFICIENTS:

$g_{33} = 22 \times 10^{-3}$ volt meters/newton

$g_{31} = -11 \times 10^{-3}$ volt meters/newton

$g_{15} = 37 \times 10^{-3}$ volt meters/newton

COUPLING COEFFICIENTS:

$k_{33} = 0.66$

$k_{31} = 0.35$

$k_{15} = 0.69$

REMANENT POLARIZATION: $P_r = 23$ $\mu coul/cm^2$

MATERIAL: G-1512 (Lead Zirconate Titanate) MANUFACTURER: Gulton Industries, Inc.

DENSITY: = >7.4 gm/cm^3

SPECIFIC WEIGHT: = 0.26 lb/in^3

ELASTIC MODULI:

$Y^E_{33} = 5.4 \times 10^{10} \frac{newtons}{m^2}$ or 0.78×10^7 psi

$Y^E_{11} = 6.3 \times 10^{10} \frac{newtons}{m^2}$ or 0.91×10^7 psi

$Y^E_{55} = 2.6 \times 10^{10} \frac{newtons}{m^2}$ or 0.38×10^7 psi

ONE-DIMENSIONAL WAVE VELOCITY: $c = 2.69 \times 10^5$ cm/sec or 1.06×10^5 in/sec

CURIE TEMPERATURE: °C >240

FREE DIELECTRIC CONSTANTS:

$K_3 = 2600$

$K_1 = 2200$

PIEZOELECTRIC CHARGE COEFFICIENTS:

$d_{33} = 500 \frac{pcb}{newton}$ or $2220 \frac{pcb}{lb}$

$d_{31} = -232 \frac{pcb}{newton}$ or $-1030 \frac{pcb}{lb}$

$d_{15} = 680 \frac{pcb}{newton}$ or $3100 \frac{pcb}{lb}$

PIEZOELECTRIC VOLTAGE COEFFICIENTS:

$g_{33} = 20 \times 10^{-3}$ volt meters/newton

$g_{31} = -9.3 \times 10^{-3}$ volt meters/newton

$g_{15} = 35 \times 10^{-3}$ volt meters/newton

COUPLING COEFFICIENTS:

$k_{33} = 0.72$

$k_{31} = 0.37$

$k_{15} = 0.78$

REMANENT POLARIZATION: $P_r = 23$ $\mu coul/cm^2$

MATERIAL: G-2000 (Lead Metaniobate)

MANUFACTURER: Gulton Industries, Inc.

DENSITY: = >5.8 gm/cm^3

SPECIFIC WEIGHT: = 0.21 lb/in^3

ELASTIC MODULI:

$Y^E_{33} = 4.7 \times 10^{10} \frac{newtons}{m^2}$ or 0.68×10^7 psi

$Y^E_{11} = 4.0 \times 10^{10} \frac{newtons}{m^2}$ or 0.58×10^7 psi

$Y^E_{55} = 1.8 \times 10^{10} \frac{newtons}{m^2}$ or 0.26×10^7 psi

ONE-DIMENSIONAL WAVE VELOCITY: $c = 2.85 \times 10^5$ cm/sec or 1.12×10^5 in/sec

CURIE TEMPERATURE: °C >400

FREE DIELECTRIC CONSTANTS:

$K_3 = 250$

$K_1 = 250$

PIEZOELECTRIC CHARGE COEFFICIENTS:

$d_{33} = 80 \frac{pcb}{newton}$ or $356 \frac{pcb}{lb}$

$d_{31} = -10 \frac{pcb}{newton}$ or $44.5 \frac{pcb}{lb}$

$d_{15} = 115 \frac{pcb}{newton}$ or $511 \frac{pcb}{lb}$

PIEZOELECTRIC VOLTAGE COEFFICIENTS:

$g_{33} = 36 \times 10^{-3}$ volt meters/newton

$g_{31} = -4.5 \times 10^{-3}$ volt meters/newton

$g_{15} = 50 \times 10^{-3}$ volt meters/newton

COUPLING COEFFICIENTS: $k_{33} = 0.38$

$k_{31} = 0.04$

$k_{15} = 0.33$

REMANENT POLARIZATION: P_r = --- $\mu coul/cm^2$

MATERIAL: Ceramic "B" MANUFACTURER: Clevite Corp.

DENSITY: $= 5.55 \ gm/cm^3$

SPECIFIC WEIGHT: $= 0.2 \ lb/in^3$

ELASTIC MODULI: $Y^E_{33} = 11.1 \times 10^{10} \frac{newtons}{m^2}$ or 1.61×10^7 psi

$Y^E_{11} = 11.6 \times 10^{10} \frac{newtons}{m^2}$ or 1.68×10^7 psi

$Y^E_{55} =$

ONE-DIMENSIONAL WAVE VELOCITY: $c = 4.48 \times 10^5$ cm/sec or 1.65×10^5 in/sec

CURIE TEMPERATURE: °C 115°

FREE DIELECTRIC CONSTANTS: $K_3 = 1200$

$K_1 = 1300$

PIEZOELECTRIC CHARGE COEFFICIENTS: $d_{33} = 149 \ \frac{pcb}{newton}$ or $662 \ \frac{pcb}{lb}$

$d_{31} = -58 \ \frac{pcb}{newton}$ or $258 \ \frac{pcb}{lb}$

$d_{15} = 242 \ \frac{pcb}{newton}$ or $1070 \ \frac{pcb}{lb}$

PIEZOELECTRIC VOLTAGE COEFFICIENTS: $g_{33} = 14.1 \times 10^{-3}$ volt meters/newton

$g_{31} = -5.5 \times 10^{-3}$ volt meters/newton

$g_{15} = 21 \times 10^{-3}$ volt meters/newton

COUPLING COEFFICIENTS: $k_{33} = 0.48$

$k_{31} = -0.194$

$k_{15} = 0.48$

REMANENT POLARIZATION: $P_r =$ ---- $coul/cm^2$

MATERIAL: PZT-2 MANUFACTURER: Clevite Corp.

DENSITY: = 7.6 gm/cm^3

SPECIFIC WEIGHT: = 0.27 lb/in^3

ELASTIC MODULI: Y_{33}^E =

Y_{11}^E =

Y_{55}^E =

ONE-DIMENSIONAL WAVE VELOCITY: c =

CURIE TEMPERATURE: °C 370

FREE DIELECTRIC CONSTANTS: K_3 =

K_1 =

PIEZOELECTRIC CHARGE COEFFICIENTS: d_{33} = 152 $\frac{pcb}{newton}$ or 675 $\frac{pcb}{lb}$

d_{31} = -60.2 $\frac{pcb}{newton}$ or 268 $\frac{pcb}{lb}$

d_{15} = 440 $\frac{pcb}{newton}$ or 1952 $\frac{pcb}{lb}$

PIEZOELECTRIC VOLTAGE COEFFICIENTS: g_{33} = 38.1x 10^{-3} volt meters/newton

g_{31} =-15.1x 10^{-3} volt meters/newton

g_{15} = 50.3x 10^{-3} volt meters/newton

COUPLING COEFFICIENTS: k_{33} = 0.626

k_{31} = -0.28

k_{15} = 0.701

REMANENT POLARIZATION: P_r = ---- $coul/cm^2$

MATERIAL: PZT-4 MANUFACTURER: Clevite Corp.

DENSITY: $= 7.5 \quad gm/cm^3$

SPECIFIC WEIGHT: $= 0.27 \quad lb/in^3$

ELASTIC MODULI: $Y^E_{33} = 6.6 \times 10^{10} \frac{newtons}{m^2}$ or 0.96×10^7 psi

$Y^E_{11} = 8.2 \times 10^{10} \frac{newtons}{m^2}$ or 1.19×10^7 psi

$Y^E_{55} =$

ONE-DIMENSIONAL WAVE VELOCITY: $c = 2.97 \times 10^5$ cm/sec or 1.17×10^5 in/sec

CURIE TEMPERATURE: °C 328

FREE DIELECTRIC CONSTANTS: $K_3 = 1300$

$K_1 = 1475$

PIEZOELECTRIC CHARGE COEFFICIENTS: $d_{33} = 289 \frac{pcb}{newton}$ or $1240 \frac{pcb}{lb}$

$d_{31} = -123 \frac{pcb}{newton}$ or $-546 \frac{pcb}{lb}$

$d_{15} = 496 \frac{pcb}{newton}$ or $2201 \frac{pcb}{lb}$

PIEZOELECTRIC VOLTAGE COEFFICIENTS: $g_{33} = 26.1 \times 10^{-3}$ volt meters/newton

$g_{31} = -11.1 \times 10^{-3}$ volt meters/newton

$g_{15} = 39.4 \times 10^{-3}$ volt meters/newton

COUPLING COEFFICIENTS: $k_{33} = 0.70$

$k_{31} = 0.334$

$k_{15} = 0.71$

REMANENT POLARIZATION: $P_r =$ ---- $coul/cm^2$

MATERIAL: PZT5A

MANUFACTURER: Clevite Corp.

DENSITY:

$= 7.75 \quad gm/cm^3$

SPECIFIC WEIGHT:

$= 0.28 \quad lb/in^3$

ELASTIC MODULI: $Y^E_{33} =$

$Y^E_{11} =$

$Y^E_{55} =$

ONE-DIMENSIONAL WAVE VELOCITY: $c =$

CURIE TEMPERATURE: °C 365

FREE DIELECTRIC CONSTANTS: $K_3 =$

$K_1 =$

PIEZOELECTRIC CHARGE COEFFICIENTS:

$d_{33} = 374 \quad \frac{pcb}{newton}$ or $1660 \quad \frac{pcb}{lb}$

$d_{31} = -171 \quad \frac{pcb}{newton}$ or $-760 \quad \frac{pcb}{lb}$

$d_{15} = 584 \quad \frac{pcb}{newton}$ or $2598 \quad \frac{pcb}{lb}$

PIEZOELECTRIC VOLTAGE COEFFICIENTS:

$g_{33} = 24.8 \times 10^{-3}$ volt meters/newton

$g_{31} = -11.4 \times 10^{-3}$ volt meters/newton

$g_{15} = 38.2 \times 10^{-3}$ volt meters/newton

COUPLING COEFFICIENTS: $k_{33} = 0.705$

$k_{31} = -0.344$

$k_{15} = 0.685$

REMANENT POLARIZATION: $P_r =$ ---- $coul/cm^2$

MATERIAL: PZT-5H MANUFACTURER: Clevite Corp.

DENSITY. = 7.5 gm/cm^3

SPECIFIC WEIGHT: = 0.27 lb/in^3

ELASTIC MODULI: Y^E_{33} =

Y^E_{11} =

Y^E_{55} =

ONE-DIMENSIONAL WAVE VELOCITY: c =

CURIE TEMPERATURE: °C 193

FREE DIELECTRIC CONSTANTS: K_3 =

K_1 =

PIEZOELECTRIC CHARGE COEFFICIENTS: d_{33} = 593 $\frac{pcb}{newton}$ or 2639 $\frac{pcb}{lb}$

d_{31} = -274 $\frac{pcb}{newton}$ or -1220 $\frac{pcb}{lb}$

d_{15} = 741 $\frac{pcb}{newton}$ or 3299 $\frac{pcb}{lb}$

PIEZOELECTRIC VOLTAGE COEFFICIENTS: g_{33} = 19.7x 10^{-3} volt meters/newton

g_{31} =-9.11x 10^{-3} volt meters/newton

g_{15} = 26.8x 10^{-3} volt meters/newton

COUPLING COEFFICIENTS: k_{33} = 0.752

k_{31} = -0.388

k_{15} = 0.675

REMANENT POLARIZATION: P_r = ---- $coul/cm^2$

SECTION V

COMPUTATIONS UTILIZING BASIC RELATIONSHIPS AND CIRCUITS

EXAMPLES OF COMPUTATIONS USING BASIC RELATIONSHIPS

In the previous two sections of this report, the basic relationships between pertinent quantities were given, as well as values for material properties of several materials. In this section, sample calculations are given to illustrate the use of the equations and material properties, and to give indications of actual numerical values for the various parameters of interes, such as currents and voltages. These sample calculations will be based upon the following two crystals:

1. Quartz disk, 1/2 in. dia. x 0.10 in. thick (identified by "g")
2. HST-41 disk, 1/2 in. dia. x 0.10 in. thick (identified by "h")

a. Crystal capacitance

$$C = \frac{K_o A \varepsilon_{11}^S}{h}$$

q: $$C = \frac{(8.85 \times 10^{-12}) \ \frac{\pi}{4}(\frac{1}{2})^2 \ (0.115)}{0.10}$$

$$C = 2.0 \text{ pfd}$$

h: $$C = \frac{(8.85 \times 10^{-12}) \ \frac{\pi}{4}(\frac{1}{2})^2 \ (45.6)}{0.10}$$

$$C = 795 \text{ pfd}$$

b. Voltage across capacitor for open circuit conditions:

$$V = Q/C$$

q: $V = (10.2 \text{ pcb/lb})/2.0 \text{ pfd}$

$V = 5.1$ volts/lb at applied force (for one-dimensional stress)

h: $V = (1440 \text{ pcb/lb})/795 \text{ pfd}$

$V = 1.82$ volts/lb of applied force (for one-dimensional stress)

c. Short circuit current across faces of a loaded crystal:

$$i_{sc}(t) = \frac{d_{em}\sigma(t)Ac}{h}, \text{ for } t < h/c.$$

q: $$i_{sc} = \frac{(10.2 \text{ pcb/lb})(.196 \text{ in}^2)(216{,}000 \text{ in/sec})}{0.10}$$

$= 4.3\mu$ amp/psi, for $t < .46\mu$ sec (for one-dimensional stress)

h: $$i_{sc} = \frac{(1440 \text{ pcb/lb})(.196 \text{ in}^2)(2.77 \times 10^5 \text{ in/sec})}{0.10}$$

$= 792\mu$ amp/psi, for $t < .36\mu$ sec (for one-dimensional stress)

d. Energy stored in capacitor:

$$E = \frac{Q^2}{2C}$$

q: $E = \frac{(10.2 \text{ pcb/lb})^2}{2 \times 2.0 \text{ pfd}}$

$E = 26.2 \times 10^{-12}$ joules/lb of applied force

h: $E = \frac{(1440 \text{ pcb/lb})^2}{2 \times 795 \text{ pfd}}$

$E = 1.31 \times 10^{-9}$ joules/lb of applied force

Equation (11) will be used to illustrate the current and energy output which would be expected from a piezoelectric generator in an application where the input pulse rise time is long compared to the transit time through the pulse. The case considered will be one for which the input pulse is a ramp type, and the impedance of all elements of the system are matched. Figure 3a shows the pulse and system components, and 3b shows the expected current time pulse. Figure 4 shows the effect of various rise times of input pulse. The charge generated (area under i(t) curve) is the same in each case, but since energy involves current squared, the energy released is increased as the rise time of the pulse is decreased.

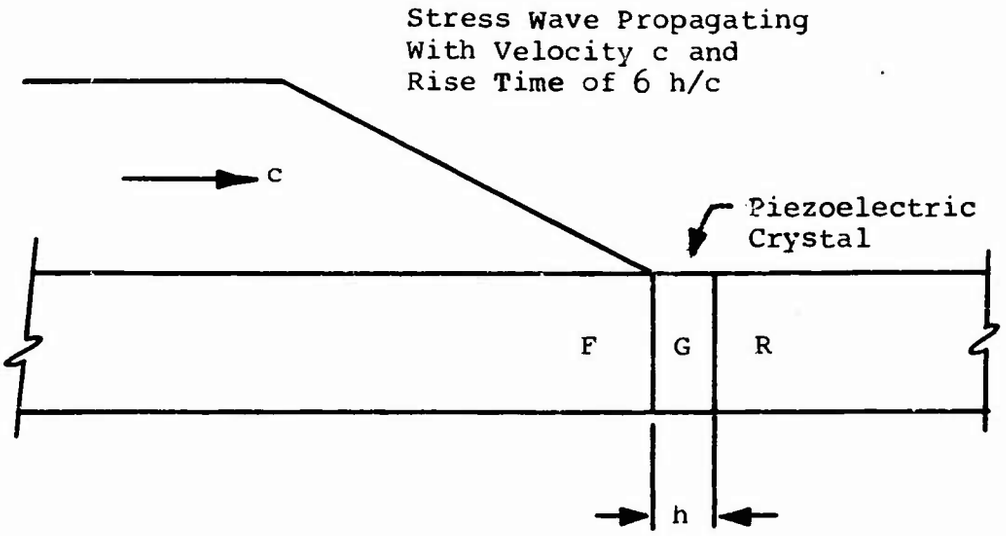

Note: The mechanical impedance of elements F,G, and R are assumed equal for this example.

(a)

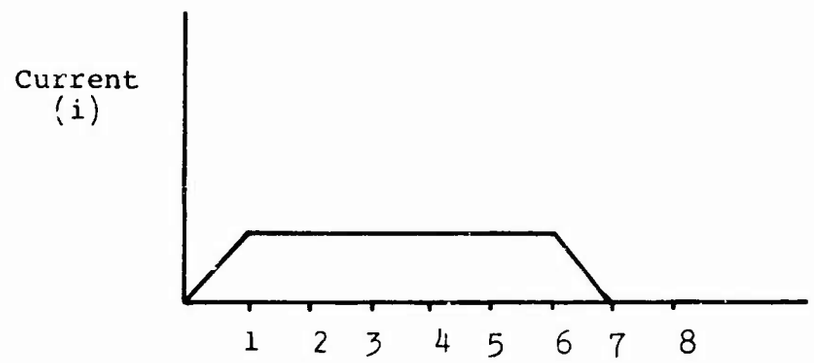

(b)

Figure 3. Example for Finite Rise Time Pulse

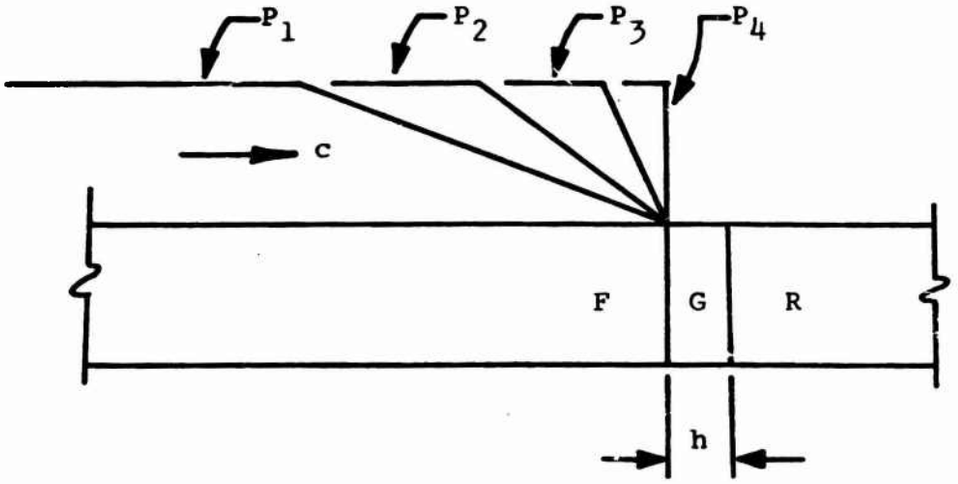

(a)

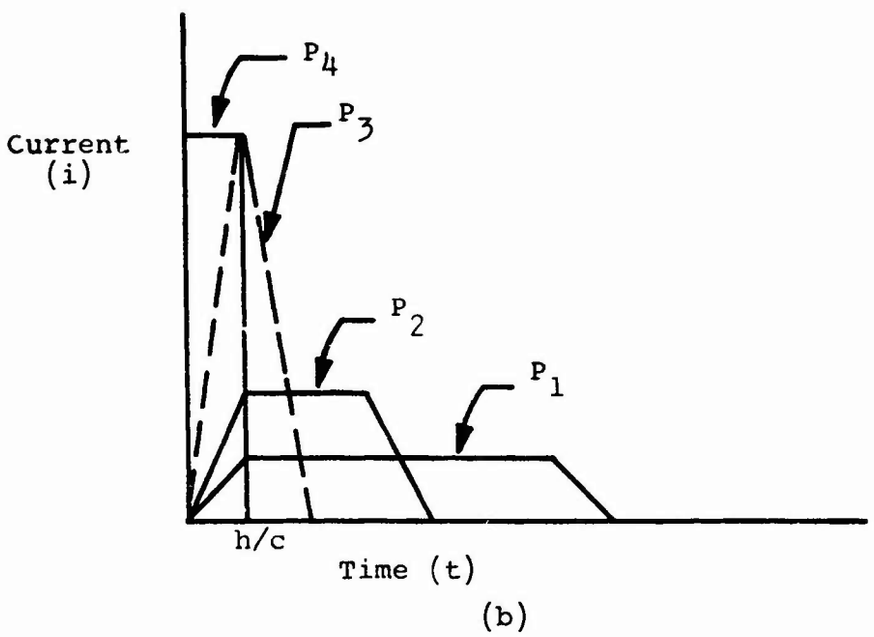

(b)

Figure 4. Effect of Rise Time on Crystal Output

STUDY OF BEHAVIOR OF IDEAL CIRCUIT

Equation (9) gives the differential equation relating the current generated, i_q or i_{sc}, to the current passing through the load resistor in which the energy will be dissipated. For any experiment conducted on a crystal, i_R may be measured, but i_q is the one predicted by theory, Equation (8). This section gives the results of a study made of the effect of the circuit parameter R_L and C_T on i_R for assumed forms of i_q.

Equation (9) wqs programmed for evaluation on a digital computer. This solutions was evaluated for two forms of $i_q(t)$: a ramp function and a haversine pulse. These two functions were selected since they approximate the excitation applied to the crystal for two of the types of tests planned.

The parameters describing these pulses were defined as follows:

τ_R = Rise time for ramp function and pulse duration for haversine.

RC = Time constant of the circuit.

XK = τ_R/RC

Runs were made for values of XK from 10.0 to 10,000 for the ramp function, and 100 to 50,000 for the haversine. It was believed that these ranges would more than amply cover that encountered in the experimental work.

Figure 5 shows examples of the results for each of the inputs. The curves plotted represent those for the parameter values resulting in the greatest deviation in the two currents.

Table I gives the computer output obtained for the runs made for the ramp input. Similar results are given in Table II for the haversine. The one undefined term in these tables is "DFCRP." This is the percent difference between i_q and i_R, based upon the maximum i_q. These tables may be used to estimate the difference in i_q and i_R for experimental data involving similar inputs. A study of these tables shows that, in general, the difference between the two quantities is small and that significant difference occur only from τ_R/RC less than 500. This condition could be easily satisfied for the test conditions utilized in this work.

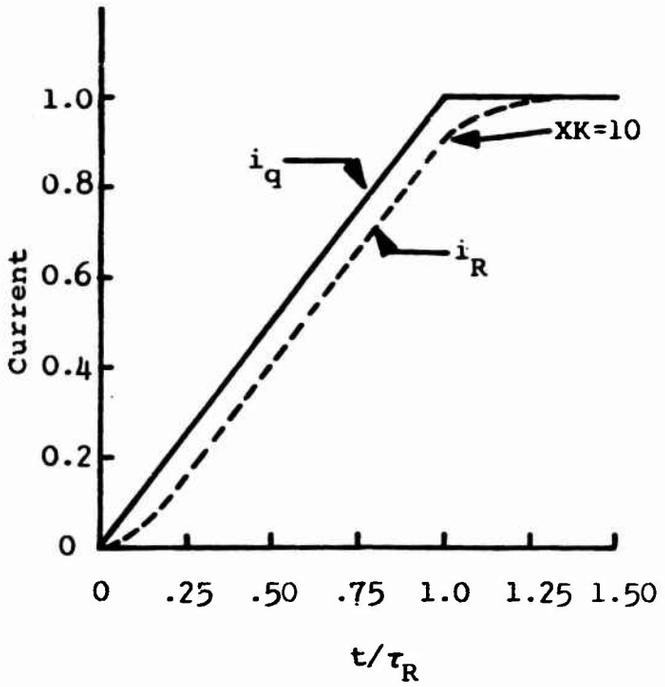

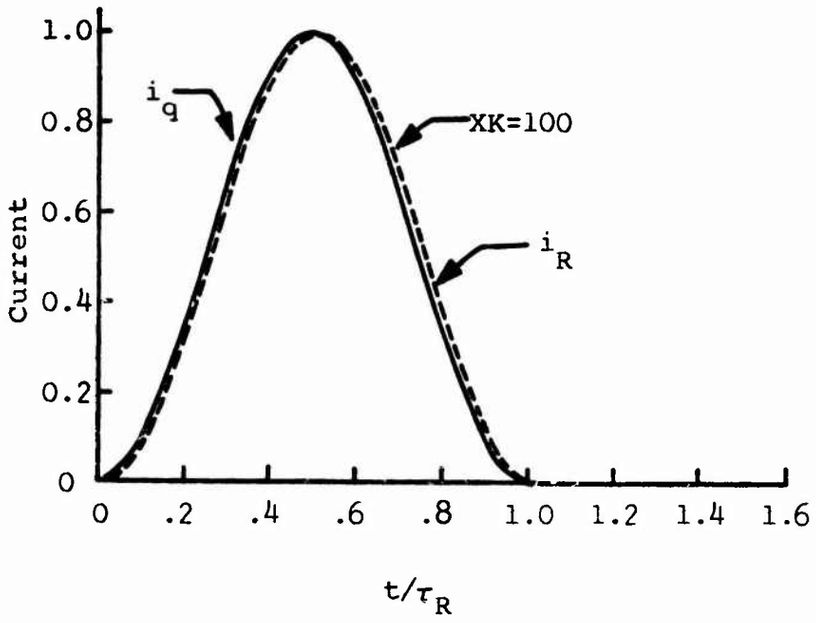

Figure 5. Example of Results from Study of Ideal Circuit

TABLE 1. Results for Ramp Function Input to Ideal Circuit

VALUE OF RC = 4.0000E-08
VALUE OF XK = 10.0010 RISE TIME = 4.0000E-07

TIME INCREMENT	CURRENTIQ	CURRENTIR	DFCRP
2.0000000E-08	5.0000000E-02	1.0653066E-02	3.9346934E+00
4.0000000E-08	1.0000000E-01	3.6787944E-02	6.3212056E+00
6.0000000E-08	1.5000000E-01	7.2313016E-02	7.7686984E+00
8.0000000E-08	2.0000000E-01	1.1353353E-01	8.8646472E+00
1.0000000E-07	2.5000000E-01	1.5820850E-01	9.1791500E+00
1.2000000E-07	3.0000000E-01	2.0497871E-01	9.5021293E+00
1.4000000E-07	3.5000000E-01	2.5301974E-01	9.6980262E+00
1.6000000E-07	4.0000000E-01	3.0183156E-01	9.8168436E+00
1.8000000E-07	4.5000000E-01	3.5111090E-01	9.8889100E+00
2.0000000E-07	5.0000000E-01	4.0067379E-01	9.9326205E+00
2.2000000E-07	5.5000000E-01	4.5040868E-01	9.9591323E+00
2.4000000E-07	6.0000000E-01	5.0024788E-01	9.9752125E+00
2.6000000E-07	6.5000000E-01	5.5015034E-01	9.9849656E+00
2.8000000E-07	7.0000000E-01	6.0009119E-01	9.9908812E+00
3.0000000E-07	7.5000000E-01	6.5005531E-01	9.9944692E+00
3.2000000E-07	8.0000000E-01	7.0003355E-01	9.9966454E+00
3.4000000E-07	8.5000000E-01	7.5002035E-01	9.9979653E+00
3.6000000E-07	9.0000000E-01	8.0001234E-01	9.9987659E+00
3.8000000E-07	9.5000000E-01	8.5000749E-01	9.9992515E+00
4.0000000E-07	1.0000000E+00	9.0000454E-01	9.9995460E+00

VALUE OF RC = 8.0000E-09
VALUE OF XK = 50.0010 RISE TIME = 4.0000E-07

TIME INCREMENT	CURRENTIQ	CURRENTIR	DFCRP
2.0000000E-08	5.0000000E-02	3.1641700E-02	1.8358300E+00
4.0000000E-08	1.0000000E-01	8.0134759E-02	1.9865241E+00
6.0000000E-08	1.5000000E-01	1.3001106E-01	1.9988938E+00
8.0000000E-08	2.0000000E-01	1.8000091E-01	1.9999092E+00
1.0000000E-07	2.5000000E-01	2.3000007E-01	1.9999925E+00
1.2000000E-07	3.0000000E-01	2.8000001E-01	1.9999994E+00
1.4000000E-07	3.5000000E-01	3.3000000E-01	1.9999999E+00
1.6000000E-07	4.0000000E-01	3.8000000E-01	2.0000000E+00
1.8000000E-07	4.5000000E-01	4.3000000E-01	2.0000000E+00
2.0000000E-07	5.0000000E-01	4.8000000E-01	2.0000000E+00
2.2000000E-07	5.5000000E-01	5.3000000E-01	2.0000000E+00
2.4000000E-07	6.0000000E-01	5.8000000E-01	2.0000000E+00
2.6000000E-07	6.5000000E-01	6.3000000E-01	2.0000000E+00
2.8000000E-07	7.0000000E-01	6.8000000E-01	2.0000000E+00
3.0000000E-07	7.5000000E-01	7.3000000E-01	2.0000000E+00
3.2000000E-07	8.0000000E-01	7.8000000E-01	2.0000000E+00
3.4000000E-07	8.5000000E-01	8.3000000E-01	2.0000000E+00
3.6000000E-07	9.0000000E-01	8.8000000E-01	2.0000000E+00
3.8000000E-07	9.5000000E-01	9.3000000E-01	2.0000000E+00
4.0000000E-07	1.0000000E+00	9.8000000E-01	2.0000000E+00

TABLE I (continued)

VALUE OF RC = 4.0000E-09
VALUE OF XK = 100.0000 RISE TIME = 4.0000E-07

TIME INCREMENT	CURRENTIQ	CURRENTIR	DFCRP
2.0000000E-08	5.0000000E-02	4.0067379E-02	9.9326205E-01
4.0000000E-08	1.0000000E-01	9.0000454E-02	9.9995460E-01
6.0000000E-08	1.5000000E-01	1.4000000E-01	9.9999969E-01
8.0000000E-08	2.0000000E-01	1.9000000E-01	1.0000000E+00
1.0000000E-07	2.5000000E-01	2.4000000E-01	1.0000000E+00
1.2000000E-07	3.0000000E-01	2.9000000E-01	1.0000000E+00
1.4000000E-07	3.5000000E-01	3.4000000E-01	1.0000000E+00
1.6000000E-07	4.0000000E-01	3.9000000E-01	1.0000000E+00
1.8000000E-07	4.5000000E-01	4.4000000E-01	1.0000000E+00
2.0000000E-07	5.0000000E-01	4.9000000E-01	1.0000000E+00
2.2000000E-07	5.5000000E-01	5.4000000E-01	1.0000000E+00
2.4000000E-07	6.0000000E-01	5.9000000E-01	1.0000000E+00
2.6000000E-07	6.5000000E-01	6.4000000E-01	1.0000000E+00
2.8000000E-07	7.0000000E-01	6.9000000E-01	1.0000000E+00
3.0000000E-07	7.5000000E-01	7.4000000E-01	1.0000000E+00
3.2000000E-07	8.0000000E-01	7.9000000E-01	1.0000000E+00
3.4000000E-07	8.5000000E-01	8.4000000E-01	1.0000000E+00
3.6000000E-07	9.0000000E-01	8.9000000E-01	1.0000000E+00
3.8000000E-07	9.5000000E-01	9.4000000E-01	1.0000000E+00
4.0000000E-07	1.0000000E+00	9.9000000E-01	1.0000000E+00

VALUE OF RC = 8.0000E-10
VALUE OF XK = 500.0000 RISE TIME = 4.0000E-07

TIME INCREMENT	CURRENTIQ	CURRENTIR	DFCRP
2.0000000E-08	5.0000000E-02	4.8000000E-02	2.0000000E-01
4.0000000E-08	1.0000000E-01	9.8000000E-02	2.0000000E-01
6.0000000E-08	1.5000000E-01	1.4800000E-01	2.0000000E-01
8.0000000E-08	2.0000000E-01	1.9800000E-01	2.0000000E-01
1.0000000E-07	2.5000000E-01	2.4800000E-01	2.0000000E-01
1.2000000E-07	3.0000000E-01	2.9800000E-01	2.0000000E-01
1.4000000E-07	3.5000000E-01	3.4800000E-01	2.0000000E-01
1.6000000E-07	4.0000000E-01	3.9800000E-01	2.0000000E-01
1.8000000E-07	4.5000000E-01	4.4800000E-01	2.0000000E-01
2.0000000E-07	5.0000000E-01	4.9800000E-01	2.0000000E-01
2.2000000E-07	5.5000000E-01	5.4800000E-01	2.0000000E-01
2.4000000E-07	6.0000000E-01	5.9800000E-01	2.0000000E-01
2.6000000E-07	6.5000000E-01	6.4800000E-01	2.0000000E-01
2.8000000E-07	7.0000000E-01	6.9800000E-01	2.0000000E-01
3.0000000E-07	7.5000000E-01	7.4800000E-01	2.0000000E-01
3.2000000E-07	8.0000000E-01	7.9800000E-01	2.0000000E-01
3.4000000E-07	8.5000000E-01	8.4800000E-01	2.0000000E-01
3.6000000E-07	9.0000000E-01	8.9800000E-01	2.0000000E-01
3.8000000E-07	9.5000000E-01	9.4800000E-01	2.0000000E-01
4.0000000E-07	1.0000000E+00	9.9800000E-01	2.0000000E-01

TABLE I (continued)

VALUE OF RC = 4.0000E-10

VALUE OF XK = 1000.0000 RISE TIME = 4.0000E-07

TIME INCREMENT	CURRENTIQ	CURRENTIR	DFCRP
2.0000000E-08	5.0000000E-02	4.9000000E-02	1.0000000E-01
4.0000000E-08	1.0000000E-01	9.9000000E-02	1.0000000E-01
6.0000000E-08	1.5000000E-01	1.4900000E-01	1.0000000E-01
8.0000000E-08	2.0000000E-01	1.9900000E-01	1.0000000E-01
1.0000000E-07	2.5000000E-01	2.4900000E-01	1.0000000E-01
1.2000000E-07	3.0000000E-01	2.9900000E-01	1.0000000E-01
1.4000000E-07	3.5000000E-01	3.4900000E-01	1.0000000E-01
1.6000000E-07	4.0000000E-01	3.9900000E-01	1.0000000E-01
1.8000000E-07	4.5000000E-01	4.4900000E-01	1.0000000E-01
2.0000000E-07	5.0000000E-01	4.9900000E-01	1.0000000E-01
2.2000000E-07	5.5000000E-01	5.4900000E-01	1.0000000E-01
2.4000000E-07	6.0000000E-01	5.9900000E-01	1.0000000E-01
2.6000000E-07	6.5000000E-01	6.4900000E-01	1.0000000E-01
2.8000000E-07	7.0000000E-01	6.9900000E-01	1.0000000E-01
3.0000000E-07	7.5000000E-01	7.4900000E-01	1.0000000E-01
3.2000000E-07	8.0000000E-01	7.9900000E-01	1.0000000E-01
3.4000000E-07	8.5000000E-01	8.4900000E-01	1.0000000E-01
3.6000000E-07	9.0000000E-01	8.9900000E-01	1.0000000E-01
3.8000000E-07	9.5000000E-01	9.4900000E-01	1.0000000E-01
4.0000000E-07	1.0000000E+00	9.9900000E-01	1.0000000E-01

VALUE OF RC = 8.0000E-11

VALUE OF XK = 5000.0000 RISE TIME = 4.0000E-07

TIME INCREMENT	CURRENTIQ	CURRENTIR	DFCRP
2.0000000E-08	5.0000000E-02	4.9800000E-02	2.0000000E-02
4.0000000E-08	1.0000000E-01	9.9800000E-02	2.0000000E-02
6.0000000E-08	1.5000000E-01	1.4980000E-01	2.0000000E-02
8.0000000E-08	2.0000000E-01	1.9980000E-01	2.0000000E-02
1.0000000E-07	2.5000000E-01	2.4980000E-01	2.0000000E-02
1.2000000E-07	3.0000000E-01	2.9980000E-01	2.0000000E-02
1.4000000E-07	3.5000000E-01	3.4980000E-01	2.0000000E-02
1.6000000E-07	4.0000000E-01	3.9980000E-01	2.0000000E-02
1.8000000E-07	4.5000000E-01	4.4980000E-01	2.0000000E-02
2.0000000E-07	5.0000000E-01	4.9980000E-01	2.0000000E-02
2.2000000E-07	5.5000000E-01	5.4980000E-01	2.0000000E-02
2.4000000E-07	6.0000000E-01	5.9980000E-01	2.0000000E-02
2.6000000E-07	6.5000000E-01	6.4980000E-01	2.0000000E-02
2.8000000E-07	7.0000000E-01	6.9980000E-01	2.0000000E-02
3.0000000E-07	7.5000000E-01	7.4980000E-01	2.0000000E-02
3.2000000E-07	8.0000000E-01	7.9980000E-01	2.0000000E-02
3.4000000E-07	8.5000000E-01	8.4980000E-01	2.0000000E-02
3.6000000E-07	9.0000000E-01	8.9980000E-01	2.0000000E-02
3.8000000E-07	9.5000000E-01	9.4980000E-01	2.0000000E-02
4.0000000E-07	1.0000000E+00	9.9980000E-01	2.0000000E-02

TABLE I (continued)

VALUE OF RC = 4.0000E-11

VALUE OF XK = 10000.0000 RISE TIME = 4.0000E-07

TIME INCREMENT	CURRENTIQ	CURRENTIR	DFCRP
2.0000000E-08	5.0000000E-02	4.9900000E-02	1.0000000E-02
4.0000000E-08	1.0000000E-01	9.9900000E-02	1.0000000E-02
6.0000000E-08	1.5000000E-01	1.4990000E-01	1.0000000E-02
8.0000000E-08	2.0000000E-01	1.9990000E-01	1.0000000E-02
1.0000000E-07	2.5000000E-01	2.4990000E-01	1.0000000E-02
1.2000000E-07	3.0000000E-01	2.9990000E-01	1.0000000E-02
1.4000000E-07	3.5000000E-01	3.4990000E-01	1.0000000E-02
1.6000000E-07	4.0000000E-01	3.9990000E-01	1.0000000E-02
1.8000000E-07	4.5000000E-01	4.4990000E-01	1.0000000E-02
2.0000000E-07	5.0000000E-01	4.9990000E-01	1.0000000E-02
2.2000000E-07	5.5000000E-01	5.4990000E-01	1.0000000E-02
2.4000000E-07	6.0000000E-01	5.9990000E-01	1.0000000E-02
2.6000000E-07	6.5000000E-01	6.4990000E-01	1.0000000E-02
2.8000000E-07	7.0000000E-01	6.9990000E-01	1.0000000E-02
3.0000000E-07	7.5000000E-01	7.4990000E-01	1.0000000E-02
3.2000000E-07	8.0000000E-01	7.9990000E-01	1.0000000E-02
3.4000000E-07	8.5000000E-01	8.4990000E-01	1.0000000E-02
3.6000000E-07	9.0000000E-01	8.9990000E-01	1.0000000E-02
3.8000000E-07	9.5000000E-01	9.4990000E-01	1.0000000E-02
4.0000000E-07	1.0000000E+00	9.9990000E-01	1.0000000E-02

TABLE II. Results for Haversine Input to Ideal Circuit

VALUE OF RC = 1.0000E-07
VALUE OF XK = 100.0000 RISE TIME = 1.0000E-05

TIME INCREMENT	CURRENTIQ	CURRENTIR	DFCRP
5.0000000E-07	2.4491283E-02	1.5671869E-02	7.8194138E-01
1.0000000E-06	9.5565841E-02	7.8750436E-02	1.6815405E+00
1.5000000E-06	2.0626084E-01	1.9208368E-01	2.4177161E+00
2.0000000E-06	3.4573204E-01	3.1656156E-01	2.9170487E+00
2.5000000E-06	5.0031612E-01	4.5901000E-01	3.1306123E+00
3.0000000E-06	6.5486923E-01	6.2449438E-01	3.0374850E+00
3.5000000E-06	7.9425056E-01	7.5778266E-01	2.6667902E+00
4.0000000E-06	9.0480559E-01	8.8483757E-01	1.9968021E+00
4.5000000E-06	9.7570379E-01	9.5419182E-01	1.1511971E+00
5.0000000E-06	9.9999960E-01	9.9807145E-01	1.9281494E-01
5.5000000E-06	9.7531289E-01	9.8315745E-01	-7.8445640E-01
6.0000000E-06	9.0406208E-01	9.2091087E-01	-1.6848784E+00
6.5000000E-06	7.9322728E-01	8.1742969E-01	-2.4202410E+00
7.0000000E-06	6.5366643E-01	6.8285148E-01	-2.9185044E+00
7.5000000E-06	4.9905163E-01	5.3036019E-01	-3.1308561E+00
8.0000000E-06	3.4452974E-01	3.7489467E-01	-3.0364931E+00
8.5000000E-06	2.0523851E-01	2.3168511E-01	-2.6446597E+00
9.0000000E-06	9.4823628E-02	1.1476105E-01	-1.9937418E+00
9.5000000E-06	2.4101903E-02	3.5576971E-02	-1.1475067E+00
1.0000000E-05	1.5989323E-06	1.3901590E-03	-1.8885600E-01

VALUE OF RC = 2.0000E-08
VALUE OF XK = 500.0000 RISE TIME = 1.0000E-05

TIME INCREMENT	CURRENTIQ	CURRENTIR	DFCRP
5.0000000E-07	2.4491283E-02	2.2623580E-02	1.8677035E-01
1.0000000E-06	9.5565841E-02	9.1934395E-02	3.6314451E-01
1.5000000E-06	2.0626084E-01	2.0122141E-01	5.0394317E-01
2.0000000E-06	3.4573204E-01	3.3977831E-01	5.9537297E-01
2.5000000E-06	5.0031612E-01	4.9403135E-01	6.2847697E-01
3.0000000E-06	6.5486923E-01	6.4886911E-01	6.0001215E-01
3.5000000E-06	7.9425056E-01	7.8912289E-01	5.1276706E-01
4.0000000E-06	9.0480559E-01	9.0105270E-01	3.7528868E-01
4.5000000E-06	9.7570379E-01	9.7369334E-01	2.0104509E-01
5.0000000E-06	9.9999960E-01	9.9992854E-01	7.1060898E-03
5.5000000E-06	9.7531289E-01	9.7718818E-01	-1.8752906E-01
6.0000000E-06	9.0406208E-01	9.0770001E-01	-3.6379290E-01
6.5000000E-06	7.9322728E-01	7.9827146E-01	-5.0441771E-01
7.0000000E-06	6.5366643E-01	6.5962271E-01	-5.9562718E-01
7.5000000E-06	4.9905163E-01	5.0533649E-01	-6.2848596E-01
8.0000000E-06	3.4452974E-01	3.5052749E-01	-5.9977502E-01
8.5000000E-06	2.0523851E-01	2.1036158E-01	-5.1230705E-01
9.0000000E-06	9.4823628E-02	9.8570136E-02	-3.7465085E-01
9.5000000E-06	2.4101903E-02	2.5104823E-02	-2.0029192E-01
1.0000000E-05	1.5989323E-06	6.4712694E-05	-6.3113761E-03

TABLE II (continued)

VALUE OF RC = 1.0000E-08

VALUE OF XK = 1000.0000 RISE TIME = 1.0000E-05

TIME INCREMENT	CURRENTIQ	CURRENTIR	DFCRP
5.0000000E-07	2.4491283E-02	2.3538534E-02	9.5274913E-02
1.0000000E-06	9.5565841E-02	9.3733924E-02	1.8319164E-01
1.5000000E-06	2.0626084E-01	2.0372922E-01	2.5316197E-01
2.0000000E-06	3.4573204E-01	3.4274873E-01	2.9833126E-01
2.5000000E-06	5.0031612E-01	4.9717338E-01	3.1427448E-01
3.0000000E-06	6.5486923E-01	6.5187494E-01	2.9942977E-01
3.5000000E-06	7.9425056E-01	7.9169804E-01	2.5525137E-01
4.0000000E-06	9.0480559E-01	9.0294492E-01	1.8606725E-01
4.5000000E-06	9.7570379E-01	9.7471724E-01	9.8655017E-02
5.0000000E-06	9.9999960E-01	9.9998382E-01	1.5780355E-03
5.5000000E-06	9.7531289E-01	9.7626942E-01	-9.5653539E-02
6.0000000E-06	9.0406208E-01	9.0589723E-01	-1.8351440E-01
6.5000000E-06	7.9322728E-01	7.9576126E-01	-2.5339725E-01
7.0000000E-06	6.5366643E-01	6.5665100E-01	-2.9845601E-01
7.5000000E-06	4.9905163E-01	5.0219440E-01	-3.1427648E-01
8.0000000E-06	3.4452974E-01	3.4752283E-01	-2.9930881E-01
8.5000000E-06	2.0523851E-01	2.0778870E-01	-2.5501932E-01
9.0000000E-06	9.4823628E-02	9.6681026E-02	-1.8574683E-01
9.5000000E-06	2.4101903E-02	2.5084680E-02	-9.8277623E-02
1.0000000E-05	1.5989323E-06	1.3405295E-05	-1.1806363E-03

VALUE OF RC = 2.0000E-09

VALUE OF XK = 5000.0000 RISE TIME = 1.0000E-05

TIME INCREMENT	CURRENTIQ	CURRENTIR	DFCRP
5.0000000E-07	2.4491283E-02	2.4297720E-02	1.9356304E-02
1.0000000E-06	9.5565841E-02	9.5196887E-02	3.6895385E-02
1.5000000E-06	2.0626084E-01	2.0575264E-01	5.0820006E-02
2.0000000E-06	3.4573204E-01	3.4513438E-01	5.9766037E-02
2.5000000E-06	5.0031612E-01	4.9968755E-01	6.2857081E-02
3.0000000E-06	6.5486923E-01	6.5427133E-01	5.9790322E-02
3.5000000E-06	7.9425056E-01	7.9374190E-01	5.0866197E-02
4.0000000E-06	9.0480559E-01	9.0443600E-01	3.6958958E-02
4.5000000E-06	9.7570379E-01	9.7550948E-01	1.9431030E-02
5.0000000E-06	9.9999960E-01	9.9999960E-01	-4.6181547E-07
5.5000000E-06	9.7531289E-01	9.7550721E-01	-1.9431908E-02
6.0000000E-06	9.0406208E-01	9.0443168E-01	-3.6959705E-02
6.5000000E-06	7.9322728E-01	7.9373595E-01	-5.0866740E-02
7.0000000E-06	6.5366643E-01	6.5426434E-01	-5.9790607E-02
7.5000000E-06	4.9905163E-01	4.9968020E-01	-6.2857080E-02
8.0000000E-06	3.4452974E-01	3.4512740E-01	-5.9765751E-02
8.5000000E-06	2.0523851E-01	2.0574670E-01	-5.0819462E-02
9.0000000E-06	9.4823628E-02	9.5192574E-02	-3.6894638E-02
9.5000000E-06	2.4101903E-02	2.4295458E-02	-1.9355425E-02
1.0000000E-05	1.5989323E-06	7.9949312E-07	7.9943914E-05

TABLE II (continued)

VALUE OF RC = 1.0000E-09

VALUE OF XK = 10000.0000 RISE TIME = 1.0000E-05

TIME INCREMENT	CURRENTIO	CURRENTIR	DFCRP
5.0000000E-07	2.4491283E-02	2.4394314E-02	9.6969509E-03
1.0000000E-06	9.5565841E-02	9.5381204E-02	1.8463694E-02
1.5000000E-06	2.0626084E-01	2.0600663E-01	2.5421639E-02
2.0000000E-06	3.4573204E-01	3.4543315E-01	2.9889149E-02
2.5000000E-06	5.0031612E-01	5.0000184E-01	3.1428565E-02
3.0000000E-06	6.5486923E-01	6.5457034E-01	2.9889078E-02
3.5000000E-06	7.9425056E-01	7.9399634E-01	2.5421503E-02
4.0000000E-06	9.0480559E-01	9.0462095E-01	1.8463507E-02
4.5000000E-06	9.7570379E-01	9.7560682E-01	9.6967313E-03
5.0000000E-06	9.9999960E-01	9.9999840E-01	-1.9985987E-05
5.5000000E-06	9.7531289E-01	9.7541023E-01	-9.7347453E-03
6.0000000E-06	9.0406208E-01	9.0424704E-01	-1.8495839E-02
6.5000000E-06	7.9322728E-01	7.9348173E-01	-2.5444985E-02
7.0000000E-06	6.5366643E-01	6.5396545E-01	-2.9901411E-02
7.5000000E-06	4.9905163E-01	4.9936592E-01	-3.1428540E-02
8.0000000E-06	3.4452974E-01	3.4482851E-01	-2.9876768E-02
8.5000000E-06	2.0523851E-01	2.0549249E-01	-2.5398115E-02
9.0000000E-06	9.4823628E-02	9.5007941E-02	-1.8431332E-02
9.5000000E-06	2.4101903E-02	2.4198493E-02	-9.6589213E-03
1.0000000E-05	1.5989323E-06	1.0016619E-06	5.9727035E-05

VALUE OF RC = 2.0000E-10

VALUE OF XK = 50000.0000 RISE TIME = 1.0000E-05

TIME INCREMENT	CURRENTIO	CURRENTIR	DFCRP
5.0000000E-07	2.4491283E-02	2.4471859E-02	1.9423969E-03
1.0000000E-06	9.5565841E-02	9.5528888E-02	3.6952969E-03
1.5000000E-06	2.0626084E-01	2.0620998E-01	5.0861866E-03
2.0000000E-06	3.4573204E-01	3.4567225E-01	5.9788073E-03
2.5000000E-06	5.0031612E-01	5.0025327E-01	6.2857134E-03
3.0000000E-06	6.5486923E-01	6.5480946E-01	5.9768388E-03
3.5000000E-06	7.9425056E-01	7.9419973E-01	5.0824424E-03
4.0000000E-06	9.0480559E-01	9.0476869E-01	3.6901438E-03
4.5000000E-06	9.7570379E-01	9.7568442E-01	1.9363398E-03
5.0000000E-06	9.9999960E-01	9.9999967E-01	-7.1580128E-06
5.5000000E-06	9.7531289E-01	9.7533239E-01	-1.9499546E-03
6.0000000E-06	9.0406208E-01	9.0409910E-01	-3.7017236E-03
6.5000000E-06	7.9322728E-01	7.9327819E-01	-5.0908527E-03
7.0000000E-06	6.5366643E-01	6.5372625E-01	-5.9812558E-03
7.5000000E-06	4.9905163E-01	4.9911449E-01	-6.2857044E-03
8.0000000E-06	3.4452974E-01	3.4458948E-01	-5.9743731E-03
8.5000000E-06	2.0523851E-01	2.0528929E-01	-5.0777616E-03
9.0000000E-06	9.4823628E-02	9.4860465E-02	-3.6837064E-03
9.5000000E-06	2.4101903E-02	2.4121191E-02	-1.9287765E-03
1.0000000E-05	1.5989323E-06	1.4478701E-06	1.5106218E-05

SECTION VI

SUMMARY OF EXPERIMENTAL WORK ON PROJECT

The work done on the crystal phase of the contract has included both analytical and experimental studies involving both static and dynamic tests. This section of this report describes the work done, and gives data, results, and conclusions where applicable.

STATIC TESTS

Static load tests were conducted on several different materials in order to measure the piezoelectric charge coefficient, d_{33}. Information on these tests has been summarized in earlier quarterly progress reports, and this will be repeated where necessary and supplemented.

The loads were applied to the crystals using two different machines. Loads less than 5000 lb. were applied in a Dillon tensile testing machine (using a compression cage), and loads greater than this were applied with a Reihle universal testing machine. Figure 6 shows the hardware and method used to apply loads to the crystals.

Recording of the data during loading was done with an X-Y recorder for convenience. Since the piezoelectric charge coefficient has dimensions of charge per unit of force, it was necessary to develop measuring techniques and circuitry to record these quantities.

In the low force ranges, measurement of force was accomplished with a Kistler Corporation load cell and charge amplifier. In the higher force ranges, measurement was accomplished with a special load cell designed and constructed at The University of New Mexico (UNM). Figure 7 describes this transducer, and Figure 8 gives the calibration data and curves for it. In obtaining this calibration curve, the gages on the transducer were connected in the customary bridge circuit. The bridge current was adjusted to give the output as indicated by the specified calibrated resistor and the corresponding deflections.

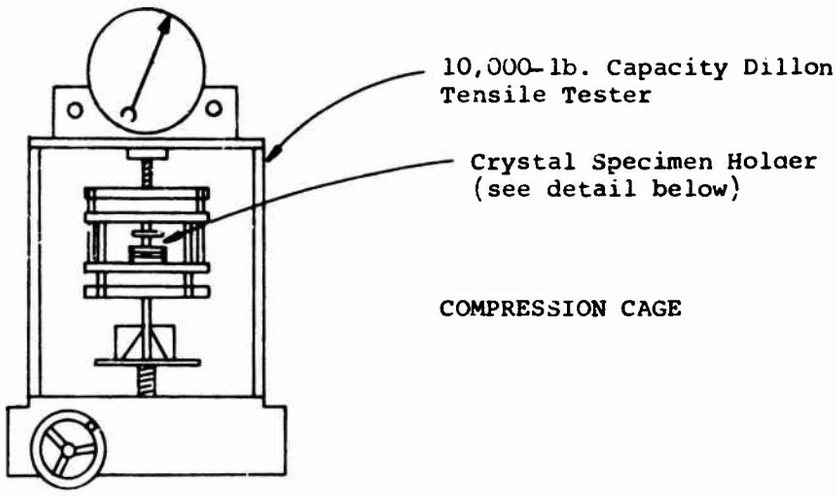

CROSS SECTION DETAIL OF SPECIMEN HOLDER

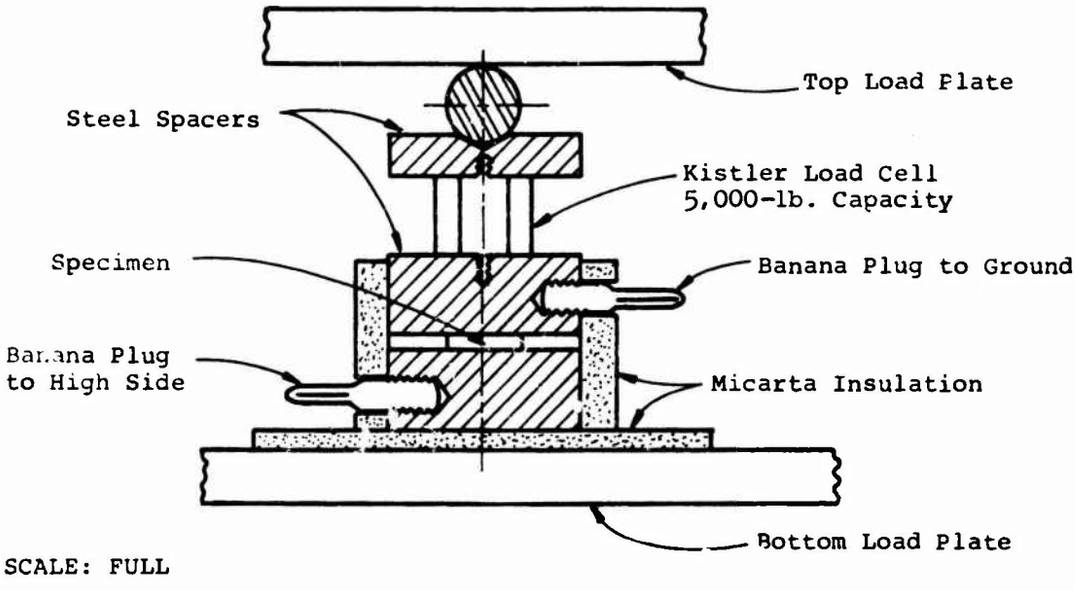

SCALE: FULL

Figure 6. Hardware for Static Tests on Ferroelectric Crystals

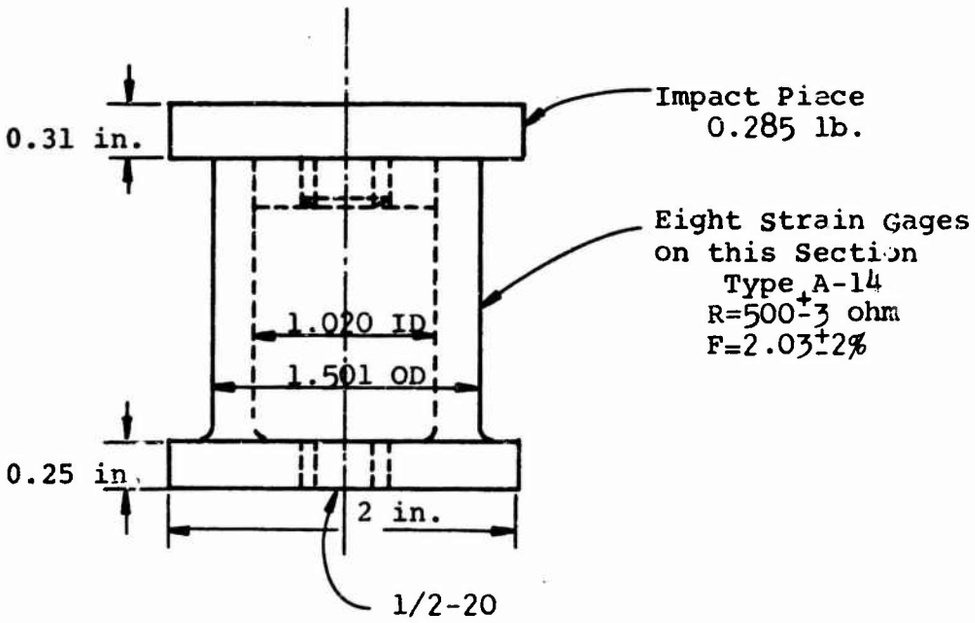

MATERIAL: MILD STEEL

MODULUS=29×10^6 psi

SPRING CONSTANT=22×10^6 lb/in

NATURAL FREQUENCY=20,500 Hz

Figure 7. High Range Force Transducer

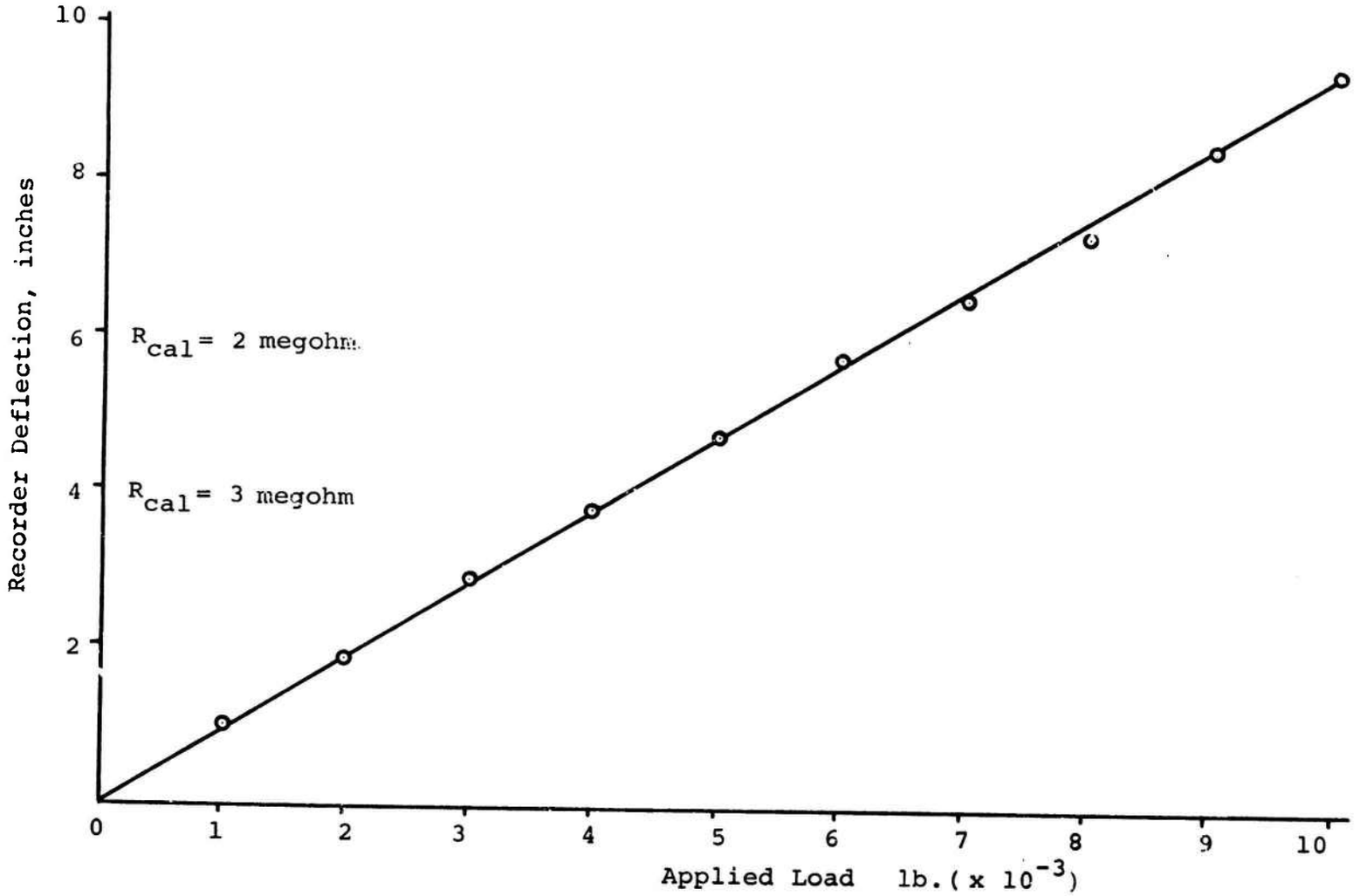

Figure 8. Calibration Plot - Strain Gage Force Transducer

Figure 9 gives a general description of the recording technique for these tests. The circuitry for recording the charge developed is shown here. The series capacitor, C_c, charged with an appropriate voltage from the power supply was used to calibrate the circuit. The shunt capacitor, C_s, was used to load the circuit in order that the cathode follower would not be overdriven, and as an adjustment on the signal into the X-Y recorder to have adequate indicator deflection over a wide range of charge.

Figures 10, 11, and 12 give the results of the calibration tests on this circuitry. Three curves are given to cover different ranges of charge. The curves on Figure 12 illustrate two points: 1) Repeatability of the calibration curve after a time lapse of several days, and 2) the fact that small deviation in C_c has a negligible effect on the calibration curve as long as $C_s >>> C_c$.

The test equipment was used initially with a quartz crystal. The properties of quartz are well known, and the results of this test were used as a check on the measuring system. The 1/2-inch diameter quartz disc was loaded to 4300 lb. and unloaded. The charge-force relation was plotted on the X-Y recorder. The results showed a linear relationship with essentially no hysteresis. The slope of the curve was computed to be 1.93 pcb/N, which compares quite favorably with the d_{11} constant for quartz shown on page 4. It was concluded that the test equipment was adequate for making the desired measurements, and two samples each of HST-41, PZT-4 and PST-5 were tested.

One series of tests on HST-41 were conducted primarily on one sample. Table III describes these tests and gives experimental values for d_{33}. Runs 1 through 4 indicate that the d_{33} constant under low stress values is repeatable, but an upward shift is indicated even for these low values of stress. A typical curve from one of these tests is shown in Figure 13. This curve shows a small hysteresis loop and some nonlinearity during the loading phase of the curve.

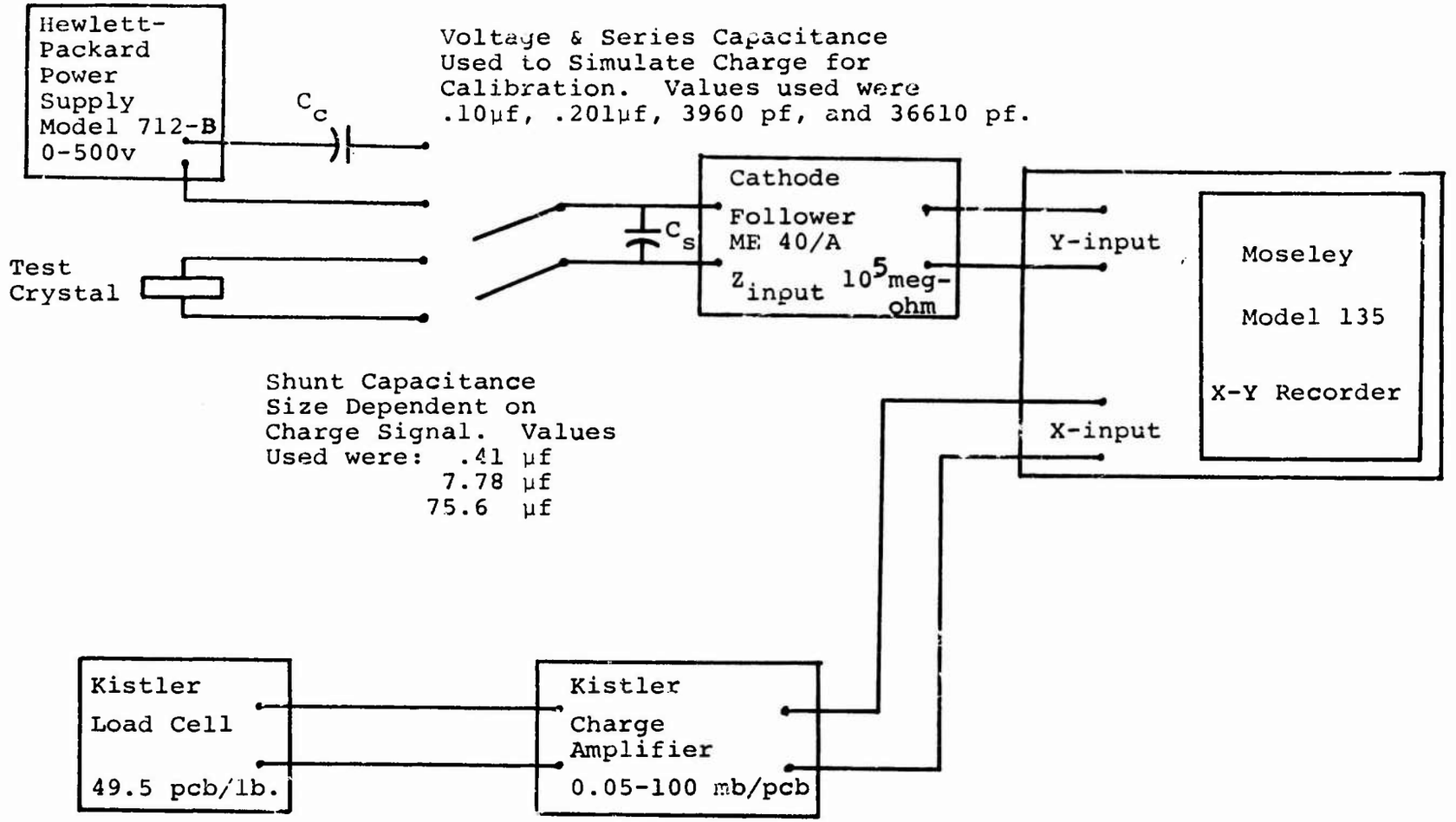

Figure 9. Circuitry for Static Tests on Ferroelectric Crystals

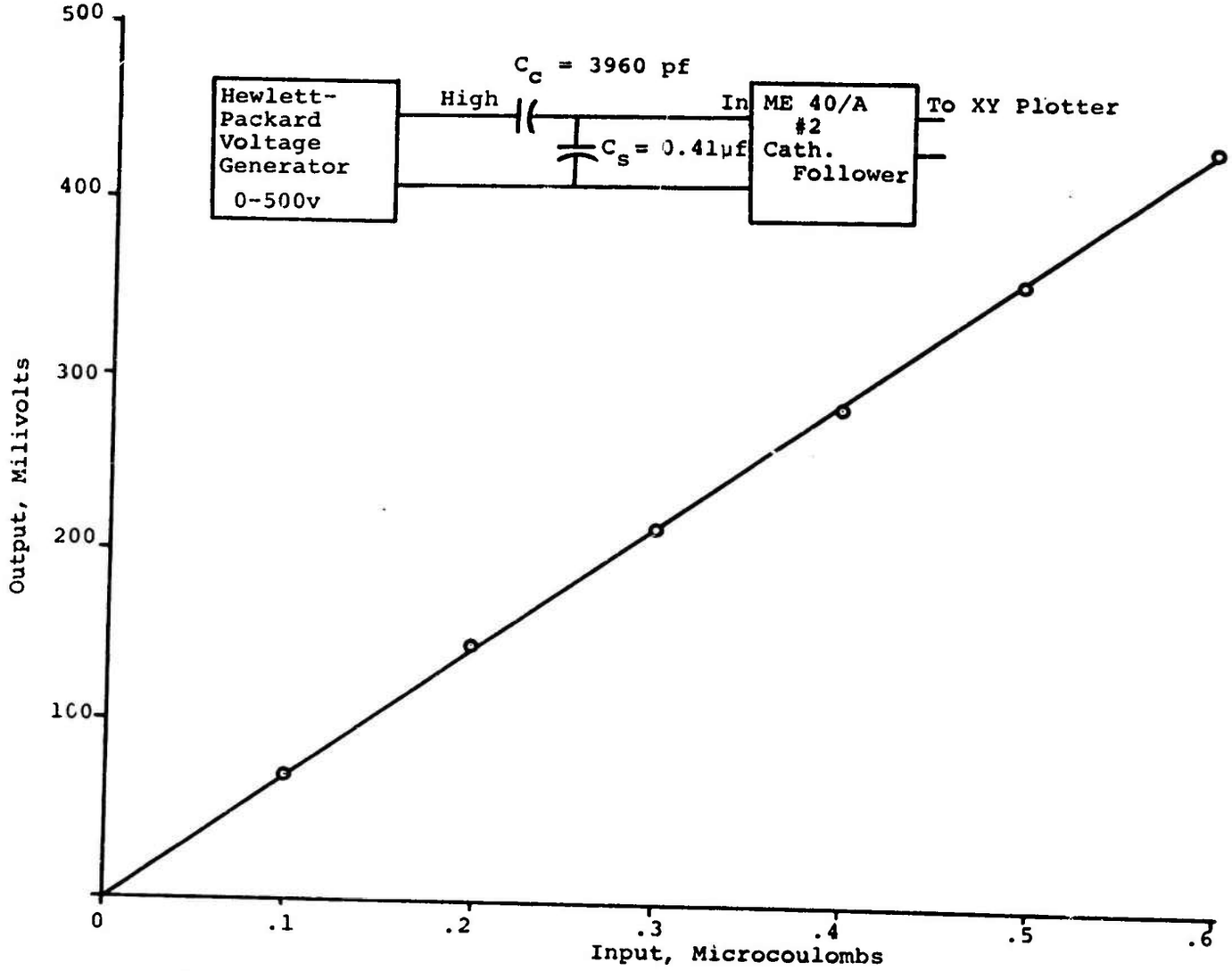

Figure 10. Calibration Curve "A" for Low Loads

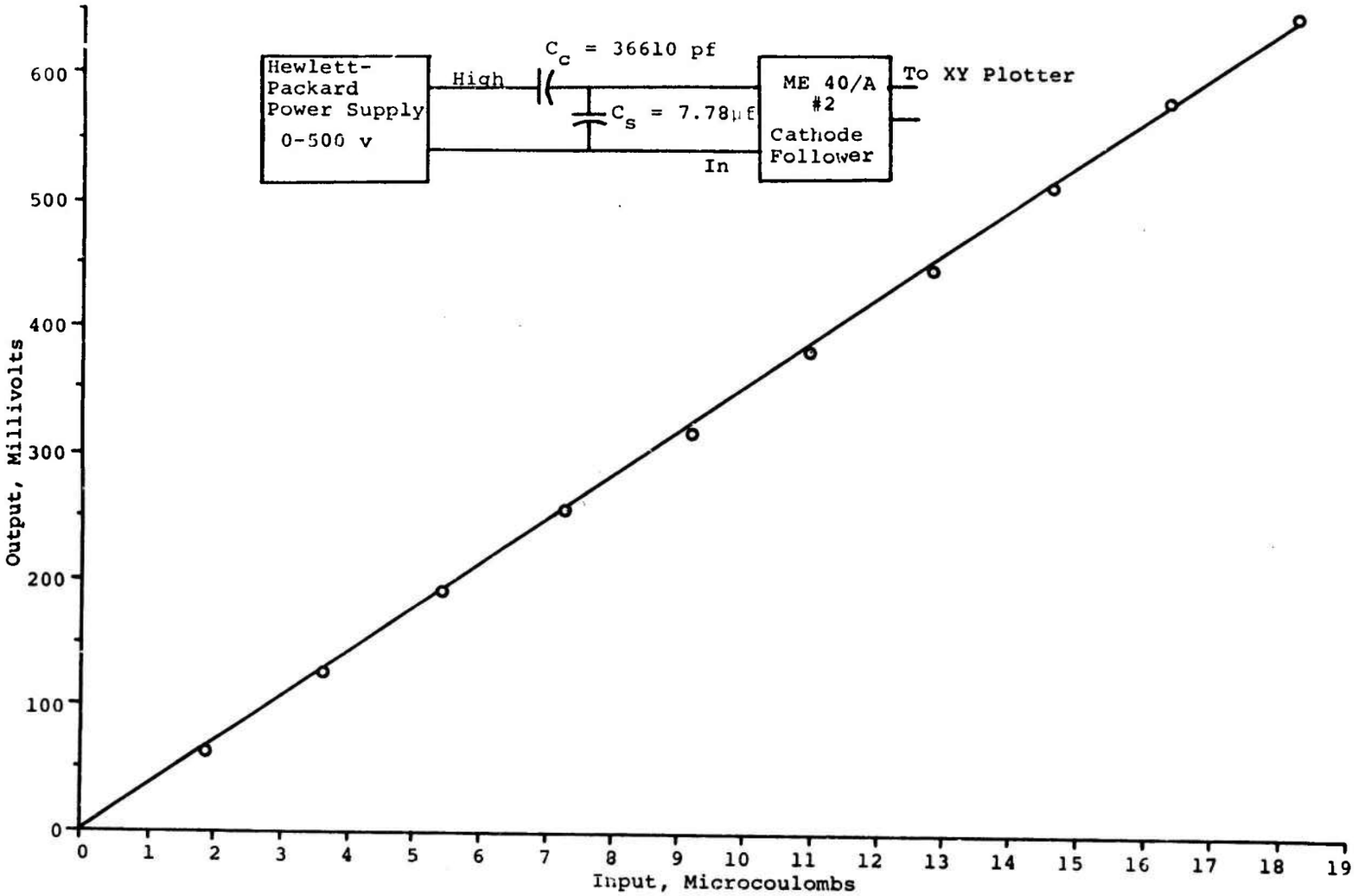

Figure 11. Calibration Curve "B" for High Loads

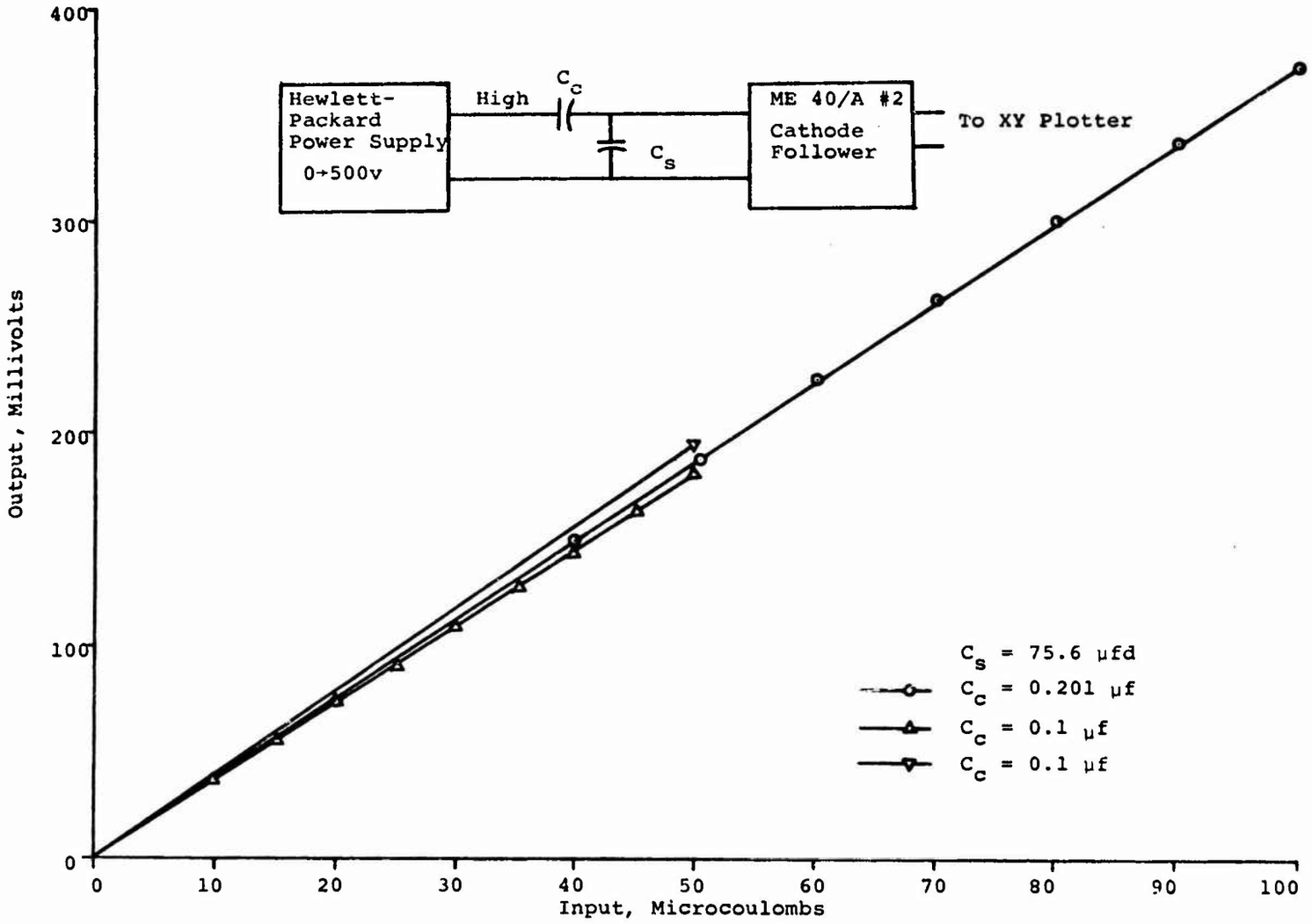

Figure 12. Calibration Curves "C" and "D"

TABLE III

RESULTS OF STATIC LOAD TESTS ON HST-41

Test No.	Purpose	Peak force[1] lb.	d_{33}[2] pcb/N
1	Repeatability of d_{33} for low force.	19.3	2245
2		20.6	2261
3		18.3	2368
4		20.9	2610
5	Change of charge-force behavior when cycled to alternating high and low force.	1218	5670
6		19.4	2034
7		1220	2945
8		20.2	1487
9		2215	5260
10		24.0	1249
11		2215	3930
12 through 22 23	Change of charge-force behavior when cycled to the same force.	2000	----
24	Check for recovery of crystal after 30 days without testing.	2222	2430
25		2262	2122
26		10,000	1690
27		9,150	660
28		9,100	450
29		9,050	398

[1]The crystal tested was 1/2 in. dia., for an area of .196 in.^{2}. Therefore, approximate stress values can be computed by multiplying the force value by 5.

[2]The values given here were computed from the final readings of the charge and force, and as such do not represent any slope associated with the curve where nonlinearities exist.

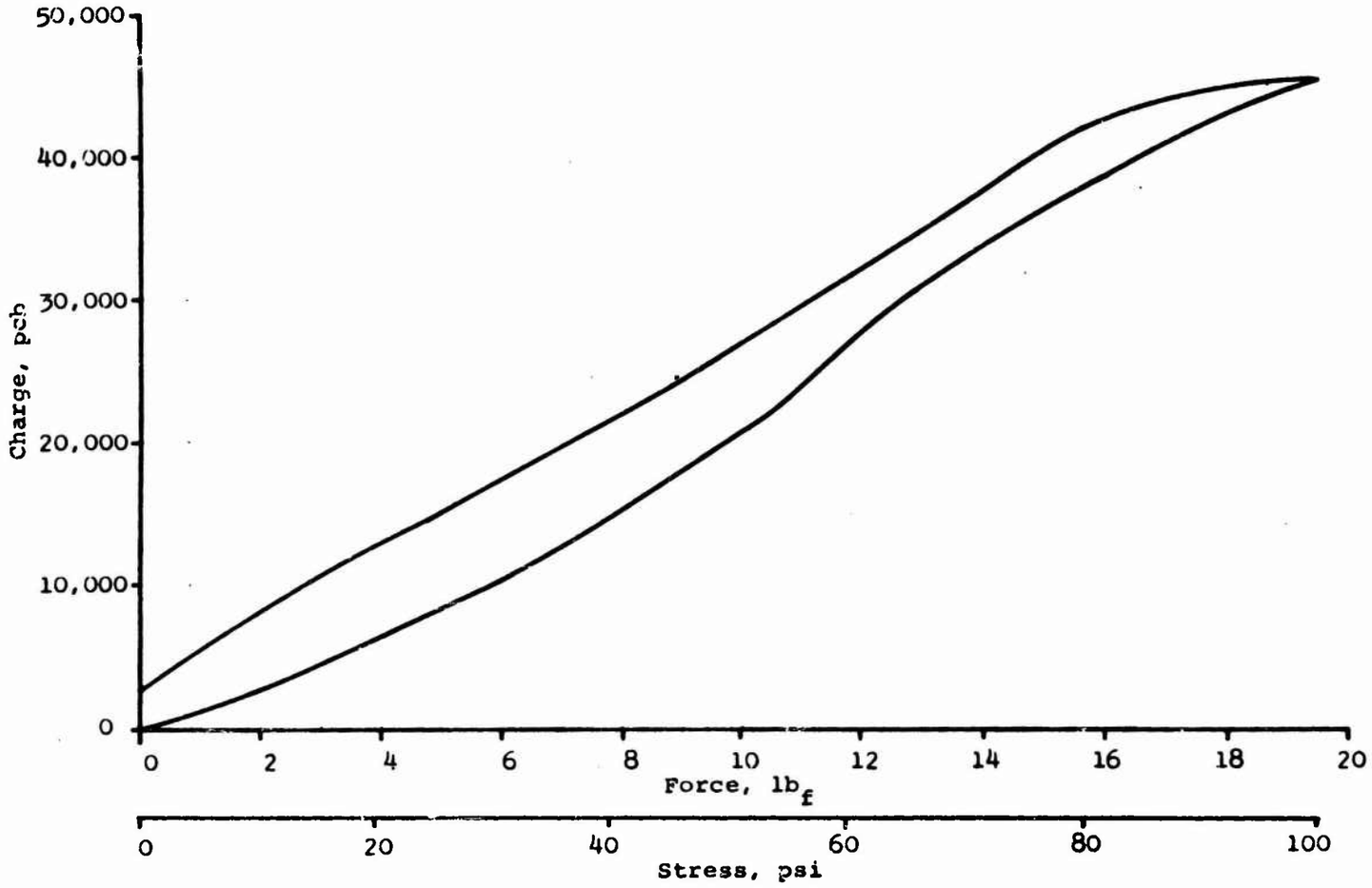

Figure 13. Typical Charge-Force Curve for HST-41 for Low-Stress Amplitude

Runs 5 through 11 were conducted to study the behavior of the crystal when cycled with alternating high and low force values. Figure 14 shows the curve obtained with the first high force value. The behavior for the low force tests was similar to that shown in Figure 13, except the hysteresis loop was slightly larger. This series of tests covered a time interval of approximately 1 hour. Repeated tests to this stress level do show a decrease in the charge developed.

Runs 12 through 22 were conducted one right after another, each to the same load. Figure 15 shows the results of this series; as before, a degradation in the charge developed was noted. Run 23 was made after the crystal "rested" for 30 minutes. A small amount of recovery is noted.

The crystal was then allowed to remain unloaded for 30 days. Re-testing then indicated a further recovery of charge producing capability, but not to the original level.

Tests 26 through 29 were conducted to very high stress levels -- approximately 50,000 psi. Figure 16 shows the results of test 26. In it noted that at the high stress levels, very little additional charge is developed as the force increases. Repeated tests to the same stress level show a significant decrease in "d_{33}."

Table IV shows the results of the tests on PZT-4. Figure 17 shows the results of test 2 on sample 2 and test 4 on sample 3. Figure 18 shows results of tests at stress levels of approximately 5000 psi., and Figure 19 shows results of several tests at the 50,000 psi. level.

A review of the above mentioned table and figures gives the following indications regarding the behavior of PZT-4.

1) There may be considerable variation in d_{33} among samples of this material.
2) The force-charge relation is closer to being linear than for HST-41 up through 5000 psi, and there is less hysteresis.
3) At stress levels of 50,000 psi, the curve is beginning to flatten out.

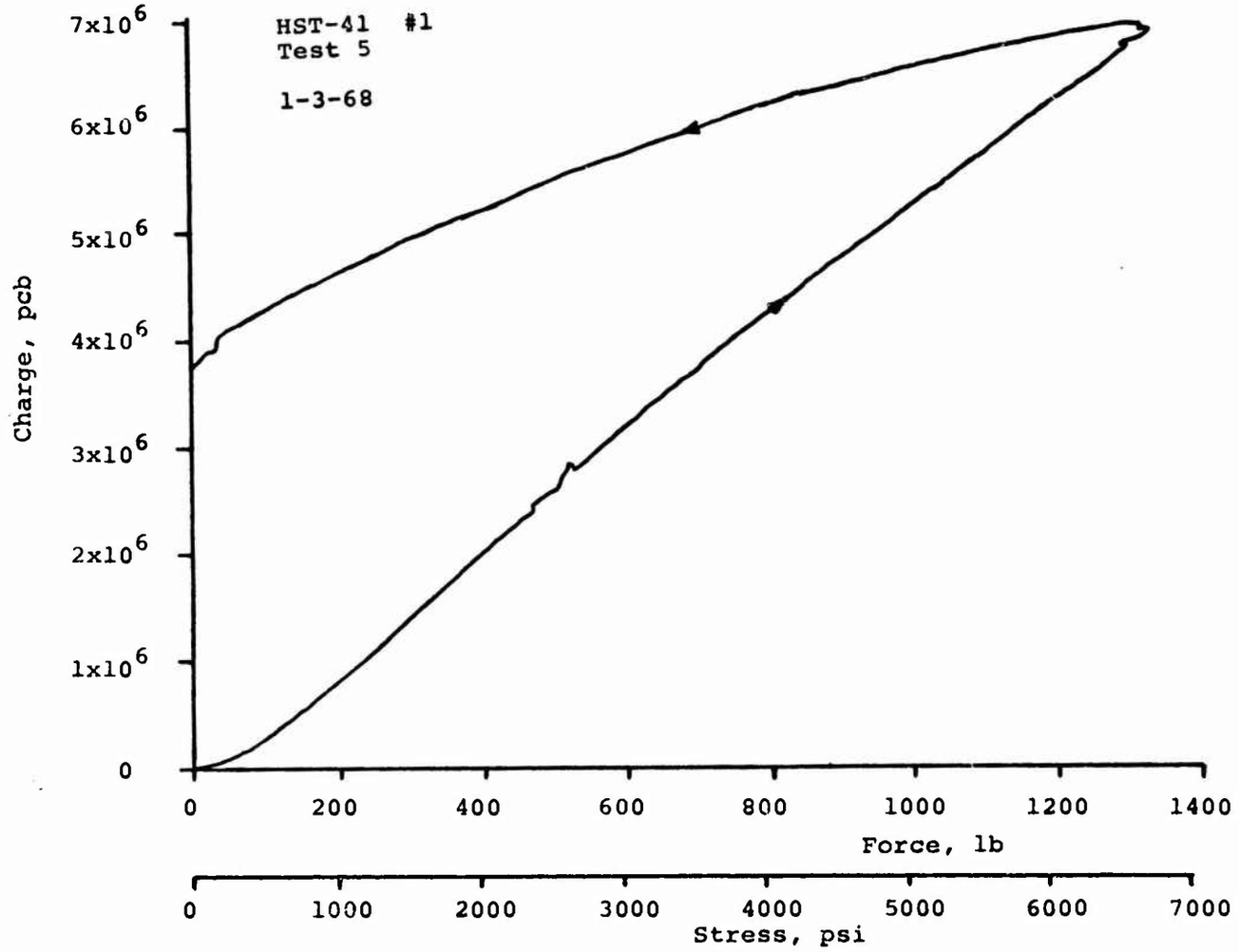

Figure 14. Charge-Force Curve for HST-41 Under Initial Loading to 6200 psi

Sample 1
Tests 12 through 23

——— Loading

-------- Unloading

1. Curve number shown indicates load test of this series only; i.e., number 1 here corresponds to run 12 of Table III.
2. Unloading curves not shown for runs 2 through 9 to avoid confusion.

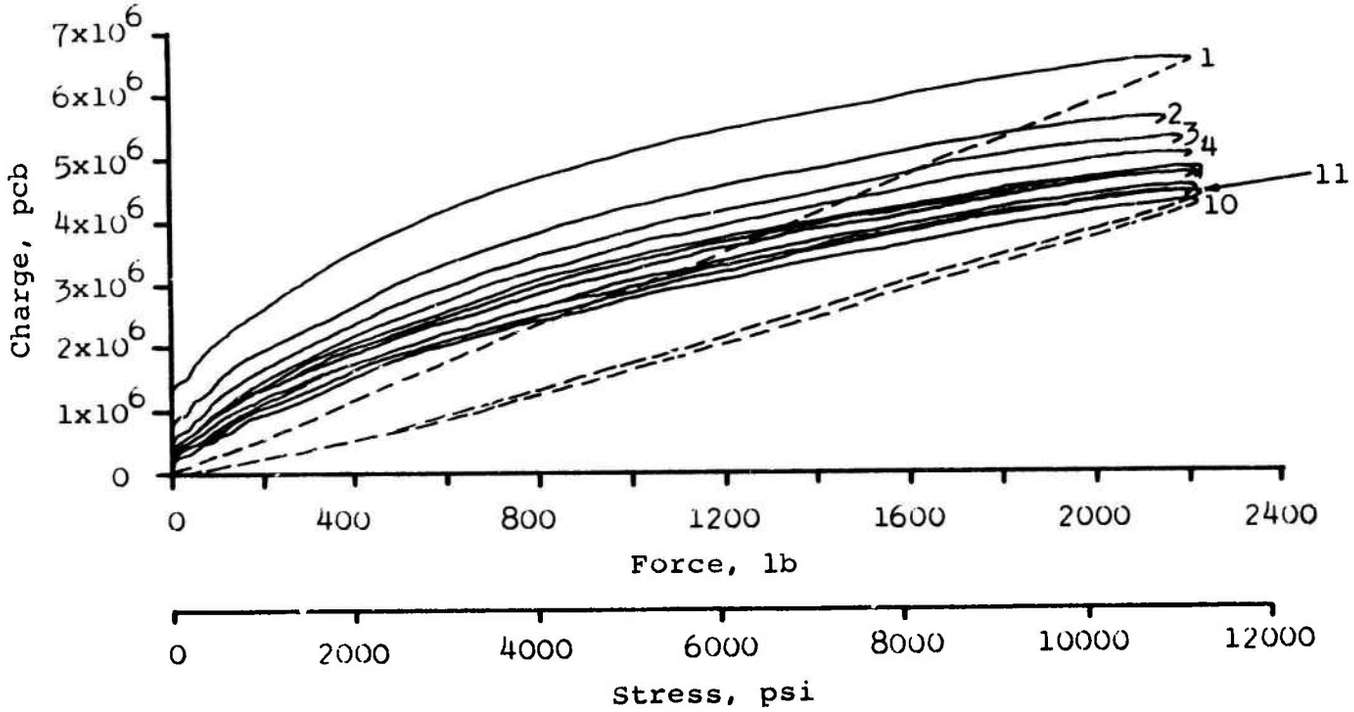

Figure 15. Results of Sequential Load Tests on HST-41

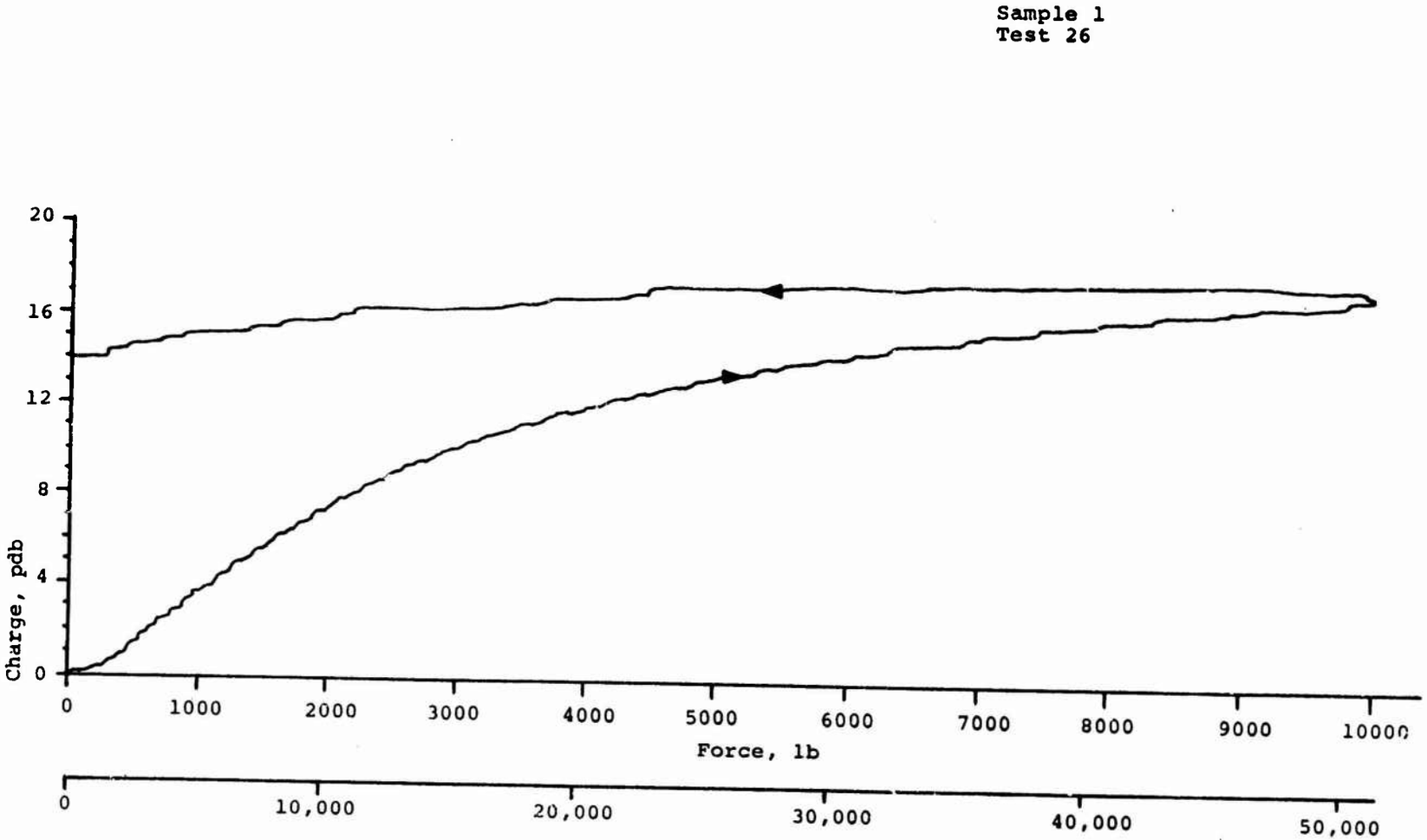

Figure 16. Charge-Force Curve for HST-41 to Compressive Stress of 50,000 psi

TABLE IV

RESULTS ON PZT-4

Test No.	SAMPLE 2		SAMPLE 3	
	Stress psi	d_{33}[1] pcb/lb	Stress psi	d_{33} pcb/lb
1	180	1042	---	---
2	174	988	103	1052
3	188	1046	159	1701
4	195	1045	185	1456
5	---	---	184	1487
6	5100	1060	186	1392
7	5100	980	5370	1694
8			5340	1575
9			10,300	2215
10			10,200	2120
11			11,300	2620
12			51,000	2990
13			46,900	3100
14			46,900	2450
15			46,900	1795

[1]The values given here were computed from the final readings of the charge and force, and as such do not represent any slope associated with the curve where nonlinearities exist.

[2]There was a 30-day wait between test 10 and 11 on crystal 3.

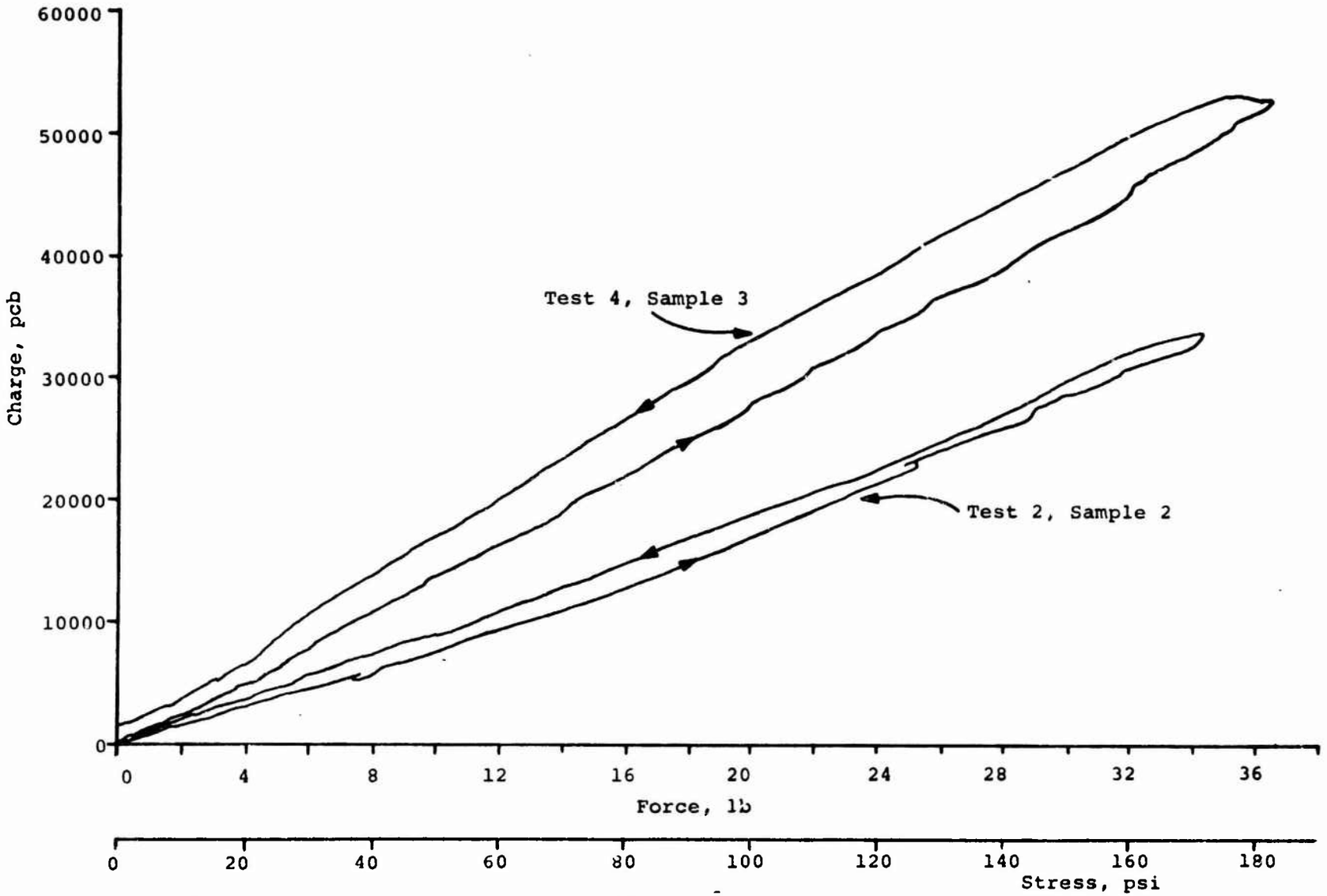

Figure 17. Charge-Force Relations for PZT-4 at Low-Stress Levels

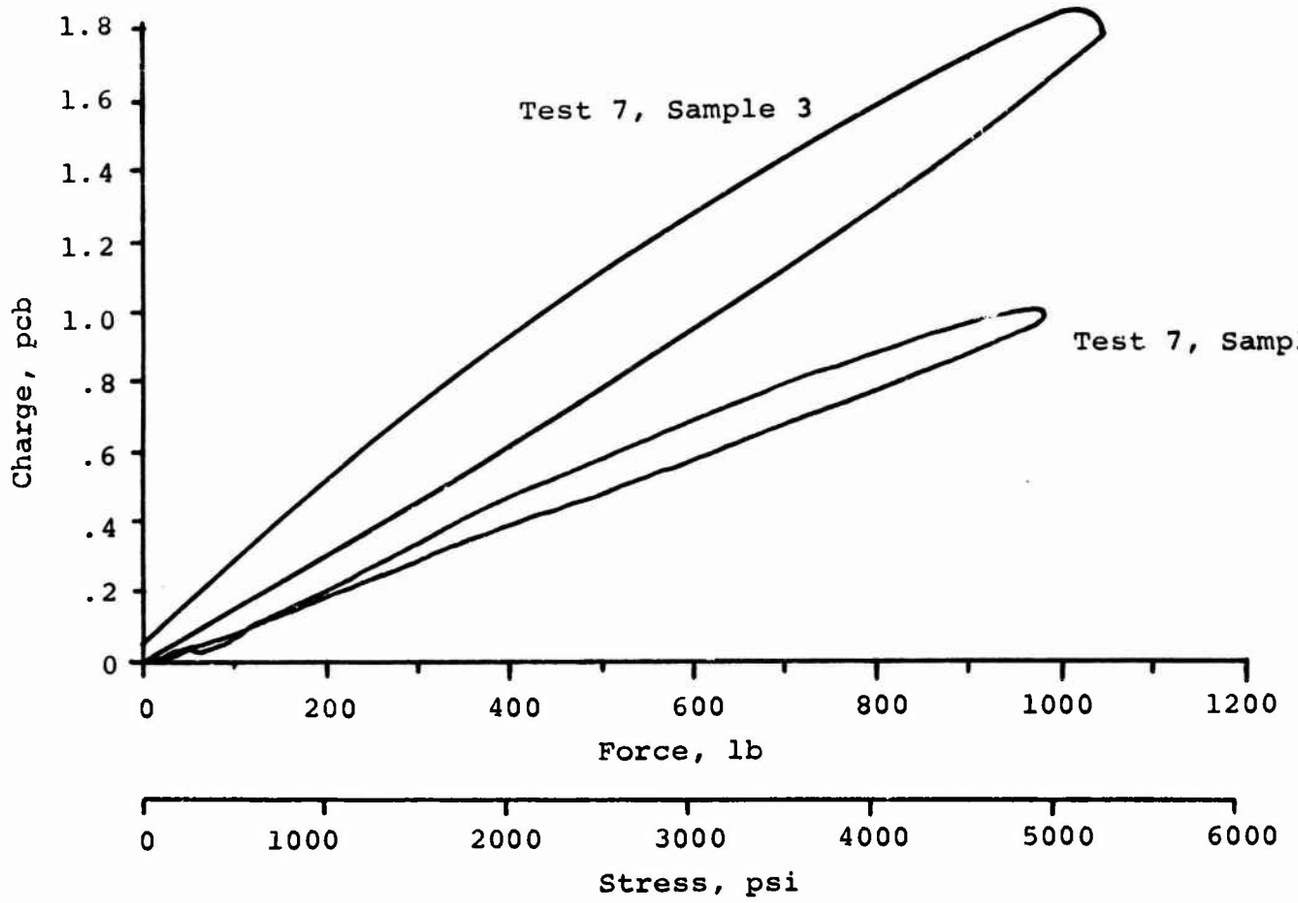

Figure 18. Charge-Force Relations for PZT-4 at Stress Levels of 5000 psi

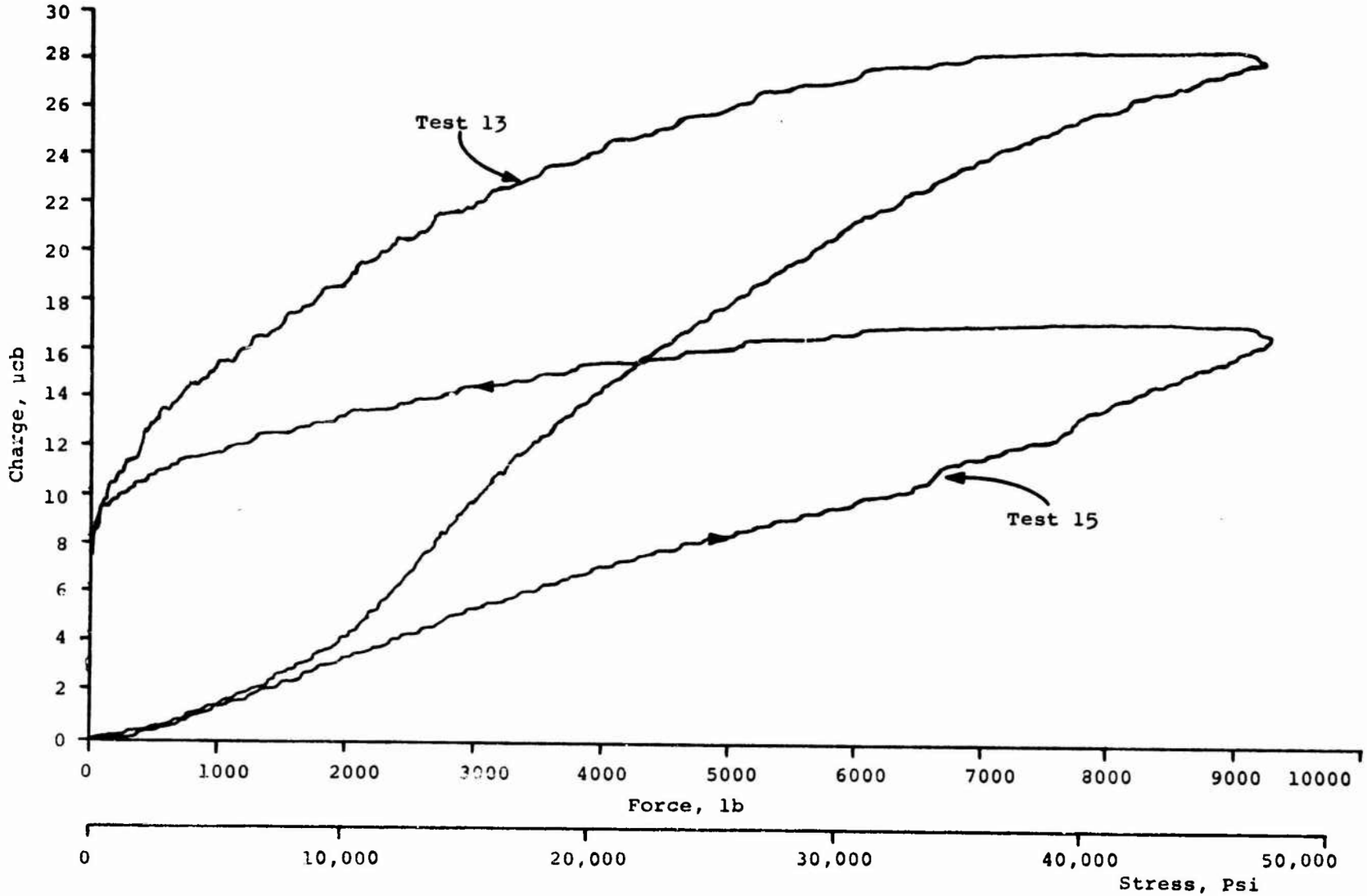

Figure 19. Charge-Force Relations for PZT-4 at 50,000 psi

A summary of the results of the tests on PZT-5 is shown in Table V. Figures 20, 21, and 22 show typical results from these tests.

A second series of tests was conducted to determine a basis for obtaining a nonlinear and uniaxial stress charge coefficient for HST-41 at high stress levels. For this series a new crystal was used for each test. In order to insure a state of uniaxial stress, a slightly different loading technique was used. The crystals were loaded through two bars having the same diameter as the crystal, as shown in Figure 23. This method was used since the boundary conditions on the crystals in the static tests would approximate those for the split Hopkinson bar tests which would be conducted in the dynamic tests. Two different materials, steel and aluminum, were used for bars though which the load was applied, and two different thicknesses of crystal were used, -- 0.50 inch and .100 inch. Again this was done to duplicate the later dynamic tests. The various combinations of bar materials and crystals are shown below.

	Bar Material	Crystal Thickness (inches)
Test 1	Aluminum	.100
Test 2	Aluminum	.100
Test 3	Aluminum	.100
Test 4	Steel	.100
Test 5	Steel	.100
Test 6	Steel	.050

Tests were conducted on a Riehle Universal Testing machine using the same Kistler load cell in the earlier test series to monitor the load. Figure 23 also shows the load washer and test specimen. Recording was done as before, using a large shunt capacitor to prevent the test crystal from overdriving the Kistler charge amplifiers. A second Kistler charge amplifier was used in conjunction with the load cell. Both charge

TABLE V

RESULTS ON PZT-5

Test No.	Stress psi	d_{33}[1] pcb/lb
1	79	1995
2	100	2300
3	113	2228
4	126	1859
5	5810	4100
6	6140	7590
7	5810	6060
8	5850	2080
9	412	780
10	475	481
11	441	839
12	371	1210
13[2]	2180	4959
14	50,900	997
16	35,203	348

[1]The values given here were computed from the final readings of the charge and force, and as such do not represent any slope associated with the curve where nonlinearities exist.

[2]Crystal given a 30-day rest prior to this test.

[3]Crystal fractured at this load.

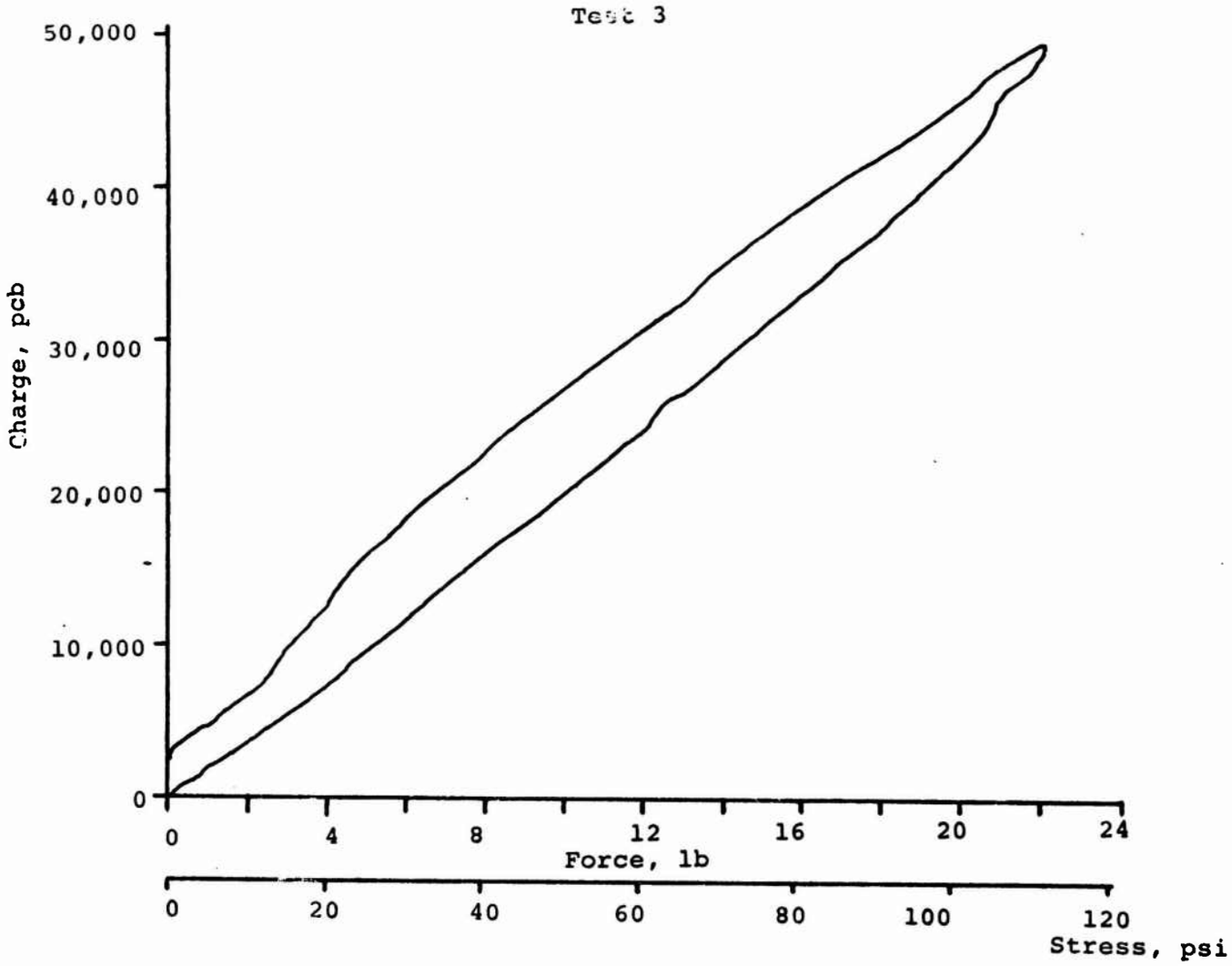

Figure 20. Charge-Force Curve for PZT-5 for Low-Stress Amplitude

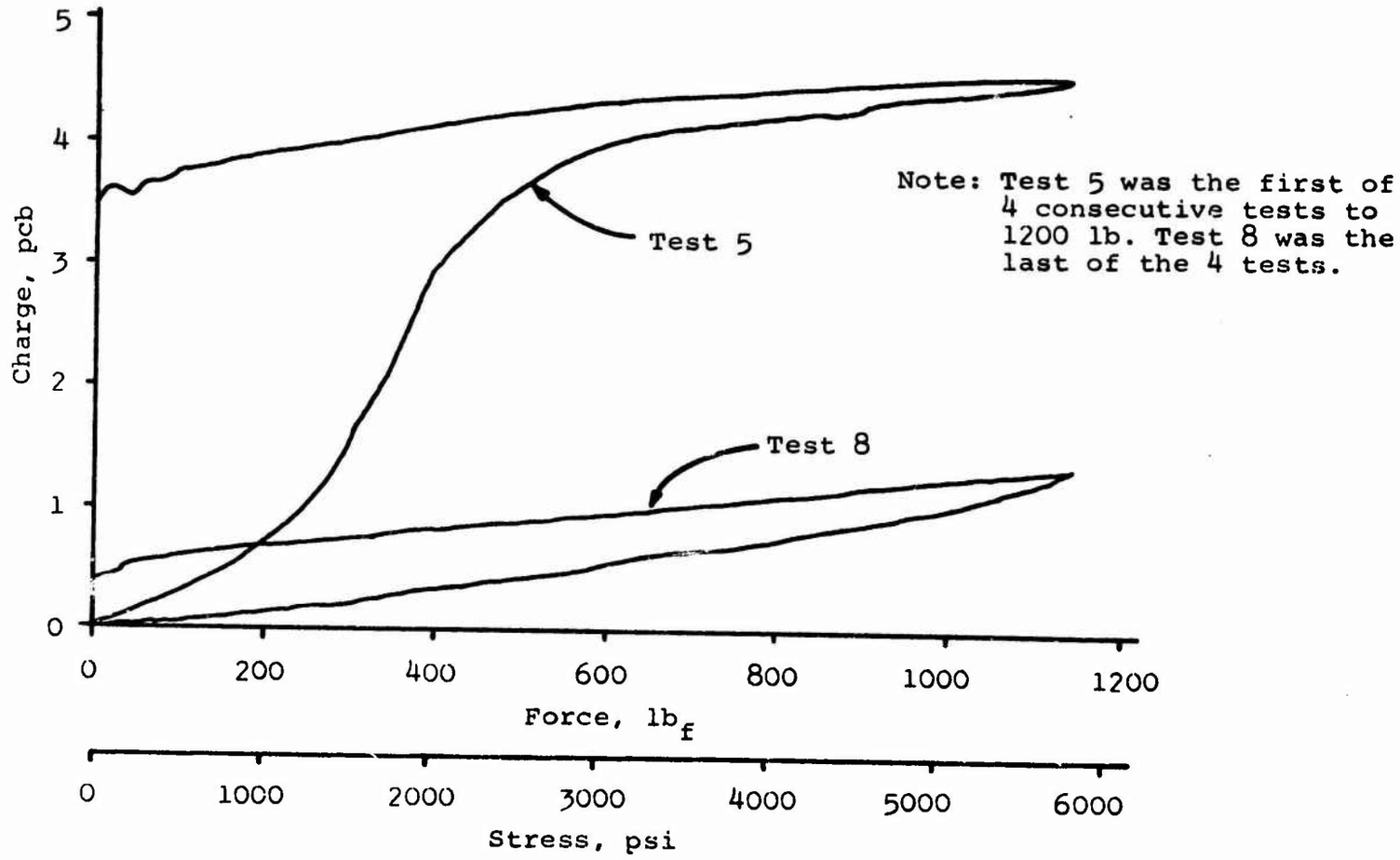

Figure 21. Charge-Force Curves for PZT-5 Under Consecutive Loadings

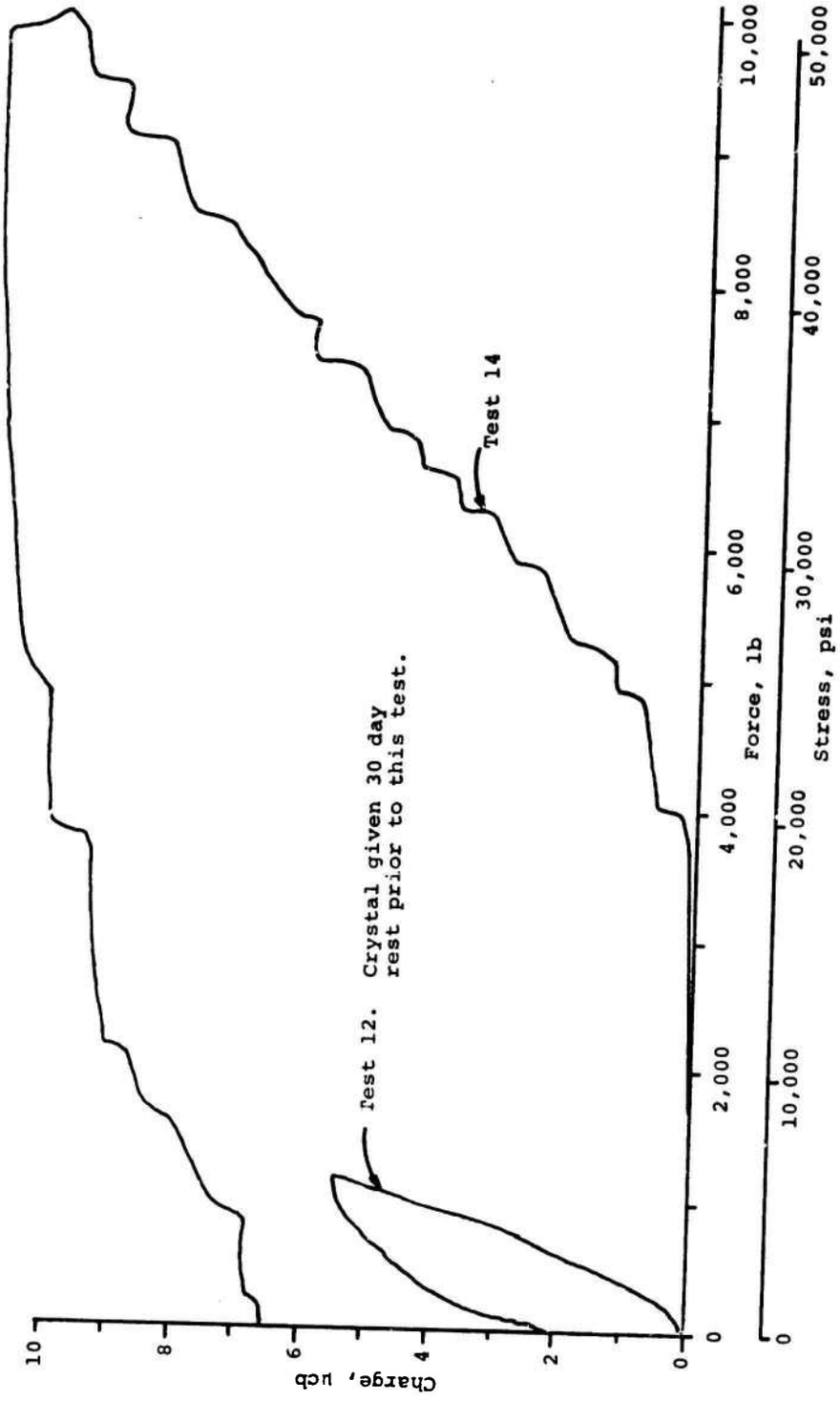

Figure 22. Charge-Force Curves for PZT-5

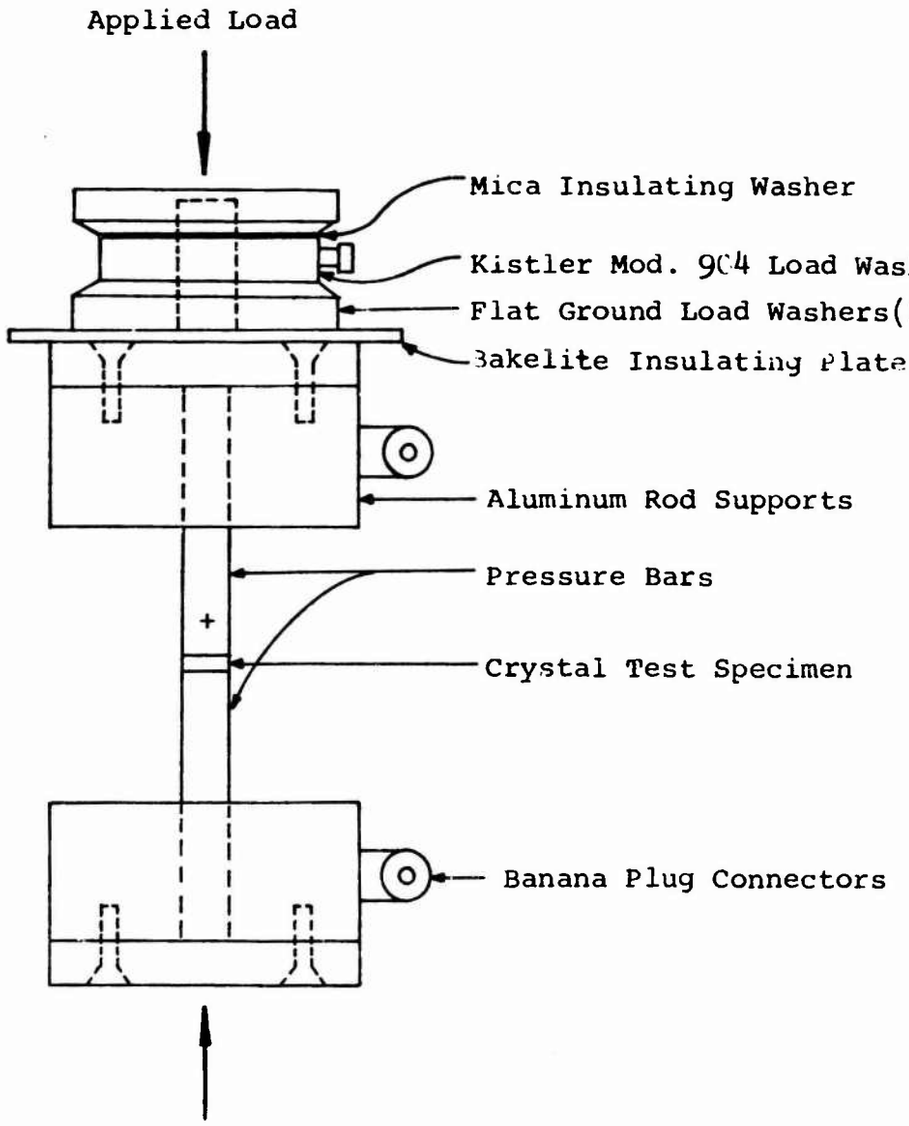

Figure 23. Test Fixture Used for Determining the Static Charge-Force Relation for HST-41

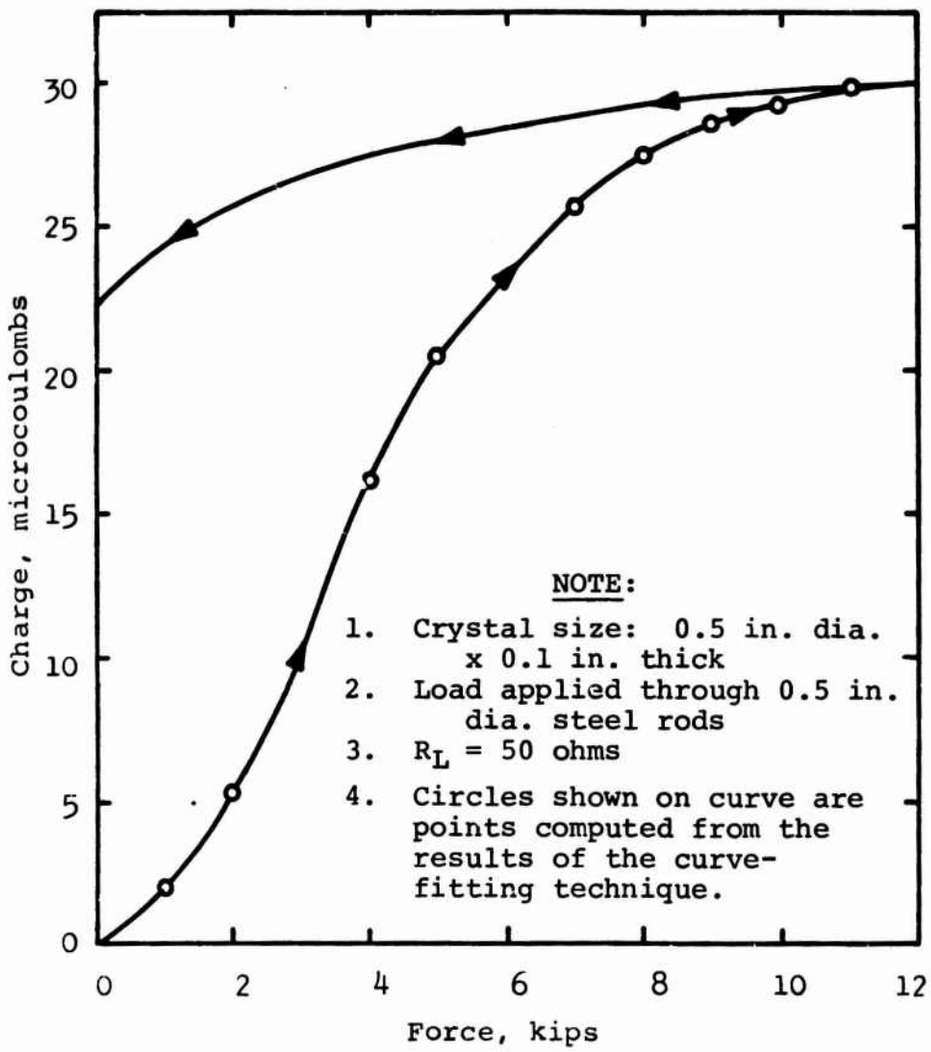

Figure 24. Charge Force Relation for HST-41 (Determined for use in numerical work)

amplifiers then drove the Moseley X-Y plotter. Calibration was done directly on the recording circuits by using a DC power supply and a series capacitor to simulate a charge on the crystal.

The crystals were loaded through the aluminum bars to about 20,000 psi, and to about 40,000 psi through the steel bars. Data were taken on the initial loading only. The curves for all of the six tests fell within a band which was quite narrow, possibly within the range of variation of specimen properties. Therefore, only one experimentally-determined curve is shown for this test searies. Test 5 was taken as representative of all data and is shown in Figure 24. It was used for determining the charge stress functions as needed in the numerical work.

Two factors concerning these tests should be noted. One is that the zero load charge coefficient determined experimentally in this test series agrees very closely with that given by the manufacturer. However, at a load of about 16,000 psi, the charge coefficient has increased to four times that at zero load. At very high loads then the charge coefficient drops off to less than 10% of the zero load value. This is expected since, as the load increases, the charge generated approaches the maximum available charge given by Equation 12. For these tests the maximum charge approaches about 32 μcb. This charge coefficient-average stress relation is later used in the reduction of the data from the Hopkinson bar tests.

The second factor is that the output of the new crystals was substantially higher than for the older crystals. Hence it is suspected that the ferroelectric materials do lose some of their charge potential with age. It is not believed that the nonlinear charge coefficient function determined for the new crystals would be valid for the older crystals.

DYNAMIC TESTS--SHOCK TUBE

A considerable amount of work has been done in earlier investigations on response of crystals to shock wave inputs.

This type of input requires that the initial contact with the face of the crystal be plane, and achieving this condition experimentally can be something of a problem. The air driven shock tube was used as the initial test vehicle on the crystals since the loading condition satisfied this requirement, the tests could be run quickly, and the tests were nondestructive (in the sense the crystal was not broken during each test). These factors were of importance in the first series of tests. The tests were undertaken to accomplish the following: (1) to check the theory associated with use of the piezoelectric effect as an energy generator, as presented in Section III; (2) as an initial probe into the problems involved in the circuitry and measuring techniques; and (3) in order to determine the effects of the measuring instruments in crystal circuits. Figures 25 and 26 describe the hardware and recording techniques used in these tests.

Materials tested were quartz and HST-41. The recording circuit used is shown in Figure 27. The termination resistor was 50 ohm on all tests. For one series of tests, which was run only on HST-41, the effect of increasing the shock tube driving pressure was studied. The load resistance, R_L, was zero for these tests. Figure 28 shows typical data for this series and a sketch of the data for all of the tests conducted. It is observed that the voltage drop across R_{TERM} increases with driving pressure, as expected. It should be pointed out that the driving pressure does not represent the pressure applied to the crystal, but is the charge pressure in the shock tube.

Another series of tests run on HST-41 only involved a study of the effect of crystal thickness. Tests were run on crystals varying in thickness from 0.02 to 0.25 inch. The results of these tests are shown in Figure 29. Theory indicates that the current generated will vary inversely with thickness (Eq. 4, p. 3). Figure 29 shows that while the voltage drop across R_{TERM} is dependent on the thickness, Equation 4 is not applicable for the inputs of these tests. It is believed

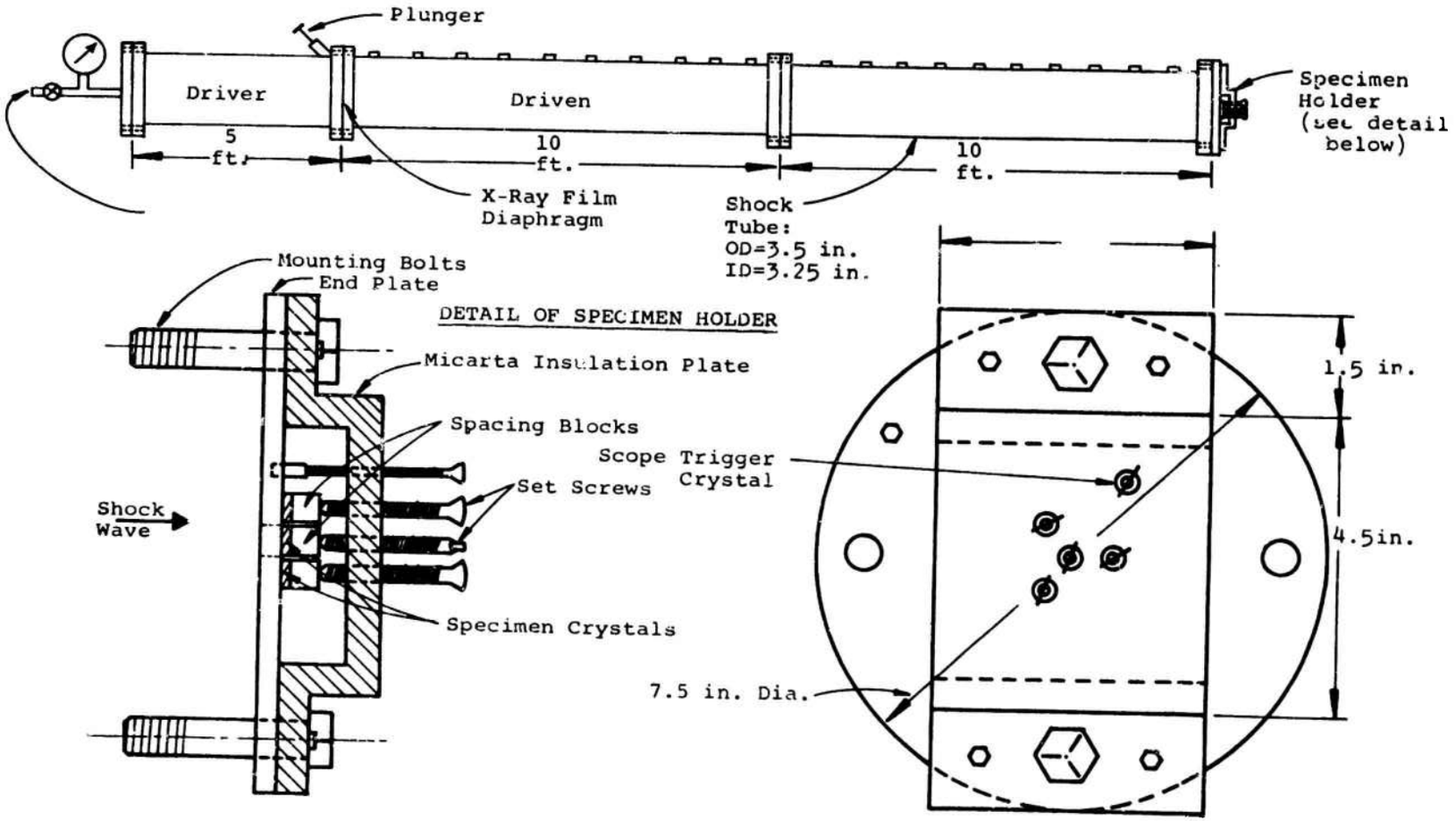

Figure 25. Hardware for Shock Tube Tests

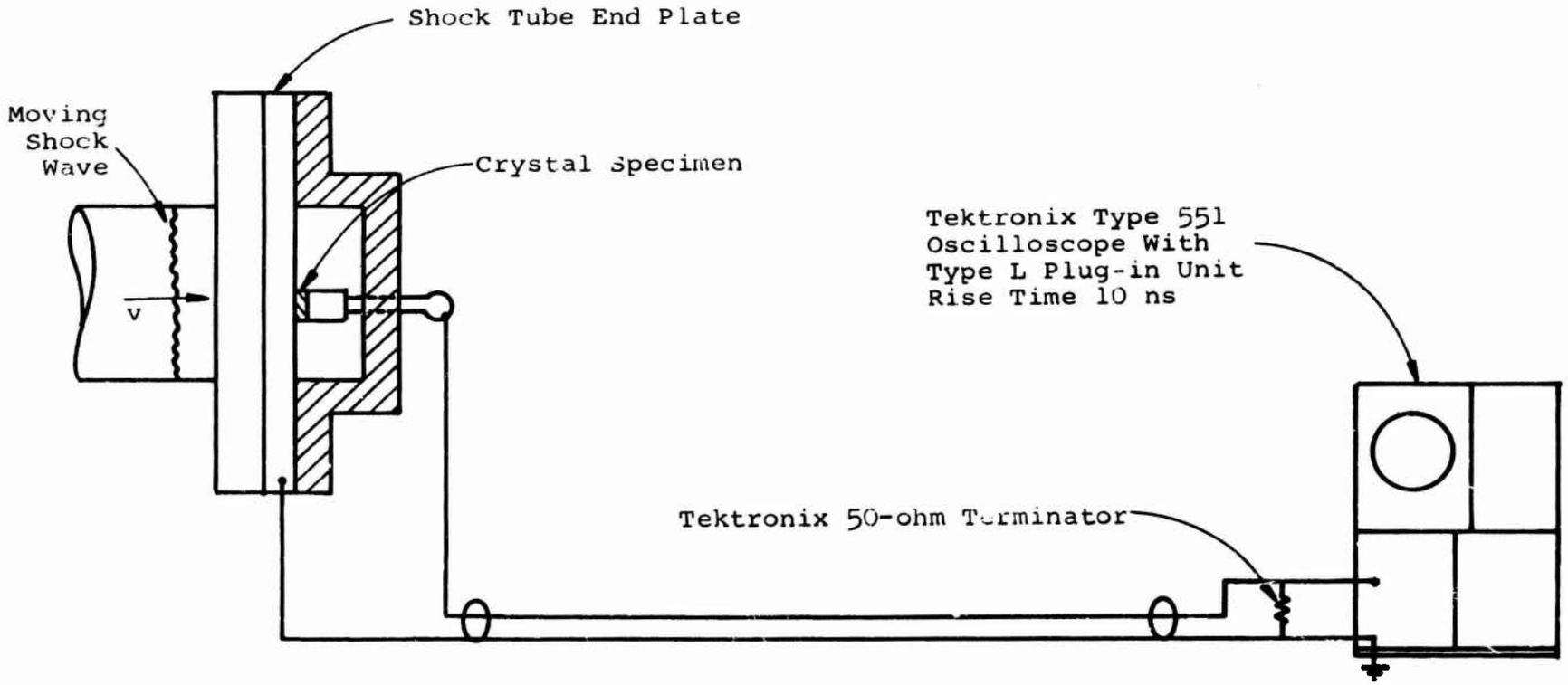

Figure 26. Recording Technique Circuitry for Shock Tube Tests on Crystals

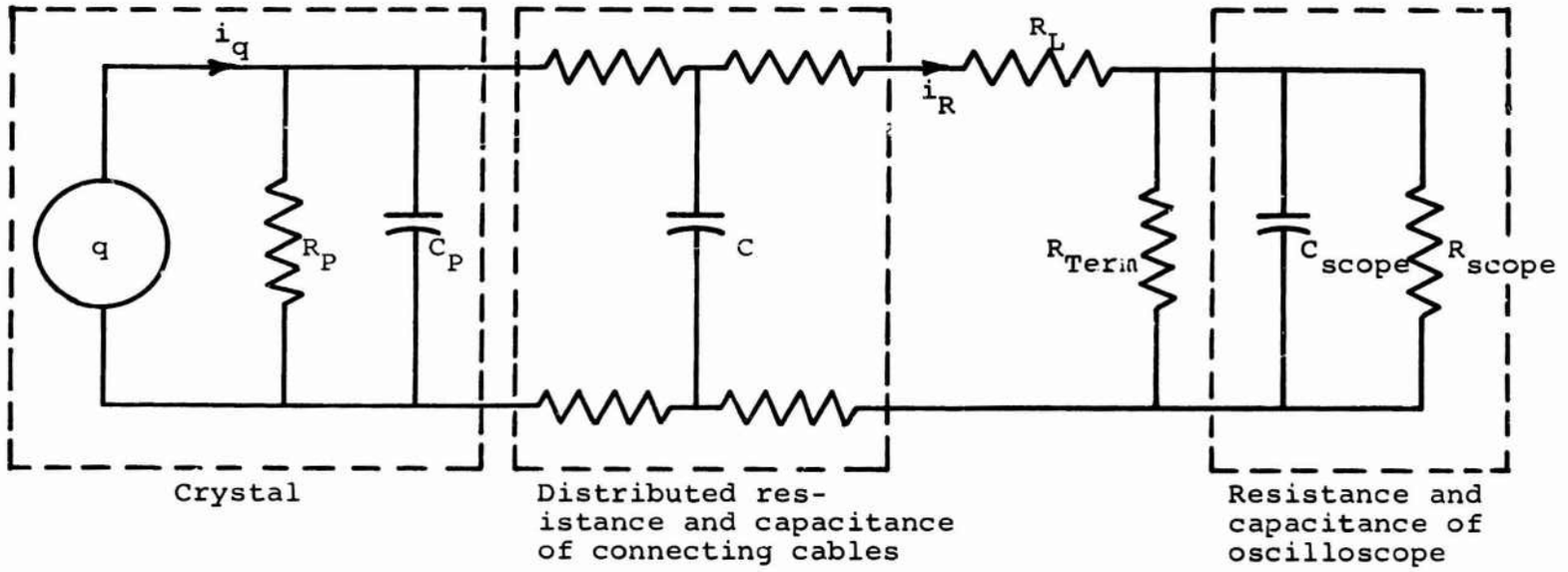

Figure 27. Recording Circuit Diagram

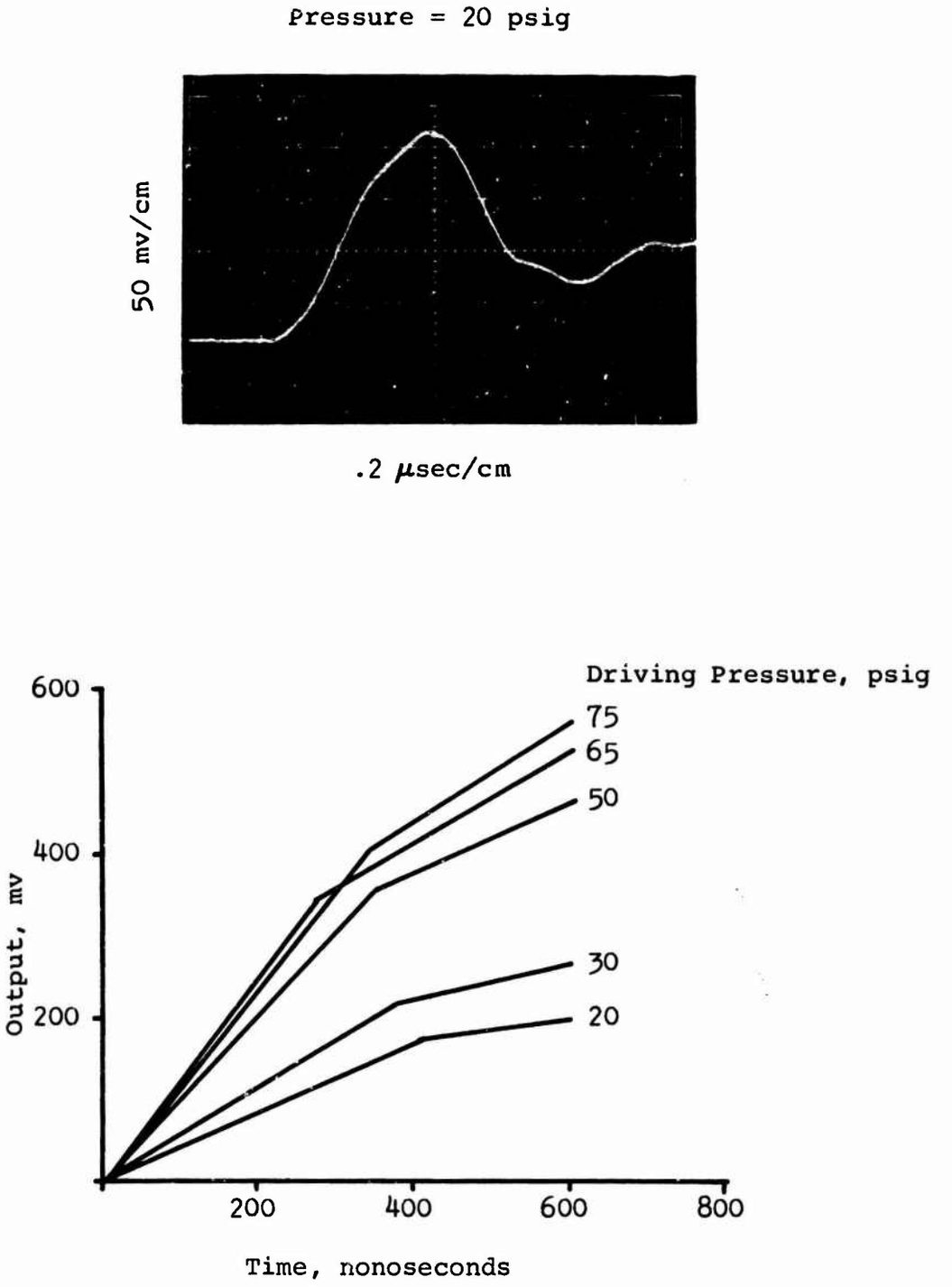

Figure 28. Typical Data and Results for Shock Tube Tests on HST-41 Crystal (.50 in. dia. x 0.10 in. thick)

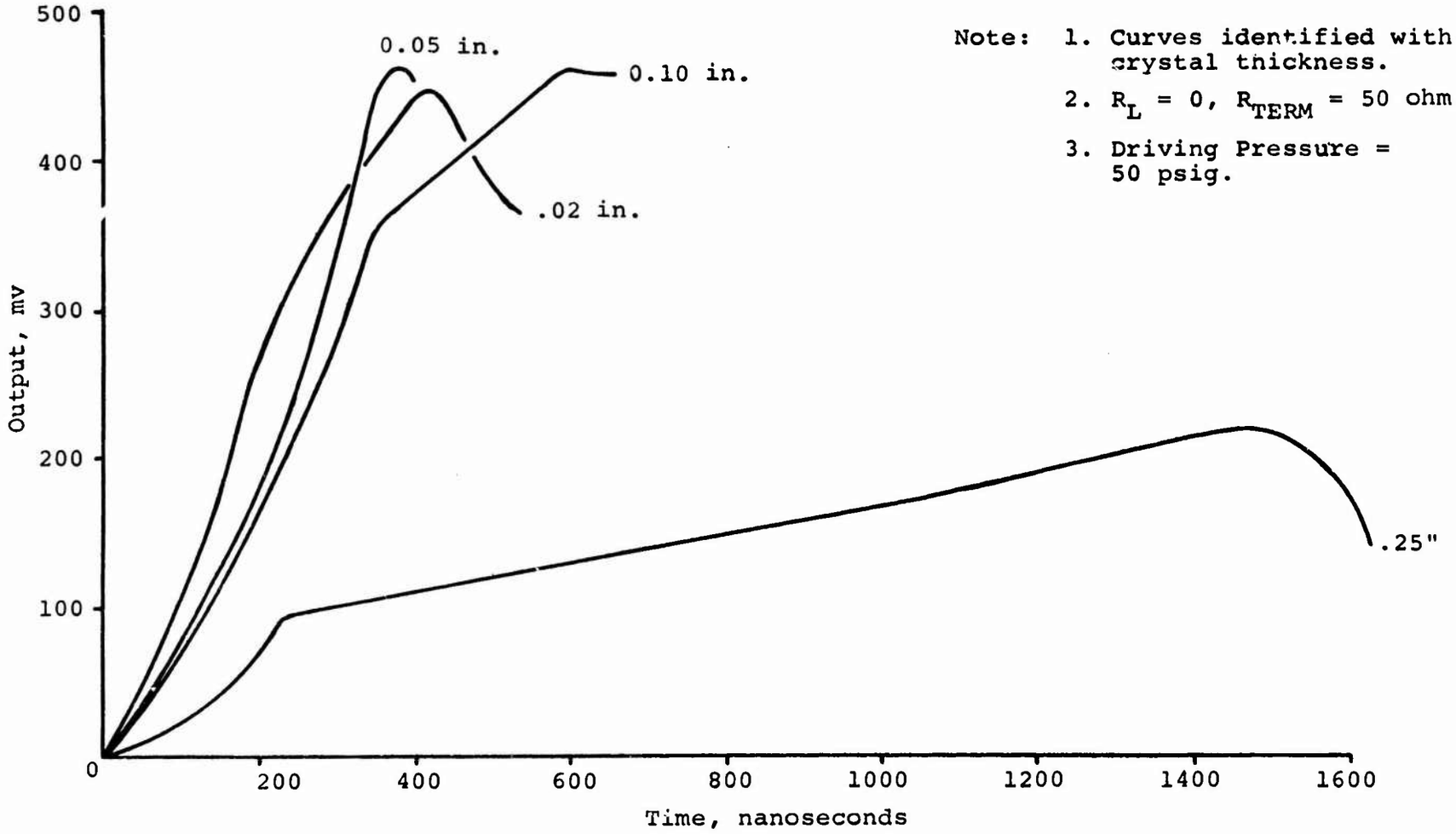

Figure 29. Effect of Crystal Thickness on Output for HST-41

that the deviation from the theory is the result of the inherent lack of planeness of the force input to the crystal.

A study of the effect of load resistance, R_L, on current and energy generated was made for quartz and HST-41. The load resistance was varied from zero to 100,000 ohm and driving pressure was 50 psig for all tests. Figures 30 and 31 show typical data on quartz and HST-41, respectively. Figure 32 summarizes the pulse signatures for all runs for quartz, and similarly, Figure 33 for HST-41.

The data obtained for the range of load resistors has been used in further studies related to the problem. These are as follows:

1. Study of the effect of the impedance of measuring instruments in the circuit used with the crystals.
2. Study of the effect of input pulse on the response of the circuit.
3. Study of current generation - specifically to predict currents generated, and effect of R_L on current.
4. Investigation into the amounts of energy generated for these tests.

Details of these studies will be discussed in the above order.

Items 1 and 2 above were investigated with the same approach. The circuit diagram of Figure 27 includes essentially all the elements involved. Analysis of this circuit would be quite difficult. This circuit was first reduced to the one labelled "real" in Figure 34. In doing this, the following assumptions were made:

1. $R_p >>> R_L$

2. $R_{DIST} <<< R_L$

3. $C_{SCOPE} >> C_p + C_{DIST}$

4. $C_{TOTAL} = C_p + C_{DIST}$

Driving Pressure = 50 psig, all tests.
Total Capacitance = 150 pfd, all tests.

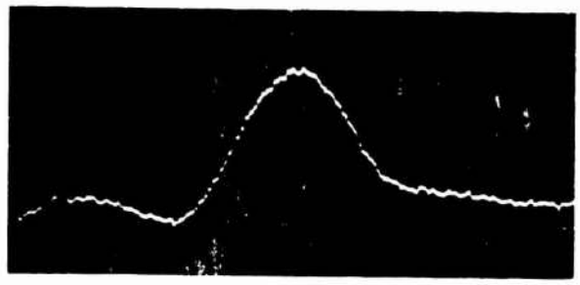

2 mv/cm

R_L = 1000 ohm

.2 μsec/cm

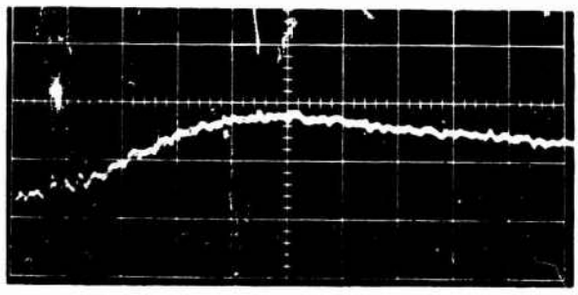

1 mv/cm

R_L = 8000 ohm

.2 μsec/cm

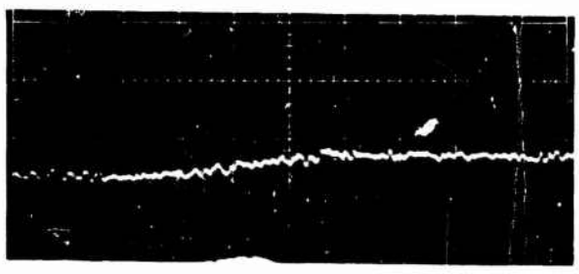

1 mv/cm

R_L = 50,000 ohm

.2 μsec/cm

Figure 30. Examples of Data from Shock Tube Tests on Quartz (0.50 in dia. x 0.10 in. thick)

Driving Pressure = 50 psig, all tests.
Total Capacitance = 834 pfd, all tests.

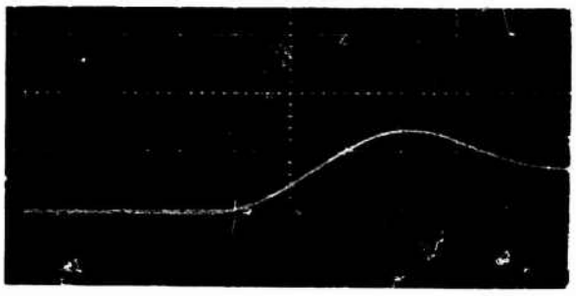

200 mv/cm

R_L = 500 ohm

.2 μsec/cm

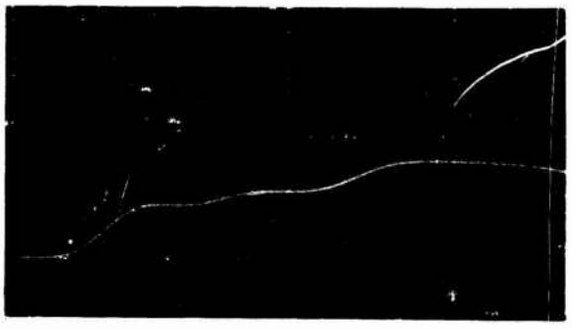

50 mv/cm

R_L = 5000 ohm

.5 μsec/cm

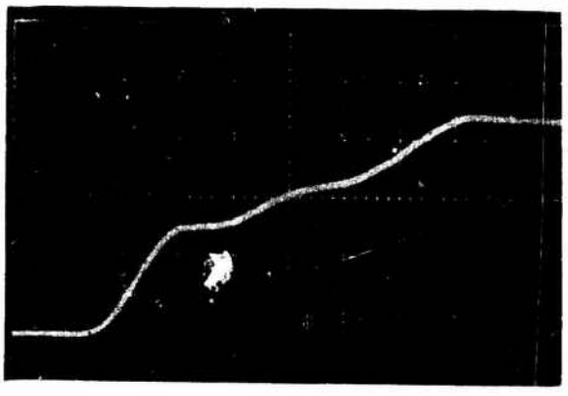

5 mv/cm

R_L = 50000 ohm

.5 μsec/cm

Figure 31. Examples of Data from Shock Tube Tests on HST-41 (0.50 in. dia. x 0.10 in. thick)

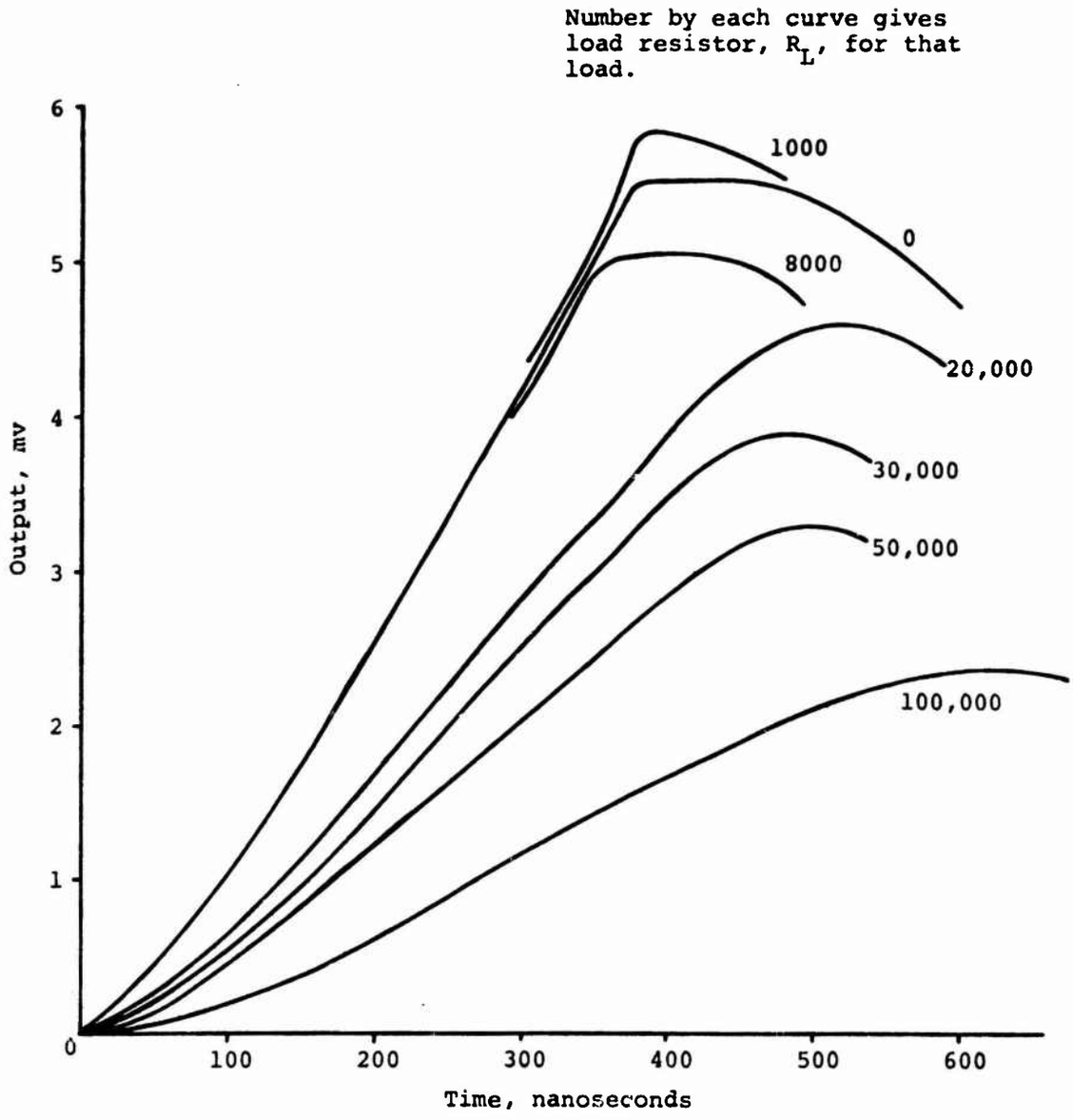

Figure 32. Summary of Data for Quartz Shock Tube Tests

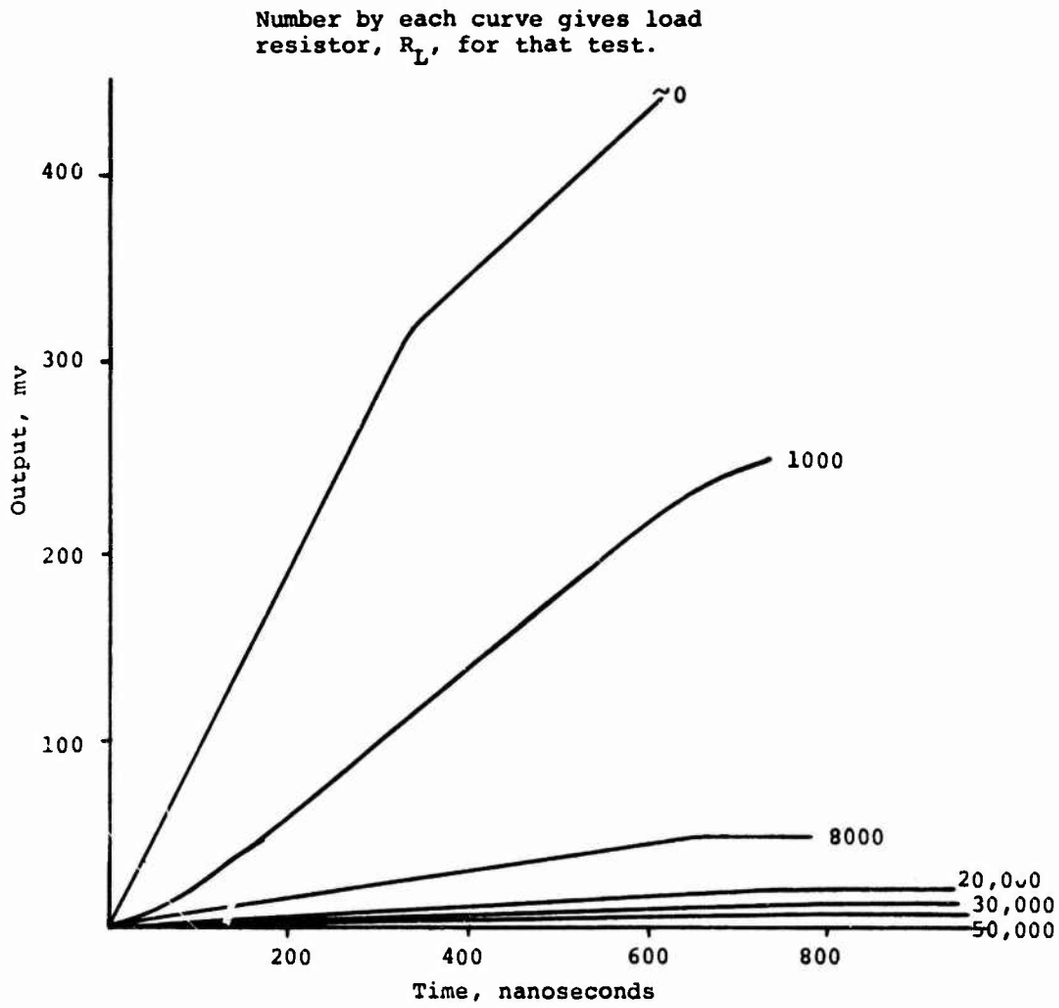

Figure 33. Summary of Data for HST-41 Shock Tube Tests

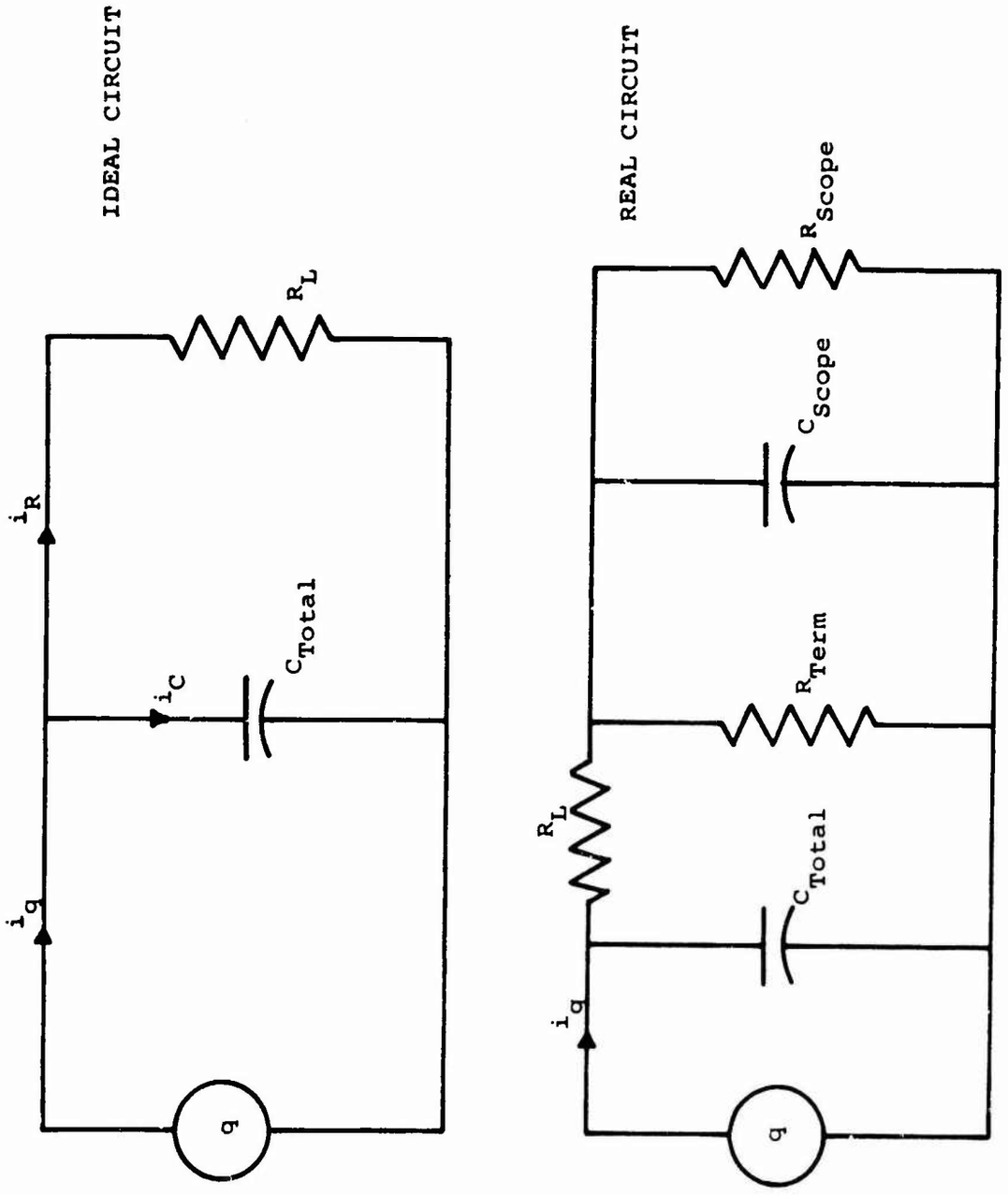

Figure 34. Circuits Used

This circuit retains the principal characteristics of the actual circuit, i.e., the impedance of the measuring instrument, and will permit investigation of its effect on the measured crystal output. The applicable circuit when the measuring instrument is not being used is shown as the "ideal circuit" in Figure 34.

The values of the parameters used were those from the test series, and computations were made using a piezoelectric charge coefficient for both quartz and HST-41. Solutions for the required currents for the ideal circuit could be made using analytical techniques. However, an analytical solution to the differential equations for the real circuit would be quite messy, and a numerical technique was adopted.

This numerical technique made use of the computer program "ECAP", which was obtained from IBM. Use of the program requires insertion of the desired impedance values between the appropriate node points in the circuit. The program then, in essence, sets up the differential equations and determines the desired currents and voltages.

These two circuits were solved for both a step input and a ramp input. Figures 35 and 36 show the results for the quartz and HST-41, respectively. A study of these figures permits the following conclusions to be made:

1. For the value of R_L used in this study, the presence of the measuring instrument in the circuit reduces the current through the load resistor a noticeable amount. The amount of this reduction is apparently dependent upon the parallel capacitance in the circuit, since the percent reduction is greater for the HST-41 than the quartz.
2. The ECAP program does not give results in complete agreement with analytical solutions to very simple circuits, as evidenced by the lack of agreement between solutions of the same problem by each technique. This difference in solutions is greater for the step input than for the ramp. However, this

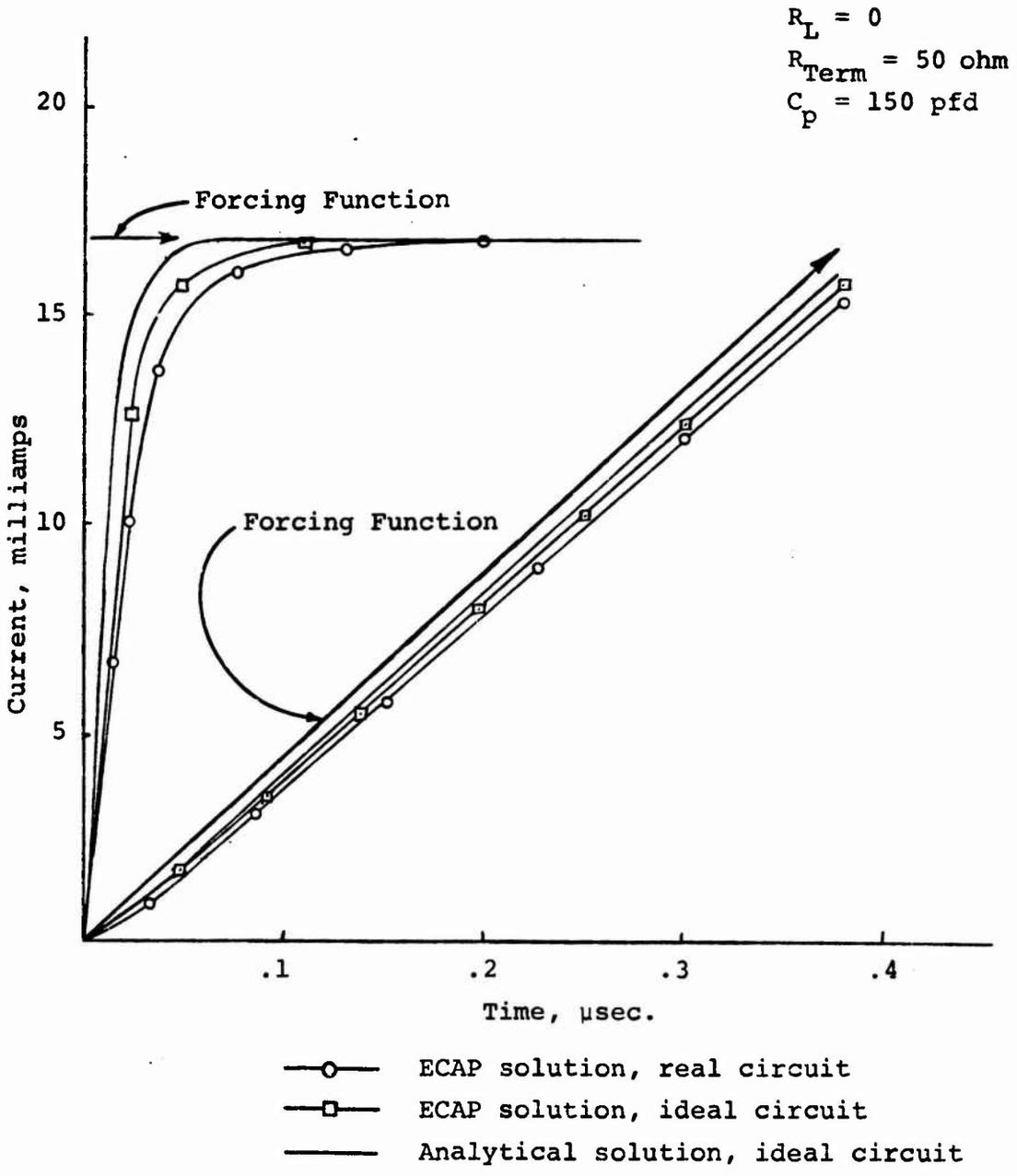

Figure 35. Results of Circuit Studies, Quartz Crystal

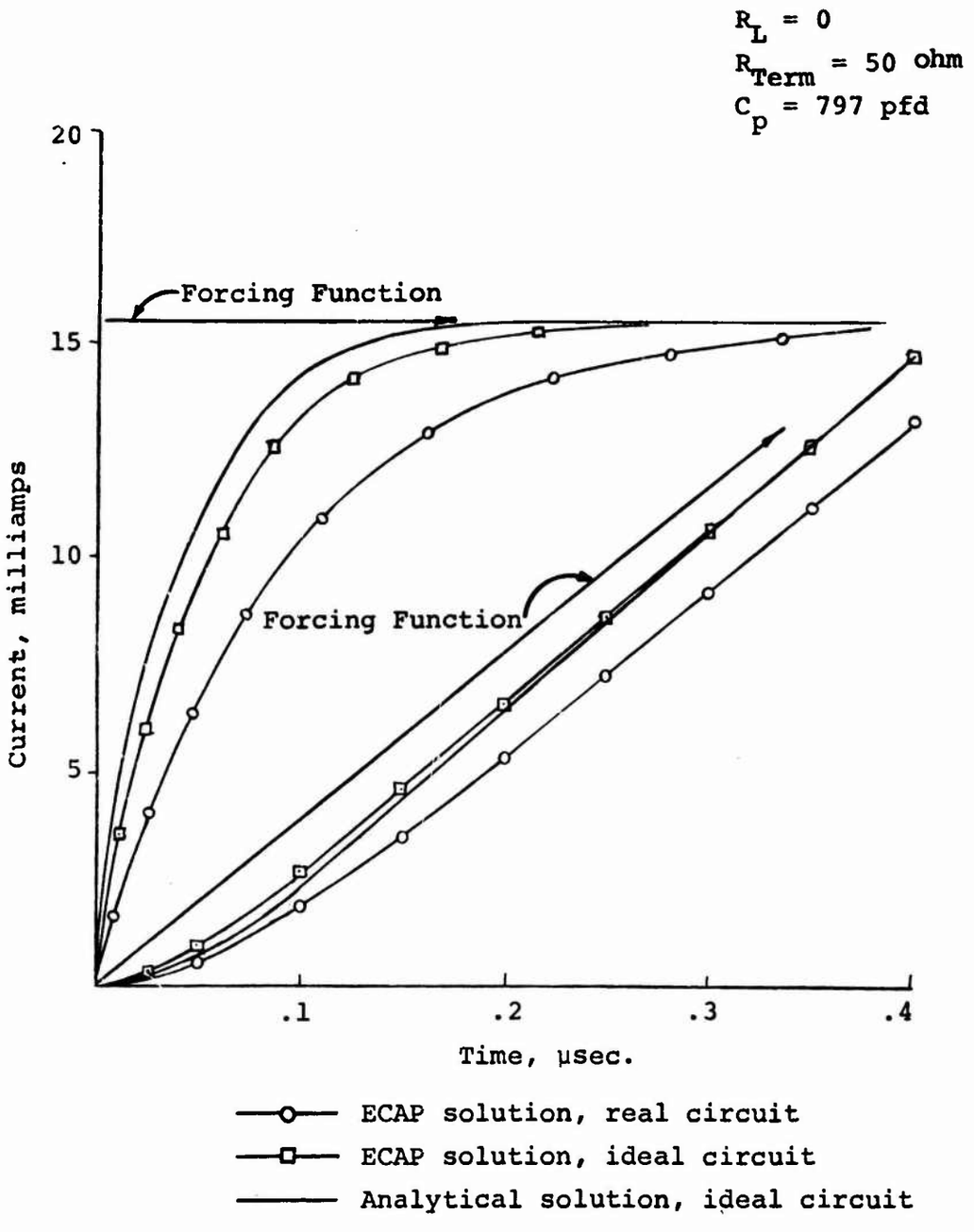

Figure 36. Results of Circuit Studies, HST-41 Crystal

apparent error in the ECAP method is considered small enough for the results to still be useful.

3. The crystal is being subjected to an approximate ramp input by the shock tube having a rise time of about 0.4 μsec. This is indicated since the characteristics of the recorded signal are similar to those of the predicted currents for the ramp input (see Fig. 28).

The theory presented earlier specifies the current generated when a quartz crystal is struck by a shock wave. The data presented gives measured currents for quartz and HZT-41. The work discussed in the following pages is that of computation of current generated using theory and comparison with some of the measured values.

These computations were made based upon the piezoelectric theory presented in Section III. The parameters used in the computations were as follows:

	Quartz	HST-41
Driving Pressure, P_c, psig	50	50
Pressure on Crystal, P_r, psia	37.2	37.2
Pressure transmitted through crystal	.495 P_r	.66 P_r
Pulse shape	Ramp	Ramp
Rise time, μsec	.38	.38
d_{33}	10.2 pcb/lb.	1440 pcb/lb.
R_{TERM}, ohms	50	50
C_p, pfd	130	777
C_{Total}, pfd	150	797

The "ideal" circuit was used in the computations for i_R.

Figure 37 shows the results of these computations for quartz and Figure 38 for HST-41. Points from the experimentally determined curves presented earlier have been shown on each of these figures.

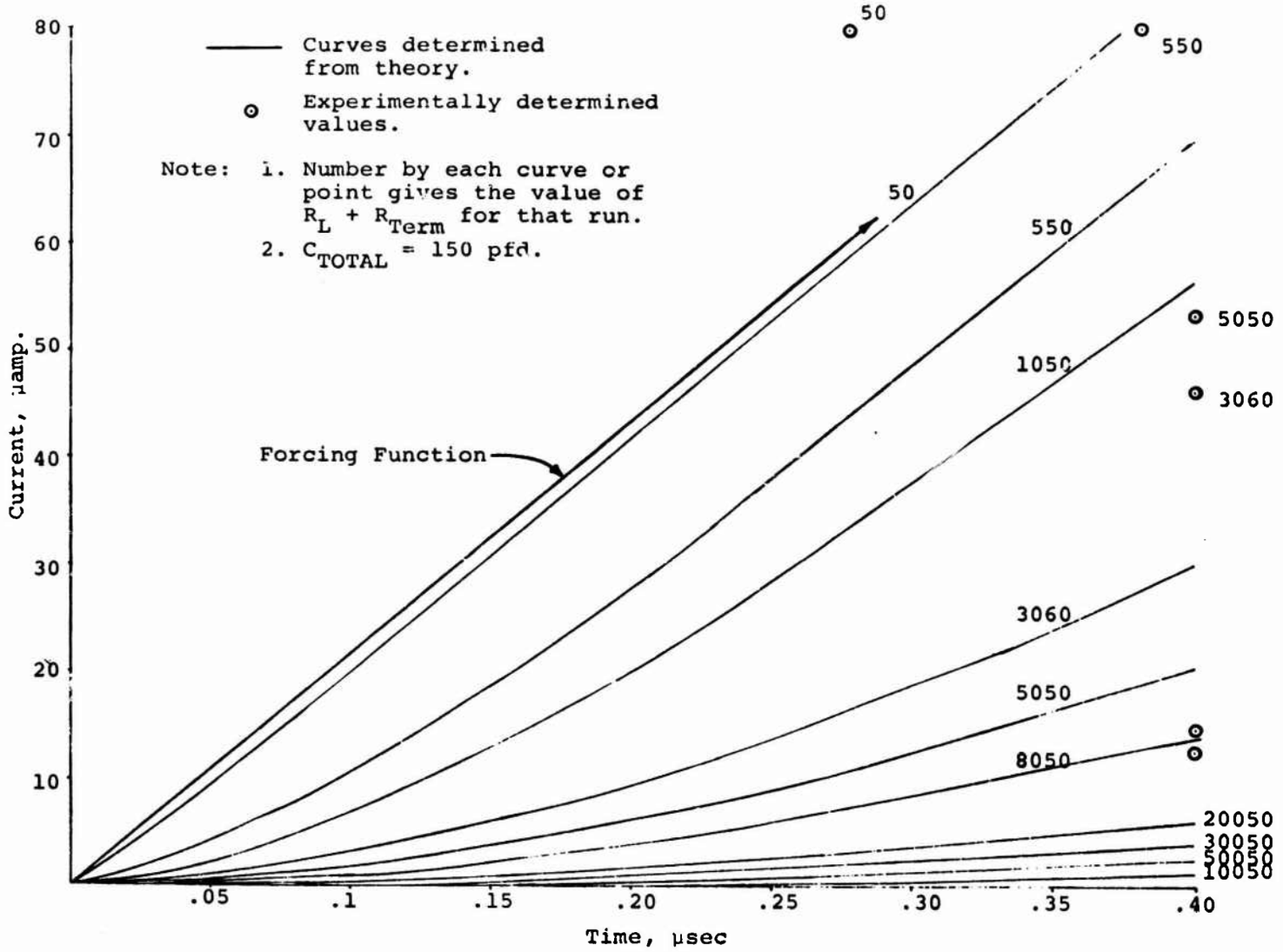

Figure 37. Effect of Size of Load Resistor on Current Generated by Quartz

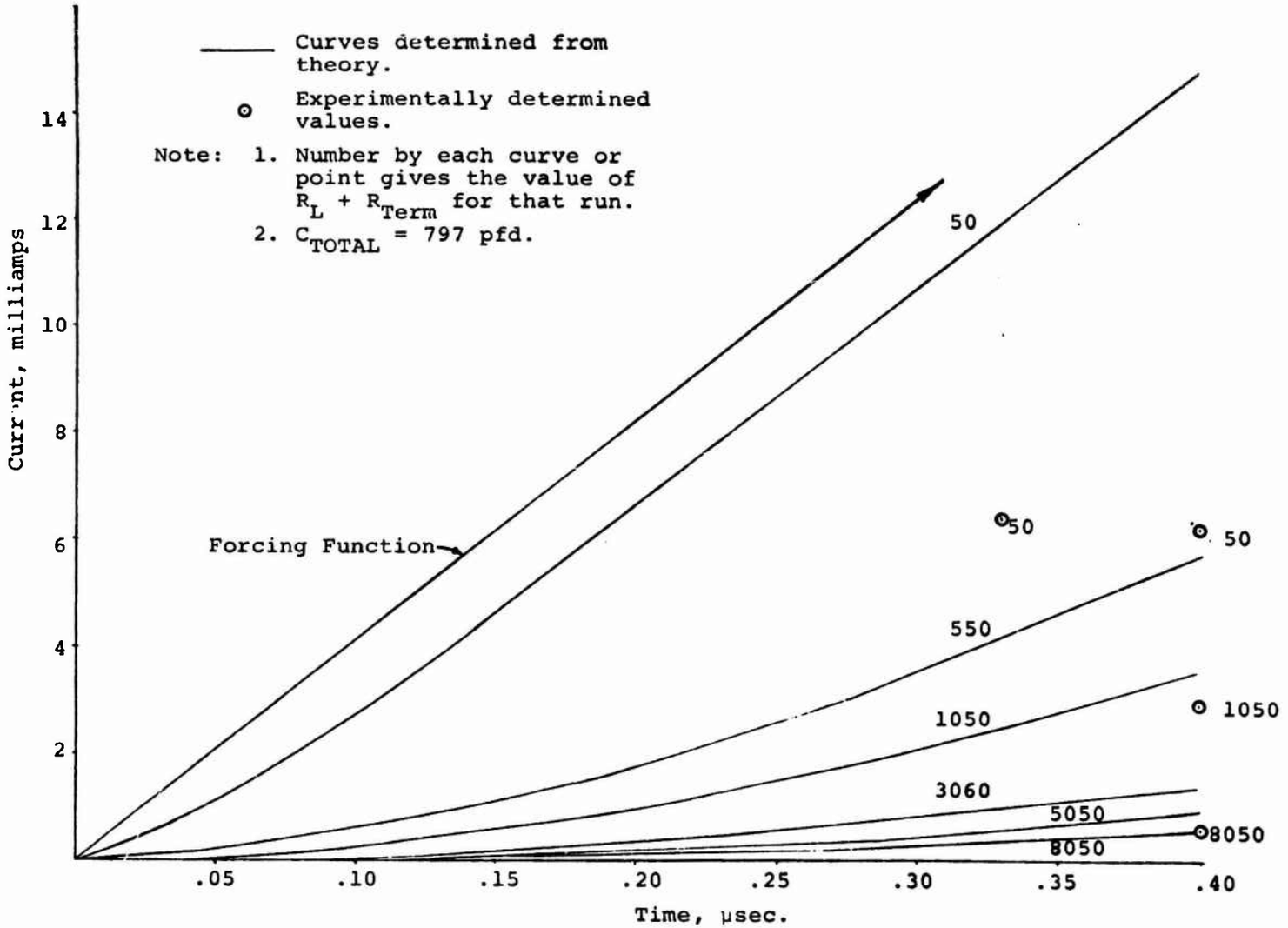

Figure 38. Effect of Size of Load Resistor on Current Generated by HST-41

A study of these figures indicates the following:

1. Theory and experiment are in general agreement for low stresses used in this phase of the work.
2. The agreement between the computed and measured values of current improves as the size of the load resistor increases. This is indicative of improper assumptions and/or measurement regarding circuit impedance. As the resistance becomes large, its impedance in the circuit then overrides the other effects.

The computed current time histories presented above were used to determine the energy dissipated in the load and termination resistor. The significant results from these computations are presented in Figures 39 and 40 for quartz and HST-41, respectively. These figures give representative values of energy generated for this type of excitation and give some indication of the effect of circuit resistance. These figures show that there will be some optimum value of total load resistance for maximum energy generation.

DYNAMIC TESTS--VACUUM-GUN FACILITY

Tests on the crystals utilizing the shock tube give very low applied stresses. The vacuum-gun facility was constructed for which the function was to test crystals under conditions of shock excitation similar to the shock tube, but to higher stress levels. Figure 41 shows a schematic of the gun. The gun is termed a vacuum gun since the chamber between the impact plate and projectile is evacuated before each shot. This serves two purposes: (1) it eliminates the air cushion between the projectile and the target, thus decreasing pulse rise time, and (2) it permits the atmospheric pressure to be used for the driving force.

Preliminary tests have been run with the gun and impact velocities up to 50 fps have been obtained. The most effective way of controlling the impact velocity is with the initial position of the projectile in the barrel, rather than the amount of vacuum drawn.

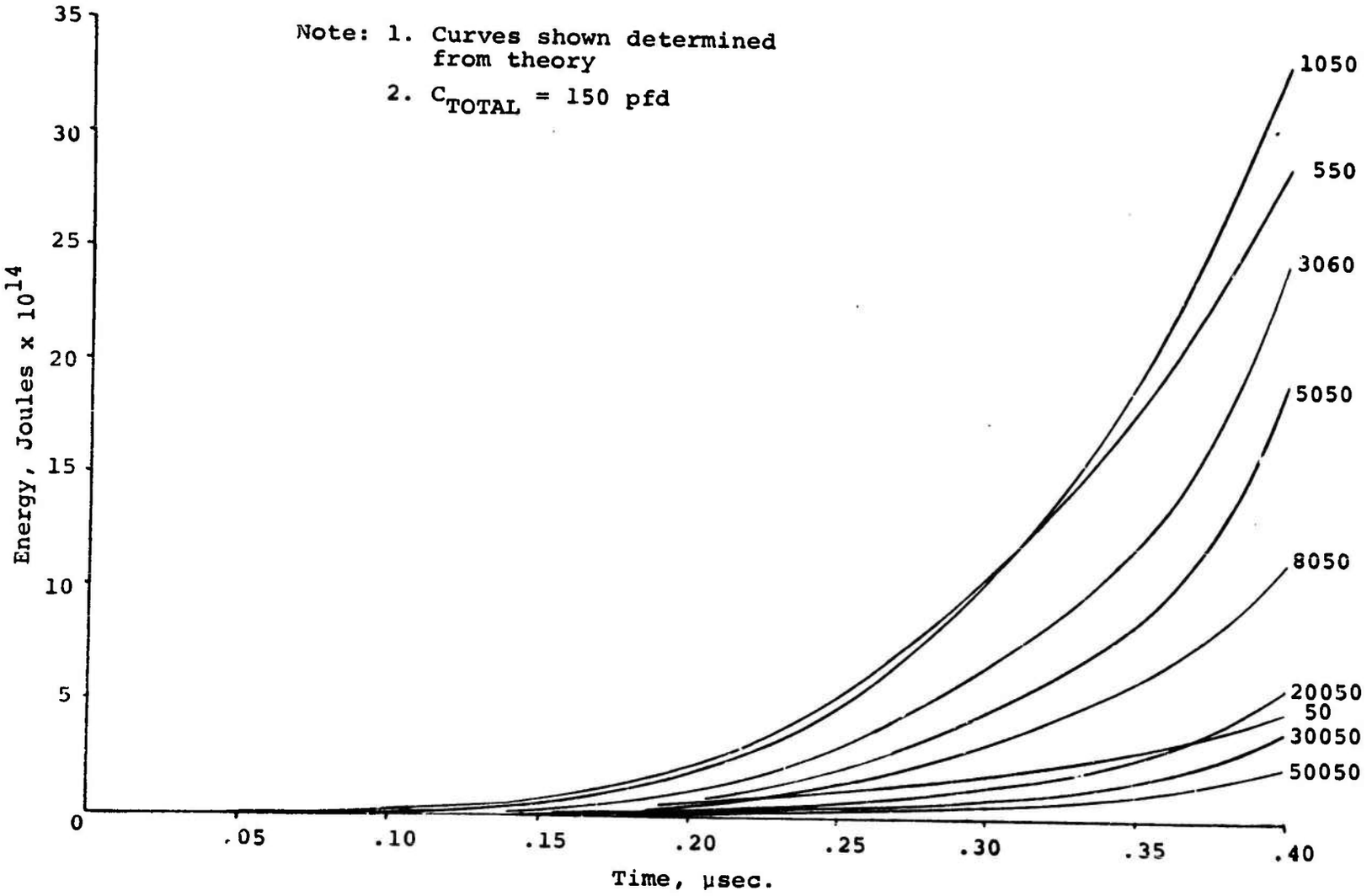

Figure 39. Effect of Size of Load Resistor on Energy Generated by Quartz

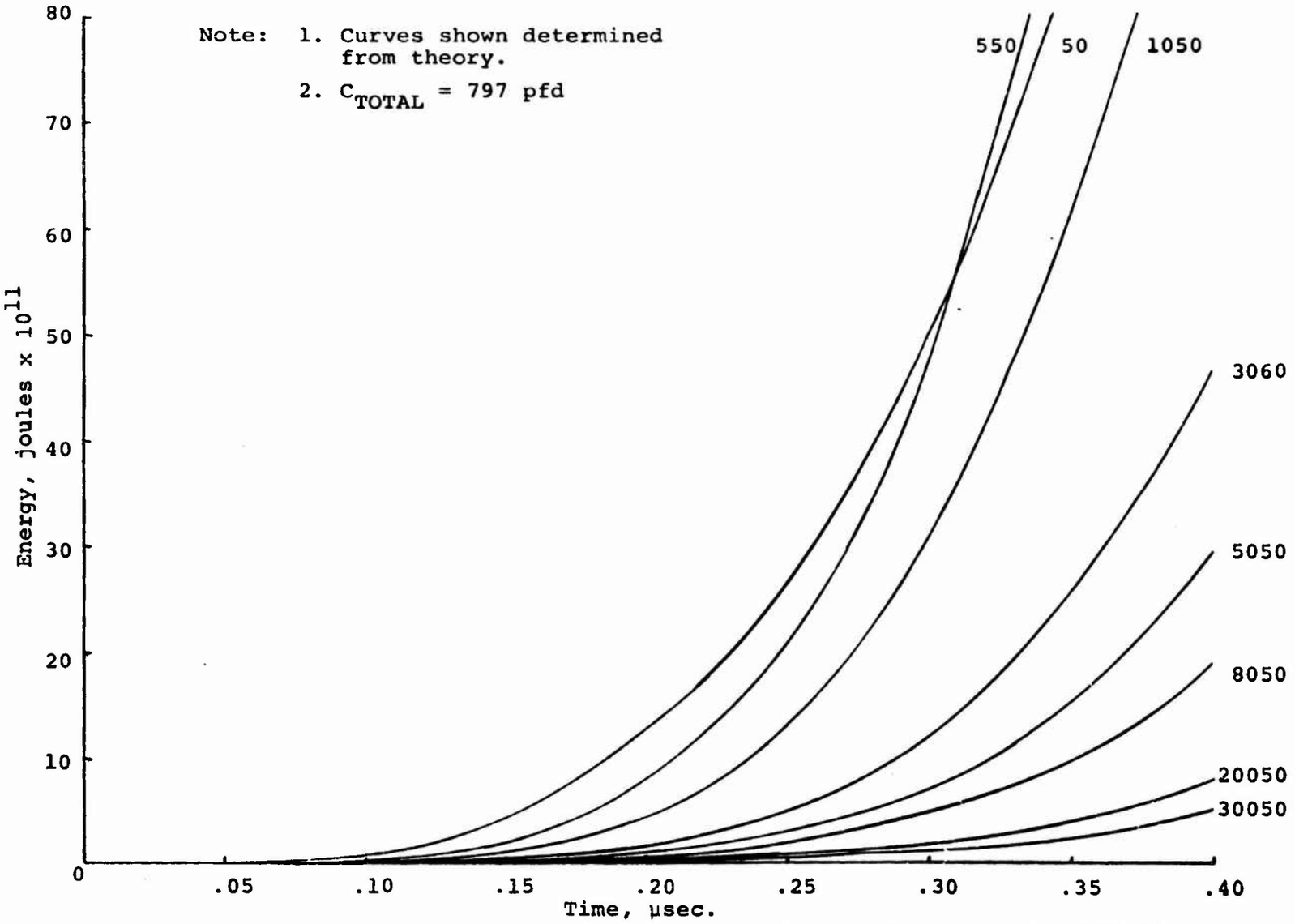

Figure 40. Effect of Size of Load Resistor on Energy Generated by HST-41

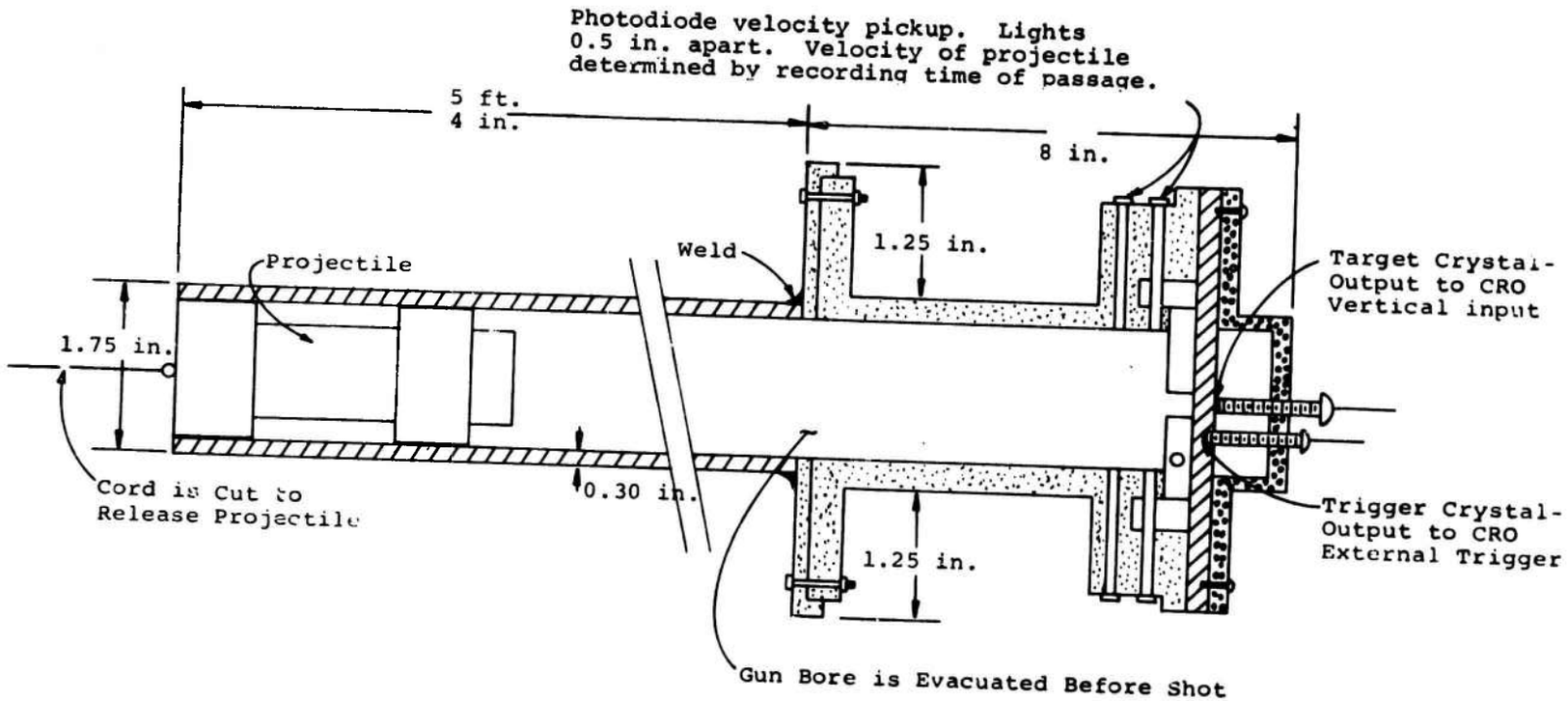

Figure 41. Vacuum-Gun Schematic

The initial tests also showed that the fit of the projectile in the barrel was not sufficiently close to give the desired planeness of impact. An indication of the importance of planeness of impact is given by this expression from Ref. 10:

$$\tan\phi = \frac{c}{U_o} \tan\theta$$

where θ = angle between impacting surfaces

ϕ = angle of wavefront in crystal

U_o = impact speed.

A study of this expression shows that the tilt angle of the impacting surfaces will be amplified by the ratio c/Uo. For low velocity impact of the magnitude being considered for this study, this amplification will be large, and θ must be minimized. Considerable time was spent grinding and polishing the base, and machining the projectiles to obtain a θ small enough. However, with the equipment available, it was not possible to obtain a sufficiently small θ for the wavefront developed in the crystal to be considered plane.

DYNAMIC TESTS--SPLIT HOPKINSON PRESSURE BAR

Work was also done on impulsive loading of crystals using a split Hopkinson pressure bar. The desirable characteristics of this method are that the input pulse may be controlled to a greater degree than with the other methods discussed, information on the pulse signature may be obtained from measurements rather than from the crystal, and geometry is one which could possible be applied to a proposed system. The geometry used is shown in Figure 42. The impulse to the input rod was applied with a projectile from the gas-gun developed for this contract, and strain gages were used to monitor the input pulse to the crystal. With this geometry, impact on the input rod does not have to be as nearly plane as for the case when the projectile strikes the crystal directly. When nonplanar impact occurs, the wavefront approaches the planar

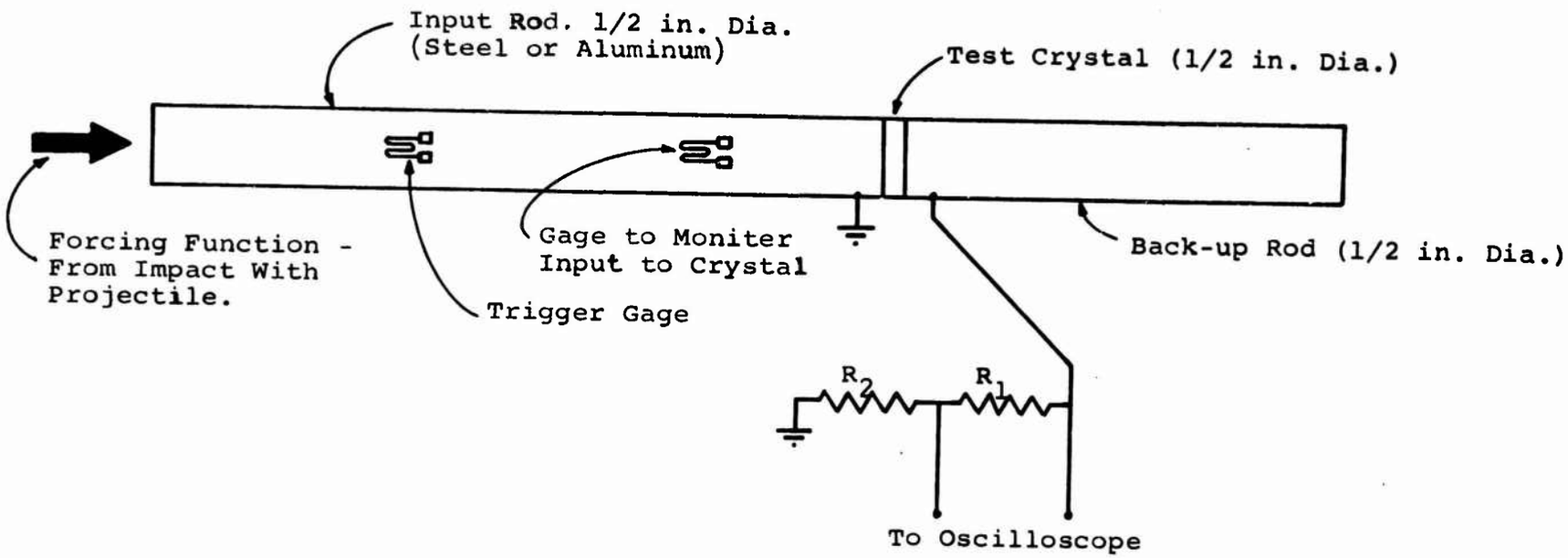

Figure 42. Schematic of Split Hopkinson Pressure Bar Test

condition as it moves down the rod. Since this geometry is less sensitive to the alignment of the impacting surfaces at impact, it is somewhat more feasible for use under conditions not found outside the test laboratory.

Since the purpose of this work was to determine energy levels which could be obtained from crystals under impact, the work for this type of loading was planned as follows:

1. Develop through the use of appropriate theory, an analytical method for predicting current and energy levels put out by the crystals under the test conditions.
2. Conduct several experiments to determine the system input and output during actual tests.
3. Verify the analytical model through comparison of measured outputs with computed values for the same system and system input.

Once the analytical model had been verified, it would have been possible to make studies with computer simulation in order to maximize the energy output.

The work done in pursuit of the above investigation will be presented in three subsections. The first subsection will be a discussion of the appropriate theory and computational procedures used in data reduction. The second subsection will describe the experimental phase of the work, and the last subsection will present the results.

THEORY AND COMPUTATIONAL PROCEDURES

When the input rod is struck on the end by the projectile, the disturbance initiated propagates down the rod and passes through the crystal. Therefore, the theory and analytical procedures required are wave propagation, current generation, and determination of energy dissipated by current through a resistor. This subsection is divided into the above three subsections.

1) Wave Propagation

The governing equations for the propagation of the disturbance in the rod initiated by projectile contact may be written in terms of the field equations

$$\frac{\partial \sigma}{\partial x} - \rho \frac{\partial v}{\partial t} = 0 \tag{13}$$

$$\frac{\partial \varepsilon}{\partial t} - \frac{\partial v}{\partial x} = 0 \tag{14}$$

and the constitutive relation

$$\frac{\partial \varepsilon}{\partial t} = f(\sigma,\varepsilon) \frac{\partial \sigma}{\partial t} \tag{15}$$

which is the assumed stress-deformation law for the materials in which the wave is propagating. Equation (13) results from the application of momentum priniciples to an element of the rod, and Equation (14) is the continuity requirement.

The above field equations were derived under the assumption that (1) plane cross section of the bar initially perpendicular to the axis remain plane and perpendicular to the axis at all times; (2) the axial stress component is the only non-zero stress; (3) the stress is uniformly distributed over the cross section; and (4) the longitudinal strain is given by the engineering strain, $\partial u/\partial x$, and it is the only non-zero component of strain. These equations are therefore based upon a one-dimensional theory.

The solutions to the field equation depends upon the stress-strain relation used. If the material is linearly elastic, we have

$$f(\sigma,\varepsilon) = \frac{1}{E_o} \tag{15a}$$

and if it is an elastic-plastic solid,

$$f(\sigma,\varepsilon) = \frac{1}{F(\varepsilon)} \tag{15b}$$

In the above two equations, $f(\sigma,\varepsilon)$ is the function in Equation (15) and $F(\varepsilon)$ is the static stress-strain function.

Equations (13), (14), and (15), when solved with the appropriate initial condition and boundary conditions for the problem of interest, would give stress and/or strain as a function of time at any cross section along the test specimen. The stress information at the cross sections located at the two faces of the crystal permits computation of the current through the circuit associated with the crystal, with the use of Equation (11).

This system of equations is hyperbolic and therefore is soluble by graphical integration along characteristics in the (x,t) plane even when the constitutive relation is of a form complex enough to prevent obtaining a close form analytical solution. This method, as it applies to wave propagation problems, has been discussed in detail in numerous papers (33,34), and it will not be discussed in detail here. However, a general description of the numerical procedure used will be given.

The significant relations upon which the numerical solution is based are the characteristics

$$\frac{dx}{dt} = \begin{cases} \pm c_o \\ \\ \pm c(\sigma,\varepsilon) \end{cases} \tag{16}$$

and the characteristic relations

$$dv = \pm \begin{cases} \frac{1}{\rho c_o} \, d\sigma \\ \\ \frac{1}{\rho c} \, d\sigma \end{cases} \tag{17}$$

$$d\varepsilon = \begin{cases} \frac{1}{E} \, d\sigma \\ \\ f(\sigma,\varepsilon)\, d\sigma \end{cases} \tag{18}$$

where

$$c(\sigma,\varepsilon) = \sqrt{\frac{1}{\rho f(\sigma,\varepsilon)}} \tag{19}$$

$$C_o = \sqrt{\frac{E_o}{\rho}} \tag{20}$$

The initial conditions for this problem are

$$t = 0, \quad x > 0: \qquad \sigma = \varepsilon = v = 0$$

and the boundary conditions are

$$t > 0, \quad x = 0: \quad \varepsilon = \varepsilon(t)$$ (as determined with a strain gage measurement.)

$$t > 0, \quad x \to \infty: \quad \sigma = \varepsilon = v = 0$$

The interfaces between the input rod and the crystal will be defined as x_1, and the interface between the crystal and the backup rod will be defined as x_2. Then,

$$v^1(x_1,t) = v^2(x_1,t) \tag{21}$$

$$\sigma^1(x_1,t) = \sigma^2(x_1,t) \tag{21a}$$

and

$$v^2(x_2,t) = v^3(x_2,t) \tag{22}$$

$$\sigma^2(x_2,t) = \sigma^3(x_2,t) \tag{22a}$$

In the above four conditions, the superscript identifies the element of the test specimen referred to: 1 is the input rod, 2 is the crystal, and 3 is the backup rod. Conditions 21 and 22 are the result of the crystal being securely bonded to the input and backup rod during the test duration of interest. Conditions 21a and 22a are the result of a force balance at the interfaces between the rods and the crystals, and the fact that the areas of all three elements are equal.

Since the solution in closed analytical form is seldom known for quasi-linear systems, such as this one, a finite difference method was used to obtain numerical solutions to the problem. Existence, uniqueness and stability of the solution of the initial value problem for the hyperbolic system of 'n' quasi-linear first-order partial differential equations have been established by various authors in the literature.

It is the direct replacement of the derivative along the characteristics that form the basis of the finite difference method. The following procedure was used for computing the solution of the initial value problem of Equations (17) and (18). The respresentative points in the (x,t) net are illustrated in Figure 43. Initially, only the conditions along α_0 characteristic are known. This characteristic has a slope of c_0^1 in the medium 1, c_0^2 in the medium 2 and c_0^3 $(=c_0^1)$ in the medium 3. Points of distance Δt apart are marked off along the t axis, and points of distance $c_0^1\Delta t$ in medium 1, $c_0^2\Delta t$ in medium 2 and c_0^3 in medium 3 are marked off on the x axis as shown in Figure 43. The solution for the characteristics and the field variables can then be made by approximation from time t to time $t+\Delta t$. As an example, the procedure for finding the values of σ, ε and v and therefore the slopes of α and β characteristics along the CD line will be described, assuming that the variables on the line AB are known from earlier computations.

From the values of σ, ε and v on AB, the slope of the α and β characteristics along AB are known to be $\pm \sqrt{1/\ f(\sigma,\varepsilon)}$, and this is shown in Figure 44. These slopes are used to draw straight-line approximations to the characteristics throughout

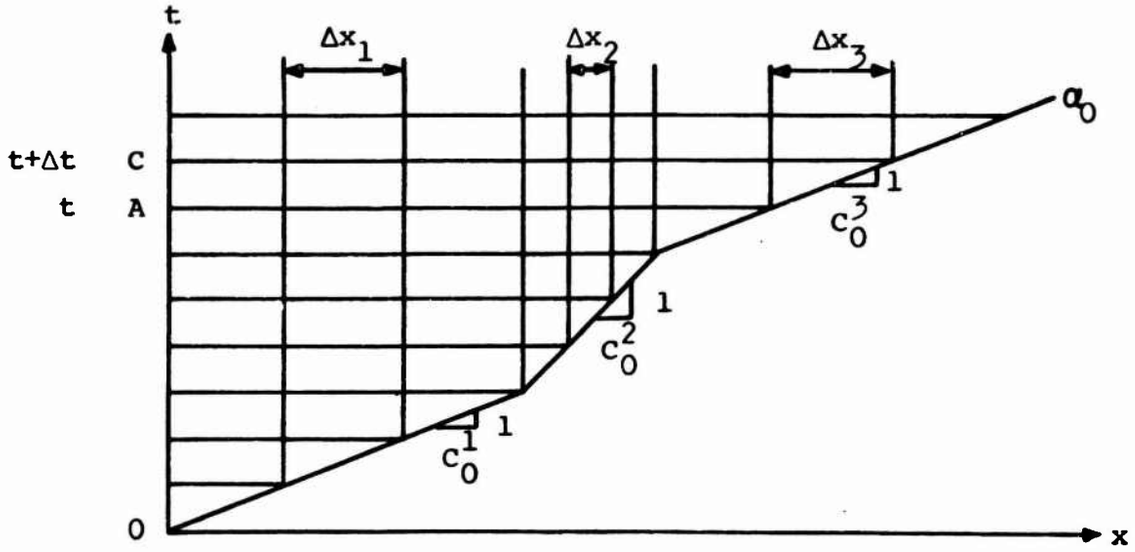

Figure 43. Characteristic Plane

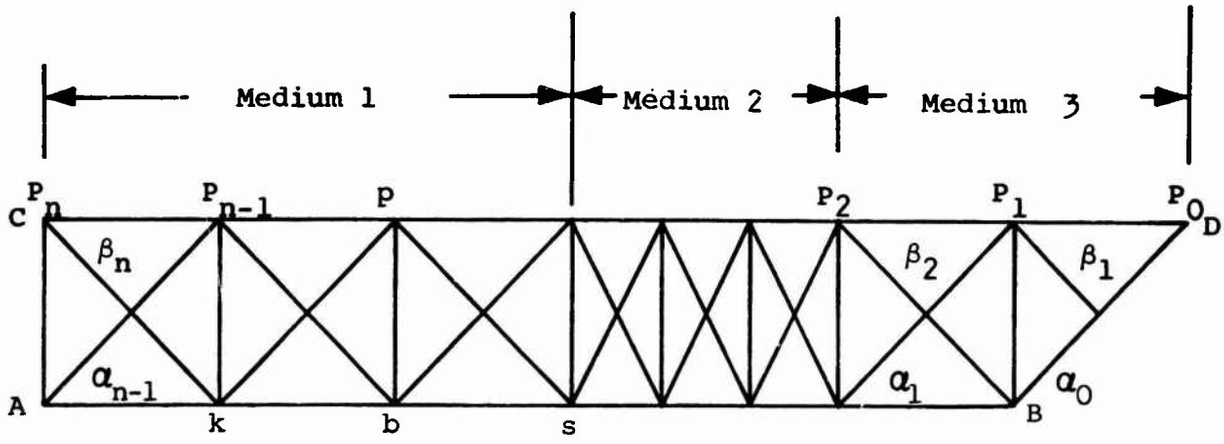

(a) Elastic Case

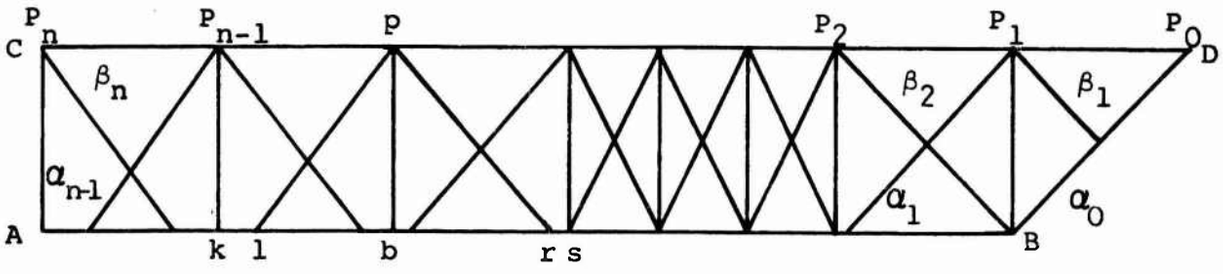

(b) Plastic Case

Figure 44. Region ABCD Removed from Characteristic Plane (Enlarged for Clarity)

the region ABCD. Through each of the points P_0, P_1, P_2, ..., P_{n-1}, P_n on CD, the characteristics are drawn by means of the slopes along AB. For determining the field variables along CD from the known values along AB, the following relations derived from Equations (17) and (18) are used:

Elastic case:

$$\varepsilon_p - \varepsilon_b - \frac{1}{E}(\sigma_p - \sigma_b) = 0$$

$$v_p - v_k - \frac{1}{\rho c_o}(\sigma_p - \sigma_k) = 0 \qquad (23)$$

$$v_p - v_s - \frac{1}{\rho c_o}(\sigma_p - \sigma_s) = 0$$

Plastic case:

$$\varepsilon_p - \varepsilon_b - f_b(\sigma_p - \sigma_b) = 0$$

$$v_p - v_\ell + \frac{1}{\rho c_\ell}(\sigma_p - \sigma_\ell) = 0 \qquad (23a)$$

$$v_p - v_r - \frac{1}{c_r}(\sigma_p - \sigma_r) = 0$$

From the known values of σ, ε and v at the mesh points k and b, the values of σ_ℓ, ε_ℓ and v_ℓ are known by linear interpolation. Similarly from the known values of σ, ε and v at the mesh points b and s, the values of σ_r, ε_r and v_r are known by linear interpolation. From the interpolated values σ, ε and v at ℓ and r, the slopes of the characteristics through ℓ and r; i.e., c_ℓ and c_r are known from Equation (19).

Equations (23) and/or (23a) can then be solved simultaneously, for determination of the values of σ_p, ε_p and v_p. The same

process is used to find the values of σ, ε and v at all mesh points P_o, P_1, ..., P_{n-1}, P_n along CD. By linear interpolation, the values of σ, ε and v at any arbitrary location on CD can be found from the computed values of σ, ε and v at the neighboring left and right mesh points on CD. In Equation (23) and (23a), the superscripts identifying the medium in which the point lies have been omitted from ρ, c, E, σ, and ε, for generality. When specific computations are made, the correct superscript must be used.

Successive applications of the scheme will enable the solution to be advanced in time as long as necessary.

2) Current Generation.

The short circuit current from a crystal loaded with a split Hopkinson pressure bar is given by Equation (5), repeated here for convenience:

$$i_{sc}(t) = \frac{d_{em}\, \Delta\sigma_m(t)\, Ac}{h} \qquad (5)$$

The difference in stress on the front and rear face of the crystal, $\Delta\sigma_m$, occurs in the split Hopkinson pressure bar test when the propagating pulse is in the rise or decay portion.

As previously mentioned, d_{em} in Equation (5) is the coefficient relating charge generated to force on the crystal, and as such, implies the relation is linear. This is known to be the case for quartz.* However, the static tests have shown this not to be true for the ferroelectric materials.

The current generated by the ferroelectric materials was determined by utilizing a nonlinear relation between charge and force. A cubic piecewise polynomial was fit to the experimental data using the method of natural cubic interpolating splines (35). This curve fitting technique was chosen because

*The values of d_{em} and c used in this equation for quartz were plane strain values, since the first passage of a strain wave in a thin disc of the type to be used is essentially plane.

it yields smoother approximations of the first derivative, which is the quantity of interest here. The curves obtained fit the experimental data quite well; there was, in fact, no visible deviation from the original data curve. See Figure 24, which shows points on the experimental curve which were determined from the curve fit routine. Being of polynomial form it is quite easy to obtain the required derivative of the approximating curve. Appendix D gives a listing of the computer program used for this curve fit.

Application of this program to Equation (5) required determination of a piezoelectric charge coefficient, which is the slope of the charge-force function, at a desired stress value. At a given instant of time in the computational procedure, the stress values used when determining the charge coefficient was the average of the stress on the faces of the crystal at that time. This technique would be correct only when the slope of the charge-force function is essentially constant within the stress range on the two faces of the crystal.

3) Energy Release

The usable energy released by the crystal is assumed to be that which is dissipated in the termination and load resistors. This may be computed as

$$E = \int_0^{t_o} i_R^2(t)\ (R_L + R_{TERM})\,dt \qquad (24)$$

This equation was evaluated with the use of a digital computer, and the program used is given as Appendix E.

In this equation, $i_R(t)$ is the current through the resistors. This current will be approximately the short circuit current; the difference between i_R and i_{sc} being due to the capacitance loading of the circuit. This affect has been investigated and the results discussed in Section V.

4) Summary

The loading of the piezoelectric-ferroelectric crystals with a split Hopkinson pressure bar occurs as a result of the passage of the strain wave through the crystal. The stress-time history on the front and rear surface of the crystal may be determined from a known input to the bar and a one-dimensional wave propagation theory. The appropriate crystal theory (with either linear or nonlinear force-charge relation) may then be used to compute the short circuit current from the crystal. This current is used to determine the electrical energy available for release in a resistor.

The discussion just completed has presented the appropriate theory and described the computational procedures used. These computational procedures were programmed for solution on a digital computer, and listings of these programs are given as Appendices.

Appendix B gives the program which computes the short circuit current and energy release through a resistor from a known strain-time input to the split Hopkinson pressure bar. This program is usable for a crystal which has either a linear or nonlinear force-charge relation. However, it is restricted to the case for which the intensity of impact is such that only elastic waves propagate in the pressure bar. Appendix C gives a listing of the program which is applicable when the impact on the bar is great enough to exceed the elastic limit of the material. In programming for this case, the strain-rate independent theory of plastic wave propagation was used. All other aspects of this program are similar to the one in Appendix B.

EXPERIMENTAL WORK

The actual test specimens used in this study were similar to that shown in Figure 42. Tests were conducted on specimens for which the bars were made of AISI 1095 steel and 6061-T6 aluminum. The input rod was 6 inches long, and the backup rod was 4 inches long.

The two different piezoelectric materials, x-cut quartz and HST-41 were used for the tests. The disks were 1/2-inch

in diameter, and two thicknesses of each material were used, .050 in. and .100 in. The x-cut quartz was chosen as one of the materials because its properties are well known and there is considerable documentation of its previous usage in transient measurements in the literature. In addition, it has a nearly constant charge coefficient and shows little sensitivity to strain in other than the x-direction, hence the effect of violating the assumptions of uniaxial stress or strain is limited to the difference in mechanical stiffness between the two cases about 10%) which is well understood. It was felt that the quartz tests would serve as a rough check on the validity of the computer solution of the wave equations, the crystal current output equation, and experimental technique.

The HST-41 was chosen as a representative ferroelectric. It has a nonlinear charge coefficient, and is a readily available material, but it also has a high cross-sensitivity (to both manual and shear strain), and a high electro-mechanical coupling coefficient (about .3 to .6). The nonlinearity of the charge coefficient made it necessary to use the nonlinear charge force relation developed for this purpose from static tests.

The piezoelectric discs were bonded to the appropriate surfaces of the bar with an epoxy adhesive. The incident wave through the crystal was measured with foil resistance strain gages mounted in opposed pairs on the surface of the rod. Two sets of gages were used. One set was mounted 2 in. in front of the tests disc to serve as trigger gages for the recording oscilloscopes. The incident strain pulse profile was measured by a second pair 1 in. in front of the disc. For recording, the gages were wired in opposite arms of a 4-arm Wheatstone bridge to cancel any bending strains.

Recording of both the strain gage signals and the crystal signal was done on Type 555 Tektronix oscilloscopes equipped with Type 1A5 plug-ins. This system had a bandwidth from DC to 30 MHz (at maximum plug-in gain), which was more than adequate to faithfully display the signals from the sensors. The signal from the crystals was terminated using a Tektronix 50-ohm terminator.

Tests on these specimens were conducted at two locations. The low speed impact tests were conducted at The University of New Mexico. The projectile was driven by the air gun constructed for use on the studies supported by this contract. The high speed tests were conducted at Arnold Engineering Development Center, Arnold Air Force Station, Tennessee.

The impact speeds for the tests conducted at the UNM facility were selected to cause only elastic strains in the input rod. The approximate impact speed used for all tests was 50 fps. This yielded stress levels in the steel input rod of about 40,000 psi, and about 20,000 psi in the aluminum rod. The projectile used on all tests was a 1/2 in. diameter steel rod, about 6 in. long, supported in the air gun barrel on each end by nylo sealing rings. The sealing rings also served to keep the rod aligned in the gun barrel. This type of projectile was chosen for two reasons. First, it allowed the impact problem to be simplified to that of impact between two bars of the same diameter, and second, it minimized momentum transfer to the test rod, thereby reducing the damage done to the bar and instrumentation when its motion was arrested after impact.

The first two series of tests were conducted with the end of the projectile ground flat. However, it was decided that any misalignment between the test rod and the projectile would produce bending stress waves in the rod. While this would not effect the output of the strain circuitry, it would effect the output of the crystal. Consequently, subsequent tests were made with the impact end of the projectile ground slightly spherical. There was, however, no observable difference in either case.

One entry was made on the "G" Range at AEDC, to determine crystal output for very high impact speeds. The "G" range at AEDC is a two-state powder-nitrogen gun approximately 100 ft. long.

The projectile used in these tests was a 2-1/2 inch diameter aluminum slug, 2-1/2 inches long. The recording equipment used during these tests was essentially the same as that used for the tests at UNM.

Two types of specimens were used; one identical to that shown in Figure 42, and the other a similar geometry in which the crystal was omitted. The rod was continuous, and strain gages were mounted on the rod at the crystal station. The purpose of the tests on the second type of specimen was to determine the amount of attenuation of the propagating wave from the monitoring station to the crystal location.

Six tests were conducted at AEDC on these types of specimens; three without a crystal and three with. Due to the difficulties encountered with noise, triggering, and gain settings, usable data were obtained only on one specimen without a crystal and two with the crystal. Data from these tests is shown in Figures 45, 46, 47 and 48.

Four series of crystal tests were conducted on the air gun at UNM. By a series of tests, it is meant one entry on the gun with a group of prepared test specimens. This procedure was used since the input rod and back-up rod could be reused after each test. So preparing a specimen, after the rods were once made, consisted of cleaning and bonding new crystals in place.

In the first three series of tests the ferroelectric crystals used were some furnished earlier by AFWL. It was later discovered that their exact origin and age could not be accurately determined, and data had indicated this to be a factor. Consequently, for the fourth series of tests, a new quantity of HST-41 crystals was ordered. The results of the tests on these crystals is considered the most valid. The crystals used in the static determination of the nonlinear charge coefficient were also from this new set of HST-41 crystals.

The x-cut quartz specimens used in all tests were, however, of known origin. Since the piezoelectric properties of quartz are natural, they are not affected by age and so all of the tests in the 5 series will be used.

Table VI summarizes the tests run at UNM. Figures 49 through 65 show the data obtained for these tests.

I. Test Specimen

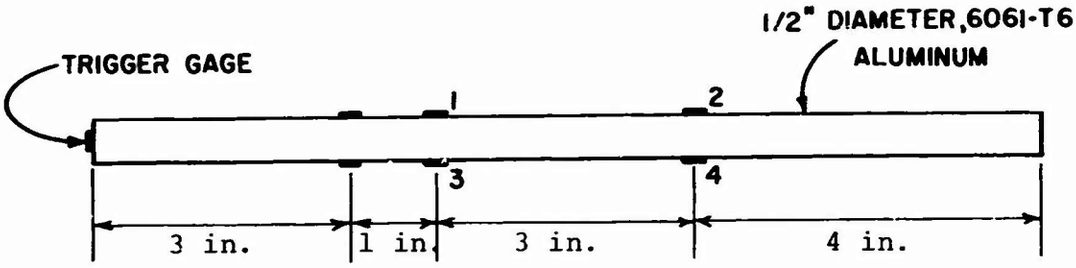

All measuring gages are type HE-111 (Budd Co.), 1/16 in. gage length (F =2.04, R = 120 ohm).

II. Projectile

2½ inch diameter x 2½ inch long aluminum.

Impact speed: 8190 fps

III. Circuit Information

Each measuring gage was the only active gage in a bridge circuit.

Gage 1: R_{cal}: 12,000 ohms Scale factor: 4950 με/cm.

Gage 3: R_{cal}: 20,000 ohms Scale factor: 2985 με/cm.

Gage 4: R_{cal}: 20,000 ohms Scale factor: 2985 με/cm.

IV. Scope Data

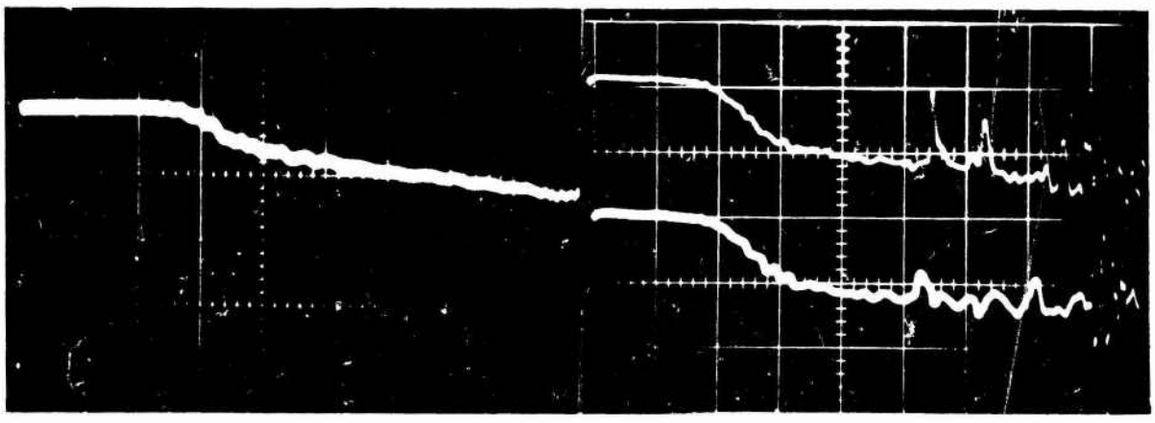

Upper beam: Gage 1
Lower beam: Radiometer(trigger)
Sweep: 5μsec/cm→
Delay: 5μsec

Upper beam: Gage 3
Lower beam: Gage 4
Sweep: 5μsec/cm→
Delay: 25μsec

Figure 45. Data for Rod Test Without Crystal AEDC Test No. 1204 (Data from other scopes on the above gages were obtained, but those shown were the best.)

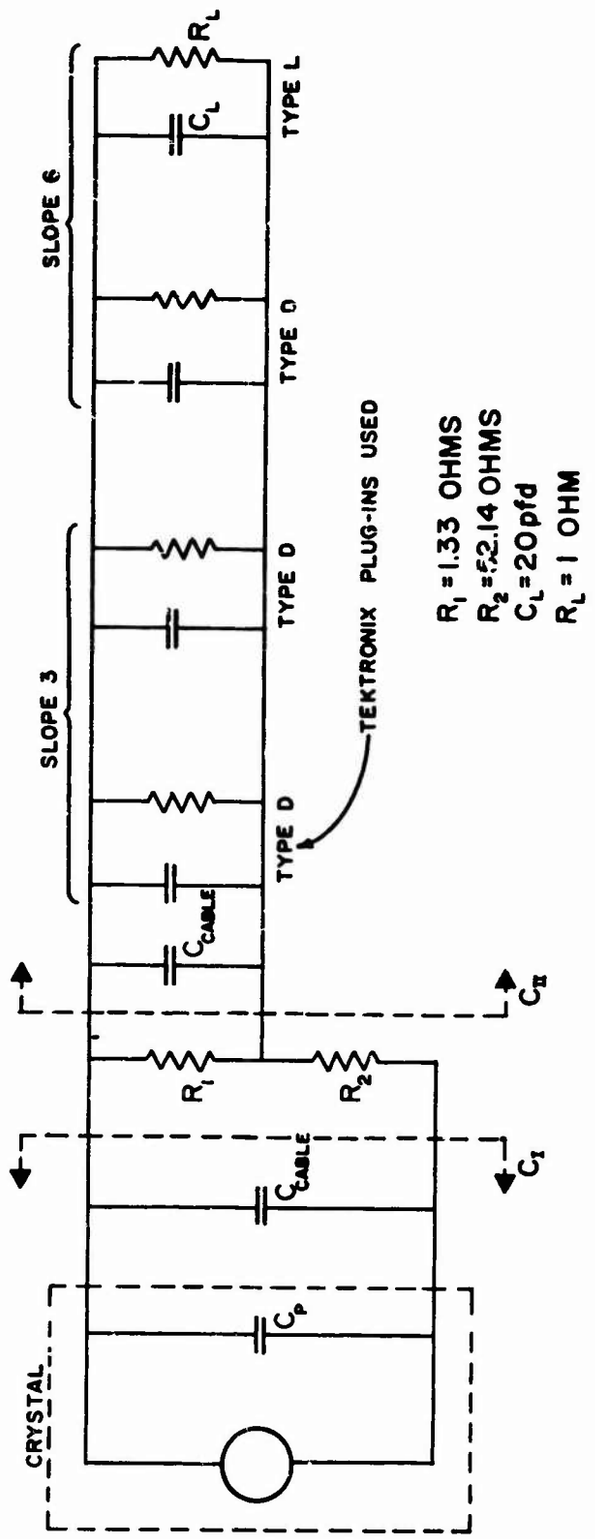

Figure 46. Recording Circuit Data for Crystal Tests Run at AEDC

I. Test Specimen

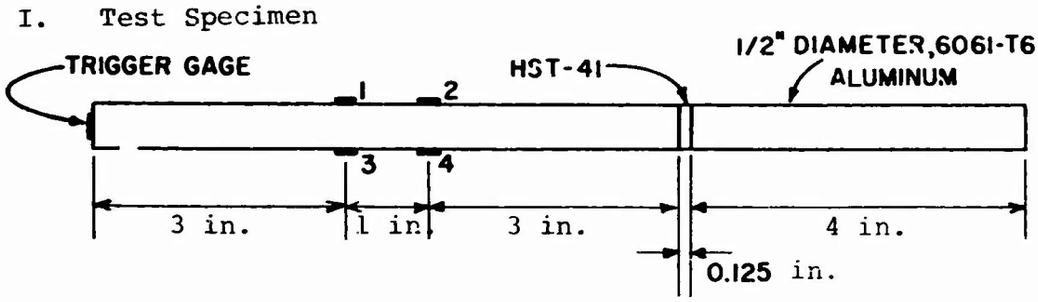

All measuring gages are type HE-111 (Budd Co.), 1/16 gage length (F =2.04, R = 120

II. Projectile: 2½ inch diameter x 2½ inch long aluminum

Impact speed: 8380 fps

III. Circuit Information

Crystal Circuit: C_I = 1210 pfd
C_{II} = 611 pfd See Figure 46
C_p = 587 pfd

Gage circuit, Gages 3 and 4: R_{cal}: 20,000 ohm
Scale factor: 2985 με/cm

IV. Scope Data

Crystal data

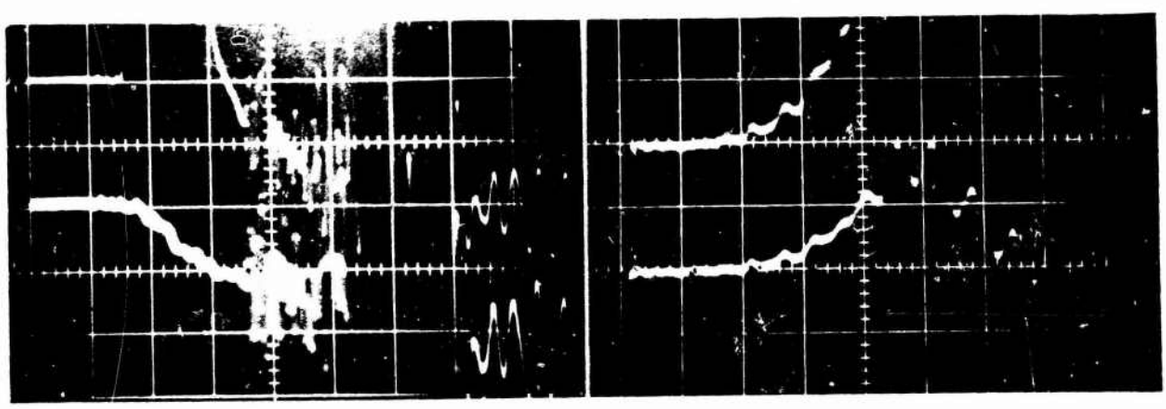

Scope 2 Upper Beam: Gage 3 Scope 3 Upper Beam: 2v/cm
Lower Beam: Gage 4 Lower Beam: 5v/cm
Sweep: 5μsec/cm → Sweep: 2μsec/cm
Delay: 10μsec Delay: 29μsec

Figure 47. Data for Rod Test with Crystal. AEDC Test No. 1206 (Data from other scopes were obtained, but those shown were used in data reduction.)

I. Test Specimen

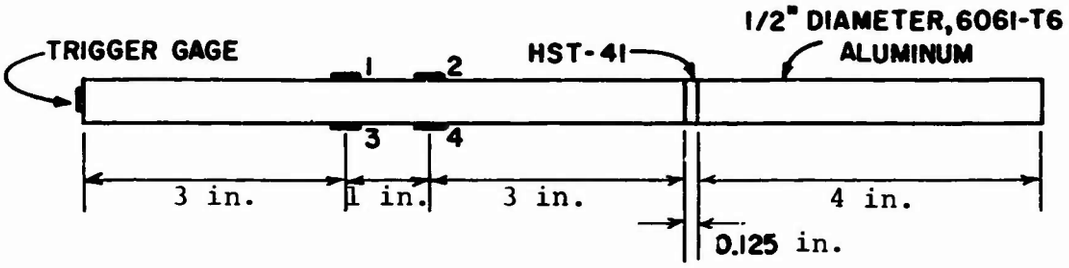

All measuring gages are type HE-111 (Budd Co.), 1/16 in. gage length (F = 2.04, R = 120 ohm).

II. Projectile: 2½ in. diameter x 2½ in. long aluminum

Impact speed: 8150 fps

III. Circuit Information

Crystal circuit: C_I = 1175 pfd

C_{II} = 615 pfd

C_p = 600 pfd

Gage circuit: Gages 3 and 4: R_{cal}: 20,000 ohm

Scale factor: 2985 με/cm

IV. Scope Data

Crystal data

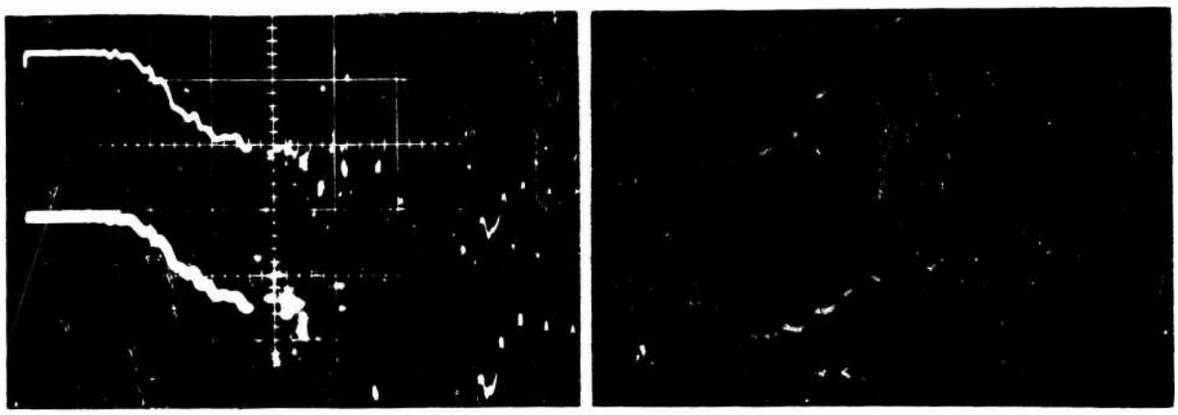

Scope 2 Upper beam: Gage 3
Lower beam: Gage 4
Sweep: 5μsec/cm→
Delay: 10μsec

Scope 3 Upper beam: 2v/cm
Lower beam: 5v/cm
Sweep: 2μsec/cm→
Delay: 29μsec

Figure 48. Data for Rod Test with Crystal. AEDC Test No. 1207 (Data from other scopes were obtained, but those shown were used in data reduction.)

TABLE VI

SUMMARY OF TESTS RUN AT UNM

Series	Test	Crystal Mat'l	Thick-ness, Inch	Rod Mat'l	Data Obtained	Comments
1	1	PZT-4	.100	Steel	Yes	
	2	Quartz	.050	Steel	No	gain set wrong
	3	Quartz	.050	Alum	Yes	
	4	Quartz	.100	Alum	Yes	
	5	Quartz	.100	Steel	Yes	
2	1	Quartz	.050	Steel	No	bad connection
	2	Quartz	.050	Alum	Yes	
	3	Quartz	.100	Steel	Yes	
	4	Quartz	.100	Alum	Yes	
	5	PZT-4	.100	Steel	Yes	
	6	Pzt-4	.100	Steel	Yes	
3	1	Quartz	.050	Steel	No	no trigger
	2	HST-41	.050	Steel	No	late trigger
	3	HST-41	.050	Steel	Yes	
	5	Quartz	.100	Alum	Yes	
	6	Quartz	.050	Alum	Yes	
4	1	HST-41	.100	Steel	Yes	peak current lost
	2	HST-41	.050	Steel	Yes	
	3	Quartz	.050	Alum	Yes	
	4	HST-41	.050	Steel	Yes	
	5	HST-41	.100	Steel	Yes	

I. Test Specimen

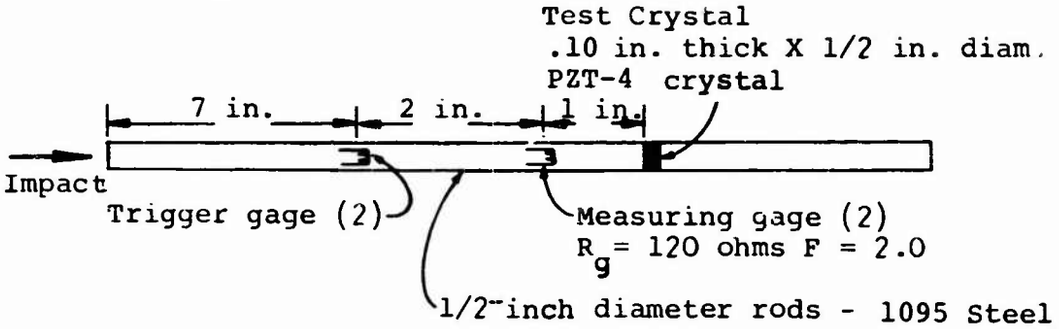

II. Projectile and Velocity Information

Projectile length - 6.7 in. Time increment - 14216 µsec.

Firing pressure - 3.5 psig. Impact Velocity - 39.? fps.

III. Circuit Information

a. Strain circuit.

Number of active arms - 2
Bridge current - 30 milliamps
Equivalent strain - 750 µin/in/division
R_{cal} = 20 K ohms/2 divisions

b. Current circuit.

R_L = 50 ohms
R_{term} = 50 ohms (50-ohm Tektronix terminating resistor was used.)

IV. Scope Data

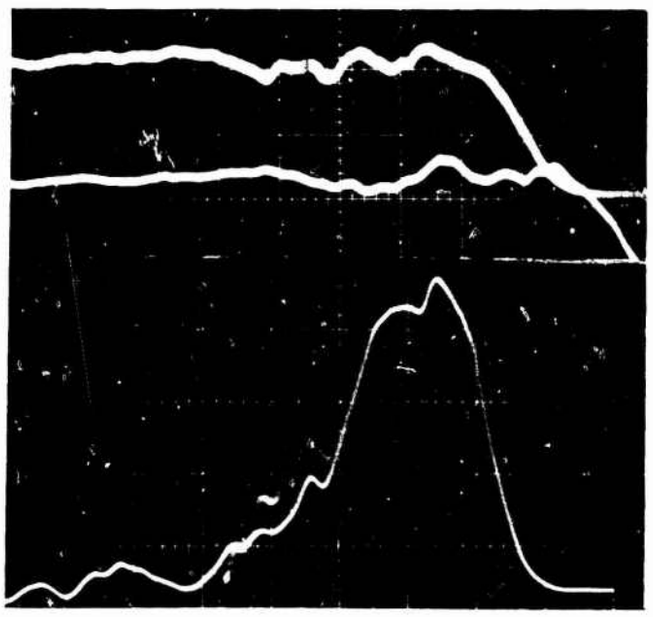

Upper trace - Strain
Sweep - 5 µsec/div
Gain - 750 µin/in/div (equivalent)

Lower trace - current
Sweep - 5 µsec/div
Gain - 20 volts/div
Delay - 5 µsec from strain data

Figure 49. Data for Crystal Test 1, Series 1

I. Test Specimen

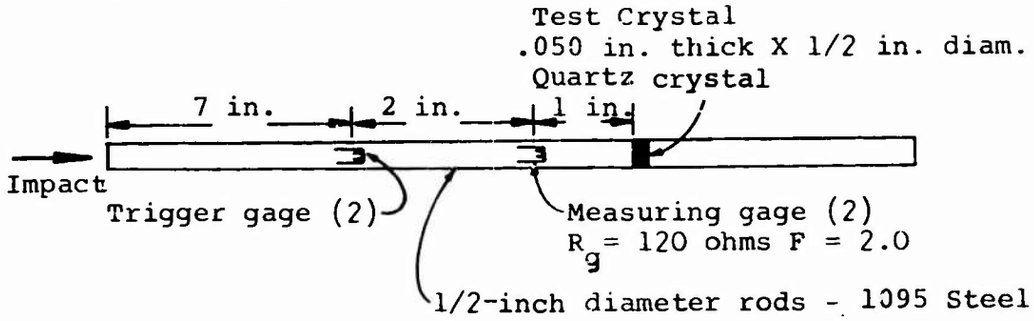

II. Projectile and Velocity Information

Projectile length - 6.7 in. Time increment - 13697 μsec.

Firing pressure - 3.5 psig. Impact Velocity - 40.7 fps.

III. Circuit Information

a. Strain circuit.

Number of active arms - 2
Bridge current - 30 milliamps
Equivalent strain - 750 μin/in/division
R_{cal} = 20 K ohms/2 divisions

b. Current circuit.

R_L = 50 ohms
R_{term} = 50 ohms (50-ohm Tektronix terminating resistor was used.)

IV. Scope Data

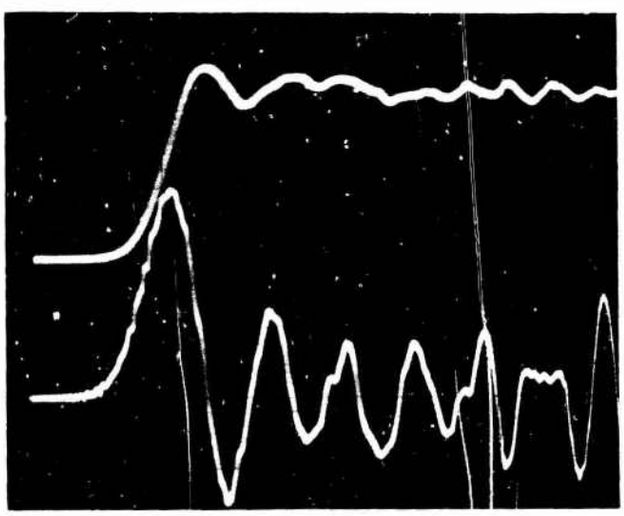

Upper trace - Strain
Sweep - 5 μsec/div
Gain - 750 μin/in/div (equivalent)

Lower trace - current
Sweep - 5 μsec/div
Gain - .2 volts/div
Delay - 5 μsec from strain data

Figure 50. Data for Crystal Test 3, Series 1

I. Test Specimen

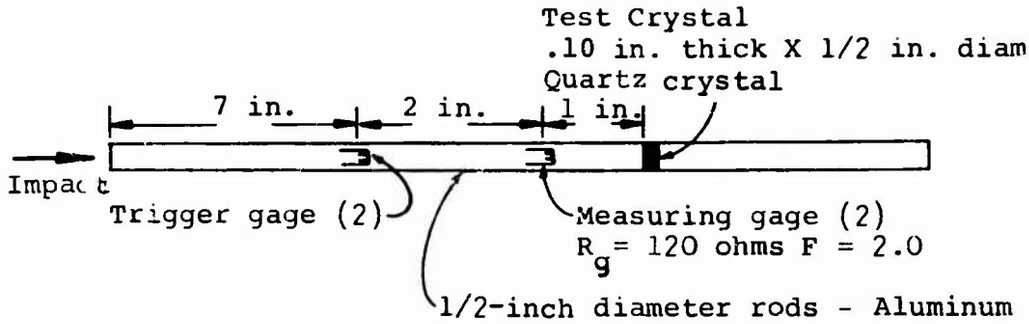

II. Projectile and Velocity Information

Projectile length - 6.7 in. Time increment - 13643 μsec.

Firing pressure - 3.5 psig. Impact Velocity - 40.9 fps.

III. Circuit Information

a. Strain circuit.

Number of active arms - 2
Bridge current - 30 milliamps
Equivalent strain - 750 μin/in/division
R_{cal} = 20 K ohms/2 divisions

b. Current circuit.

R_L = 50 ohms
R_{term} = 50 ohms (50-ohm Tektronix terminating resistor was used.)

IV. Scope Data

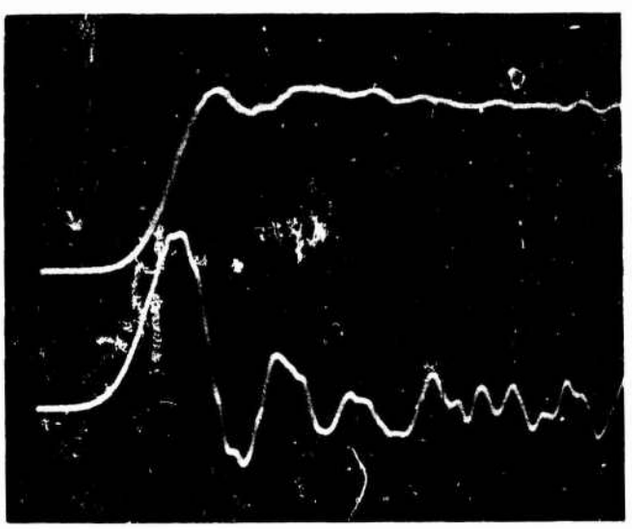

Upper trace - Strain
Sweep - 5 μsec/div
Gain - 750 μin/in/div (equivalent)

Lower trace - current
Sweep - 5 μsec/div
Gain - .2 volts/div
Delay - 5 μsec from strain data

Figure 51. Data for Crystal Test 4, Series 1

I. Test Specimen

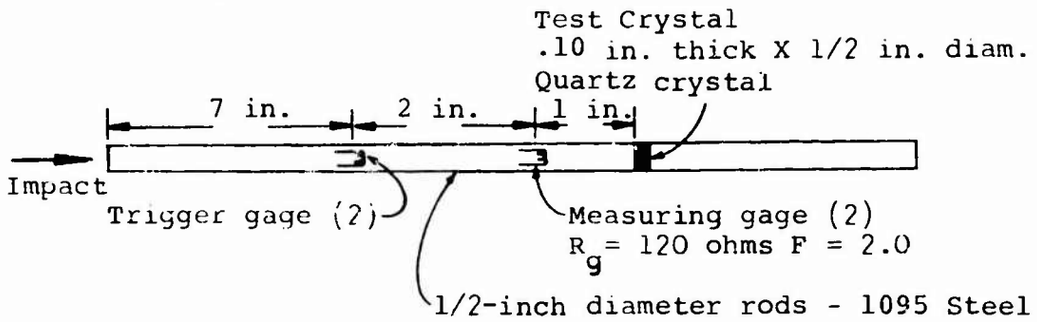

II. Projectile and Velocity Information

Projectile length - 6.7 in. Time increment - 13915 μsec.

Firing pressure - 3.5 psig. Impact Velocity - 40.1 fps.

III. Circuit Information

a. Strain circuit.

Number of active arms - 2
Bridge current - 30 milliamps
Equivalent strain - 750 μin/in/division
R_{cal} = 20 K ohms/2 divisions

b. Current circuit.

R_L = 50 ohms
R_{term} = 50 ohms (50-ohm Tektronix terminating resistor was used.)

IV. Scope Data

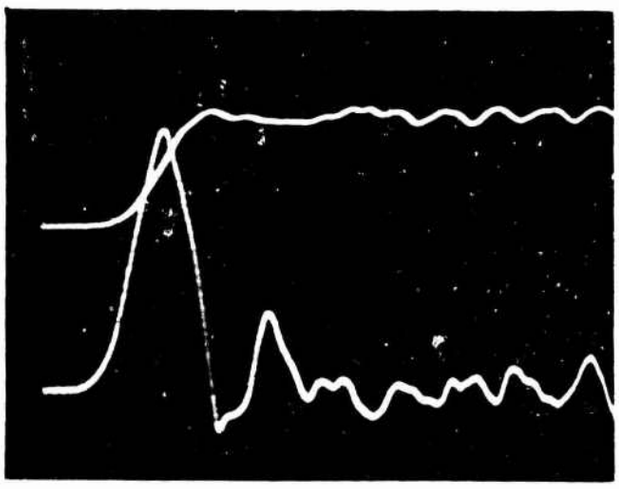

Upper trace - Strain
Sweep - 5 μsec/div
Gain - 750 μin/in/div (equivalent)

Lower trace - current
Sweep - 5 μsec/div
Gain - .2 volts/div
Delay - 5 μsec from strain data

Figure 52. Data for Crystal Test 5, Series 1

I. Test Specimen

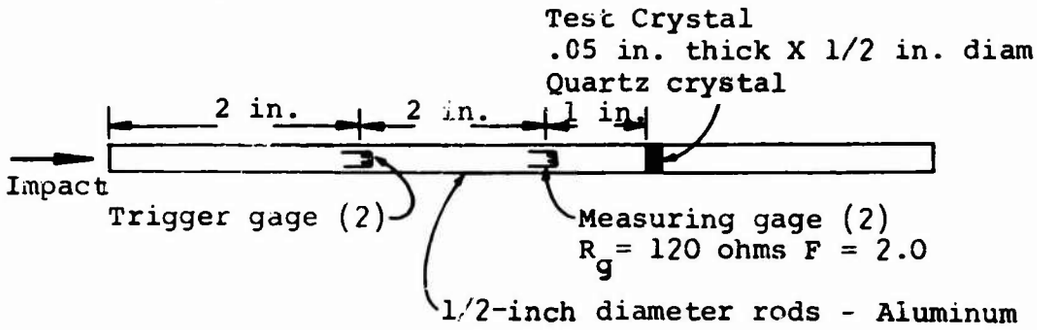

II. Projectile and Velocity Information

Projectile length - 6.7 in. Time increment - 13595 μsec.

Firing pressure - 3.5 psig. Impact Velocity - 41.0 fps.

III. Circuit Information

a. Strain circuit.

Number of active arms - 2
Bridge current - 30 milliamps
Equivalent strain - 750 μin/in/division
R_{cal} = 20 K ohms/2 divisions

b. Current circuit.

R_L = 50 ohms
R_{term} = 50 ohms (50-ohm Tektronix terminating resistor was used.)

IV. Scope Data

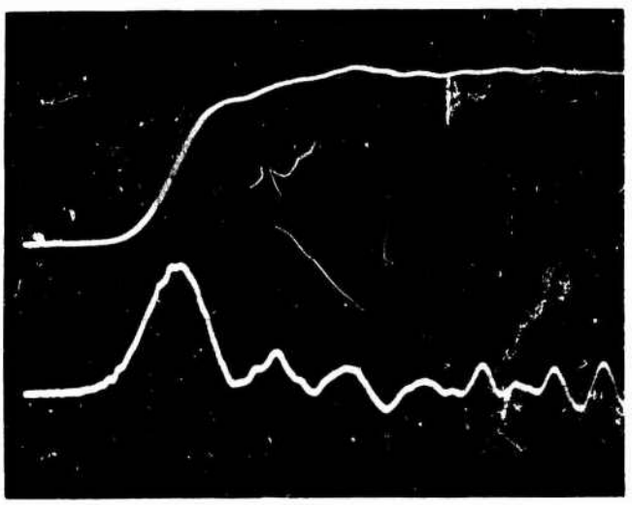

Upper trace - Strain
Sweep - 5 μsec/div
Gain - 750 μin/in/div (equivalent)

Lower trace - current
Sweep - 5 μsec/div
Gain - .2 volts/div
Delay - 5 μsec from strain data

Figure 53. Data for Crystal Test 2, Series 2

I. Test Specimen

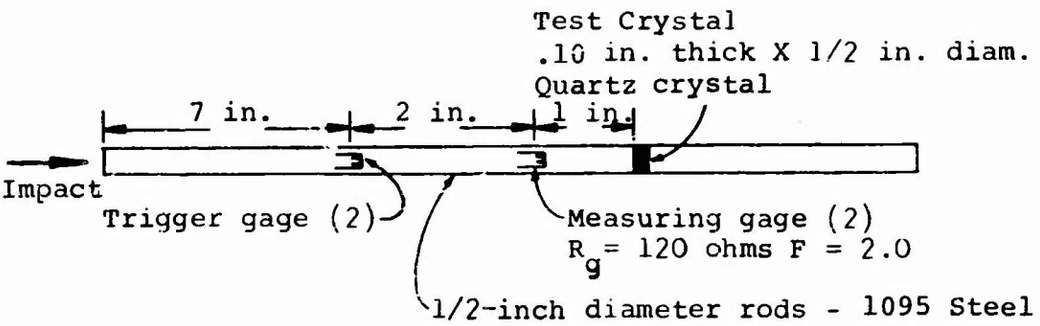

II. Projectile and Velocity Information

Projectile length - 6.7 in. Time increment - 13775 μsec.

Firing pressure - 3.5 psig. Impact Velocity - 40.5 fps.

III. Circuit Information

a. Strain circuit.

Number of active arms - 2
Bridge current - 30 milliamps
Equivalent strain - 750 μin/in/division
R_{cal} = 20 K ohms/2 divisions

b. Current circuit.

R_L = 50 ohms
R_{term} = 50 ohms (50-ohm Tektronix terminating resistor was used.)

IV. Scope Data

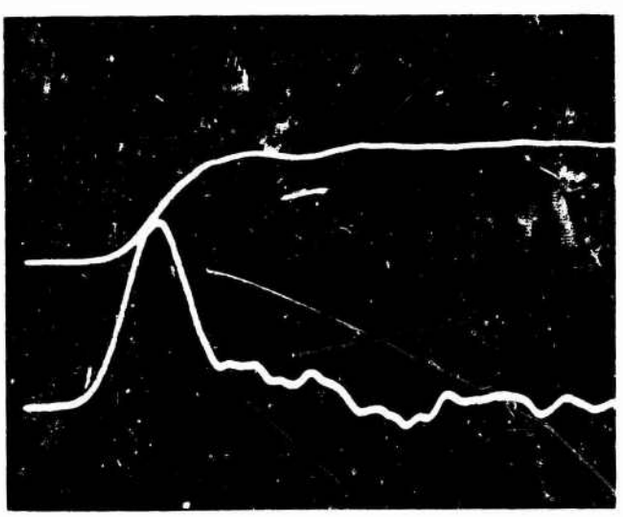

Upper trace - Strain
Sweep - 5 μsec/div
Gain - 750 μin/in/div (equivalent)

Lower trace - current
Sweep - 5 μsec/div
Gain - .2 volts/div
Delay - 5 μsec from strain data

Figure 54. Data for Crystal Test 3, Series 2

I. Test Specimen

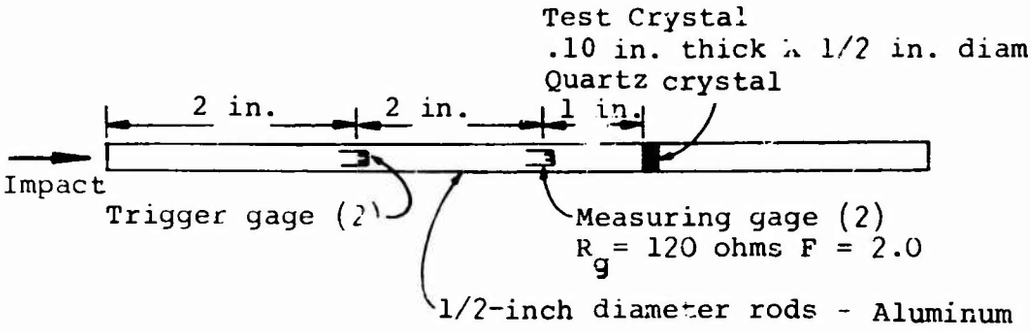

II. Projectile and Velocity Information

Projectile length - 6.7 in. Time increment - 13555 μsec.

Firing pressure - 3.5 psig. Impact Velocity - 41.1 fps.

III. Circuit Information

a. Strain circuit.

Number of active arms - 2
Bridge current - 30 milliamps
Equivalent strain - 750 μin/in/division
R_{cal} = 20 K ohms/2 divisions

b. Current circuit.

R_L = 50 ohms
R_{term} = 50 ohms (50-ohm Tektronix terminating resistor was used.)

IV. Scope Data

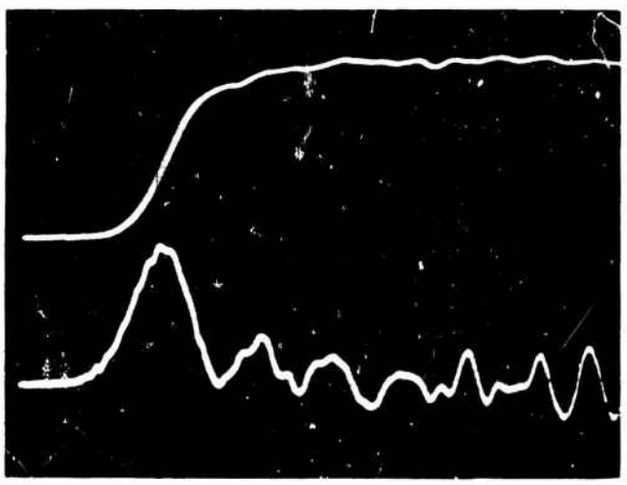

Upper trace - Strain
Sweep - 5 μsec/div
Gain - 750 μin/in/div (equivalent)

Lower trace - current
Sweep - 5 μsec/div
Gain - .2 volts/div
Delay - 5 μsec from strain data

Figure 55. Data for Crystal Test 4, Series 2

I. Test Specimen

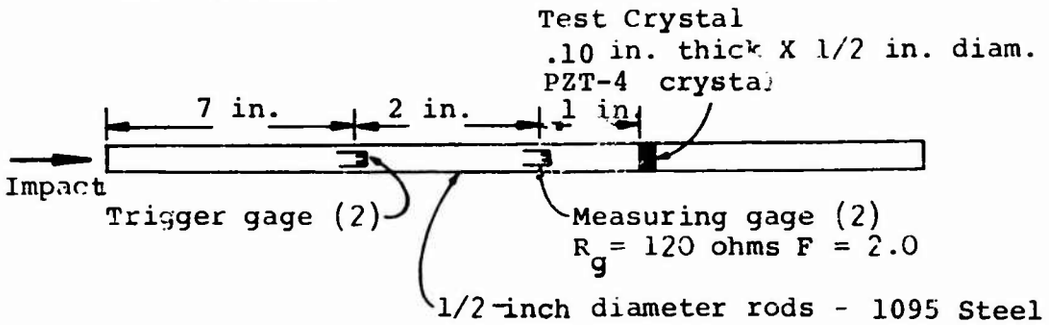

II. Projectile and Velocity Information

Projectile length - 6.7 in. Time increment - 13770 μsec.

Firing pressure - 3.5 psig. Impact Velocity - 40.5 fps.

III. Circuit Information

a. Strain circuit.

Number of active arms - 2
Bridge current - 30 milliamps
Equivalent strain - 750 μin/in/division
R_{cal} = 20 K ohms/2 divisions

b. Current circuit.

R_L = 50 ohms
R_{term} = 50 ohms (50-ohm Tektronix terminating resistor was used.)

IV. Scope Data

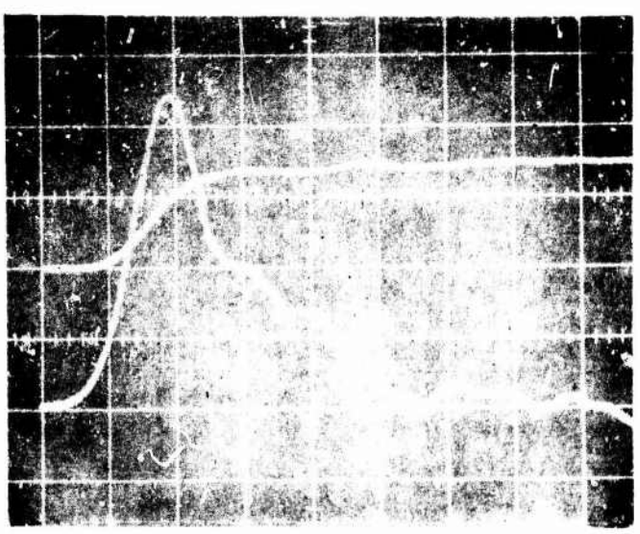

Upper trace - Strain
Sweep - 5 μsec/div
Gain - 750 μin/in/div (equivalent)

Lower trace - current
Sweep - 5 μsec/div
Gain - 20 volts/div
Delay - 5 μsec from strain data

Figure 56. Data for Crystal Test 5, Series 2

I. Test Specimen

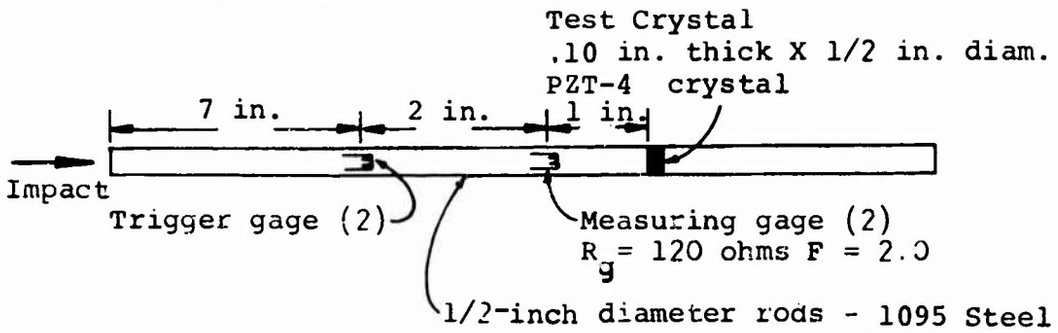

II. Projectile and Velocity Information

Projectile length - 6.7 in. Time increment - 13640 μsec.

Firing pressure - 3.5 psig. Impact Velocity - 40.9 fps.

III. Circuit Information

a. Strain circuit.

Number of active arms - 2
Bridge current - 30 milliamp
Equivalent strain - 750 μin/in/division
R_{cal} = 20 K ohms/2 divisions

b. Current circuit.

R_L = 50 ohms
R_{term} = 50 ohms (50-ohm Tektronix terminating resistor was used.)

IV. Scope Data

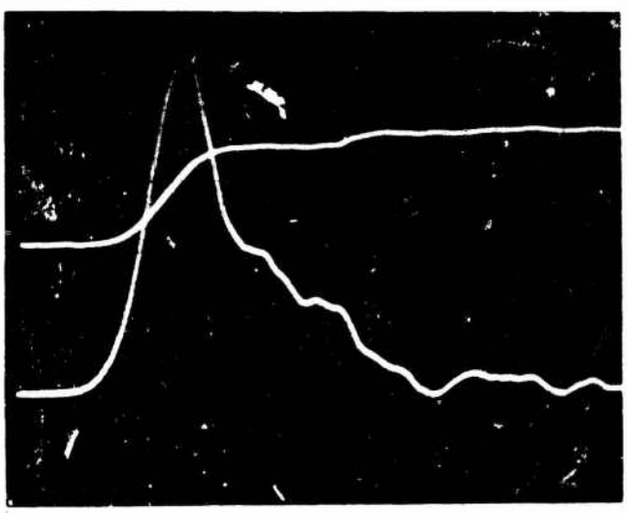

Upper trace - Strain
Sweep - 5 μsec/div
Gain - 750 μin/in/div (equivalent)

Lower trace - current
Sweep - 5 μsec/div
Gain - 20 volts/div
Delay - 5 μsec from strain data

Figure 57. Data for Crystal Test 6, Series 2

I. Test Specimen

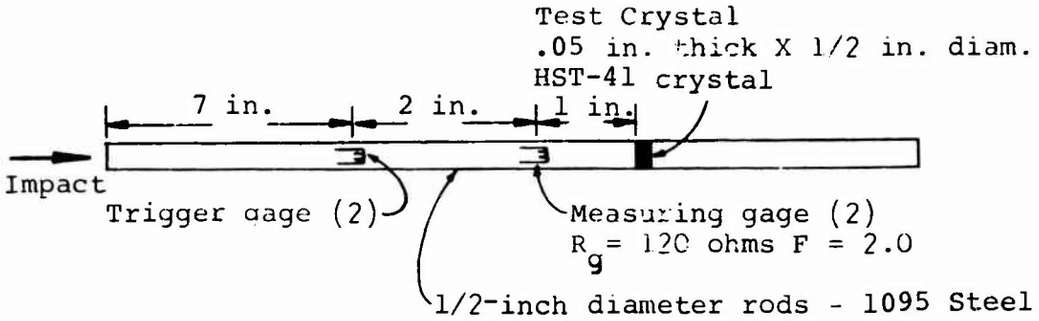

II. Projectile and Velocity Information

Projectile length - 6.7 in. Time increment - no data

Firing pressure - 3.5 psig. Impact Velocity - approx 40 fps.

III. Circuit Information

a. Strain circuit.

Number of active arms - 2
Bridge current - 30 milliamps
Equivalent strain - 750 μin/in/division
R_{cal} = 20 K ohms/2 divisions

b. Current circuit.

R_L = 50 ohms
R_{term} = 50 ohms (50-ohm Tektronix terminating resistor was used.)

IV. Scope Data

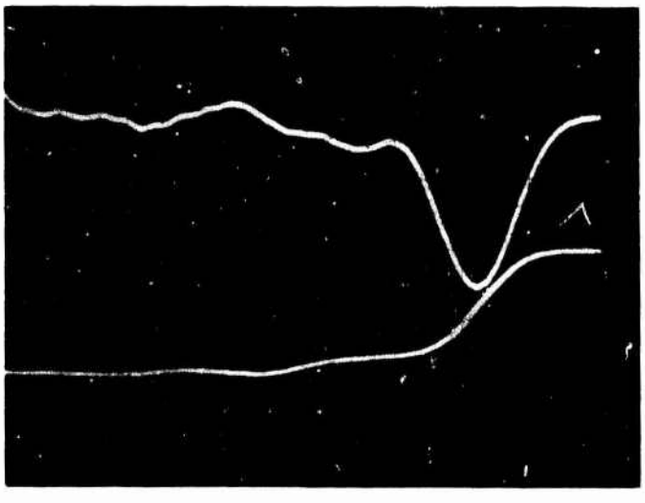

Upper trace - Strain
Sweep - 5 μsec/div
Gain - 750 μin/in/div (equivalent)

Lower trace - current
Sweep - 5 μsec/div
Gain - 20 volts/div
Delay - 5 μsec from strain data

Figure 58. Data for Crystal Test 3, Series 3

I. Test Specimen

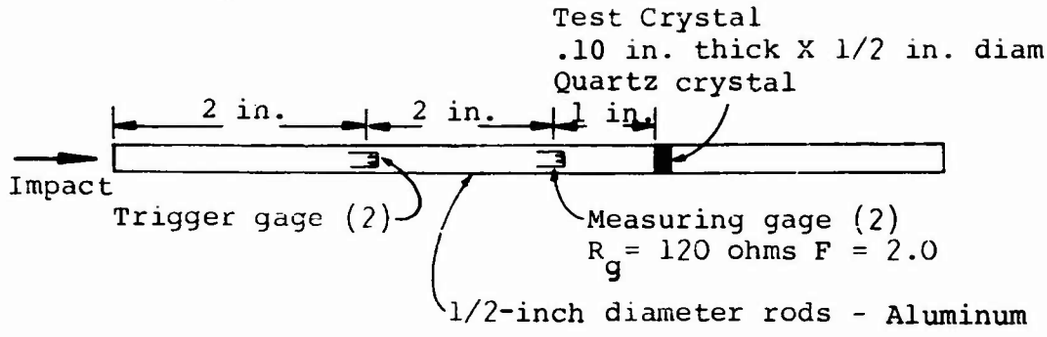

II. Projectile and Velocity Information

Projectile length - 6.7 in. Time increment - 12964 μsec.

Firing pressure - 3.5 psig. Impact Velocity - 43.0 fps.

III. Circuit Information

a. Strain circuit.

Number of active arms - 2
Bridge current - 30 milliamps
Equivalent strain - 750 μin/in/division
R_{cal} = 20 K ohms/2 divisions

b. Current circuit.

R_L = 50 ohms
R_{term} = 50 ohms (50-ohm Tektronix terminating resistor was used.)

IV. Scope Data

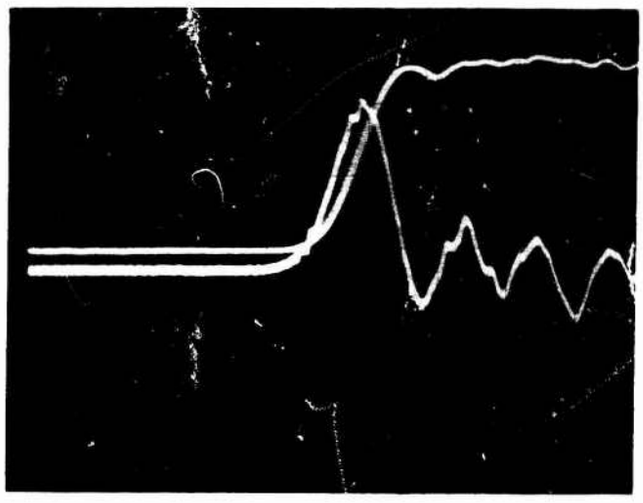

Upper trace - Strain
Sweep - 5 μsec/div
Gain - 750 μin/in/div (equivalent)

Lower trace - current
Sweep - 5 μsec/div
Gain - .2 volts/div
Delay - 5 μsec from strain data

Figure 59. Data for Crystal Test 5, Series 3

I. Test Specimen

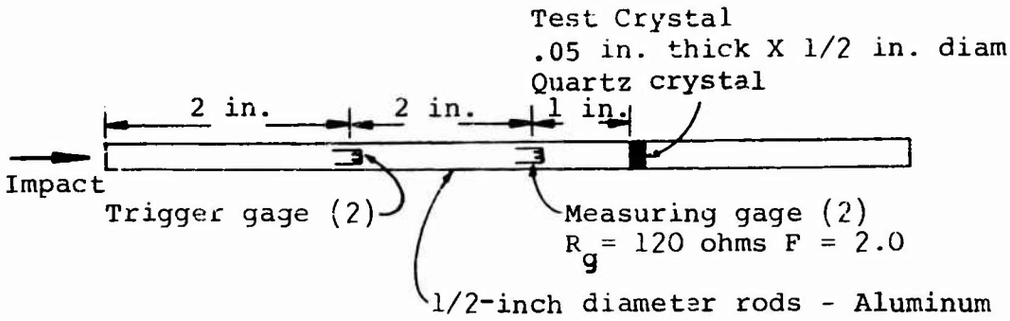

II. Projectile and Velocity Information

Projectile length - 6.7 in. Time increment - 13277 μsec.

Firing pressure - 3.5 psig. Impact Velocity - 42.0 fps.

III. Circuit Information

a. Strain circuit.

Number of active arms - 2
Bridge current - 30 milliamps
Equivalent strain - 750 μin/in/division
R_{cal} = 20 K ohms/2 divisions

b. Current circuit.

R_L = 50 ohms
R_{term} = 50 ohms (50-ohm Tektronix terminating resistor was used.)

IV. Scope Data

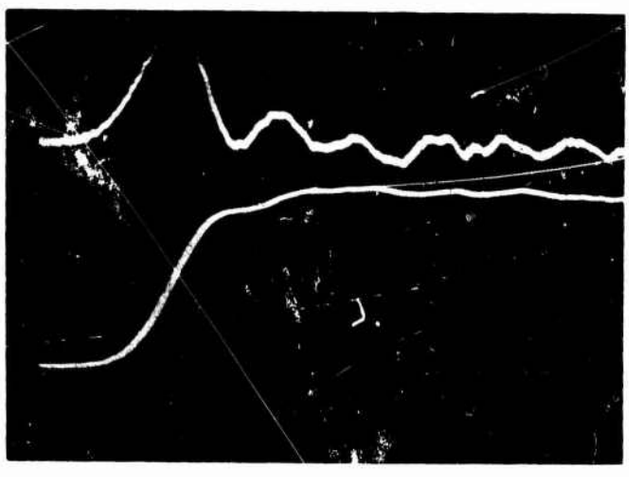

Upper trace - Strain
Sweep - 5 μsec/div
Gain - 750 μin/in/div (equivalent)

Lower trace - current
Sweep - 5 μsec/div
Gain - .2 volts/div
Delay - 5 μsec from strain data

Figure 60. Data for Crystal Test 6, Series 3

I. Test Specimen

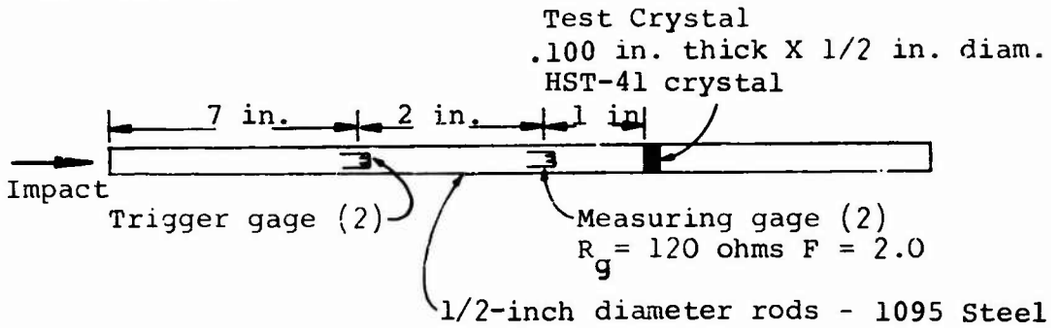

II. Projectile and Velocity Information

Projectile length - 6.7 in. Time increment - 13133 μsec.

Firing pressure - 3.5 psig. Impact Velocity - 42.5 fps.

III. Circuit Information

a. Strain circuit.

Number of active arms - 2
Bridge current - 30 milliamps
Equivalent strain - 750 μin/in/division
R_{cal} = 20 K ohms/2 divisions

b. Current circuit.

R_L = 50 ohms
R_{term} = 50 ohms (50-ohm Tektronix terminating resistor was used.)

IV. Scope Data

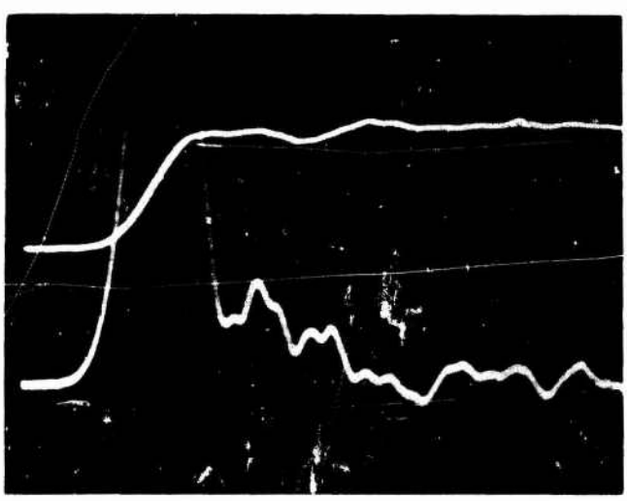

Upper trace - Strain
Sweep - 5 μsec/div
Gain - 750 μin/in/div (equivalent)

Lower trace - current
Sweep - 5 μsec/div
Gain - 20 volts/div
Delay - 5 μsec from strain data

Figure 61. Data for Crystal Test 1, Series 4

I. Test Specimen

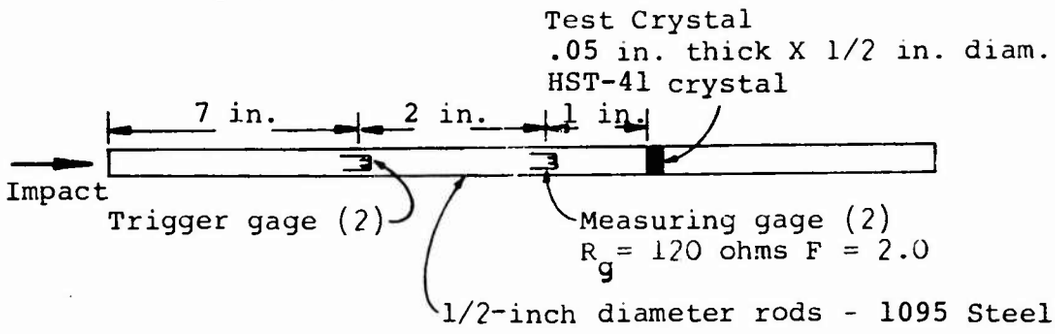

II. Projectile and Velocity Information

Projectile length - 6.7 in. Time increment - 13261 μsec.

Firing pressure - 3.5 psig. Impact Velocity - 42.0 fps.

III. Circuit Information

a. Strain circuit.

Number of active arms - 2
Bridge current - 30 milliamps
Equivalent strain - 750 μin/in/division
R_{cal} = 20 K ohms/2 divisions

b. Current circuit.

R_L = 50 ohms
R_{term} = 50 ohms (50-ohm Tektronix terminating resistor was used.)

IV. Scope Data

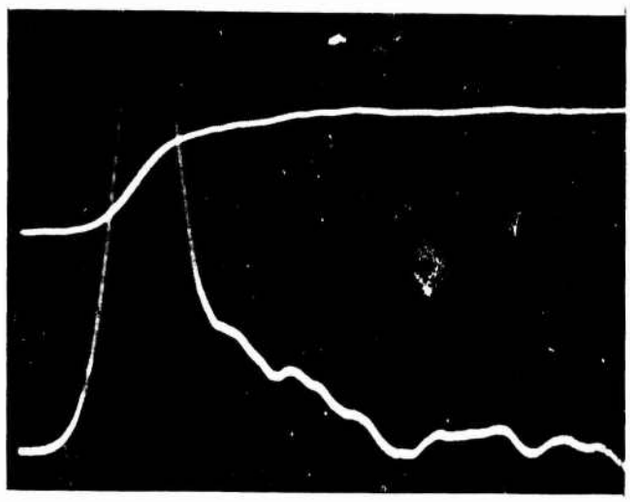

Upper trace - Strain
Sweep - 5 μsec/div
Gain - 750 μin/in/div (equivalent)

Lower trace - current
Sweep - 5 μsec/div
Gain - 20 volts/div
Delay - 5 μsec from strain data

Figure 62. Data for Crystal Test 2, Series 4

I. Test Specimen

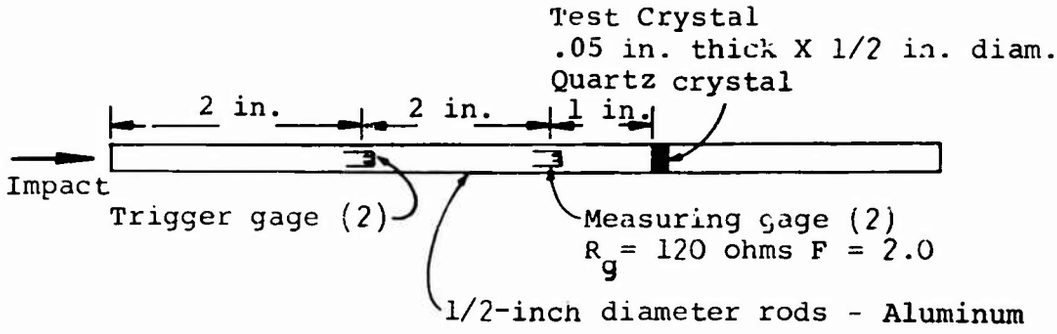

II. Projectile and Velocity Information

Projectile length - 6.7 in. Time increment - 13370 μsec.

Firing pressure - 3.5 psig. Impact Velocity - 41.7 fps.

III. Circuit Information

a. Strain circuit.

Number of active arms - 2
Bridge current - 30 milliamps
Equivalent strain - 750 μin/in/division
R_{cal} = 20 K ohms/2 divisions

b. Current circuit.

R_L = 50 ohms
R_{term} = 50 ohms (50-ohm Tektronix terminating resistor was used.)

IV. Scope Data

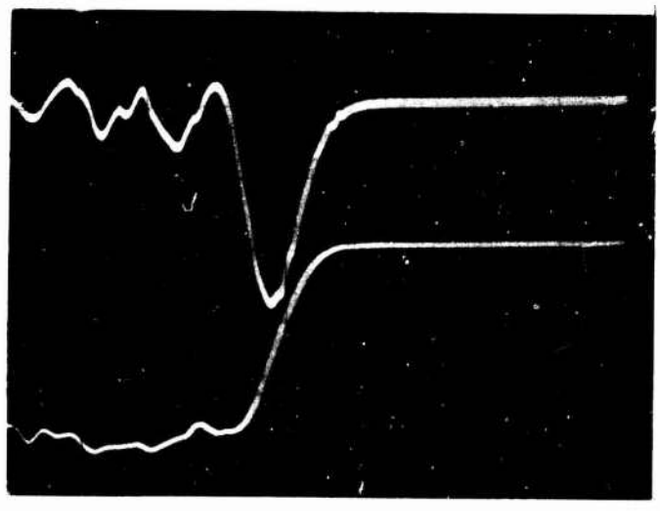

Upper trace - Strain
Sweep - 5 μsec/div
Gain - 750 μin/in/div (equivalent)

Lower trace - current
Sweep - 5 μsec/div
Gain - .2 volts/div
Delay - 5 μsec from strain data

Figure 63. Data for Crystal Test 3, Series 4

I. Test Specimen

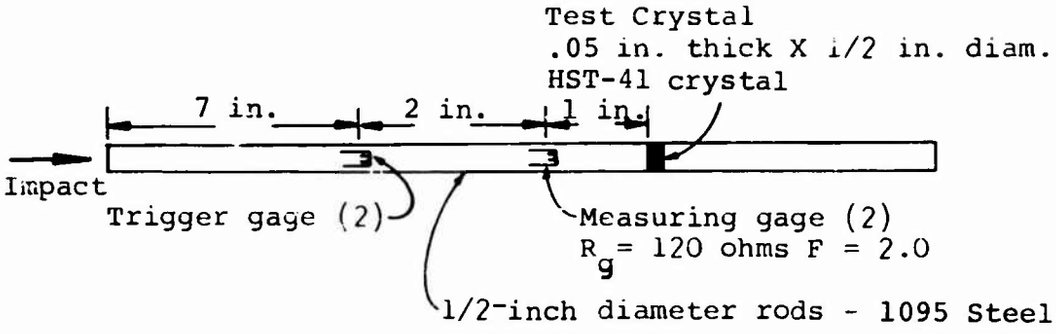

II. Projectile and Velocity Information

Projectile length - 6.7 in. Time increment - 13458 μsec.

Firing pressure - 3.5 psig. Impact Velocity - 41.4 fps.

III. Circuit Information

a. Strain circuit.

Number of active arms - 2
Bridge current - 30 milliamps
Equivalent strain - 750 μin/in/division
R_{cal} = 20 K ohms/2 divisions

b. Current circuit.

R_L = 50 ohms
R_{term} = 50 ohms (50-ohm Tektronix terminating resistor was used.)

IV. Scope Data

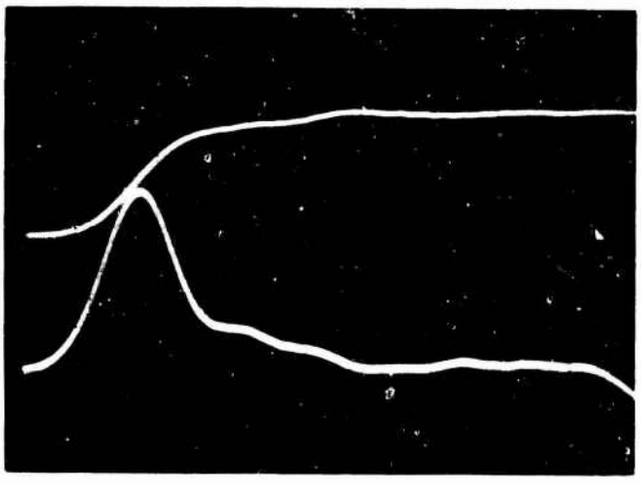

Upper trace - Strain
Sweep - 5 μsec/div
Gain - 750 μin/in/div (equivalent)

Lower trace - current
Sweep - 5 μsec/div
Gain - 50 volts/div
Delay - 5 μsec from strain data

Figure 64. Data for Crystal Test 4, Series 4

I. Test Specimen

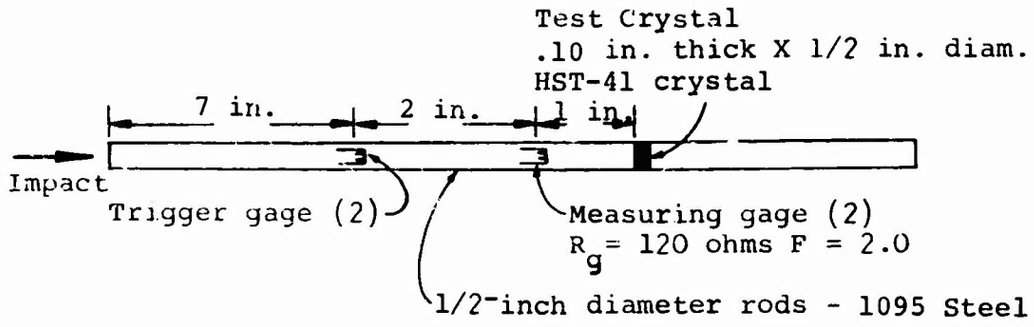

II. Projectile and Velocity Information

Projectile length - 6.7 in. Time increment - 13185 μsec.

Firing pressure - 3.5 psig. Impact Velocity - 42.3 fps.

III. Circuit Information

a. Strain circuit.

Number of active arms - 2
Bridge current - 30 milliamps
Equivalent strain - 750 μin/in/division
R_{cal} = 20 K ohms/2 divisions

b. Current circuit.

R_L = 50 ohms
R_{term} = 50 ohms (50-ohm Tektronix terminating resistor was used.)

IV. Scope Data

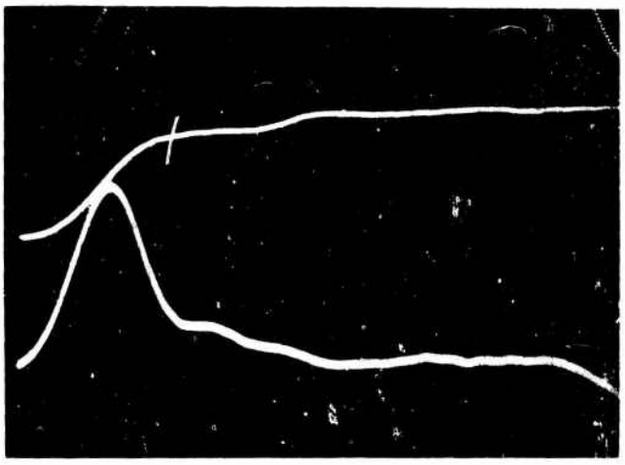

Upper trace - Strain
Sweep - 5 μsec/div
Gain - 750 μin/in/div (equivalent)

Lower trace - current
Sweep - 5 μsec/div
Gain - 50 volts/div
Delay - 5 μsec from strain data

Figure 65. Data for Crystal Test 5, Series 4

RESULTS

The data from the tests were reduced in two steps. One involved using the strain gage output from the measuring gages; i.e., the gages at the axial position on the input rod nearest the crystal as the input to the program of Appendix B or C. The output from this program included tabulated values of current-time and energy-time. These values are called the theoretical values in subsequent discussion.

The second step in the data reduction was the use of the measured current-time function to compute the electrical energy dissipated in a load resistor. This was done by programming for computation on a digital computer. Appendix E gives a listing of the program used for this. This program is basically the last section of the programs in Appendix B and C. The only difference is that the program of Appendix E uses experimental values for current, while those of Appendix B and C use theoretical values for current.

Earlier work had shown that for the values of capacitance and resistive loading of the circuit (with cables and scope plug-in) encountered with the circuits used in the experimental work, the current out of the crystal is, for practical purposes, equal to that which passes through the loading resistors. Consequently, no correction was made for the effect of the measuring instruments on the current available.

The data from the trace on the oscilloscope picture was digitized for use with the computer with a Telereader.

Considering first the results of the tests on the x-cut quartz crystals, it was anticipated that the linearized equation for the current output (Equation 5) would accurately predict the experimentally determined current. This is because the majority of the assumptions made in deriving this equation are essentially satisfied. The only major assumption which is not satisfied is the one on the state of strain in the crystal. In the test situation, the crystal is loaded somewhere between plane stress and plane strain, and it was assumed that the

crystal was in plane strain for data reduction. The difference in the charge coefficient between the plane stress and strain states is about 10%. This is due to the difference in mechanical stiffness between the two states.

The data of three runs were selected for reduction, and the resulting plots are shown in Figures 66, 67 and 68. These graphs show that the combination of the simple linear charge-force relation for quartz, the one-dimensional elastic wave propagation equation and its computer solution gave excellent results for predicting the current output and energy release for two cases, with results in agreement only to the same order of magnitude for the third case.

The test data on quartz which was reduced was selected to permit comparison of the effect of crystal thickness and the effect of rod material. In Figures 66 and 67, the only different parameter in the tests was the bar material. There was insufficient time to determine if this was the cause for the disagreement between the numerical and experimental values for Figure 67. However, the results of a duplicate test of a different series; i.e., run 5 of series 1, was in agreement with Figure 67.

In Figures 66 and 68, the only different test parameter was the crystal thickness. A study of these graphs indicates the crystal output is not a strong function of this parameter.

A study of the oscilloscope trace for all the tests indicates that the crystal output was the same order of magnitude for all tests, and that the shape of the input pulse may be the most significant parameter which affects the output for a particular crystal material. Even minor variations in the shape of the strain/pulse were noted to have an effect on the output. It is believed that the best way to investigate the effect of such things as crystal thickness, material properties of input and back-up rod, and shape of input pulse would be to use computer simulation. This is possible due to the apparent validity of the computer program.

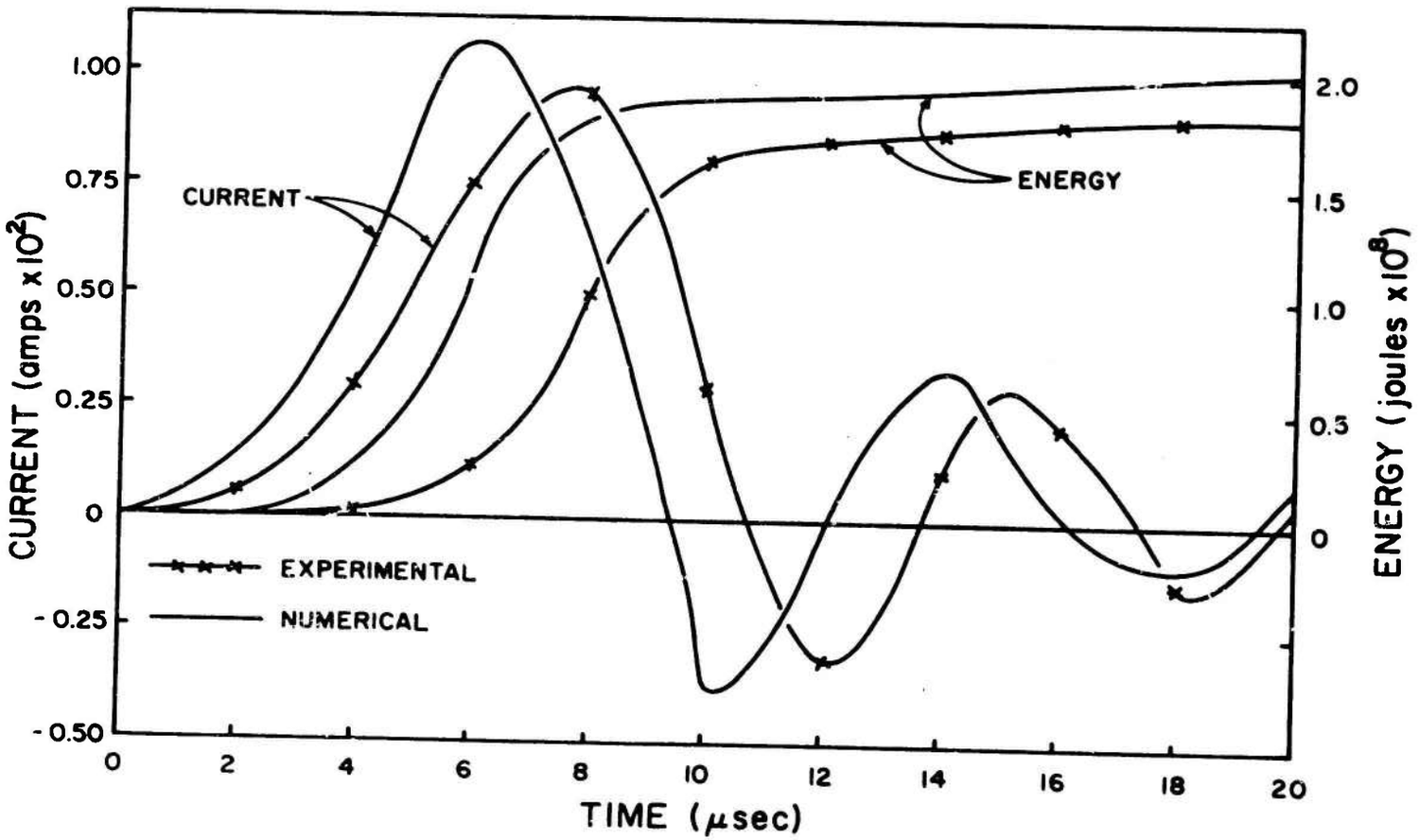

Figure 66. Results of Test on Quartz Crystal 0.1" Thick with Aluminum Bar (Series 1, Test 4)

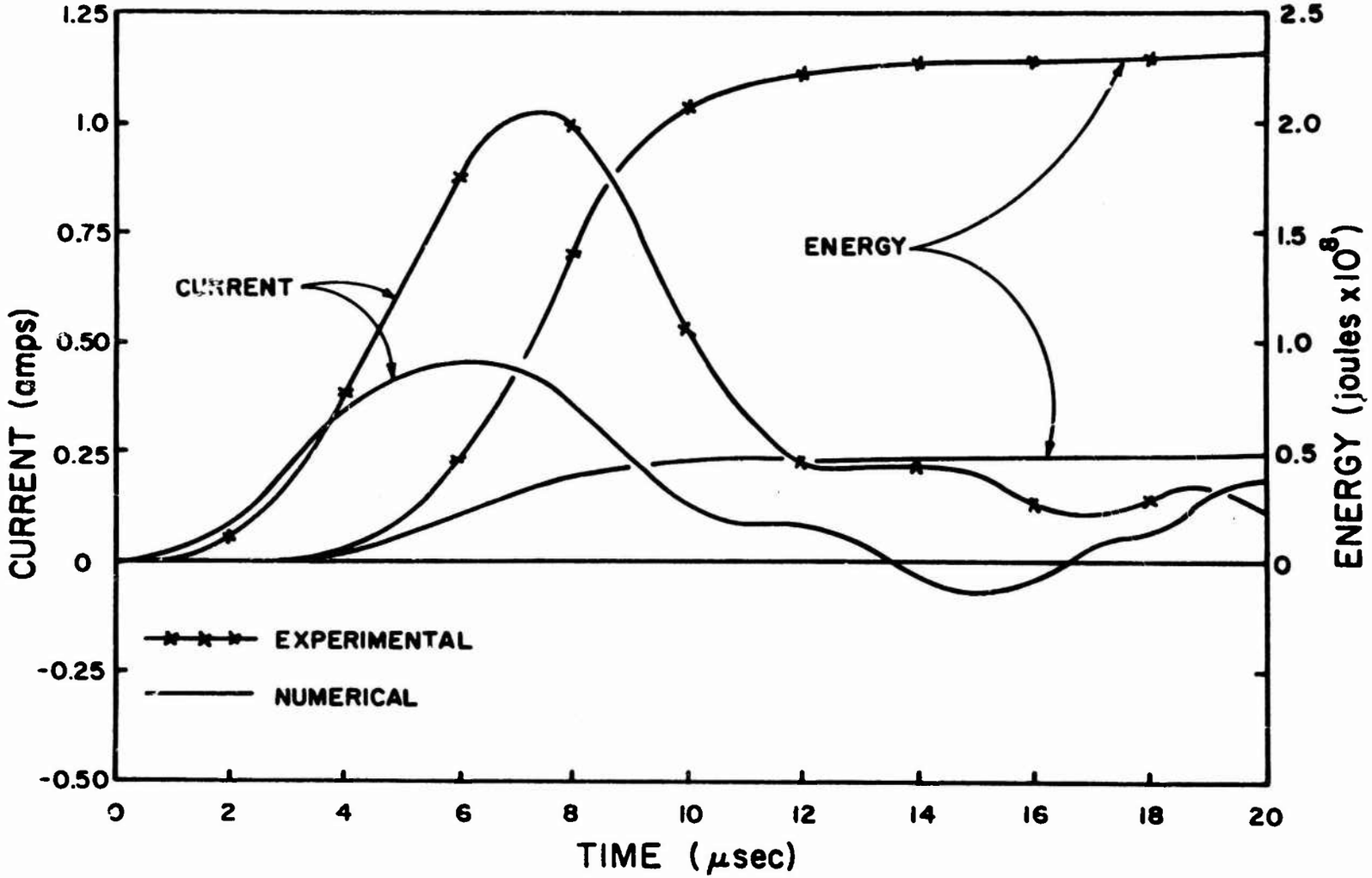

Figure 67. Results of Test on Quartz Crystal 0.1" Thick with Steel Pressure Bar (Series 2, Test 3)

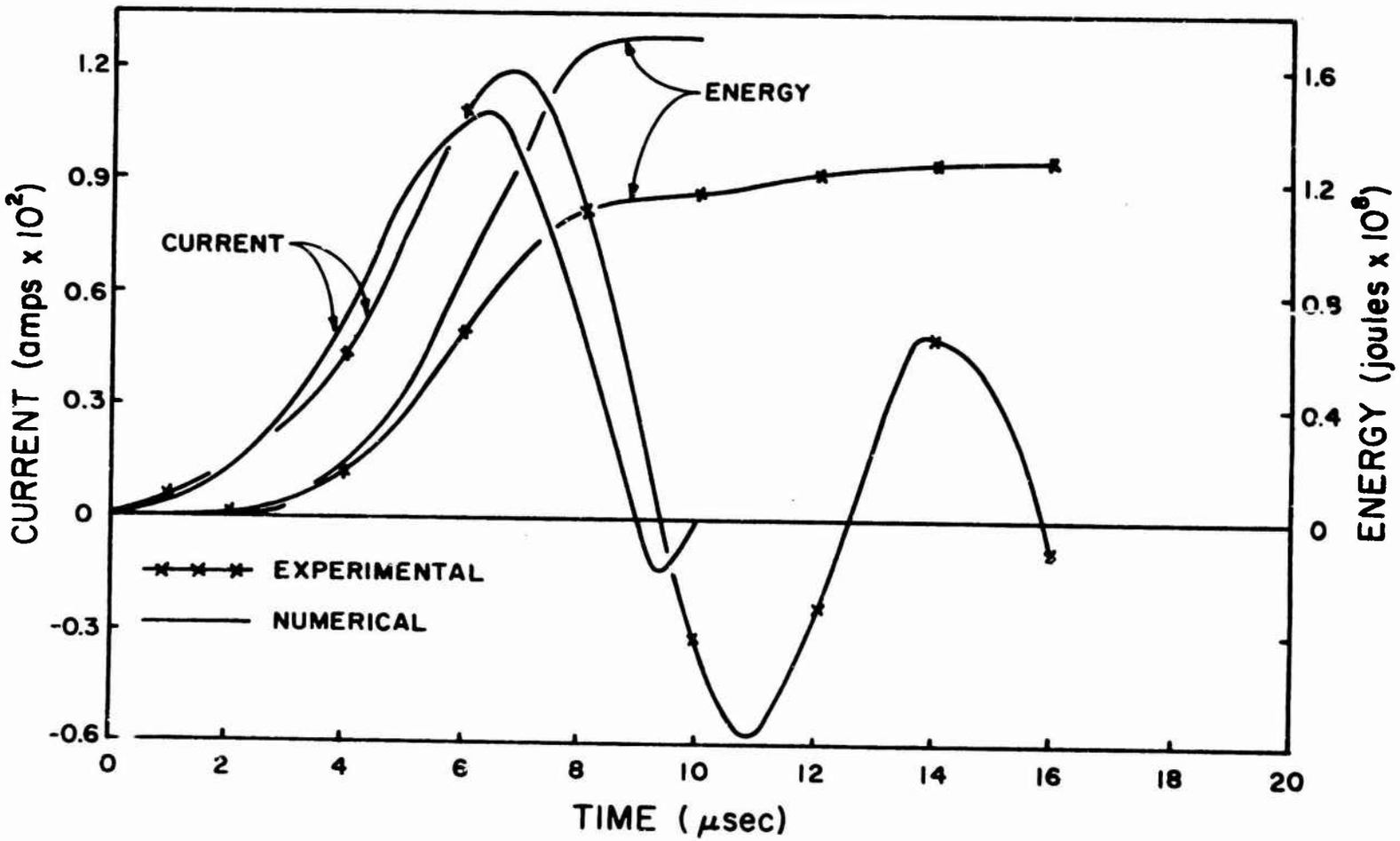

Figure 68. Results of Test on Quartz Crystal 0.05" Thick with Aluminum Pressure Bar (Series 1, Test 3)

The results of the tests on the "new" HST-41 crystals; i.e., from series 4, for which the data was reduced is shown in Figures 69 and 70. The pressure bar was always in the elastic range, so the computer program in Appendix B was used in the data reduction. The high impact speed tests which were run at AEDC were reduced utilizing the plastic wave propagation program (Appendix C). The results of these tests are shown in Figures 71 and 72. The crystals used in these tests were from the old batch, and this would introduce some discrepancies in the results. The numerical solutions for all tests were obtained by using the nonlinear charge coefficient determined from the static tests.

Figures 69 and 70 show that the numerical technique presented for computing current and energy from the crystal gives reasonably good quantitative and qualitative agreement with the experimental results and can be considered adequate for a first order approximation. Since the work on quartz has shown that the numerical technique can give excellent agreement, the differences in the numerical and experimental results for the HST-41 is attributed to deficiencies in the charge-force relation, as determined, and/or as considered in the theory. The most significant reasons for these differences are believed to be

1. The effect of current generated by radial and shear waves is not negligible for HST-41, and must be included for improved agreement. The one-dimensional wave propagation theory used precludes easy incorporation of this change into the program.
2. The effect of the electromechanical coupling has also been neglected in this one-dimensional theory.
3. Any effect of strain rate on the force-charge relation (or current generated) for the crystal has been neglected. The function determined under quasi-static loading has been used for

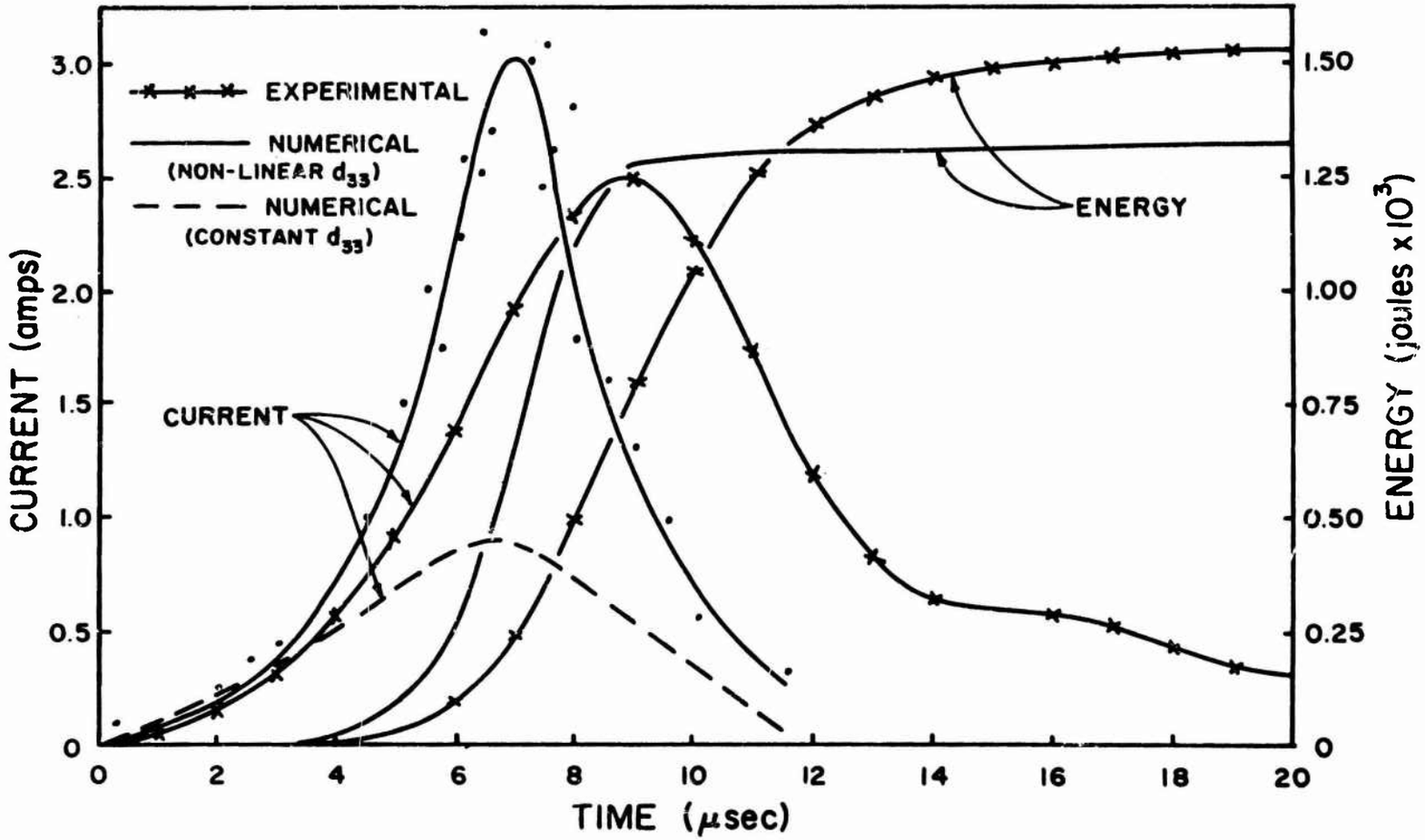

Figure 69. Results of Test on HST-41 Crystal 0.05" Thick with Steel Pressure Bar (Series 4, Test 4)

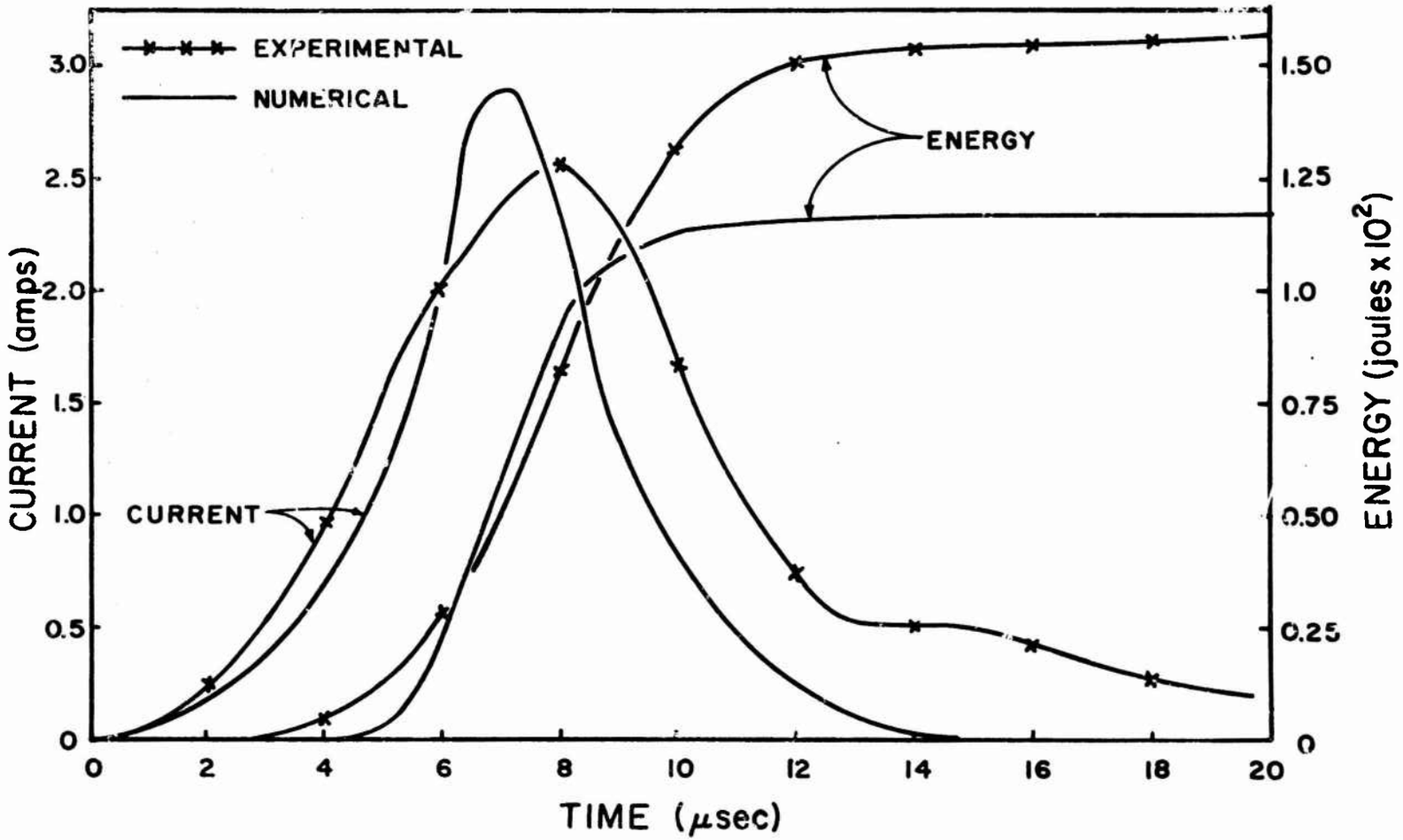

Figure 70. Results of Test on HST-41 Crystal 0.1" Thick with Steel Pressure Bar (Series 4, Test 5)

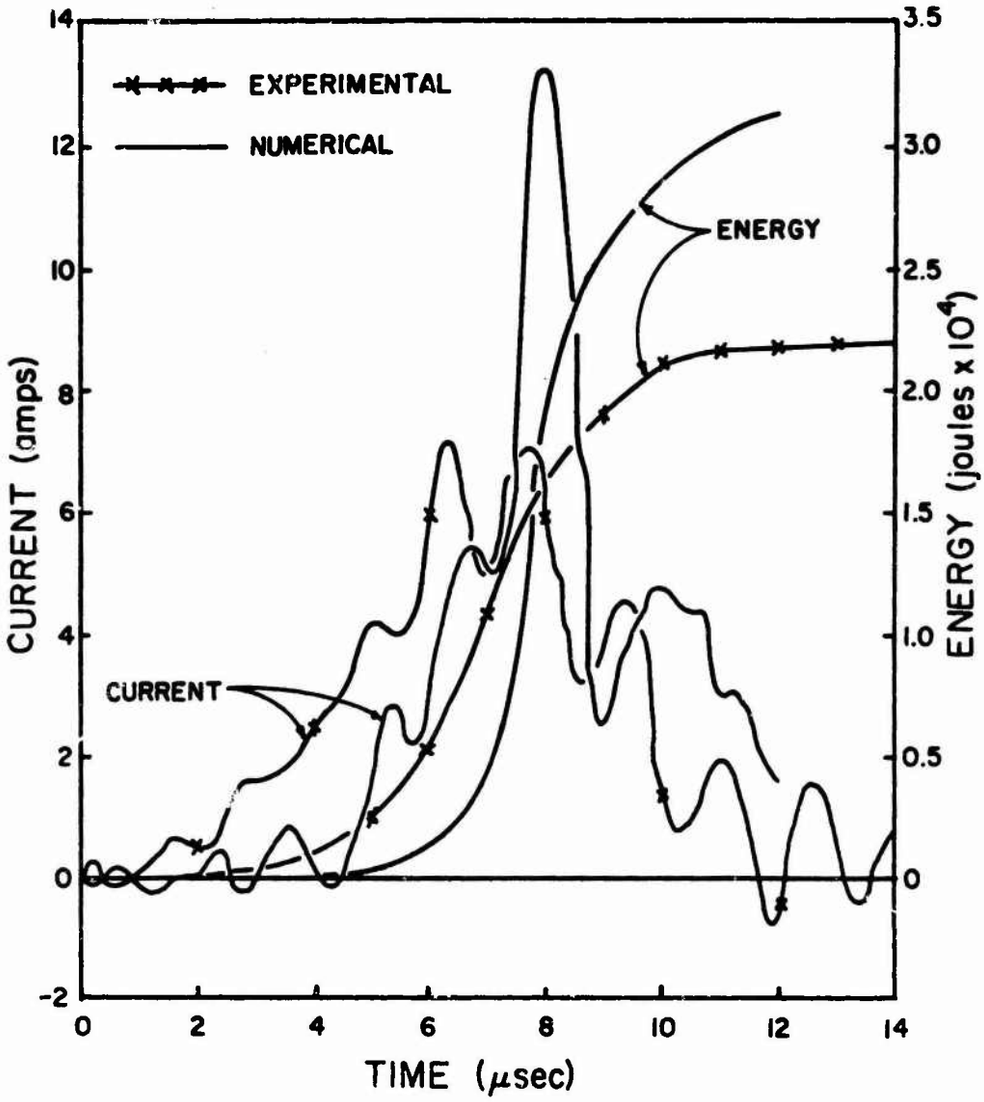

Figure 71. Results of Test on HST-41 Crystal 0.125" Thick with Aluminum Pressure Bar (AEDC Run 1206)

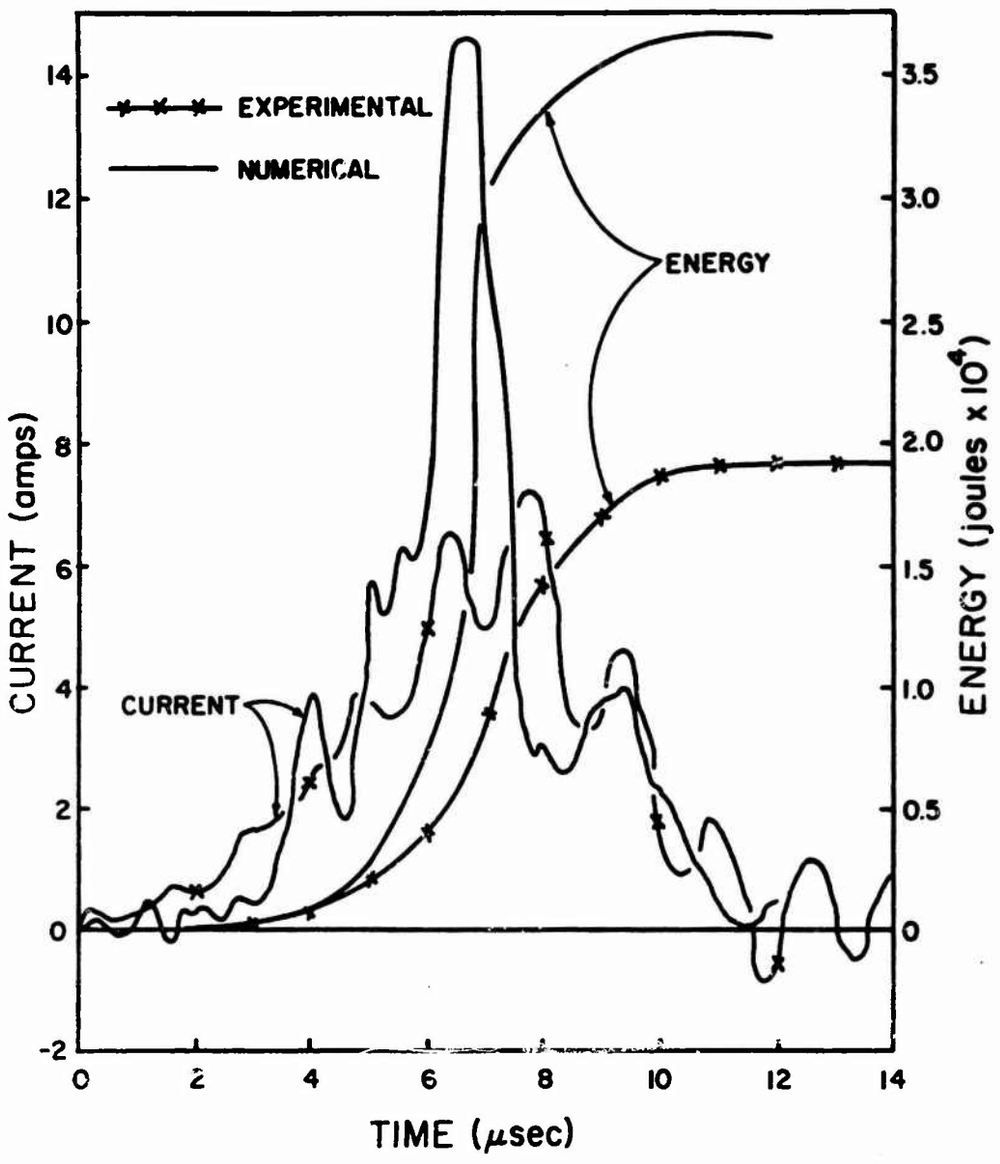

Figure 72. Results of Test on HST-41 Crystal 0.125" Thick with Aluminum Pressure Bar (AEDC Run 1207)

the dynamic case, where loading occurs in about 10 μsec.

Two additional items of importance are shown in Figure 69. One is the current curve determined from theory utilizing a linear charge-force relation for the crystal. (The charge coefficient used was one determined from the end points in Figure 24). When this curve is compared to the one determined with the nonlinear relation, it is noted that the quantitative agreement is much better when the nonlinear relation is used.

Also shown in Figure 69 are the plotting data from which the numerical curve was determined. This plotting data indicates that there was considerable noise in the numerical solutions for the current output. This occurred for both the quartz and the HST-41 crystals, and the scatter in plotting dots shown here is typical of that for all computed results in Figures 66 through 70. This scatter was caused by errors in the data reduction technique used and the subsequent amplification of these errors by the finite difference solution of the wave propagation problem. All of the experimental data was recorded by photographing the trace on the oscilloscopes. The traces on the film were then digitized using a Telereader. This required approximating the vertical center of the trace on the film. There are errors in this approximation. Where the slope of the curve is the greatest, the errors in approximation were the greatest. These errors were further amplified by the finite difference technique used. Unfortunately, the peak current also occurs where the slope of the strain curve was the greatest and hence the peak values of current are the least accurately defined. values.

The noise could be greatly reduced and more accurate results obtained by fitting polynomials piecewise to the strain data in the same manner as was done to obtain the nonlinear charge-force relation; i.e., with natural cubic interpolatory splines. This would require some additional computer work but would yield much smoother results.

It should be noted that although there is noise in the numerical current solution, the energy computed was relatively smooth. This is the result of the averaging effect of the intergration process required to get energy from current.

The results shown in Figure 71 and 72 were determined for impact speeds of about 8000 fps, whereas the results in Figures 69 and 70 were for impact speeds of about 50 fps. When the current and energy for these two curves are compared, it is noted that they are of the same order of magnitude. It should be noted that essentially all of the energy from the crystal is included in the curves of Figures 69 and 70, but such is not the case in Figures 71 and 72. For these tests, the energy given is that dissipated in the 1.33-ohm resistor across which the voltage drop was measured, but the total energy generated by the crystal is dissipated in the 1.33-ohm and 52.14-ohm resistor which are in series. When a correction is made for this, the energy available from the crystal for the high-speed shots was about 7.8×10^{-3} joules, as compared to about 1.5×10^{-3} joules for the low-speed shots. (Values given are those from measured currents.)

It is of interest to note that the energy from the quartz crystal was about 2×10^{-8} joules, as compared to 1.5×10^{-3} joules from the HST-41 crystal for identical test conditions.

SECTION VII

CONCLUSIONS AND RECOMMENDATIONS

Conclusions based upon the static tests conducted on the crystals used in this study are as follows:

1. The test set-up developed is adequate for determining the force-charge relation for piezoelectric or ferroelectric materials, as indicated by the results obtained with quartz.
2. The variation of the charge-force relation with previous load history is large.
3. There is an indication of a variation in the charge-force relation with age for ferroelectric materials.
4. The charge-force relation is highly nonlinear for the ferroelectrics, but at low-stress amplitudes, it may be approximated as linear. The stress level to which the linear approximation may be used is dependent on the material.
5. When loaded to high stresses, i.e., 50,000 psi, the increase in charge developed per increment of force becomes very small.
6. The variation between the d_{33} values for the three materials tested is small; generally, smaller than variations in values occuring between different crystals of a given material.

The most significant conclusions based upon the results of the dynamic tests on the crystals are:

1. The theory and computer programs developed for prediction of the current and energy from either quartz or ferroelectric materials, when loaded in a split Hopkinson pressure bar, gives agreement with experimental results which is at least within the same order of magnitude. The qualitative agreement was excellent for quartz and good for the ferrorelectric materials.

2. The lack of good agreement between computed and experimental results for the ferroelectric materials is attributed to the omission of phenomenon such as electromethanical coupling, the use of a one-dimensional wave propagation theory, and the fact that the equation for the short circuit current from a crystal may be only an approximation for ferroelectric materials.
3. With the test geometry used, energy levels up to about 2×10^{-3} joules were obtained from the ferroelectric materials.
4. The amount of energy obtainable from the test geometry used in this work, for a given material, could be increased by
   a. Using the optimum size load resistor in series with the crystal.
   b. Moving the crystal very near the impact end of the Hopkinson presure bar. (This would tend to decrease the rise time of the input pulse.)
   c. Selection of the material for the input and back-up rods to maximize the stress difference.
5. The computer program developed for predicting current and energy release would be of value in maximizing energy release by ferroelectric materials through variation and selection of the values of appropriate material parameters of the pressure bar to accomplish this. Further experimental work is required to determine the optimum load resistor size. A two-dimensional wave propagation theory would be required to properly simulate the phenomonon if the crystal were very near the impact end. (This would be the minimum refinement in theory. Further refinements in other applicable theories might also be required.)

The recommendations which could be made for further work in this area are numerous, since the work completed has been

primarily in the exploratory stage. It is believed the most significant areas for further study would be:

1. Studies of the effect on the crystal behavior of such phenomena as load history, storage time, radiation, temperature, and/or other environment to which the crystal will be subjected in an application.
2. Research to improve the relation for the short circuit current generated by ferroelectric material under shock or dynamic loading.
3. Studies to maximize the energy release by ferroelectric materials to a load resistor, for the specific test geometry used in this work; i.e., the split Hopkinson pressure bar.
4. Studies to optimize the method of loading of the ferroelectric materials in the field (i.e., not under laboratory conditions) to give the maximum energy release. For example, it is possible that crystals in series in a pressure bar could increase the energy level, or it is possible that a shear deformation could result in a greater energy release.

APPENDIX A

ABSTRACTS FROM LITERATURE REVIEW

NOTE: The numbering system in Appendix A corresponds to the References (p. 182). Those references that do not have an abstract either cover introductory material or have a title that is self-explanatory.

APPENDIX A

LITERATURE REVIEW

6. F. W. Nielson, "Ferromagnetic and Ferroelectric One-Shot Explosive-Electric Transducers,"

"This memorandum presents the theories of operation and the initial experimental verification of these theories for ferromagnetic and ferroelectric one-shot transducers which convert a portion of the energy of a high explosive to electrical energy with suitable power, current, and voltage.

The transducers are shown to be extremely small, simple, and versatile."

9. R. A. Graham, F. W. Neilson, W. B. Benedick, "Piezoelectric Current from Shock-Loaded Quartz - A Submicrosecond Stress Gauge,"

"Current from X-cut quartz disks may be used to detect stress-time profiles induced by shock loading. The current amplitude and its time dependence are functions of the dielectric, piezoelectric, and mechanical properties of quartz under shock-loading conditions. The results of an extensive experimental study of the current from shock-loaded quartz disks are reported for shock stress up to 50 kbar. The experiment is performed by impacting precisely aligned X-cut quartz disks upon each other at various measured velocities and observing the current in one of the disks during the first wave transit. Within the low signal range, the piezoelectric stress constant e_{11} is found to be 0.174 $C\text{-}m^{-2}$. The coefficient relating current jump to stress jump in one-dimensional strain is found to be 2.04×10^{-8} $C\text{-}cm^{-2}\text{-}kbar^{-1}$ up to 6 kbar and 2.15×10^{-8} $C\text{-}cm^{-2}\text{-}kbar^{-1}$ from 9 to 18 kbar. The wave velocity was determined to be constant to 25 kbar. The observed current waveform could be fully interpreted in terms of rate-independent properties. Determinations of distortions to the current from apparently minor deviations from one-dimensional conditions were also made."

10. W. J. Halpin, "Current from a Shock-Loaded Short-Circuited Ferroelectric Ceramic Disk,"

"Thin circular disks of polarized ferroelectric ceramics were equipped with electrodes on their faces, and the electrodes were connected by a short circuit. Each disk was traversed by a stress wave, and the resulting current pulse through the short circuit was measured. The stress wave was generated by impact and made to propagate along the disk axis in a direction opposite to that of polarization. Current-pulse data are presented from tests with

PZT 95/5, both normally sintered and hot-pressed, and with PSZT 68/7 for impact stresses ranging from a few to several tens of kilobars. Over this range of stress both the shape of the current pulse and its time integral are found to be strongly stress dependent. It is concluded that this behavior results from the combined effects of stress on (1) remanent polarization, (2) polarizability, and (3) conductivity of the ferroelectric material enveloped by the wave. In a narrow range of stress where remanent polarization is reduced to near zero and where conductivity is negligible, the observed behavior can be adequately described by means of a mathematical model which is developed. The model includes the effect of stress wavefront tilt which occurs in impact experiments to an extent that influences significantly the character of the current pulse. Some conclusions are drawn about permittivity of shock-loaded ferroelectrics and the extent to which remanent polarization is affected by the rapidly applied large electric fields which accompany the process of current production."

11. C. W. Beadle and J. W. Dally, "Experimental Methods for Investigating Strain-Wave Propagation and Associated Charge Release in Ferroelectric Materials,"

"Study of strain levels associated with electric charge release in barium-titanate-base ferroelectric ceramic which may be utilized as single-shot, high-energy power supply, correlation between charge release and stress level were made for stress levels up to 16 kbar; in addition, fracture wave propagation was determined, and time between fracture and charge release was established."

12. O. M. Stuetzer, "Secondary Stresses in a Stress-Pulse-Activated Piezoelectric Element,"

"Previous treatments of stress-pulse-activated piezoelectric and ferroelectric stress gauges and power generators neglect the secondary stresses produced by circuit-enforced fields in not-directly-stressed parts of the transducer. It is pointed out that under short-circuit conditions these secondary stresses generate strong effects in materials with high electromechanical coupling factors. To demonstrate this, a thin plate activated by a plane rectangular low-amplitude stress front is considered. A rigorous theoretical analysis is sketched for this configuration. It is found that short-circuit current pulses generated by the stress-front transit are not rectangular, but vary exponentially in time. The exponent is proportional to the square of the electromechanical coupling factor and depends on the mechanical boundary conditions. Supporting experiments are reported."

13. H. Krueger and D. Berlincourt, "Effects of High Static Stress on the Piezoelectric Properties of Transducer Materials,"

"Piezoelectric ceramic elements in high-power acoustic transducers are subjected to high static as well as dynamic stress. This is particularly true of well-matched transducers operating in deep water, since the static stress in the piezoelectric element may be several times the water pressure. The present study was undertaken in an effort to determine the effects of static compressive stress on the piezoelectric properties of two commercial lead titanate zirconate compositions, PZT-4 and PZT-5, and of two barium-titanate compositions, commercial Ceramic B (a barium calcium titanate), and the composition 88 wt% barium titanate, 12 wt% lead titanate (BaPb12Ti). The permanent effects of stress exposure, determined at zero stress after exposure to a given stress, were found to be more severe with stress parallel to the polar axis than with perpendicular stress, as expected. Under maintained stress, however, the effects of perpendicular stress are more severe. PZT-4 and BaPb12Ti, generally better suited for use as radiating transducers, show effects dependent upon exposure time but independent of the number of stress cycles. Ceramic B and PZT-5 show effects dependent upon the number of stress cycles and less dependent upon the total period of stress exposure. Of the compositions tested, PZT-4 and BaPb12Ti were least affected by high static stress, suffering relatively little from exposure to stress as high as 15000 psi. Of these two compositions, PZT-4 has markedly higher coupling (κ_{33}=0.64 compared to 0.365) and therefore offers higher transducer bandwidth."

14. D. Berlincourt and H. Krueger, "Domain Processes in Lead Titanate Zirconate and Barium Titanate Ceramics,"

"The amount of 90° reorientation during poling was determined from mechanical strains measured during the poling process. With tetragonal lead titanate zirconate 53% of the possible 90° reorientation occurred during poling, but this figure dropped to 44% upon removal of the poling field. With barium titanate the figures are only 17% and 12%, respectively. Comparison of the polarization of poled polycrystalline barium titanate with that for single crystals indicates that 180° reorientation is virtually perfect. Application of very high compressive stress parallel to the polar axis causes 90° switching of nearly all aligned domains, and, therefore, removes virtually all polarization. Curves of released charge as function of mechanical strain are nearly linear, but curves of released charge as function of stress are strongly nonlinear. Application of high compressive

stress perpendicular to the polar axis also causes 90° domain reorientation and a reduction in the total polarization of the ceramic. This domain reorientation may be interpreted as a shift of the polar axes of some domains into a position more closely corresponding to the plane of cross expansion, and typically the total electric moment is reduced by less than 10%. High electric stress causes 180° as well as 90° reorientation. With prepoled specimens dc fields in the same direction as the poling field cause 90° switching, while reverse dc fields cause both 90° and 180° reorientation, with the latter predominating."

15. D. G. Doran, "Shock-Wave Compression of Barium Titanate and 95/5 Lead Zirconate Titanate,"

"The shock compression of the ceramics $BaTiO_3$ (5%$CaTiO_3$) and Pb $(Zr_{0.95}Ti_{0.05})O$ (1wt%NB_2O_5) was measured in the ranges 5-200 kbar and 2-140 kbar, respectively. Barium titanate exhibits a two-wave structure above 30 kbar; the first wave has a velocity of 6.27 mm/μsec. The cusp in the Hugoniot at 30 kbar is interpreted as a dynamic elastic limit. Comparison of the first wave velocity with the measured longitudinal sound speeds of the tetragonal (ferroelectric) and cubic (paraelectric) phases (5.4 and 6.2 mm/μsec, respectively) suggests, as does other evidence, that the material begins to transform to the cubic phase in the neighborhood of 7 kbar. Below 7 kbar, subsonic velocities are observed and it is speculated that this phenomenon is associated with domain reorientation.

The particular lead zirconate composition studied has a two-wave structure above about 40 kbar; the position of the cusp in the Hugoniot depends sensitively on initial density. This cusp is presumably the Hugoniot elastic limit. A weak cusp is also observed at about 2 kbar. The wave velocity is essentially sonic below 2 kbar and subsonic above 2 kbar, increasing to about sonic in the neighborhood of 40 kbar."

17. R. K. Linde, "Depolarization of Ferroelectrics at High Strain Rates,"

"Poled specimens of barium titanate (BT) and lead zirconate titanate (PZT) ceramics have been successfully recovered after shock loading antiparallel to the polarization vector (short-circuit configuration) in the 3- to 23kbar range. It has been shown that permanent depoling as a result of phase transitions or of domain switching can occur within the microsecond time scale of a shock experiment. Results of dynamic charge release measurements made during shock transit in PZT 52/48 tend to corroborate the finding of other investigations. Techniques for recovery of shock-loaded specimens were discussed."

18. C. E. Reynolds and G. E. Seay, "Two-Wave Shock Structures in the Ferroelectric Ceramics Barium Titanate and Lead Zirconate Titanate,"

"Pb $(Zr_{0.52},Ti_{0.48})O_3$ with 1 wt% Nb_2O_5 and pure $BaTiO_3$, were studied under plane shock waves having pressures ranging from 2 to 175 kilobar which were produced by high-explosive driving systems; 2-wave structures are characteristic of elastic properties of materials and are not due to phase transitions from ferroelectric to paraelectric.

19. W. J. Halpin, "Resistivity Estimates for Some Shocked Ferroelectrics,"

"It has been observed previously that the shape of the current pulse delivered to an external short circuit by a shock-loaded ferroelectric ceramic specimen undergoes an abrupt change when a sufficiently high shock stress level is reached. This change was explained qualitatively as being due to the onset of electrical conduction in the specimen. Here a quantitative analysis of short-circuit current waveshapes from some typical ferroelectric materials is made on the basis of a previously developed model that has been extended to include the effect of conduction. Finite resistivity is assumed in the stressed region of a specimen and evaluated in terms of the various model parameters and experimental quantities, particularly the short-circuit current itself. With the analysis an estimate is made that the resistivity of the ferroelectric materials under shock stress in the range of 25 to 35 kbar is of the order of 100 Ω-cm with accompanying fields greater than about 20,000 V/cm."

20. R. A. Graham, W. H. Halpin, "Dielectric Breakdown and Recovery of X-Cut Quartz Under Shock Wave Compression,"

"While a shock wave is traversing a disk of X-cut quartz, a piezoelectric current flows in an external circuit connected across the faces of the disk. In this paper measurements of this current are used to study dielectric breakdown and subsequent recovery which occurs in quartz. Quartz specimen disks were impacted at various stress levels in such a way as to produce shock waves that propagated along the X axis either in the direction of or opposite to that of the pressure-induced polarization. In the latter case, short-circuit current measurements show that breakdown occurs at a threshold stress greater than 10 and less than 13 kbar. Since the impact experiment produced one-dimensional electrical and mechanical conditions in the specimen disk, it was possible to formulate a mathematical model that permitted solutions for internal electrical fields and resistivity in terms of the measured current. Computations with this model show that the field in the stressed portion of the disk

at breakdown is about 7.0×10^5 V/cm, which is an order of magnitude lower than the value observed at atmospheric pressure. Computations with the model also show that recovery from breakdown to essentially infinite values of resistivity occurs during the transit time of the shock wave when the field in the stressed region of the disk is "quenched" to a value of about 1.9×10^5 V/cm. This critical field appears to be the same for all shock stress levels investigated from 13 to 35 kbar. The dependence of the initiation of breakdown on the direction of wave propagation relative to the polarization direction indicates that the shock-wave front furnishes a source of free electrons."

21. R. A. Graham, "Dielectric Anomaly in Quartz for High Transit Stress and Field,"

"Neilson and Benedick have reported an anomalous piezoelectric behavior for negatively-oriented synthetic alpha-quartz crystals when subjected to transient stress of about 65 kbar. This paper describes the piezoelectric behavior of negatively-oriented quartz in the stress region of from 5 to 50 kbar. The first indication of anomalous behavior occurs at 8 kbar. Between 8 and 24 kbar the negative x-current waveforms show evidence of partial electric breakdown in the quartz. Between 25 and 34 kbar disruptive breakdown occurs. Above 34 kbar disruptive breakdown is followed by gross conduction with positive currents being observed for stress greater than about 50 kbar. The fields associated with the piezoelectric behavior are lower than the field for steady-state electric breakdown at atmospheric pressure. It is proposed that the anomaly is triggered by stress-induced dislocation motion resulting in liberated electrons which are accelerated into the stressed region of the specimen by the high negative electric field."

22. R. A. Graham, "Technique for Studying Piezoelectricity Under Transient High Stress Conditions,"

"An experimental technique is described which is being successfully used to study the transient high stress piezoelectric behavior of synthetic alpha-quartz. Short, flat-faced cylinders of quartz are impacted upon each other at high velocity to produce the desired transient stress in the range from 5-70 kilobar. Precision is maintained in the alignment of the flat impact surfaces so that the Hugoniot conservation of momentum and the relationship governing the impact of flat cylinders may be used to compute the stress imparted to the target cylinders of quartz. Electric charge release data are taken in conjunction with the initial passage of the stress wave produced by impact."

23. E. A. Ripperger and D. Hart, "Stress-Charge Release Relationships for Ferroelectric Ceramics,"

"The relationship between charge released, electrical load, and stress has been studied for two ferroelectric materials, barium titanate (ceramic B) and lead zirconium titanate (52-48). Stresses which cover the range from zero to 10 kilobars are applied dynamically, in the axial mode, by allowing stress waves generated by an impact to pass through a specimen of the material. The stress applied is measured by the split pressure-bar technique. By properly correlating stress and charge measurements which are recorded as functions of time, stress-charge curves for a given electrical load are constructed. These curves show that the two materials investigated have a dynamic stress-charge relationship. The saturation stress, or the stress at which all the available charge is released is between 4 and 5 kilobars for both materials. Charge released is virtually independent of electrical load for pure ohmic loads between 8 and 1000 ohms. Electrical energy released increases almost directly with electrical load.

A PZT in the "Far Rhombohedral" range (92-8) was also studied briefly. Charge release from this material seems to be dependent, on both rate of stress application, and stress amplitude."

24. R. W. Rhode, O. E. Jones, "Mechanical and Piezoelectric Properties of Shock-Loaded X-Cut Quartz at 573°K,"

"Properties of uniaxially strained X-cut quartz were studied at 573°K over stress range of 6 to 21 kbar by monitoring current output from shock-loaded quartz disk; in addition to providing fundamental knowledge of behavior of quartz under these conditions, results yield data necessary for application of quartz as submicrosecond stress gage at this temperature; experimental results on temperature-stress dependence of piezoelectric and mechanical properties of uniaxially strained X-cut alpha quartz ar· presented."

25. .. A. Krueger, "Stress Sensitivity of Piezoelectric Ceramics-2, 3,"

"Measurements on two piezoelectric ceramics used for high-power, high-stress applications for which stabilizing heat treatment has reduced changes in permittivity; stabilizing effect shown to be permanent; several stress cycles to 10 to 20 kpsi stabilize these ceramics; measurements of changes in permittivity, loss and piezoelectric constants for piezoelectric ceramic transducer materials subject to high stress perpendicular to polar axis; difference in stress sensitivity for "hard" ceramics and "soft" donor-doped ceramics."

26. E. Fatuzzo, W. J. Merz, Selected Topics in Solid State Physics, Vol. 7, Ferroelectricity,

"A number of books and review articles have been published on the subject, however, since the advances made in the last few years, this book offers an up to date review of ferroelectricity. Little space is devoted to the "classical aspects" i.e. dependence of the dielectric properties on pressure, temperature, strain, etc. and the applications of ferroelectricity are only briefly summarized. These intentional omissions apart, the book gives a thorough physical picture of the ferroelectric phenomena. The various topics include: microwave and infrared studies, fatigue effects, thermodynamic theory, static and dynamic properties of domains, lattice dynamic theory, theory of polarization and radiation damage. A chapter is devoted to recent developments in ferroelectric research, these include special effects like optical second-harmonic generation, semi-conducting properties and temperature autostabilization effects in ferroelectrics. As shown above the book deals with purely scientific problems and would be of value to the research worker."

27. D. Berlincourt, "Piezoelectric and Ferroelectric Energy Conversion,"

"The parameters of the materials involved and the principles of these electromechanical energy conversion methods are discussed in general terms. Use of some of these materials for high-voltage thermoelectric energy conversion is discussed briefly; power conversion efficiency appears limited to the 1 percent range."

28. J. C. Muirhead, W. J. Fenrick, "Studies on Shock Wave Pressure-Time Gauges III: The Spontaneous Charge Release Effect,"

"This note describes further studies on spontaneous charge release and absorption in piezoelectric ceramics. Charges that are developed by stressing ceramics (or are impressed on the ceramic from a power source) tend to change the polarities of individual crystals within the ceramics, which thereby store charges. Application of pressure pulses assists in returning these modified crystals to their normal state. This in turn releases the stored electrical charges, which show up on pressure-time records as spontaneous charge release or absorption."

29. W. Ohlwiler, "High Temperature Ferroelectric Materials,"

"This report reviews published data on high-temperature ferroelectric materials. Applicable terms are defined and some characteristics of this type of material are given. High temperature ferroelectric materials studied

were lead metaniobate, lithium tantalate, potassium niobate, lead titanate, and lead metantantalate. Other ferroelectric materials with less supporting data are discussed also."

30. H. Jaffe, D. A. Berlincourt, "Piezoelectric Transducer Materials,"

"Properties of piezoelectric crystals and ceramics are reviewed as they affect use of such materials in electroacoustic transducers. Extensive data on lead titanate-zirconate ceramics are presented to help in selection of the appropriate material for a variety of applications in the lower and medium frequency range, up to several megacycles per second. Quartz and several recently discovered piezoelectric crystals will share the higher megacycle range."

31. Bruce D. Wedlock, "Properties of Piezoelectric Materials,"

"The purpose of this monograph is to provide a source of data on a wide variety of piezoelectric materials which will be useful to those conducting research in this area as well as to the engineer designing ultrasonic transducers, filters, and other piezoelectric devices. The numerical data are given in the rationalized MKS system in accordance with the IRE Standards on Piezoelectricity, as are the symbols employed. Table I defines the symbols employed and gives their MKS unit. Since a large amount of literature still uses the CGS system, Table II presents the factors to convert CGS units to MKS units. On the data pages, the digits in the data columns are to be multiplied by the power of ten in the column immediately to the right of the symbol to obtain the value in the MKS system. The compounds are arranged alphabetically by chemical name. The pure compounds are followed by the binary alloys, followed by ternary compounds, etc. The multiple component compounds are arranged alphabetically by main constituent, secondary constituent, etc., and by decreasing amount of main constituent."

32. I. Lefkowitz, K. Kramer, and P. Kroeger, "Ferroelectrics: Their Electrical Behavior During, and Subsequent to, Ionizing Radiations,"

"A study was made on certain ferroelectric materials which are mong those used extensively in military applications, both in a polarized condition in such items as impact fuzes and in an unpolarized condition as capacitors. The transient voltages across a load produced by charge generated on the surface of various types of ferroelectric specimens during irradiation have been measured. These outputs were found to vary widly in amplitude and polarity even from specimens ostensibly alike (i.e., from the same lot of a given manufacturer),

and even from a single specimen pulsed repeatedly with gamma and neutron radiation. Pulses were found to vary from background levels to a high of 300 volts on a large specimen with a load of 10^7 ohms and radiation of 5.4 x 10^{14} fast (Pu) neutrons and associated gammas. The maximum voltage possible is unknown, as are the factors causing the variation. Both polarized and unpolarized specimens showed outputs well above background transients. Some specimens were identical to those used in impact fuze applications and were in simulated housings which reproduce the mechanical environment of the device. Some fuze circuits in present use are discussed with reference to their use of ferroelectric materials and a calculation of the energy transferred by a voltage pulse to a load is presented."

APPENDIX B

LIST OF COMPUTER PROGRAM

FOR

ELASTIC WAVE PROPAGATION IN A COMPOSITE BAR

General:

The program "CRYSTAL" instructs the computer to perform the following operations in the order listed:

(1) Read in the structural data including geometry and material properties and circuitry data.

(2) Read in the time increment.

(3) Read in the strain input data from the experimental scope recordings.

(4) Calcualte the initial values of the field variables.

(5) Calculate the one dimensional wave velocity, $C = \sqrt{E/\rho}$ for the three media.

(6) Calculate the values of the field variables, σ, ε, and v for each mesh point, up to the leading elastic wave front.

(7) Calculate the stress difference across the crystal faces.

(8) Calculate the short circuit current.

(9) Calculate the energy produced by the short circuit current.

(10) Print on the field variables at desired mesh points. Also print on the stress difference, short circuit current and energy.

(11) Repeat steps (6) through (10) for each time increment.

Data:

(1) E1, E2, E3, RHO1, RHO2, RHO3 (FORMAT 100)

(2) IMAX, L1, L2, X2, DIEC, DIA (FORMAT 101)

(3) M1, M2, M3, R, DT, FACT (To be given in the body of the program).

(4) XINPUT (To be given in the body of the program).

E1, E2, E3 = Youngs modulus for medium 1,2,3 resp.

RHO1, RHO2, RHO3 = Mass density for medium 1,2,3 resp.

IMAX = Total number of time increments

L1 = Spatial increment number to the front face of the crystal

L2 = Spatial increment number to the rear face of the crystal

X2 = Thickness of the crystal

DIEC = Dielectric constant for the crystal

DIA = Diameter of the bar

M1 = 1

M2 = Spatial increment number to the middle of the crystal

M3 = Spatial increment number of teh output gage in the backup bar

R = Short circuit resistance

DT = Time increment

FACT = Scope vertical gain

XINPUT = Vertical deflection of scope for input gage

SIG, STS = Stress at tiem = t and (t-DT) resp.

EPS, STR = Strain at time = t and (t-DT) resp.

VEL, V = Particle velocity at time = t and (t-DT) resp.

CI = Short circuit current

ENERGY = Energy produced by the short circuit current

T = Time

Di = 1.0/ρi*Ci; (i=1,2,3)

Ci = $\sqrt{Ei/\rho i}$; (i=1,2,3)

Running time:

If the calcualtion is done for t=o to t=30μsec DT=0.25μsec, the running time is approximately 15 seconds.

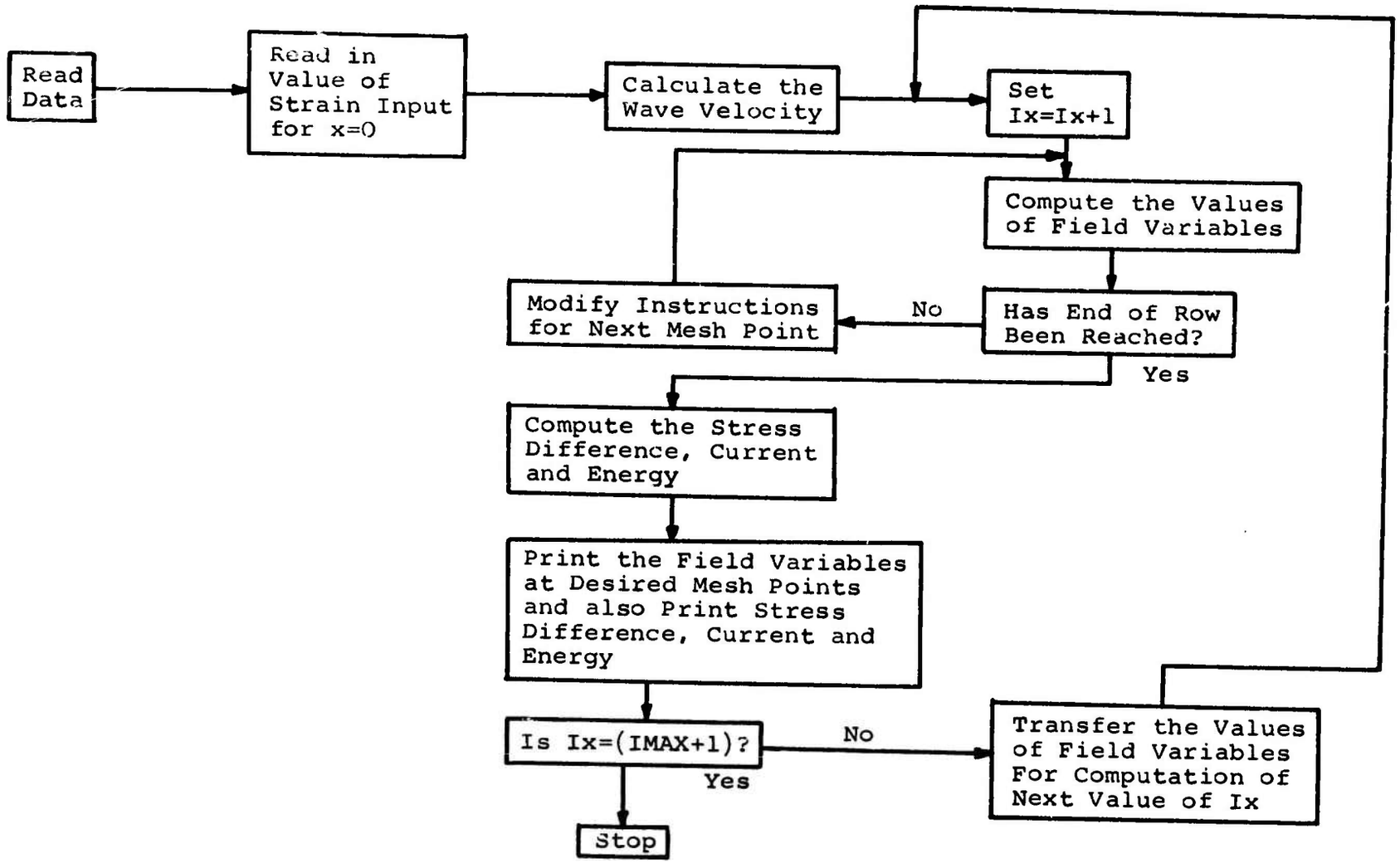

Figure 73. Computer Program Flow Chart for Elastic Wave Propagation

```
JFH,60, 30,55000.VALATHUR,5791,UNM.
RUN(S)
CRYSTAL.
'
      PROGRAM CRYSTAL(INPUT,OUTPUT)
C*****4*****4*****
C*ELASTIC WAVE PROPAGATION IN A COMPOSITE BAR *
C*************************************
      DIMENSION SIG(501),EPS(501),VEL(501),STS(501)
     1,XINPUT(501),ENERGY(501),CI(501),STR(501),V(501)
C   STRAIN INPUT PROBLEM
C   LENGTH OFMEDIUM1*X1*
C   LENGTH OFMEDIUM2*X2*
C DX1 IS THE X INCREMENT IN MEDIUM1
C DX2 IS THE X INCREMENT IN MEDIUM2
C DX3 IS THE X INCREMENT IN MEDIUM3
C E  IS YOUNGS MODULUS
C RHO IS MASS DENSITY
C     R IS RESISTANCE OF THE STRAIN GAGES IN OHMS
C   DT IS THE TIME INCREMENT
C   L1=1+X1/DX1
C   L2=L1+X2/DX2
C  L3=L2+X3/DX1
C   IMAX IS THE TOTAL NUMBER OF INCREMENTS OF TIME
C   IMAX=TOTAL TIME / DT
C NOTE**CHOOSE DT SUCH THAT (L2-L1)IS AN INTEGER**
C DATA TO BE SUPPLIED FOR THE PROBLEM
C*****
C    *NOTE ON UNITS***INCHES,POUNDS,SECONDS**
C*****4*****4*****
C  UNITS OF DATA.  E=LB/IN**2, RHO=LB-SEC**2/IN**4
C  UNITS OF THE DATA. X2=IN., DIEC=AMP-SEC/LB., DIA=IN.
450   READ 100,E1,E2,E3,RHO1,RHO2,RHO3
100   FORMAT(6E10.3)
      READ 101,IMAX,L1,L2,X2,DIEC,DIA
101   FORMAT(3I5,F10.3,E10.3,F10.3)
C   OUTPUT STRAIN GAGE LOCATIONS
C     M1 IS INPUT POINT
      M1=1
C  M2 IS THE MIDPOINT OF MEDIUM 2
C  M3 IS THE SECOND GAGE LOCATION
      AREA=3.1417*(DIA**2.)/4.
      R=53.47
      DT=0.18E-06
C DETAILS OF STRAIN INPUT FROM EXPERIMENTS
C   VALUES OF FIELD VARIABLES AT TIME=0 SPECIFIED BY
C   SUBSCRIPT(1)
      IMAXP1=IMAX+1
      T=0.0
C  XINPUT IS THE VERTICAL DEFLECTION OF SCOPES FOR
```

```
C  STRAIN GAGES
       DO 800 J=1,56
       T=T+DT
  800 XINPUT(J)=2.6E+05*T
       DO 801 J=57,112
       T=T+DT
  801 XINPUT(J)=2.6+6.0E+04*(T-10.0E-06)
       DO 802 J=113,IMAXP1
       T=T+DT
  802 XINPUT(J)=3.2
C SCALE FACTOR FOR INPUT IS*FACT*
       FACT=2924.0E-06/4.0
C END OF INPUT STRAIN
475    CONTINUE
C    THE SPEED OF PROPAGATION IS IN UNITS OF IN./SEC.
       C1=(SQRT(E1/RHO1))
       C2=(SQRT(E2/RHO2))
       C3=(SQRT(E3/RHO3))
       D1=1.0/(RHO1*C1)
       D2=1.0/(RHO2*C2)
       D3=1.0/(RHO3*C3)
       STR(1)=XINPUT(1) *FACT
       STS(1)=E1*STR(1)
       V(1)=D1*STS(1)
       ENERGY(1)=0.0
C FIELD VARIABLES FOR TIME T=DT
       EPS(1)=FACT*XINPUT(2)
       SIG(1)=STS(1)+E1*(EPS(1)-STR(1))
       VEL(1)=V(1)-D1*(SIG(1)-STS(1))
       EPS(2)=STR(1)
       SIG(2)=STS(1)
       ENERGY(2)=ENERGY(1)
       VEL(2)=V(1)
       PRINT 299
C  THE NUMBER AND DATE OF THE DATA IS PRINTED BY FORMAT 169
501    PRINT 169
  169 FORMAT(15X,23H RUN NUMBER 3 7/10/1968,/)
       PRINT 199 , IMAX
       PRINT 20 ,X2
   20 FORMAT(3X,11H THICKNESS=,F10.4)
       PRINT 808 , DIEC
808    FORMAT(3X,21H DIELECTRIC CONSTANT=,F10.3,10HAMP-SEC/LB,
      1//)
       PRINT 300
       PRINT 310
       PRINT 301 , E1,E2,E3,RHO1,RHO2,RHO3,L1,L2
       PRINT 311
       PRINT 312
       PRINT 302
       T=DT
```

```
      PRINT 303,  T,EPS(M1),SIG(L1),EPSBM1,EPS(L1),SIG(L2),
     1EPSBM3,EPS(L2),DFSTR,CI(1),ENERGY(1)
      MIX=3
      DO 200 IX=3,IMAXP1
      T=T+DT
      IX1=IX-1
      DO 201 IJ=1,IX1
      STS(IJ)=SIG(IJ)
      STR(IJ)=EPS(IJ)
  201 V(IJ)=VEL(IJ)
C AREAS OF THE MEDIA ARE EQUAL
C  AT THE INTERFACE FORCES AND VELOCITIES ARE SAME
      STR(IX)=STR(IX1)
      STS(IX)=STS(IX1)
      V(IX)=V(IX1)
      EPS(1)=FACT*XINPUT(IX)
      SIG(1)=STS(1)+E1*(EPS(1)-STR(1))
      VEL(1)=V(1)-D1*(SIG(1)-STS(1))
      SIG(IX)=STS(IX1)
      VEL(IX)=V(IX1)
      IF(IX-L1)212,213,214
  213 EPS(IX)=SIG(IX)/E2
      GO TO 216
  214 IF(IX-L2)212,212,215
  215 EPS(IX)=SIG(IX)/E3
      GO TO 216
  212 EPS(IX)=STR(IX1)
  216 DO 202 IJ=2,IX1
      IJL=IJ-1
      IJR=IJ+1
      IF(IJ-L1)203,204,205
  204 DL=1.0/D1
      DR=1.0/D2
      GO TO 209
  205 IF(IJ-L2)206,207,208
  207 DL=1.0/D2
      DR=1.0/D3
  209 VEL(IJ)=(STS(IJR)-STS(IJL)+DL*V(IJL)+DR*V(IJR))/(DL+DR)
      SIG(IJ)=STS(IJL)+DL*(VEL(IJ)-V(IJL))
      EPS(IJ)=STR(IJ)+(SIG(IJ)-STS(IJ))/E2
      GO TO 202
  206 DX=D2
      EX=E2
      GO TO 210
  208 DX=D3
      EX=E3
      GO TO 210
  203 DX=D1
      EX=E1
  210 V5L(IJ)=(V(IJR)+V(IJL)+DX*(STS(IJR)-STS(IJL)))/2.0
```

```
      SIG(IJ)=STS(IJL)+UVEL(IJ)-V(IJL))/DX
      EPS(IJ)=STR(IJ)+(SIG(IJ)-STS(IJ))/EX
  202 CONTINUE
      EPSBM1=SIG(L1)/E1
      EPSBM3=SIG(L2)/E3
C  DFSTR IS THE STRESS DIFFERENCE ACROSS THE CRYSTAL
      DFSTR=SIG(L1)-SIG(L2)
C  CONVERSION FACTOR FROM WATT-SEC TO JOULES IS 'CON'
      CON=1.0
C  CI(IX) IS THE SHORT CIRCUIT CURRENT AS CALCULATED BY
C  STRESS EQUATION AND THE UNITS ARE AMPERES.
      CI(IX)=DFSTR*AREA*C2*DIEC/X2
C  ENERGY IS THE POWER PRODUCED BY THE SHORT CIRCUIT CURRENT
C  *** ENERGY=DX/3*R*(CI(N)**2+4*CI(N+1)**2+CI(N+2)**2)
      IF(IX-MIX)600,600,700
600   CONTINUE
      ENERGY(IX)=DT/3.*R*CON*(CI(IX-2)**2+4.*CI(IX-1)**2+
     1CI(IX)**2)+ENERGY(IX-2)
211   PRINT 303, T,EPS(M1),SIG(L1),EPSBM1,EPS(L1),SIG(L2),
     1EPSBM3,EPS(L2),DFSTR,CI(IX),ENERGY(IX)
      GO TO 200
700   CONTINUE
      PRINT 303, T,EPS(M1),SIG(L1),EPSBM1,EPS(L1),SIG(L2),
     1EPSBM3,EPS(L2),DFSTR,CI(IX)
      MIX=MIX+2
  200 CONTINUE
  299 FORMAT(1H1,10X,44H ELASTIC WAVE PROPAGATION IN A
     1COMPOSITE BAR/)
  199 FORMAT(3X,6H IMAX=,I5,/)
  300 FORMAT(3X,3H E1,7X,3H E2,7X,3H E3,6X,5H RHO1,5X,
     15H RHO2,5X,5H RHO3,5X,3H L1,2X,3H L2)
301   FORMAT(6E10.3,2I5//)
302   FORMAT(//,2X,5H TIME,6X,6H EPSM1,5X,6H SIGL1,4X,
     17H EPSBM1,5X,6H EPSL1,5X,6H SIGL2,4X,7H EPSBM3,5X,
     26H EPSL2,5X,6H DFSTR,2X,8H CURRENT,4X,7H ENERGY)
303   FORMAT(E10.3,10E11.4)
310   FORMAT(1X,27H....3....(LB/IN**2).........,4X,29H......
     1(LB-SEC**2/IN**4).....)
311   FORMAT(14H****LEGEND****,/,4X,35HEPSM1=STRAIN AT FI
     1RST GAGE LOCATION,/,4X,40HSIGL1=STRESS IN MEDI
     2UM 1 AT CRYSTAL FACE,/,4X,41HEPSBM1=STRAIN IN MED
     3IUM 1 AT CRYSTAL FACE,/,4X,40HEPSL1=STRAIN IN MED
     4IUM2 AT CRYSTAL FACE,/,4X,33HSIGL2=STRESS AT CRY
     5STAL REAR FACE,/,4X,41HEPSBM3=STRAIN IN MEDIUM 3 A
     6T CRYSTAL FACE,/,4X,36HEPSL2=STRAIN IN CRYSTAL A
     7T REAR FACE)
312   FORMAT(4X,38HDFSTR=STRESS DIFFERENCE ACROSS CRYST
     1AL,/,4X,40HCURRENT=CIRCUIT CURRENT IN UNITS OF AM
     2PS,/,4X,40HENERGY=CRYSTAL ENERGY INUNITS OF JOULES,/)
1000  CONTINUE
      STOP
      END
```

EXAMPLE RUN

ELASTIC WAVE PROPAGATION IN A COMPOSITE BAR

UNM - SCR 3 TEST C - ALGP X00 - .0050 QTZ CRYSTAL
IMAX= 150

PIEZOELECTRIC CONSTANT= 4.50E-11AMP-SEC/LB

E1	E2	E3	RHO1	RHO2	RHO3	L1	L2
.....(LB/IN**2).....			.....(LB-SEC**2/IN**4).....				
1.010E+07	1.100E+07	1.010E+07	2.525E-04	2.930E-04	2.525E-04	9	7

LEGEND*
EPSM1=STRAIN AT PARDT GAGE LOCATION
SIGL1=STRESS IN MEDIUM 1 AT CRYSTAL FACE
EPSM1=STRAIN IN MEDIUM 1 AT CRYSTAL FACE
EPSL1=STRAIN IN MEDIUM 2 AT CRYSTAL FACE
SIGL2=STRESS AT CRYSTAL REAR FACE
EPSM3=STRAIN IN MEDIUM 3 AT CRYSTAL FACE
EPSL2=STRAIN IN CRYSTAL AT REAR FACE
DFSTR=STRESS DIFFERENCE ACROSS CRYSTAL
CURRENT=CIRCUIT CURRENT IN UNITS OF AMPS
ENERGY=CRYSTAL ENERGY IN UNITS OF JOULES

TIME	EPSM1	SIGL1	EPSM1	EPSL1	SIGL2	EPSM3	EPSL2	DFSTR	CURRENT	ENERGY
1.825E-07	0.	0.	0.	0.	0.	0.	0.	0.	0.	0.
3.650E-07	2.737E-06	0.	0.	0.	0.	0.	0.	0.	0.	0.
5.475E-07	2.737E-06	0.	0.	0.	0.	0.	0.	0.	0.	
7.300E-07	2.737E-06	0.	0.	0.	0.	0.	0.	0.	0.	0.
9.125E-07	5.474E-06	0.	0.	0.	0.	0.	0.	0.	0.	
1.095E-06	8.211E-06	2.955E+01	2.960E-06	2.948E-06	0.	0.	0.	2.955E+01	2.956E-04	1.7[illegible]
1.278E-06	8.211E-06	2.955E+01	2.960E-06	2.948E-06	0.	0.	0.	2.955E+01	2.956E-04	
1.460E-06	8.211E-06	2.955E+01	2.960E-06	2.948E-06	2.731E-06	2.724E-06	2.871E-06	2.956E+01	2.956E-04	1.6E4[illegible]
1.643E-06	8.211E-06	2.911E+01	2.852E-06	2.893E-06	2.731E-06	2.724E-06	2.871E-06	2.816E+01	2.561E-04	
1.825E-06	1.094E-05	7.119E+01	7.127E-06	6.208E-06	2.731E-06	2.724E-06	2.871E-06	4.447E+01	3.9E3E-04	2.1E09E-1[illegible]
2.008E-06	1.258E-05	8.079E+01	8.091E-06	7.483E-06	5.462E-06	5.448E-06	5.742E-06	2.617E+01	2.394E-04	
2.190E-06	1.094E-05	7.119E+01	7.127E-06	6.208E-06	8.193E-06	8.172E-06	8.613E-06	2.744E+00	2.49E3E-05	3.0E39E-1[illegible]
2.373E-06	2.189E-05	8.460E+01	8.482E-06	7.310E-06	5.462E-06	5.448E-06	5.742E-06	2.716E+01	2.473E-04	
2.555E-06	2.737E-05	1.134E+02	1.123E-05	9.781E-06	8.193E-06	8.172E-06	8.613E-06	4.463E+01	3.975E-04	3.7508-1[illegible]
2.738E-06	3.284E-05	1.278E+02	1.268E-05	1.097E-05	8.193E-06	8.172E-06	8.613E-06	4.460E+01	3.964E-04	
2.920E-06	4.294E-05	1.703E+02	1.703E-05	1.468E-05	1.093E-05	1.089E-05	1.148E-05	5.947E+01	5.285E-04	6.444E-1[illegible]
3.103E-06	5.337E-05	2.119E+02	2.133E-05	1.838E-05	1.366E-05	1.362E-05	1.435E-05	7.430E+01	6.605E-04	
3.285E-06	6.509E-05	2.587E+02	2.609E-05	2.248E-05	1.639E-05	1.634E-05	1.722E-05	8.914E+01	7.926E-04	1.170E-1[illegible]

APPENDIX C

LISTING OF COMPUTER PROGRAM

FOR

PLASTIC WAVE PROPAGATION IN A COMPOSITE BAR

General:

The program "WAVES" instructs the computer to perform the following operations in the order listed:

(1) Read in the structural data including geometry and material properties and circuitry data

(2) Read in the time increment

(3) Read in the strain input data from the experimental scope recordings

(4) Calculate the initial values of the field variables

(5) Calculate the one dimensional wave velocity, $C = \sqrt{E/\rho}$ for the three midia

(6) Knowing the values of the field variables at the previous instant of time ie t=t-Dt, the slopes of the characteristics starting from the previous time base and passing through the mesh points considered are calculated. This is done by calling the subroutine "INTERP". This subroutine calculates the field variables at the starting point of the characteristic by linear polation.

(7) Calculate the values of the field variables, σ, ε, and v.

(8) Repeat steps (6) and (7) for all the mesh points, up to the leading elastic wave front.

(9) Calculate the stress difference across the crystal faces.

(10) Calculate the short circuit current

(11) Calculate the energy produced by the short circuit current

(12) Print out the field variables at desired mesh points. Also print out the stress difference, short circuit current and energy

(13) Repeat steps (6) through (12) for each time increment

Data:

(1) E1, E2, E3, RHO1, RHO2, RHO3 (FORMAT 100)

(2) IMAX, L1, L2, X2, DIEC, DIA (FORMAT 101)

(3) XK, XN (FORMAT 99)

(4) YIELD, R, DT, FACT, M1 (To be given in the body of the program)

(5) XINPUT (To be given in the body of the program)

List of symbols:

E1, E2, E3 = Youngs modulus for medium 1,2,3 resp.

RHO1, RHO2, RHO3 = Mass density for medium 1,2,3 resp.

IMAX = Total number of time increments

L1 = Spatial increment number to the front face of the crystal

L2 = Spatial increment number to the rear face of the crystal

X2 = Thickness of the crystal

DIEC = Dielectric constant for the crystal

DIA = Diameter of the bar

XK, XN = Material parameters for the input bar

YIELD = Yield stress for input bar

R = Short circuit resistance

DT = Time increment

FACT = Scope vertical gain

XINPUT = Vertical deflection of scope for input gage

M1 = 1

SIG, STS = Stress at time=t and (t-DT) resp.

EPS, STR = Strain at time=t and (t-DT) resp.

VEL, V = Particle velocity at time=t and (t-DT) resp.

F, S = Function variable at time=t and (t-DT) resp.

CI = Short circuit current

ENERGY = Energy produced by the short circuit current

T = Time

Dj = 1.0/ρj*Cj; (j=1,2,3)

$$Cj = \sqrt{Ej/\rho j} \ ; \ (j=1,2,3)$$

XN1 = XN-1

XN12 = XN1/2.0

SGI, SGV, VI, VLV = Variable quantities

Running time:

If the calculation is done for t=o to t=30μsec with DT = 0.1μsec., the running time is approximately 100 seconds.

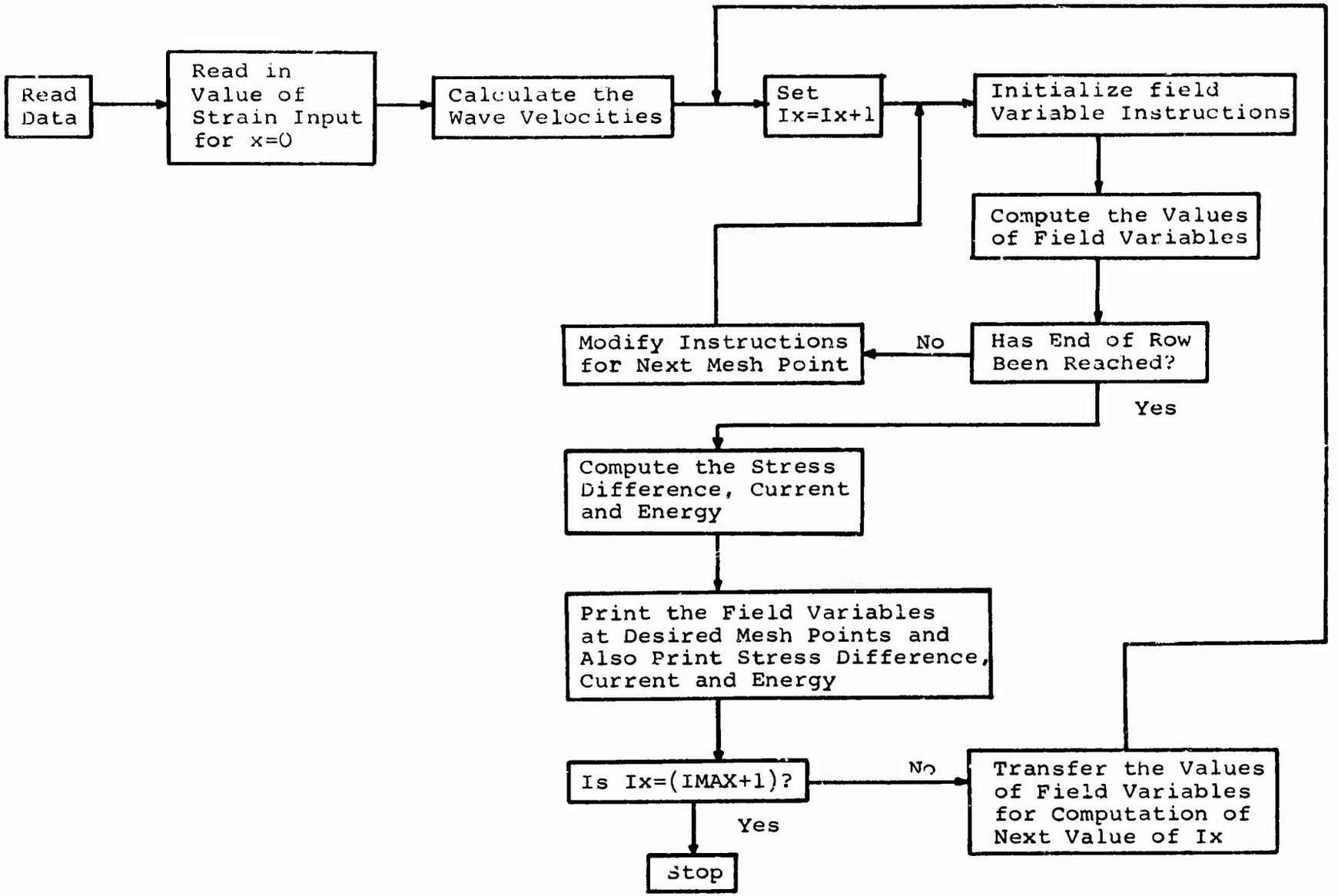

Figure 74. Computer Program Flow Chart for Plastic Wave Propagation in a Composite Bar

```
JFH,6 ,500,55000.VALATHUR,5791,UNM,3743.
RUN(S,,,,,,25000)
WAVES.
'
      PROGRAM WAVES(INPUT,OUTPUT)
      COMMON SGI,SGV,VI,VLV,RHO1,C1,XK,XN,DT,DX1,SGL,VL,
     1XE1,CF,RCF,XKN,XN1
      COMMON YIELD
      DIMENSION SIG(501),EPS(501),VEL(501),STS(501),STR(501)
     1,S(501),F(501),XINPUT(501),CI(501),ENERGY(501),V(501)
C*********************************************
C*PLASTIC WAVE PROPAGATION IN A COMPOSITE BAR *
C*********************M***********************
C     MEDIUM 2 IS IN ELASTIC STATE AND MEDIA 1AND3 ARE
C     IN PLASTIC STATE
C**********************M***
C*    STRAIN INPUT PROBLEM*
C************************
C     LENGTH OF MEDIUM2*X2*
C DX1 IS THE X INCREMENT IN MEDIUM1
C DX2 IS THE X INCREMENT IN MEDIUM2
C DX3 IS THE X INCREMENT IN MEDIUM3
C     STRESS IS EXPRESSED IN KSI UNITS
C E  IS YOUNGS MODULUS
C RHO IS MASS DENSITY
C     XK AND XN....MATERIAL PARAMETERS(RATE INDEPENDENT
C     THEORY)
C     *R* IS THE RESISTANCE OF THE CIRCUIT IN OHMS
C   DT IS THE TIME INCREMENT
C   L1=1+X1/DX1
C   L2=L1+X2/DX2
C   IMAX IS THE TOTAL NUMBER OF INCREMENTS OF TIME
C   IMAX=TOTAL TIME / DT
C NOTE**CHOOSE DT SUCH THAT (L2-L1)IS AN INTEGER**
C*****)***************4**********************
C****NOTE ON UNITS...KIPS,INCHES,SECONDS******
C*********************************************
C     UNITS OF DATA...E=KIPS/IN**2,RHO=KIPS-SEC**2/IN**4
C     UNITS OF DATA...X2=INCHES,DIEC=AMP-SEC/KIP,DIA=INCH
C DATA TO BE SUPPLIED FOR THE PROBLEM
      READ 100 ,E1,E2,E3,RHO1,RHO2,RHO3
  100 FORMAT(6E10.3)
      READ 101,IMAX,L1,L2,X2,DIEC,DIA
  101 FORMAT(3I5,F10.3,E10.3,F10.3)
      READ 99,XK,XN
   99 FORMAT(2E12.4)
C     YIELD STRESS FOR MATERIAL 1 IS EQUAL TO30 KSI(YIELD)
C
```

```
      YIELD=30.0
C
C     DETAILS OF STRAIN INPUT FROM EXPERIMENTS
C     SCALE FACTOR FOR INPUT IS *FACT*
      DT=0.15E-06
      R=53.47
      IMAXP1=IMAX+1
      T=0.0
C     XINPUT IS THE VERTICAL DEFLECTION OF SCOPES FOR
C     STRAIN GAGES
      READ 800,(XINPUT(J),J=1,IMAXP1)
  800 FORMAT(15F5.2)
C     SCALE FACTOR FOR INPUT IS FACT
      FACT=2.985E-03
C  END OF READING THE INPUT
      AREA=22.0/7.0*DIA**2/4.0
      C1=SQRT(E1/RHO1)
      C2=SQRT(E2/RHO2)
      C3=SQRT(E3/RHO3)
      D1=1.0/(RHO1*C1)
      D2=1.0/(RHO2*C2)
      D3=1.0/(RHO3*C3)
      DI=1.0/D2
      DX1=C1*DT
      DX2=C2*DT
      DX3=C3*DT
      XE1=1./E1
      XE2=1.0/E2
      XKN=XK*XN
      XN1=XN-1.0
      XN12=XN1/2.0
C    SPECIFY THE VALUES OF THE FIELD VARIABLES FOR ZERO TIME
C     BY SUBSCRIPT(1)
      STR(1)=XINPUT(1) *FACT
      STS(1)=E1*STR(1)
      V(1)=D1*STS(1)
      S(1)=1.0/E1
      ENERGY(1)=0.0
C FIELD VARIABLES FOR TIME T=DT
      EPS(1)=FACT*XINPUT(2)
      SIG(1)=STS(1)+E1*(EPS(1)-STR(1))
      STRS2=SIG(1)* SIG(1)
      F(1)=XE1+XKN*STRS2**XN12
      VEL(1)=V(1)-D1*(SIG(1)-STS(1))
      EPS(2)=STR(1)
      SIG(2)=STS(1)
      VEL(2)=V(1)
      F(2)=S(1)
      ENERGY(2)=0.0
```

```
      PRINT 299
      PRINT 169
  169 FORMAT(15X,24H RUN NUMBER ARO 8/7/1968,/)
      PRINT 808 , DISC
  808 FORMAT(3X,21H DIELECTRIC CONSTANT=,E10.3,
     112H AMP-SEC/KIP,//)
      PRINT 300
      PRINT 301 , E1,E2,E3,RHO1,RHO2,RHO3,L1,L2
      PRINT 311
      PRINT 312
      PRINT 302
      T=DT
      MIX=3
      FPM1=1.0/E1
      FPM3=1.0/E3
C     OUTPUT STRAIN GAGE LOCATIONS
C       M1 IS INPUT POINT
      M1=1
      DO 200 IX=3,IMAXP1
      T=T+DT
      IX1=IX-1
      DO 201 IJ=1,IX1
      STS(IJ)=SIG(IJ)
      STR(IJ)=EPS(IJ)
      S(IJ)=F(IJ)
  201 V(IJ)=VEL(IJ)
C   AREAS OF THE MEDIA ARE EQUAL
C   AT THE INTERFACE FORCES AND VELOCITIES ARE SAME
      STR(IX)=STR(IX1)
      STS(IX)=STS(IX1)
      V(IX)=V(IX1)
      S(IX)=S(IX1)
      EPS(1)=FACT*XINPUT(IX)
      SIG(1)=STS(1)+(EPS(1)-STR(1))/S(1)
      STRS2=SIG(1)* SIG(1)
      F(1)=XE1+XKN*STRS2**XN12
      SGI=STS(1)
      VI=V(1)
      SGV=STS(2)-STS(1)
      VLV=V(2)-V(1)
      CALL INTERP
      VEL(1)=VL-(SIG(1)-SGL)/RCF
      SIG(IX)=STS(IX1)
      VEL(IX)=V(IX1)
      IF(IX-L1)212,213,214
  213 EPS(IX)=SIG(IX)/E2
      F(IX)=1./E2
      GO TO 216
  214 IF(IX-L2)212,212,215
  215 EPS(IX)=SIG(IX)/E3
```

```
      F(IX)=1.0/E3
      GO TO 216
  212 EPS(IX,=STR(IX1)
      F(IX)=S(IX1)
  216 DO 202 IJ=2,IX1
      IJL=IJ-1
      IJR=IJ+1
      IF(IJ-L1)203,204,205
  204 SGI=STS(IJ)
      VI=V(IJ)
      SGV=STS(IJL)-STS(IJ)
      VLV=V(IJL)-V(IJ)
      CALL INTERP
      VEL(IJ)=(STS(IJR)-SGL+V(IJR)/D2+RCF*VL)/(RCF+DI)
      SIG(IJ)=STS(IJR)-(VEL(IJ)-V(IJR))/D2
      EPS(IJ)=STR(IJ)+(SIG(IJ)-STS(IJ))/E2
      F(IJ)=XE2
      EPBM1=EPBM1+(SIG(IJ)-STS(IJ))*FPM1
      STRS2=SIG(IJ)*SIG(IJ)
      FPM1=XE1+XKN*STRS2**XN12
      GO TO 202
  205 IF(IJ-L2)206,207,208
  207 SGI=STS(IJ)
      VI=V(IJ)
      SGV=STS(IJR)-STS(IJ)
      VLV=V(IJR)-V(IJ)
      CALL INTERP
      VEL(IJ)=(SGL-STS(IJL)+RCF*VL+V(IJL)/D2)/(RCF+DI)
      SIG(IJ)=STS(IJL)+(VEL(IJ)-V(IJL))/D2
      EPS(IJ)=STR(IJ)+(SIG(IJ)-STS(IJ))/E2
      F(IJ)=XE2
      EPBM3=EPBM3+(SIG(IJ)-STS(IJ))*FPM3
      STRS2=SIG(IJ)*SIG(IJ)
      FPM3=XE1+XKN*STRS2**XN12
      GO TO 202
  206 DX=D2
      EX=E2
  210 VEL(IJ)=(V(IJR)+V(IJL)+DX*(STS(IJR)-STS(IJL)))/2.0
      SIG(IJ)=STS(IJL)+(VEL(IJ)-V(IJL))/DX
      EPS(IJ)=STR(IJ)+(SIG(IJ)-STS(IJ))/EX
      F(IJ)=XE2
      GO TO 202
  208 CONTINUE
  203 SGI=STS(IJ)
      VI=V(IJ)
      SGV=STS(IJR)-STS(IJ)
      VLV=V(IJR)-V(IJ)
      CALL INTERP
      SGR=SGL
      VR=VL
```

```
      CR=CF
      RCR=RCF
      SGV=STS(IJL)-STS(IJ)
      VLV=V(IJL)-V(IJ)
      CALL INTERP
      CL=CF
      RCL=RCF
      VEL(IJ)=((SGR-SGL)/RHO1+CR*VR+CL*VL)/(CL+CR)
      SIG(IJ)=SGL+RCL*(VEL(IJ)-VL)
      EPS(IJ)=STR(IJ)+S(IJ)*(SIG(IJ)-STS(IJ))
      STRS2=SIG(IJ)*SIG(IJ)
      F(IJ)=XE1+XKN*STRS2**XN12
  304 FORMAT(I5,3E12.4)
  202 CONTINUE
      DFSTR=SIG(L1)-SIG(L2)
C  CONVERSION FACTOR FROM WATT-SEC TO JOULES IS 'CON'
      CON=1.0
C  THE UNITS OF CI ARE AMPERES.
      CI(IX)=DFSTR*AREA*C2*DIEC/X2
C  ENERGY IS THE POWER PRODUCED BY THE SHORT CIRCUIT CURRENT
      IF(IX-MIX)600,600,700
600   CONTINUE
      ENERGY(IX)=DT/3.*R*CON*(CI(IX-2)**2+4.*CI(IX-1)**2+
     1CI(IX)**2)+ENERGY(IX-2)
211   PRINT 303,  T,EPS(M1),SIG(L1), EPBM1,EPS(L1),SIG(L2),
     1EPBM3,EPS(L2),DFSTR,CI(IX),ENERGY(IX)
      GO TO 200
700   CONTINUE
      PRINT 303,  T,EPS(M1),SIG(L1), EPBM1,EPS(L1),SIG(L2),
     1EPBM3,EPS(L2),DFSTR,CI(IX)
      MIX=MIX+2
  200 CONTINUE
  299 FORMAT(1H1,10X,44H PLASTIC WAVE PROPAGATION IN A COM
     1POSITE BAR/)
  300 FORMAT(3X,3H E1,7X,3H E2,7X,3H E3,6X,5H RHO1,5X,
     15H RHO2,5X,5H RHO3,5X,3H L1,2X,3H L2)
  301 FORMAT(6E10.3,2I5)
  302 FORMAT(4X,5H TIME,7X,6H EPSM1,6X,6H SIGL1,5X,
     17H EPSBM1,6X,6H EPSL1,6X,6H SIGL2,5X,7H EPSBM3,6X,
     26H EPSL2,6X,6H DFSTR,2X,8H CURRENT,4X,7H ENERGY)
  303 FORMAT(11E12.4)
311   FORMAT(14H****LEGEND****,/,4X,35HEPSM1=STRAIN AT FI
     1RST GAGE LOCATION,/,4X,40HSIGL1=STRESS IN MEDI
     2UM 1 AT CRYSTAL FACE,/,4X,41HEPSBM1=STRAIN IN MED
     3IUM 1 AT CRYSTAL FACE,/,4X,40HEPSL1=STRAIN IN MED
     4IUM2 AT CRYSTAL FACE,/,4X,33HSIGL2=STRESS AT CRY
     5STAL REAR FACE,/,4X,41HEPSBM3=STRAIN IN MEDIUM 3 A
     6T CRYSTAL FACE,/,4X,36HEPSL2=STRAIN IN CRYSTAL A
     7T REAR FACE)
312   FORMAT(4X,38HDFSTR=STRESS DIFFERENCE ACROSS CRYST
```

```
     1AL,/,4X,40HCURRENT=CIRCUIT CURRENT IN UNITS OF AM
     2PS,/,4X,40HENERGY=CRYSTAL ENERGY INUNITS OF JOULES,/)
      STOP
      END
      SUBROUTINE INTERP
      COMMON SGI,SGV,VI,VLV,RHO1,C1,XK,XN,DT,DX1,SGL,VL,
     1XE1,CF,RCF,XKN,XN1
      COMMON YIELD
C     YIELD STRESS FOR MATERIAL 1 IS EQUAL TO 30 KSI(YIELD)
      IF(SGI+SGV- YIELD )105,105,106
  105 SGL=SGI+SGV
      VL=VI+VLV
      CF=C1
      GO TO 107
  106 XN12=XN1/2.0
      DDX=DX1/60.0
      SGLV=SGV/60.0
      SGL=SGI
      XMUL=0.0
  100 SGL=SGL+SGLV
      XMUL=XMUL+DDX
      STRS2=SGL*SGL
  104 FP=XE1+XKN*STRS2**XN12
      CF=SQRT(1.0/(RHO1*FP))
      IF(XMUL/CF-DT)102,101,101
  102 GO TO 100
  101 VL=VI+XMUL*VLV/DX1
  107 RCF=RHO1*CF
      RETURN
      END
```

EXAMPLE RUN

PLASTIC WAVE PROPAGATION IN A COMPOSITE BAR

ARO SHOT 1206 - USES CHGCOF TO COMPUTE NON-LINEAR
CHARGE COEFFICIENT FOR .100 INCH HST-41 CRYSTAL.
IMAX= 123

DIELECTRIC CONSTANT= 1.020E-08AMP-SEC/KIP
TIME DELAY= 0. SECONDS

E1	E2	E3	RHO1	RHO2	RHO3	L1	L2
.....(LB/IN**2).....			.....(LB-SEC**2/IN**4).....				
1.010E+04	8.603E+03	1.010E+04	2.525E-07	7.110E-07	2.525E-07	5	16

LEGEND*
EPSM1=STRAIN AT FIRST GAGE LOCATION
SIGL1=STRESS IN MEDIUM 1 AT CRYSTAL FACE
EPSBM1=STRAIN IN MEDIUM 1 AT CRYSTAL FACE
EPSL1=STRAIN IN MEDIUM 2 AT CRYSTAL FACE
SIGL2=STRESS AT CRYSTAL REAR FACE
EPSBM3=STRAIN IN MEDIUM 3 AT CRYSTAL FACE
EPSL2=STRAIN IN CRYSTAL AT REAR FACE
DFSTR=STRESS DIFFERENCE ACROSS CRYSTAL
CURRENT=CIRCUIT CURRENT IN UNITS OF AMPS
ENERGY=CRYSTAL ENERGY IN UNITS OF JOULES

TIME	EPSM1	SIGL1	EPSBM1	EPSL1	SIGL2	EPSBM3	EPSL2	DFSTR	CURRENT	ENERGY
1.000E-07	-2.9731E-05	0.	0.	0.	0.	0.	0.	0.	0.	0.
2.000E-07	-4.7570E-05	0.	0.	0.	0.	0.	0.	0.	0.	0.
3.000E-07	-5.3516E-05	0.	0.	0.	0.	0.	0.	0.	0.	0.
4.000E-07	-2.3785E-05	0.	0.	0.	0.	0.	0.	0.	0.	0.
5.000E-07	2.9731E-05	-3.6493E-01	-3.6132E-05	-4.2419E-05	0.	0.	0.	-3.6493E-01	-9.1392E-02	3.7231E-10
6.000E-07	5.3516E-05	-5.8389E-01	-5.7811E-05	-6.7870E-05	0.	0.	0.	-5.8389E-01	-1.4644E-01	2.4320E-09
7.000E-07	2.9731E-05	-6.5688E-01	-6.5037E-05	-7.6353E-05	0.	0.	0.	-6.5688E-01	-1.6485E-01	5.7485E-09
8.000E-07	0.	-2.9194E-01	-2.8905E-05	-3.3935E-05	0.	0.	0.	-2.9194E-01	-7.3285E-02	8.4389E-09
9.000E-07	-2.9731E-05	3.6493E-01	3.6132E-05	4.2419E-05	0.	0.	0.	3.6493E-01	9.1392E-02	8.2710E-09
1.000E-06	-1.0109E-04	6.5688E-01	6.5037E-05	7.6353E-05	0.	0.	0.	6.5688E-01	1.6485E-01	1.1362E-08
1.100E-06	-1.1892E-04	3.6493E-01	3.6132E-05	4.2419E-05	0.	0.	0.	3.6493E-01	9.1392E-02	1.3831E-08
1.200E-06	-1.1892E-04	1.0658E-14	1.0842E-18	1.0842E-18	0.	0.	0.	1.0658E-14	2.6667E-15	1.4048E-08
1.300E-06	-8.9193E-05	-2.8637E-01	-2.8353E-05	-3.3286E-05	0.	0.	0.	-2.8637E-01	-7.1691E-02	1.4429E-08
1.400E-06	-4.7570E-05	-1.1151E+00	-1.1040E-04	-1.2961E-04	0.	0.	0.	-1.1151E+00	-2.8142E-01	1.8471E-08
1.500E-06	-1.7839E-05	-1.3183E+00	-1.3053E-04	-1.5324E-04	0.	0.	0.	-1.3183E+00	-3.3386E-01	3.2644E-08
1.600E-06	1.7839E-05	-1.3969E+00	-1.3830E-04	-1.6237E-04	-2.8637E-01	-2.8353E-05	-3.3286E-05	-1.1105E+00	-2.8337E-01	4.5369E-08

APPENDIX D

LISTING OF COMPUTER PROGRAM

FOR

CURVE FIT

```
C      T8IS PROGRAM COMPUTES THE COEFFICIENTS FOR A NATURAL
C      CUBIC INTERPOLATORY SPLINE FIT TO EQUALLY SPACED
C      DATA POINTS.
C
C      INPUT AND OUTPUT VARIABLES ARE AS DEFINED BELOW
C         N - NUMBER OF SEGMENTS OR SPLINES
C         H - WIDTH OF EACH SEGMENT (NORMALIZE CLOSE TO 1
C             TO MINIMIZE COMPUTATIONAL ERRORS)
C         Y - DEPENDENT VARIABLE INPUT DATA
C         FACT(I) - THESE ARE THE MULTIPLIERS IN THE GENERAL
C             SPLINE FORMULA, INDEXED FROM 1TO N+1
      DIMENSION EM(11),U(11),F(11),B(11),FACT(13),Y(13)
      D1TA Y/0.0,1.8,5.3,10.4,15.9,20.4,23.6,25.8,27.4,
     128.5,29.3,29.9,30.1/
      H=1.0
      N=12
      NP1=N+1
      NM1=N-1
      DO 10 I=1,NM1
      EM(I)=H/6.0
      U(I)=2.0*H/3.0
      F(I)=H/6.0
   10 CONTINUE
      DO 20 J=2,N
      JM1=J-1
      JP1=J+1
      B(JM1)=(Y(JP1)-2.0*Y(J)+Y(JM1))/H
   20 CONTINUE
      DO 100 I=2,NM1
      IM1=I-1
      EM(I)=EM(I)/U(IM1)
      U(I)=U(I)-EM(I)*F(IM1)
  100 CONTINUE
      FACT(1)=0.0
      FACT(NP1)=0.0
      FACT(2)=B(1)
      DO 200 I=2,NM1
      IP1=I+1
      FACT(IP1)=B(I)-EM(I)*FACT(I)
  200 CONTINUE
      FACT(N)=FACT(N)/U(NM1)
      DO 300 J=2,NM1
      I=NP1-J
      IP1=I+1
      IM1=I-1
      FACT(I)=(FACT(I)-F(IM1)*FACT(IP1))/U(IM1)
  300 CONTINUE
      PRINT 1,(FACT(I), I=1,NP1)
    1 FORMAT(12F10.3)
      CALL EXIT
      END
/DATA
/END
```

APPENDIX E

LISTING OF COMPUTER PROGRAM FOR

DETERMINATION OF ENERGY OUTPUT FROM CURRENT

General:

The program "ELCENR" computes the energy produced from the experimental voltage input. This program instructs the computer to perform the following operations in the order listed:

(1) Read in the circuitry data
(2) Read in the time increment
(3) Read in the scope deflection data
(4) Calculate voltage, current for each time increment
(5) Calculate the energy by Simpson's rule
(6) Print out current and energy

Data:

DT, IMAX, SGAIN, R, TG (FORMAT 100)

RSC (To be given in the body of the program)

List of symbols:

DT = Time increment
IMAX = Total number of time increments
SGAIN = Scope vertical gain
R = Resistance of the strain gage
TG = Trigger delay time
RSC = Short circuit resistance
DEF = Scope deflection data
V = Voltage
I = Short circuit current
ENERGY = Energy developed
T = Time

FLOW CHART

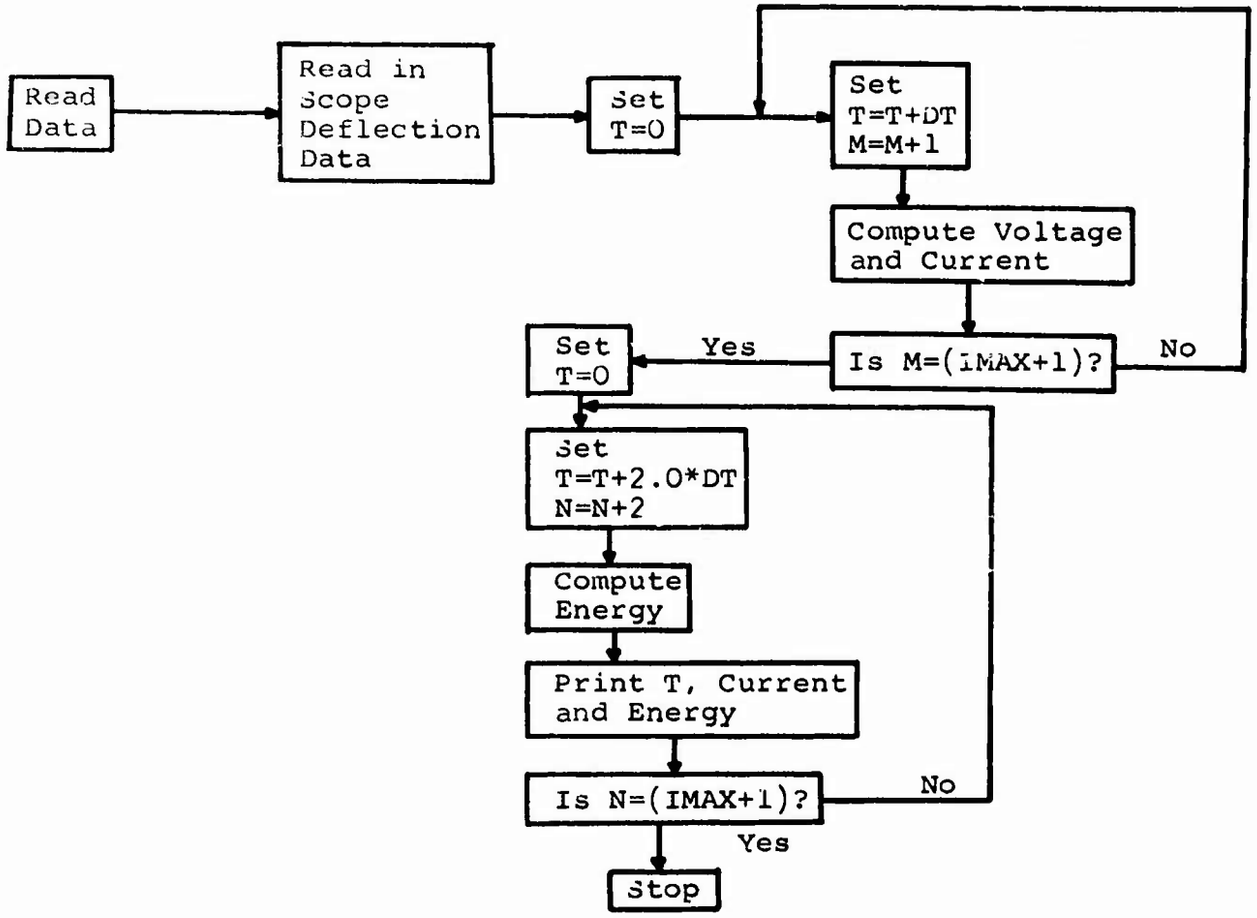

Figure 75. Computer Program Flow Chart for Determination of Energy Output from Current

```
JFH,60, 30,50000.VALATHUR,5791,UNM.
RUN(S)
ELCENR.
'
      PROGRAM ELCENR(INPUT,OUTPUT)
C     ****************************************************
C     **REDUCTION OF CRYSTAL DATA FOR ELECTRICAL ENERGY**
C     ****************************************************
      DIMENSION I(501),V(501),ENERGY(501),DEF(501)
      REAL I
C
C  READ IN TIME STEP DT, TOTAL NUMBER OF TIME INCRSMENTS
C  IMAX, SCOPE VERTICAL GAIN SGAIN, GAGE RESISTANCE R,
C  AND TRIGGER DELAY TG
C  DATA MUST BE GIVEN FOR EACH SET ACCORDING TO FORMATS
C  100 AND 101
C  DIMENSIONS. SGAIN=VOLTS/CENTIMETER, R=OHMS,DT=SECONDS,
C  TG=SECONDS
      READ 100,DT,IMAX,SGAIN,R,TG
100   FORMAT(E10.3,I10,3E10.3)
C
C     RSC = SHORT CIRCUIT RESISTANCE
      RSC=1.33
C
      IMAXP1=(2*IMAX)+1
C
C     READ IN SCOPE DEFLECTIONS AT THE PRESCRIBED TIME
C  INTERVALS
C  PUNCH SCOPE DEFLECTION DATA AT PRESCRIBED TIME INTERVAL
C  AS DETERMINED BY THE INTEGRATION METHOD
C  LET EACH VALUE CORRESPOND TO 1/2 TIME STEP (1/2*DT)
C
C  INITIALIZE  VALUES TO ZERO
      DO 33 J=1,IMAXP1
      DEF(J)=0.0
      V(J)=0.0
      I(J)=0.0
33    ENERGY(J)=0.0
C
      READ 101,(DEF(J),J=1,IMAXP1)
  101 FORMAT(16F5.2)
      DO 1 M=1,IMAXP1
C
C  CALCULATE  VOLTAGE
      V(M)=SGAIN*DEF(M)
C
C   CALCULATE  CURRENT
      I(M)=V(M)/RSC
C
1     CONTINUE
```

```
      PRINT 150
      PRINT 151
450   PRINT 169
169   FORMAT(15X,30HSHOT NO 1206 8/7/68 SCOPE NO 3,/)
180   PRINT 152,IMAX,SGAIN,R,TG
      PRINT 153
      PRINT 154
C
C  CONVERT UNITS OF ENERGY(N) FROM WATT-SEC TO JOULES
      CON=1.0
C
      T=0.0
C
C  ZERO TIME SPECIFIED BY SUBSCRIPT (1).
C
      ENERGY(1)=DT/6.*R*(I(1)**2+4.*I(2)**2+I(3)**2)*CON
      PRINT 200,T,V(1),I(1),ENERGY(1)
C
C  CALCULATE ENERGY FROM CURRENT USING SIMPSON'S RULE FOR
C  NUMERICAL INTEGRATION
C  ENERGY=1/3*(B-A)/2N*R*(I(N-1)**2+4*I(N)**2+I(N+1)**2)
C  INCREMENTS IN THAT INTERVAL. N MUST BE INTEGER.
C EXAMPLE
      DO 2 N=3,IMAXP1,2
      T=T+DT
      ENERGY(N)=DT/6.*RM(I(N-2)**2+4.*I(N-1)**2+I(N)**2)*
     1CON+ENERGY(N-2)
      PRINT 200,T,V(N),I(N),ENERGY(N)
2     CONTINUE
150   FORMAT(1H1,10X,34HWAVE PROPAGATION IN COMPOSITE BAR,/)
151   FORMAT(15X,31H EXPERIMENTAL ELECTRICAL ENERGY,//)
152   FORMAT(5X,6H IMAX=,I5,/,5X,7H SGAIN=,E10.3,/,5X,
     13H R=,F8.3,5X,7H DELAY=,E10.3,//)
153   FORMAT(5X,5H TIME,6X,8H VOLTAGE,5X,8H CURRENT,5X,
     17H ENERGY)
154   FORMAT(5X,6H (SEC),5X,8H (VOLTS),6X,7H (AMPS),4X,
     19H (JOULES),/)
200   FORMAT(2Y,E10.3,3X,E10.3,3X,E10.3,2X,E10.3)
1000  CONTINUE
C
C  IMPUT DATA ACCORDING TO FORMATS 100 AND 101
      STOP
      END
```

EXAMPLE RUN

RSC = 1.33 53.47

DT = 0.183μsec TG = 30μsec

SGAIN = 5.00 IMAX = 140

TIME	CURRENT(AMPS)	ENERGY(JOULES)
0.	.0001	9.223E-14
3.650E-07	.0001	3.506E-13
7.300E-07	.0002	9.763E-13
1.095E-06	.0004	2.681E-12
1.460E-06	.0006	6.204E-12
1.825E-06	.0006	1.319E-11
2.190E-06	.0011	2.667E-11
2.555E-06	.0014	5.548E-11
2.920E-06	.0018	1.02 E-10
3.285E-06	.0023	1.822E-10
3.650E-06	.0028	3.011E-10
4.015E-06	.0035	4.806E-10
4.380E-06	.0041	7.358E-10
4.745E-06	.0047	1.091E-09
5.110E-06	.0054	1.556E-09
5.475E-06	.0059	2.155E-09
5.840E-06	.0063	2.833E-09
6.205E-06	.0068	3.627E-09
6.570E-06	.0069	4.485E-09

REFERENCES

1. Jaffer, Bernard, A Primer on Ferroelectricity and Piezoelectric Ceramics, Clevite Corporation, Electronic Research Division, Technical Paper TP-217.

2. An Introduction to Piezoelectric Transducers, Valpey Corporation, Holliston, Mass.

3. Jaffer, Bernard, "Piezoelectricity," Encyclopedia Britannica, 1961.

4 Cady, W. G., Piezoelectricity, Vol. I and II, Dover Publications, Inc., 1964.

5 Jaffe, H., A General Look at Research on Piezoelectric Materials, Sandia Corporation Reprint, SCR-649, June 1963.

6. Nielson, F. W., Ferromagnetic and Ferroelectric One-Shot Explosive-Electric Transducers, Sandia Corporation Technical Memorandum, 230B-36-51, November 1956.

7. Berlincourt, D. and Krueger, H., Properties of Celvite Ceramics, Clevite Corporation, Technical Paper TP-226.

8. Glenite Piezoceramics, Gulton Industries, Inc., Bulletin H-500.

9. Graham, R. A., Neilson, F. W., Benedick, W. B., "Piezoelectric Current from Shock-Loaded Quartz - A Submicrosecond Stress Gauge," Journal of Applied Physics, v. 36, n. 5, May 1965.

10. Halpin, W. J., "Current from a Shock-Loaded Short-Circuited Ferroelectric Ceramic Disk," Journal of Applied Physics v. 37, n. 1, January 1966.

11. Beadle, C. W., and Dally, J. W., "Experimental Methods for Investigating Strain-Wave Propagation and Associated Charge Release in Ferroelectric Materials," Experimental Mechanics, March 1964.

12. Stuetzer, O. M., "Secondary Stresses in a Stress-Pulse-Activated Piezoelectric Element," Journal of Applied Physics, v. 38, n. 10, September 1967.

13. Krueger, H. and Berlincourt, D., "Effects of High Static Stress on the Piezoelectric Properties of Transducer Materials," Journal of the Accoustical Society of America, v. 33, n. 10, October 1961.

REFERENCES, continued

14. Berlincourt, D. and Krueger, H., "Domain Processes in Lead Titanate Zirconate and Barium Titanate Ceramics," Journal of Applied Physics, v. 30, n. 11, November 1959.

15. Doran, D. G., "Shock-Wave Compression of Barium Titanate and 95/5 Lead Zirconate Titanate," Journal of Applied Physics, v. 39, n. 1, January 1968.

16. Graham, R. A., "Piezoelectric Behavior of Impacted Quartz," Journal of Applied Physics, v. 32, n. 3, March 1961.

17. Linde, R. K., "Depolarization of Ferroelectrics at High Strain Rates," Journal of Applied Physics, v. 38, n. 12, November 1967.

18. Reynolds, C. E. and Seay, G. E., "Two-Wave Shock Structures in the Ferroelectric Ceramics Barium Titanate and Lead Zirconate Titanate," Journal of Applied Physics, v. 33, n. 7, July 1962.

19. Halpin, W. J., "Resistivity Estimates for Some Shocked Ferroelectrics," Journal of Applied Physics, v. 39, n. 8, July 1968.

20. Graham, R. A., Halpin, W. H., "Dielectric Breakdown and Recovery of X-Cut Quartz Under Shock Wave Compression," Journal of Applied Physics, v. 39, n. 11, October 1968.

21 Graham, R. A. "Dielectric Anomaly in Quartz for High Transit Stress and Field," Journal of Applied Physics, v. 33, n. 5, May 1962.

22. Graham, R. A., "Technique for Studying Piezoelectricity Under Transient High Stress Conditions," Review of Scientific Instruments, v. 32, n. 12, December 1961.

23. Ripperger, E. A. and Hart, D., Stress-Charge Release Relationships for Ferroelectric Ceramics, Structural Mechanics Research Laboratory Report, The University of Texas, June 1962.

24. Rhode, R. W. and Jones, O. E., "Mechanical and Piezoelectric Properties of Shock-Loaded X-Cub Quartz at 573°K," Review of Scientific Instruments, v. 39, n. 3, March 1968.

25. Krueger, H. A., "Stress Sensitivity of Piezoelectric Ceramics-2, 3," Journal of the Acoustical Society of America, v. 43, n. 3, March 1968.

26. Fatuzzo, E. and Merz, W. J., Selected Topics in Solid State Physics, Vol. 7, Ferroelectricity, Amsterdam: North-Holland, 1967.

27. Berlincourt, D., "Piezoelectric and Ferroelectric Energy Conversion," EEE Trans. Sonics Ultrasonics (USA), v. Su-15, n. 2, April 1968.

28. Muirhead, J. C. and Fenrick, W. J., Studies on Shock Wave Pressure-Time Gauges III: The Spontaneous Charge Release Effect, Technical Note, Suffield - TN-137, February 1964.

29. Ohlwiler, W., High Temperature Ferroelectric Materials, Air Force Systems Command Report, Wright-Patterson AFB, Ohio, AF Materials Lab., WL-TDR-64-24, AD-437307, March 1964.

30. Jaffe, H. and Berlincourt, D. A., "Piezoelectric Transducer Materials," IEEE Proceedings, v. 53, October 1965.

31. Wedlock, Bruce D., Properties of Piezoelectric Materials, Army Materials Research Agency, AMRA-MS-65-05: AD-611212, June 1965.

32. Lefkowitz, I., Kramer, K., and Kroeger, P., Ferroelectrics: Their Electrical Behavior During, and Subsequent to, Ionizing Radiations, Pitman-Dunn Research Labs, R-1779: Ad-625051, November 1965.

33. Cristescu, N., Dynamic Plasticity, North Holland Publishing Co., Wiley, New York, 1967.

34. Perzyna, P., Fundamental Problems in Viscoplasticity, Advances in Applied Mechanics, Vol. 9, Academic Press, New York, 1966.

35. Ahlberg, J. H., Nilson, E. N., and Walsh, J. L., The Theory of Spliner and Their Application, Academic Press, 1967.